Chemical Tools for Profiling the Allosteric Regulation and Interactomes of Inhibitor-Bound Protein Kinases

Linglan Fang

A dissertation

submitted in partial fulfillment of the

requirements for the degree of

Doctor of Philosophy

University of Washington

2020

Reading Committee:

Dustin J. Maly, Chair

Michael H. Gelb

Forrest Michael

Program Authorized to Offer Degree:

Chemistry

University of Washington

Abstract

Chemical Tools for Profiling the Allosteric Regulation and Interactomes of Inhibitor-Bound Protein Kinases

Linglan Fang

Chair of the Supervisory Committee:

Dustin J. Maly, Ph.D.

Department of Chemistry

This dissertation describes the development of a chemoproteomic method for profiling the interaction network of inhibitor-bound kinase complexes and chemical probes for understanding how ATP-competitive inhibitors can allosterically modulate tyrosine kinases that contain a Src-like regulatory architecture.

Small molecule inhibitors often only block a subset of the cellular functions of their protein targets. In many cases, how inhibiting only a portion of a multifunctional protein's functions affects the state of the cell is not well understood. Therefore, tools that allow the systematic characterization of the cellular interactions that inhibitor-bound proteins make would be of great utility, especially for multifunctional proteins. In the second chapter of this thesis, I describe a chemoproteomic

strategy for interrogating the cellular localization and interactomes of inhibitor-bound kinases. By developing a set of orthogonal inhibitors that contain a *trans*-cyclooctene (TCO) click handle, we are able to enrich and characterize the proteins complexed to a drug-sensitized variant of the multidomain kinase Src. We show that Src's cellular interactions are highly influenced by the intermolecular accessibility of its regulatory domains, which can be allosterically modulated through its ATP-binding site. Furthermore, we find that the signaling status of the cell also has a large effect on Src's interactome. Finally, we demonstrate that our TCO-conjugated probes can be used as a part of a proximity ligation assay to study Src's localization and interactions in situ. Together, our chemoproteomic strategy represents a comprehensive method for studying the localization and interactomes of inhibitor-bound kinases and, potentially, other druggable protein targets.

Small molecule kinase inhibitors that stabilize distinct ATP-binding site conformations can differentially modulate the global conformation of Src-family kinases (SFKs). However, it is unclear which specific ATP-binding site contacts are responsible for modulating the global conformation of SFKs and whether these inhibitor-mediated allosteric effects are general to other tyrosine kinases. In the third chapter of this thesis, I describe the development of chemical probes that allow us to deconvolute which features in the ATP-binding site are responsible for the allosteric modulation of the global conformation of Src. We find that the ability of an inhibitor to modulate the global conformation of Src's regulatory domain-catalytic domain module relies mainly on the influence it has on the conformation of a structural element called helix αC. Furthermore, by developing a set of orthogonal probes that target a drug-sensitized Src variant, we show that stabilizing Src's helix αC in an active conformation is sufficient to promote a Src-

mediated, phosphotransferase-independent alteration in cell morphology. Finally, we report that ATP-competitive, conformation-selective inhibitors can influence the global conformation of tyrosine kinases beyond the SFKs, suggesting that the allosteric networks we observe in Src are conserved in kinases that have a similar regulatory architecture. Taken together, our study highlights that an ATP-competitive inhibitor's interactions with helix αC can have a major influence on the global conformation of some tyrosine kinases in vitro and in cells.

TABLE OF CONTENTS

LIST OF ABBREVIATIONS

SFK	Src-family kinase
Abl	Abelson tyrosine kianse
CAN	Acetonitrile
Glu	Glutamine
Cys	Cystine
Ala	Alanine
ATP	Adenosine triphosphate
BME	β-Mercapto ethanol
CAM	S-carboxyamidomethylcysteine
CD	Catalytic domain
DFG	Aspartate-phenylalanine-glycine
DMEM	Dubecco's Modified Eagle Medium
DMSO	Dimethyl Sulfoxide
Dox	Doxycycline
EDTA	Ethylenediaminetetraacetic acid
EGTA	Ethylene glycol tetra acetic acid
EGFR	Epidermal Growth Factor Receptor Kinase
FAK	Focal Adhesion Kinase
FBS	Fetal Bovine Serum
GO term	Gene Ontology term
HEK293T	Human Embryonic Kidney 293T cells

HeLa	Henrietta Lacks cervical cancer cells
HPLC	High-Performance Liquid Chromatography
IC_{50}	Half-maximal inhibitory concentration
IPTG	Isopropyl β-D-1-thiogalactopyranoside
K_d	Dissociation cons
K_i	Substrate-independet half-maximal inhibitory concentration
K_m	Michaelis constant
KEGG	Kyoto Encyclopedia of Genes and Genomes
LB	Lauria Bertani Broth
Lys	Lysine
mod RIPA	Modified Radioimmunoprecipitation buffer
MS	Mass Spectrometry
m/z	Mass to charge ratio
OD	Optical Density
PAGE	Polyacrylamide Gel Electrophoresis
PBS	Phosphate Buffered Saline
PDB	Protein Data Bank
Phe	Phenylalanine
SDS	Sodium dodecyl sulfide
Ser	Serine
SH2	Src-Homology 2 domain
SH3	Src-Homology 3 domain

TBS	Tris buffered saline
TCEP	Triethyl ammonium bicarbonate
TEAB	Triethyl ammonium bicarbonate
Thr	Threonine
Tris	Tris(hydroxymethyl)aminomethane
Trp	Tryptophan
TCO	*Trans*-cyclooctene
Tz	Tetrazine
WT	Wild type

LIST OF FIGURES

ACKNOWLEDGEMENTS

"Ph.D.s are not created equally."—I can still remember these words from the orientation for new chemistry graduate students back in September of 2014. After six years of training in Dusty's lab, I would argue this statement is just a tip of the iceberg of the efforts to shape an undergrad into a peer-reviewed, community-proved scientist. I feel extremely lucky that my Ph.D. training is synthesized by so many wonderful people whom I want to acknowledge here.

Joining Dusty's lab is one of the best choices of my life. I came to UW chemistry with an only and definitive interest in pure organic synthesis and had never thought about getting my feet wet in the field of biology. I was fortunate to attend Dusty's departmental seminar in the fall quarter of 2014, and my interest in using chemical tools to solve biological questions became unstoppable ever since. It was Dusty who encouraged me to dive into the chemical biology field without worrying how much biology knowledge I had, which was technically close to none at that time. He was right—chemical biology is indeed a field where I can leverage my strength in synthesis and release my potential to a greater extend.

One of the most profound influences that Dusty has on me is the change of methodology of thinking. Thank you to Dusty for making me a results-oriented scientist by six-years of rigorous training. I sometimes got too excited about new ideas, which also means I can get distracted fairly easily and lose my initial focus on the grand purpose of the project. Dusty never discourages these new ideas and taught me how to evaluate the outcome per effort for better decision-making. This results-oriented mindset not only propelled my research progress but also had a great impact on my non-academic life. It is not uncommon for graduate students to experience a full spectrum of

emotions during graduate school. This mindset has helped me to coupe with difficult time. Secondly, Dusty is undoubtfully my biggest role model. I'm a firm believer that training as a mentee is 100% duplicating the mentor's ways of thinking and talking in your own format. I learned most of my English skills from Dusty since I moved to the United States from China. When it comes to thinking about science and making decisions for my projects, I tried to be in Dusty's shoes, thinking in the way as if he were in the same situation. Self-discipline is another trait that Dusty has enhanced in my mindset. Dusty never told us to spend more time to be in the lab, but it's hard not to see him in the office or on slack on weekends or at night, which strengthened my belief in how self-discipline and perseverance can propel one's career. I also learned how compassion and a results-oriented mindset could work harmoniously. His ability to listening to people makes him very approachable. Furthermore, I cannot stress enough on how much time Dusty has dedicated to mentoring me—including those Saturday mornings to go through presentations and second-year exam, countless one-on-one discussions to give feedback on research data and decision-making, and countless hours that we work together for papers and other application materials. He also gave me honest advice on my personalities and ideas to optimize them. I was prone to procrastinate in my early years because of the fear for imperfectness or letting people down. Dusty pointed out my tendency to procrastinate and shared his wisdom that I believe will have life-long impacts on me: "If something needs to be done, it needs to be done no matter how long you wait for it. If this thing is going to hurt someone's feeling, it's going to be more hurtful as time goes by." I have ever since been practicing this mindset and my ability to execute ideas has increased greatly. Another lesson I learned from Dusty is that "when it comes to making decisions, don't rush." Choosing a lab for postdoc training is one of the most critical decisions for a graduate student. Dusty has asked me to ponder for weeks before making the final

decision among potential labs to avoid tunnel vision because of excitements. After I finally decided to join the Kool lab, Dusty passed along what his Ph.D. mentored told him—"Once you've make a decision, don't look back"—and has been providing opportunities to get my feet wet in nucleic acid research, including collaborative projects and peer-reviewing. I can never thank him enough for creating all these opportunities for me to pursue what I'm interested in. If I had a chance to become a mentor, I would do the same to my students and hope these fantastic virtues can be passed along to the next generations of scientists.

In addition to Dusty, many others have profound impacts on my graduate school training. I want to thank Prof. Michael Gelb for inspiring me to be a curious scientist. Mike is an iconic person in our chemistry department and his sparking wisdom is self-explanatory. I'm so fortunate to interact with Mike and be "infected" by his curiosities in virtually everything. This curiosity has become one of my tools for approaching scientific challenges—trying to think as if I were a baby and knew nothing. This method helped me tremendously in critical thinking and gaining new perspectives in old concepts. Aside from being my role model, Mike gave me great career advice and encouraged my passion for becoming a PI, which I sincerely appreciate. I also want to thank Prof. Forrest Michael for witnessing how I grow from a chemist into a chemical biologist. Forrest exemplified the meaning of working ethics, as he works in his office in almost all the Saturdays. He is one of the reasons why it has been so joyful to run experiments on weekends. I'm very lucky to have him as my committee member. Dr. Jack Rose also has a significant influence on my graduate school training because of his working ethics, intelligence, and perseverance. He is my role model from the peer graduate students, and I've learned a lot by trying to follow his steps.

My dissertation work would not have been possible without the support and guidance of many people. Dr. Rama Subba Rao Vidadala helped me to start the first reaction in 2014 and contributed greatly to my first project by pioneering the development of electrophilic conformation-selective inhibitors; Dr. Jack Rose taught me the sterile techniques. Dr. Matthew Chang, Dr. Martin Golkowski, Dr. Martin Sadilek, and Dr. Priska Von Haller helped with my mass spectrometry and proteomics experiments; Dr. Sujata Chakraborty collaborated extensively with me throughout these years and performed most of the inhibitor-titrations and Src SH3 domain pull-down experiments for me; Prof. Markus Seeliger and Ms. Jessica Vilas-Boas took on Src CD crystallization. Thank you to all members of the Maly lab, past and present, for making our lab a fun and lively place to study. Additionally, thank you to Prof. Jiangchun Zhong, Dr. Jianyou Mao, and Dr. Zhiyuan Li for training me for three years in total synthesis since I was a freshman, which built a solid foundation for my graduate school training.

My Ph.D. training would also not be possible without supports from my families and friends. Thank you to my parents for your endless love and supports. I want to dedicate special thanks to my dad. He has devoted so much time of his life to my education and encouraged me to pursue my passions without worrying about any other burdens. He shaped my minds, and I'm forever in debt to him. He also taught me, by his own actions, that society will reward you as long as you work hard and contribute to the community. He also taught me to be humble when in success and grateful when defeated. I also want to thank my grandparents for reinforce the self-discipline in me and cultivated my interests in natural science in my childhood. I want to thank Ms. Zhengxin Lang, my lovely bride. Marriage with you is one of the greatest decisions in my life. You are the reason why we came to UW, which is the prerequisite for meeting all the important persons for

my graduate school training. Thank you for supporting my passions for science and tolerating my stubbornness, without which the graduate school would not have been so joyful. I'm excited about the life ahead of us, no matter it's better or worse, rich or poor. I cannot imagine life without you. My friends outside of the lab have been a constant source of fun and joy. Thank you to Fan, Xinying, Yunfei, Ren, and Yumeng. I hope you know how much I appreciate your accompany and how proud I am to call you my best friends.

DEDICATION

I dedicate this work to my families, my best friends and mentors.

I also dedicate this work to future generations of chemical biologists, especially those who are trained as international graduate students. May you find a world for your passion and talent.

VITA

2009……. No.1 High School, Jinhua, Zhejiang, China

2013……. B.S. Chemistry, China Agricultural University, Beijing, China

2020……. Ph.D. Chemistry, University of Washington, Seattle, WA

PUBLICATIONS

1. **Linglan Fang**; Jessica Vilas-Boas; Sujata Chakraborty; Zachary E. Potter; Ames C. Register; Markus Seeliger; Dustin J. Maly, How ATP-Competitive Inhibitors Allosterically Modulate Tyrosine Kinases That Contain a Src-like Regulatory Architecture. *2020. ACS Chem. Biol., 2020, in press. https://doi.org/10.1021/acschembio.0c00429.*
   - *[Selected as ACS Editors' Choice]*

2. **Linglan Fang**, Sujata Chakraborty, Emily M. Dieter, Zachary E. Potter, Chloe K. Lombard, Dustin J. Maly, Chemoproteomic Method for Profiling Inhibitor-Bound Kinase Complexes, *J. Am. Chem. Soc.,* 2019, 141, 30, 11912-11922.
   - *[Highlighted by Synfacts, 2019, 15 (10), 1194]*

3. Sujata Chakraborty, Takayuki Innukai, **Linglan Fang**, Martin Golkowski, Dustin J. Maly, Targeting Dynamic ATP-Binding Site Features Allows Discrimination Between Highly Homologous Protein Kinases, *ACS Chem. Biol.*, 2019, 14, 6, 1249-1259.

4. Ethan Ahler, Ames C. Register, Sujata Chakraborty, **Linglan Fang**, Emily M. Dieter, Katherine A. Sitko, Rama Subba Rao Vidadala, Bridget M. Trevillian, Martin Golkowski, Hannah Gelman, Jason J. Stephany, Alan F. Rubin, Ethan A. Merritt, Douglas M. Fowler, Dustin J. Maly, A Combined Approach Reveals a Regulatory Mechanism Coupling Src's Kinase Activity, Localization, and Phosphotransferase-Independent Functions, *Molecular Cell*, 2019 (74), 393-408.

5. Zachary E. Potter, Ho-Tak Lau, Sujata Chakraborty, **Linglan Fang**, Miklos Guttman, Shao-En Ong, Douglas M. Fowler, Dustin J. Maly, Parallel Chemoselective Profiling for Mapping Protein Structure, ***Cell Chem. Biol.****, 2020, accepted.*

1 Introduction

1.1 Introduction of Eukaryotic Protein Kinases and ATP-competitive kinase inhibitors

Mammalian cells sense, respond and adapt to the extracellular signals that drive cell growth and survival. Extracellular stimuli is amplified and transduced into cells, by a subset of enzymes called protein kinases either directly or indirectly. Protein kinases are a large family of enzymes consisting of at least 538 family members that catalyze γ-phosphate transfer from ATP to protein substrates containing serine, threonine or tyrosine residues.[1] Intracellular phosphorylation by protein kinases propagates cell signaling events by providing a switch-on or switch-off mechanism and initiates downstream signaling pathways.[2] In addition to substrate phosphorylation, recent studies have shown that many kinases have non-catalytic functions that extend beyond canonical phosphotransferase roles. These non-catalytic, phosphotransferase-independent functions include allosteric regulation of other proteins, protein scaffolding, and regulation of transcription,[3] allowing cells to properly respond to extracellular stimulus.[4] Misregulation of phosphotransferase dependent and independent kinase functions is one of the major mechanisms by which many cancer cells evade normal physiological growth and survival constraints.[5-6]

Despite the large size of the protein kinase family, kinases share a highly conserved, bi-lobal catalytic domain structure. The catalytic domain contains twelve highly homologous subdomains that fold into a conserved core and positions key catalytic residues for catalyzing γ-phosphate transfer of ATP.[7] The ATP-binding pocket that catalyzes ATP γ-phosphate transfer is located

between N- and C-terminal lobes. The adenosine group of ATP forms two H-bonding interactions with a flexible linker called the hinge region between the N- and C-terminal lobes. A set of conserved catalytic residues are essential for ATP binding and phosphotransferase activity: (1) A conserved glutamic acid residue (Glu) from the helix αC forms a salt-bridge with a conserved catalytic lysine residue (Lys) located on the N-lobe. This salt-bridge is believed to position the catalytic lysine in a position to coordinate the α and β phosphates of ATP, which stabilizes the build-up of negative charges that occurs during γ-phosphate transfer. (2) A catalytic aspartic acid (Asp), located in the conserved Asp-Phe-Gly sequence (also called "DFG-motif") from the activation loop, coordinates with a magnesium ion in the binding pocket which stabilizes β and γ phosphates of ATP. Disruption of any of these interactions causes kinases to be catalytically inactive.

Given their pivotal role in most signal transduction pathways and involvement in human diseases, kinases have become popular drug targets for therapeutic intervention in diseases such as cancer.[8] In recent years, many cell-permeable ATP-competitive small molecule inhibitors have been developed to target the druggable kinases pharmacologically. These inhibitors compete with ATP and abolish kinase phosphotransferase activity. In addition to their potential therapeutic applications, these ATP-competitive small molecule inhibitors are also useful tools for identifying kinase substrates and the cellular functions of kinases, which in turn provide insights for the discovery of druggable kinases. The ability of ATP-competitive inhibitors to perturb kinase phosphorylation activity allows us to study the functional roles of kinases in regulating their downstream signaling pathways and infer whether the target kinase can serve as a potential drug target for therapeutic interventions.

1.2 NON-CATALYTIC FUNCTIONS OF PROTEIN KINASES

Recent studies have demonstrated that a subset of protein kinases can affect cellular signaling through phosphotransferase-independent mechanisms. These kinase non-phosphotransferase functions include allosterically regulating other kinases and enzymes, scaffolding signaling complexes, and regulating transcription.[3] B-RAF mutants that have impaired phosphotransferase activity can still stimulate mitogen-activated protein kinase (MAPK) signaling by allosteric activation of C-RAF through heterodimerization.[9] This ability of kinases to allosterically modulate the activities of other kinases also extends to the modulation of other non-kinase enzymes. For example, the MAPK extracellular-regulated kinase 2 (Erk2) can bind to the dual-specificity phosphatase MKP3 (DUSP6), which enhances the phosphatase activity of DUSP6 by promoting a change in DUSP6's global conformation.[10-11]

A growing body of studies also demonstrates the ability of kinases to participate in the formation of signaling complexes, which plays a vital role in cell signaling. All kinases contain at least one highly homologous catalytic domain (CD) that is of similar overall architecture. Almost half of all protein kinases contain at least one auxiliary domain outside of the CD.[12] These auxiliary domains and the CD participate in numerous intermolecular binding interactions that can influence cellular signaling. For example, kinase suppressor of Ras (KSR) can function as a scaffold protein that regulates the MAPK pathway by facilitating the assembly of the Raf/Mek/Erk signaling complex in a phosphotransferase-independent manner. Upon stimulation, KSR can enhance MEK activation by interacting with RAF and MEK near the plasma membrane. Kinase-mediated

scaffolding can also regulate ubiquitination. Dual-specificity tyrosine phosphorylation-regulated kinase 2 (DYRK2) can promote the ubiquitination of katanin p60 by promoting the formation of an E3 ubiquitin ligase complex. DYRK2 serves as a scaffold for the EDVP complex, which is independent of the phosphotransferase activity of DYRK2.[13] In addition, a subset of protein kinases can regulate gene transcription in a phosphotransferase-independent manner. For example, a previous study demonstrated Erk2 as a transcriptional repressor of interferon signaling by directly binding to the DNA. Pharmacological inhibition of Erk2 had no effect on the ability of Erk2 to suppress transcription, which indicates that this function is phosphotransferase-independent.[14]

1.3 Conformation-selective kinase inhibitors for allosteric modulation of protein kinases and non-phosphotransferase activities

The efforts of drug discovery have led to increasing amounts of X-ray co-crystal structures for inhibitor-bound kinases deposited in the Protein Data Bank (PDB), covering almost half of the human kinome and containing several thousands of entries.[7] These crystal structures reveal remarkable conformation plasticity in the kinase domain, with at least three structurally divergent ATP-binding site conformations that are routinely observed in inhibitor-bound kinase complexes. Accumulated evidence has demonstrated that inhibitors that stabilize different ATP-binding site conformations can allosterically modulate a subset of protein kinases in phosphotransferase-independent manners. For example, certain inhibitor-bound B-RAF complexes can paradoxically activate the MAPK signaling pathway by stabilizing an active ATP-binding site conformation that promotes side-to-side heterodimerization of BRAF with CRAF, which leads to the activation of

C-RAF and enhancement of proliferation signals.[15-16] Crystal structures of RAF dimers demonstrate that the formation of B-RAF/C-RAF heterodimers requires the helix αC to adopt an active conformation, and inhibitors that stabilize the helix αC-out conformation disrupt the heterodimerization. Thus, inhibitors that stabilize different ATP-binding site conformations of B-RAF can differentially modulate the activation of C-RAF through promotion or disruption of B-RAF/C-RAF heterodimers. Our lab and others in the field have reported similar effects of conformation-selective inhibitors on other protein kinases. For example, Erk2 can enhance the phosphatase activity of DUSP6 when bound to a helix αC-out-stabilizing inhibitor rather than a DFG-out-stabilizing inhibitor.[11] In addition, the SH3 domains of the Src-family kinases (SFKs) and Abelson tyrosine kinase (Abl) have increased intermolecular accessibility when their catalytic domains are bound to DFG-out-stabilizing inhibitors.[17-19] Similar allosteric communication exists between the ATP-binding site of IRE1α and its RNase domain. A subset of ATP-competitive, conformation-selective inhibitors called KIRAs, can allosterically inactivate the RNase activity through the catalytic domain by disrupting the back-to-back dimerization of IRE1α[20]

While conformation-selective kinase inhibitors provide opportunities for probing and manipulating kinase phosphotransferase-independent functions in vitro and in cells, several questions regarding inhibitor-promoted allosteric modulation of protein kinases remain elusive. First, how do conformation-selective inhibitors rewire kinase interaction networks and cell signaling? Second, which ATP-binding site contacts are responsible for the divergent effects of conformation-selective inhibitors on the global conformation of protein kinases? This thesis describes my efforts to develop and utilize conformation-selective probes and a chemoproteomic platform for understanding the molecular basis and cellular outcomes of the allosteric modulation

of protein kinases. **Chapter II** describes the development of a chemoproteomic method to interrogate inhibitor-bound protein kinase complexes, which provides a framework for profiling the effects of conformation-selective inhibitors on the interactome of Src and additional kinases. **Chapter III** demonstrates the development of chemical probes for understanding which ATP-binding contacts are responsible for the allosteric modulation of SFKs and additional tyrosine kinases. This works shows that the ability of inhibitors to modulate the global conformation of Src is due to their ability to stabilize or perturb the conformation of a structural element called helix αC. Inhibitors that stabilize different ATP-binding site conformations can lead to divergent global conformations of kinases that contain a Src-like regulatory architecture, such as BTK and Abl-1 from Tec- and Abl-family kinases, respectively.

2 CHEMOPROTEOMIC METHOD FOR PROFILING INHIBITOR-BOUND KINASES COMPLEXES (CHAPTER II)

2.1 INTRODUCTION

The phenotypic effects of pharmacologically inhibiting a protein target can significantly differ compared to pre-translational disruption of function.[21-23] The slow onset of pre-translational disruption can often lead to compensatory changes within the cell. In addition, pre-translational

disruption methods usually lead to the complete loss of a target protein from a cell, while most small molecules do not lead to degradation of their inhibited protein targets. As most small molecule inhibitors block only one or two interaction sites, additional functional sites are left intact and are capable of participating in various cellular processes. In many cases, how an inhibited protein target influences cellular function is not well understood.

Kinases are of particular interest in terms of understanding how inhibitor binding affects cellular target function because almost 50% of the ~540 kinases in humans contain separate domains outside of the catalytic domain.[12] For many kinases, binding interactions distal to their active sites mediate a number of phosphotransferase-independent functions.[3, 15, 24] Even the kinase that has a single catalytic domain can contain multiple binding interaction sites that are distal to their active sites. The abilities of inhibited kinases to participate in and to modulate phosphotransferase-independent functions are not well understood. Determining how inhibitor binding affects the interactions and phosphotransferase-independent functions of protein kinase is especially important because ATP-competitive inhibitors can allosterically modulate interaction surfaces and domains that are distal to the active site.[25-27] Furthermore, because kinase inhibitors can differentially modulate distal interaction surfaces and binding domains depending on the ATP-binding site conformation that they stabilize, the interactomes and cellular localization of probe-bound kinases can vary greatly. Therefore, we sought to develop a methodology that would allow the interactions and cellular context of an inhibited protein kinase to be interrogated.

To develop a general strategy for co-enriching proteins that are non-covalently, and often weakly, associated with a probe-bound target, we required a mild and rapid bioorthogonal click reaction.

Numerous chemical proteomics strategies, such as activity-based protein profiling,[28-30] rely on the use of probes containing bioorthogonal click handles for target enrichment. The most dominant click reaction for this purpose is the copper-catalyzed alkyne-azide cycloaddition (CuAAC).[31] The robust nature of the CuAAC reaction make it attractive for enriching low abundance targets. However, we were concerned that the high concentrations of copper used in the CuAAC reaction, and the copper-mediated protein oxidation that can occur,[32-37] may result in protein complex dissociation. Strain promoted copper-free alkyne-azide cycloaddition (SPAAC)[38] have been developed but we felt its moderate reaction rate would require prolonged incubation time for enrichment, which reduces the likelihood that intact protein complexes can be captured. For these reasons, we were attracted to the inverse electron demand Diels-Alder (iEDDA) reaction between a tetrazine (Tz) and trans-cyclooctene (TCO).[29, 39-40] The iEDDA reaction has been demonstrated to be rapid (~10^5 $M^{-1}S^{-1}$), mild, and does not require additives or catalysts.

Here, we demonstrate that selective inhibitors conjugated to a TCO click handle can be used to interrogate the interactomes and cellular context of protein kinases (**Figure 2.1**). We show that the rapid, mild, and selective reaction between TCO-conjugated probes and tetrazines is ideal for interrogating the interactomes of kinases. Using a set of TCO-conjugated probes that stabilize different ATP-binding site conformations of Src kinase, we were able to obtain a comprehensive overview of how modulating the global conformation of this multi-domain protein influences its interactome. Furthermore, we were able to demonstrate the cellular context of Src profoundly influences its cellular interaction partners. Finally, we showed that our TCO-conjugated probes can be used as part of a proximity ligation assay (PLA) to study the in *situ* localization and interactions of Src. Our chemical proteomic method represents an inhibitor-focused strategy for

studying the localization and interactomes of inhibitor-bound kinases and potentially other druggable protein targets.

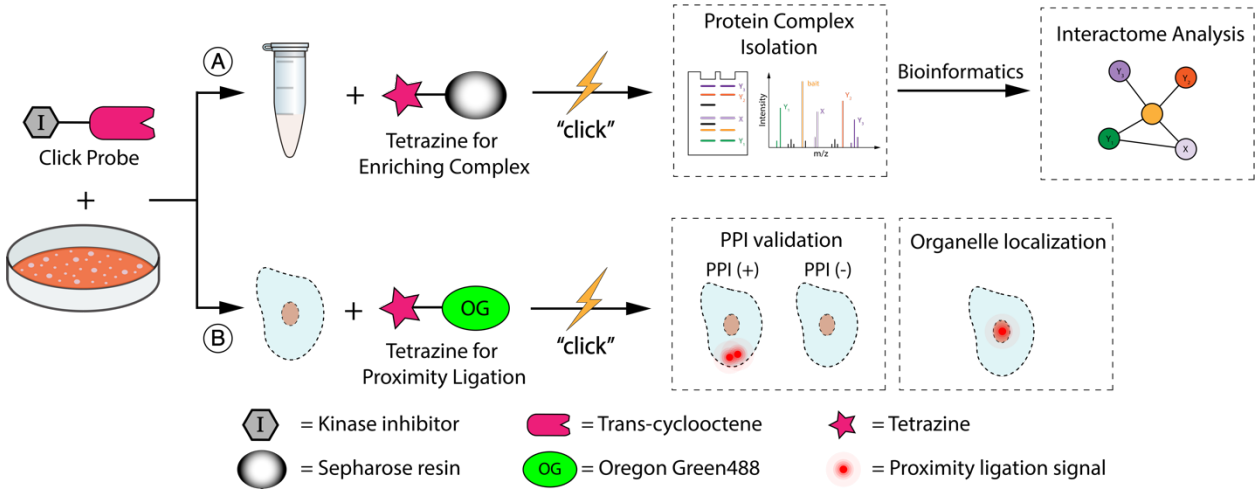

Figure 2-1. A chemoproteomic platform for characterizing inhibitor-bound protein complexes. (A) Schematic for isolating and analyzing inhibitor-bound protein complexes. (B) Schematic for validating intracellular target interactions and visualizing inhibitor-bound target localization using a proximity ligation assay.

2.2 Results and Discussion

2.2.1 Probe design and rapid enrichment of probe-bound target

We pursued a strategy that involves derivatizing selective inhibitors with a TCO moiety that can be directly enriched with Tetrazine-conjugated sepharose beads (Tz-beads). To do this, we explored whether our inhibitor-bound protein complex enrichment strategy could be integrated with a chemical genetic strategy we recently developed called Cysteine Installation for Modulating Allostery and Targeted Inhibition of Kinases (CystIMATIK).[25] CystIMATIK involves sensitizing specific kinases to electrophile-containing inhibitors, which are orthogonal to most wild-type

(WT) kinases (**Figure 2-2**), through the introduction of a cysteine residue into the N-terminal lobes of their catalytic domains.[41-44] By generating a TCO-conjugated version of our orthogonal inhibitors, this strategy should allow multiple sensitized kinases to be selectively targeted.

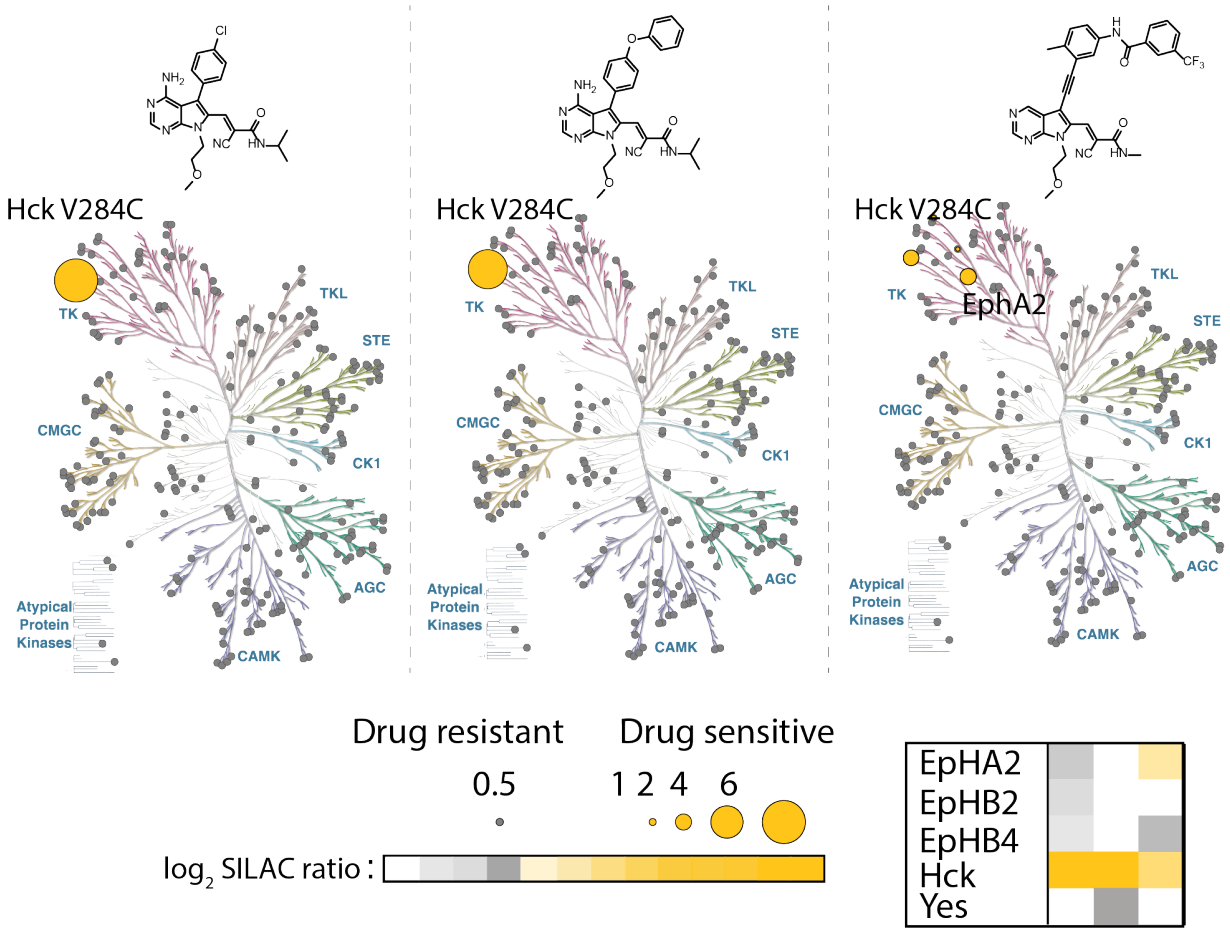

Figure 2-2. Phylogenetic trees showing the kinobead-based chemoproteomic profiling of CystIMATIK probes. Significantly competed kinases are shown as yellow circles with the size corresponding to the level of competition (larger circle, more competed). See the Supplementary Information of Mol. Cell 2019, 74, p. 393-408 for primary profiling data.

Our first target was a TCO-conjugated analog of pyrrolo[2,3]pyrimidine-based CystIMATIK probe 1 (**Figure 2-3A**, *left*). Probe **1** contains a reversible covalent electrophile at the C-6 position

and a 4-chlorophenyl moiety at the C-5 position of the pyrrolopyrimidine scaffold, which makes it highly selective for kinases that contain a threonine gatekeeper residue and a cysteine residue in the β2 strand of the N-terminal lobe that lines the roof of the ATP-binding cleft of the catalytic domain. Because only the C-terminal kinase domain of RSK2 has both of these residues at these positions, inhibitor **1** minimally interacts with most wild-type kinases (**Figure 2-2**), including Src WT. Introduction of a cysteine residue into Src, which contains a threonine gatekeeper residue, sensitizes it to probe **1** (**Figure 2-4**). Based on a co-crystal structure of **1** bound to a cysteine-containing Src mutant (Src V284C; PDB ID: 5SWH), we designed and generated **1-TCO** (**Figure 2-3A**, *right*), which contains TCO conjugated to a position directed outside of the ATP-binding pocket (**Figure 2-3B**). Like **1**, **1-TCO** potently inhibits Src V284C (**Figure 2-3C**).

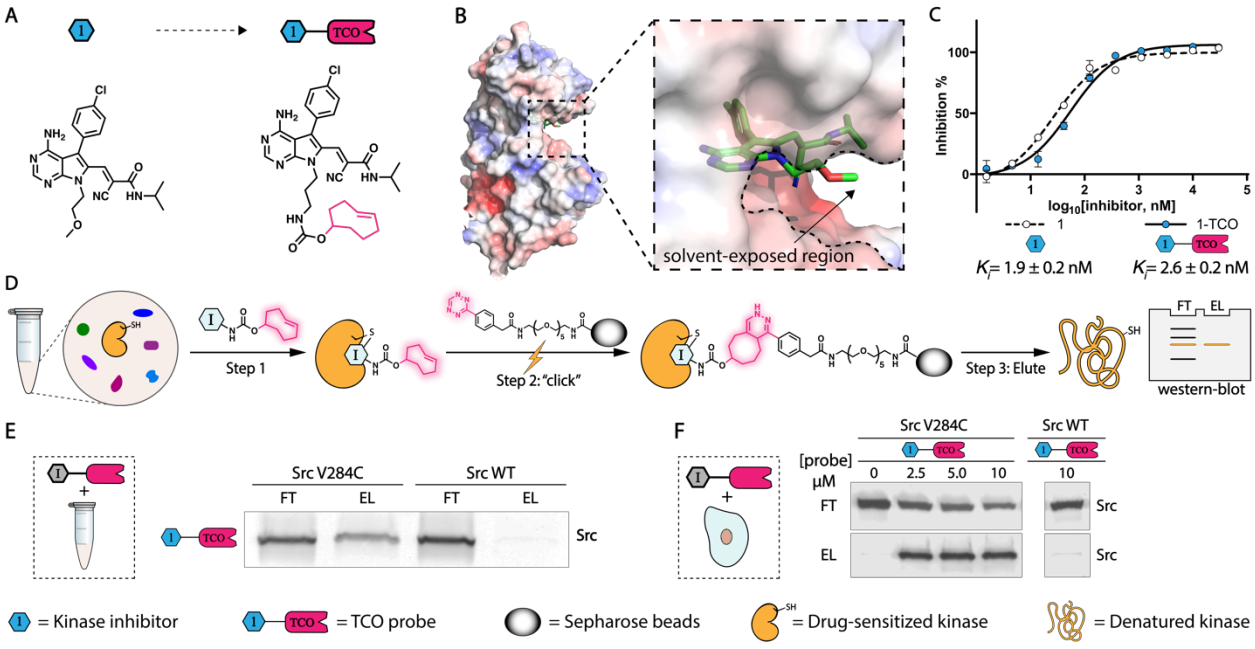

Figure 2-3. Rapid and mild enrichment of protein kinases with TCO-conjugated probes.

(A) Schematic for conversion of 1 (left) into 1-TCO (right). (B) Co-crystal structure of 1 bound to Src V284C (PDB ID: 5SWH). (C) Inhibition curves and Ki values of 1 and 1-TCO against recombinant Src V284C activity. Values shown are mean ± SEM, n = 3. (D) Schematic representation of kinase enrichment with TCO-conjugated probes. (E) 1-TCO selectively enriches a drug-sensitized Src mutant (Src V284C) from cell lysates. HEK293 cell lysates containing either Src V284C or Src WT were treated with 1-TCO (5 μM), incubated with tetrazine-conjugated sepharose beads (Tz-beads), and captured proteins were eluted under reducing and denaturing conditions. A Src immunoblot of the flow through (FT) and elution (EL) are shown. (F) 1-TCO selectively enriches Src V284C from cells. HEK293 cells expressing either Src V284C or Src WT were treated with the indicated concentrations of 1-TCO, lysed, and then incubated with Tz-beads. Captured proteins were eluted under reducing and denaturing conditions. A Src immunoblot of the flow through (FT) and elution (EL) are shown.

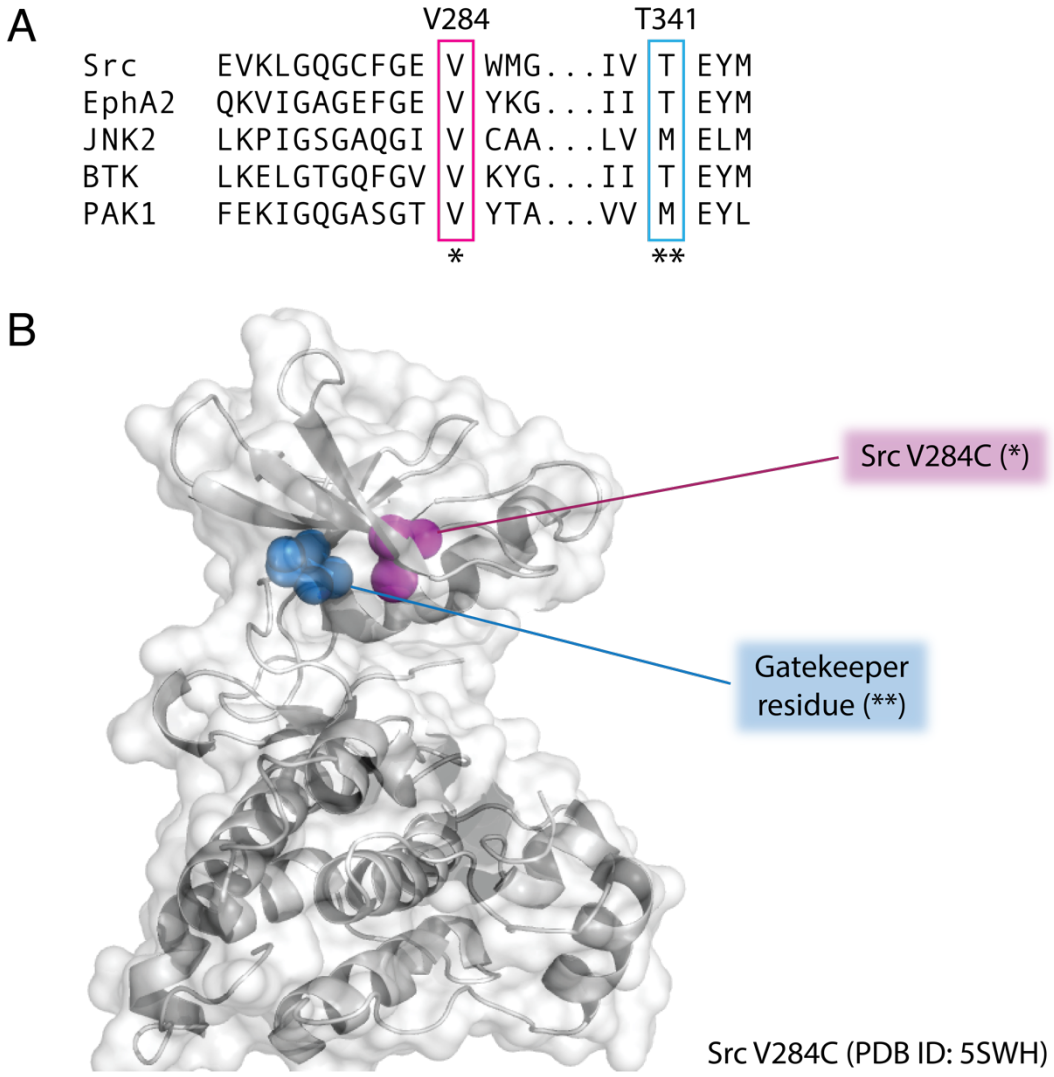

Figure 2-4**.** Sensitization of kinases to CystIMATIK probes. Introduction of a Cys at the residue homologous to V284 of Src and, if required, a Thr at the gatekeeper position sensitizes kinases to CystIMATIK probes.

(A) Sequence alignment of the nonreceptor tyrosine kinases Src and BTK, the receptor tyrosine kinase Epha2, and the serine/threonine kinases PAK1 and JNK2. Residues at the position equivalent to V284 of Src are framed in magenta. Gatekeeper residues are framed in blue. Sequences used for sequence alignment are: PDB ID (Src): 2BDF; PDB ID (EphA2): 5I9Y; PDB

ID (JNK2): 3E7O; PDB ID (BTK): 5FBO; PDB ID (PAK1): 2HY8. (B) X-ray crystal structure of the catalytic domain of Src V284C (PDB ID: 5SWH). The Cys284 residue is colored in magenta. The gatekeeper residue (T341) is colored in blue.

Next, we investigated whether our **1-TCO** probe can be used to directly enrich Src V284C from complex proteomes. To do this, we incubated **1-TCO** with HEK293T cell lysate containing either recombinant drug-sensitized Src V284C or Src WT constructs, followed by direct enrichment with Tz-beads (**Figure 2-3D**). Western blot analysis of bound proteins eluted under reducing and denaturing conditions demonstrated that a significant percentage of Src V284C was captured under these conditions, while Src WT was not (**Figure 2-3E**). We found that **1-TCO** was also capable of efficiently enriching Src V284C from live mammalian cells. Treatment of HEK293 cells stably expressing Src V284C with **1-TCO**, followed by incubation with Tz-beads immediately after cell lysis led to significant enrichment of Src V284C (**Figure 2-3F**). Thus, the click reaction between TCO and tetrazine is capable of rapidly and efficiently enriching probe-bound targets.

We also determined whether additional kinases can be sensitized to CystIMATIK probes **1** and **1-TCO**. We found that BTK (V416C), EphA2 (EphA2 V627C), JNK2 (JNK2 V40C/M108T), and PAK1 (PAK1 V286C/M346T) can be sensitized to probe **1** by introducing Cys at the residue homologous to V284 of Src and, if required, threonine at the gatekeeper position (**Figure 2-5A**). As expected, WT JNK2, EphA2 and PAK1 were insensitive to **1**. Like Src V284C, we observed that **1-TCO** was capable of selectively enriching diverse drug-sensitized kinases from lysates (**Figure 2-5B,2-5C**) or live mammalian cells (**Figure 2-5D**). Thus, **1-TCO** should be of utility for the chemical proteomic interrogation of a number of kinases beyond Src.

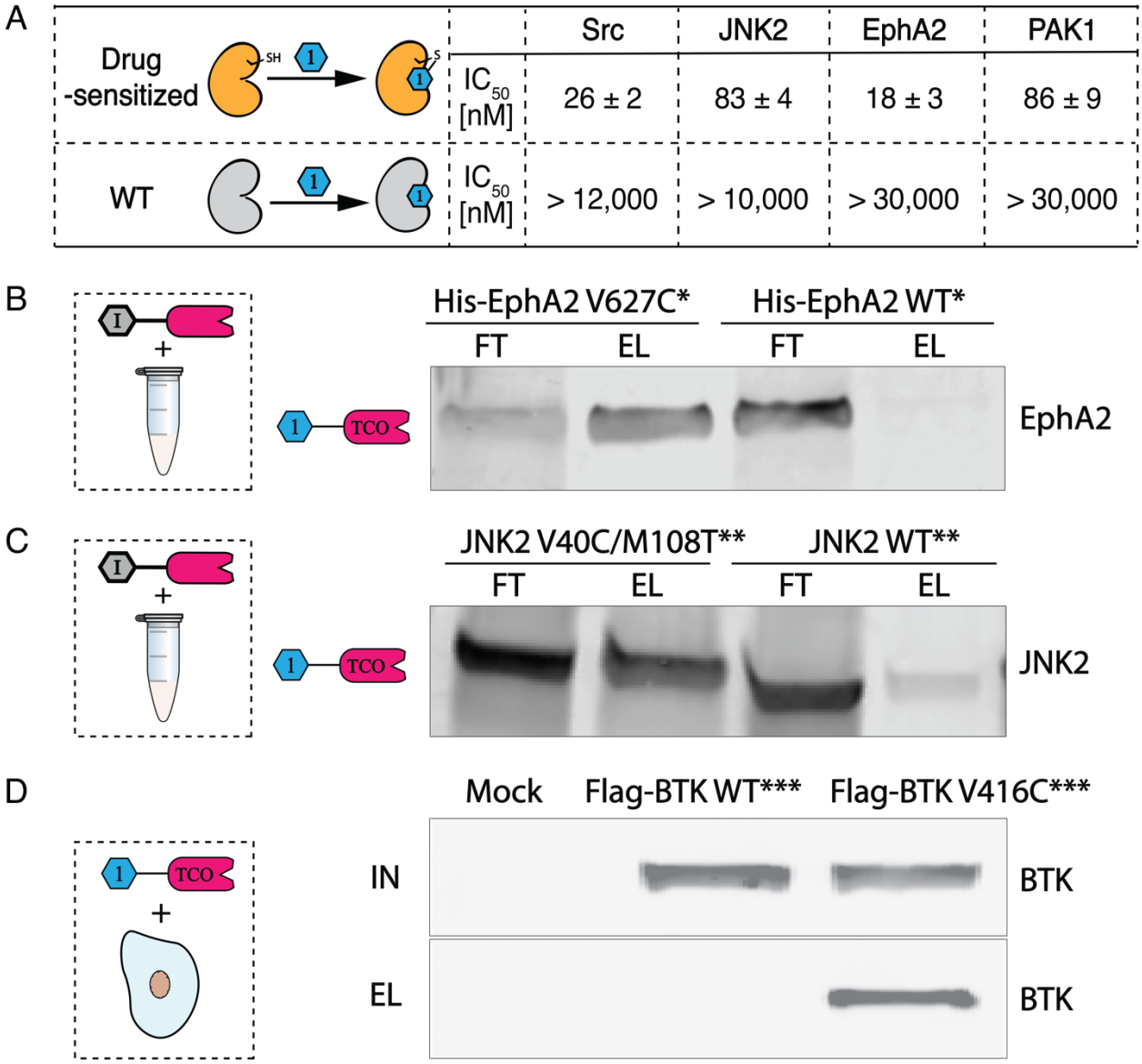

Notes: N-terminal His-tagged recombinant EphA2 (residue 590 - 876); ** Full-length reco--mbinant JNK2; *** N-terminal Flag-tagged full-length BTK*

Figure 2-5. Sensitization of diverse kinases to CystIMATIK probes **1** and **1-TCO**.

(A) IC_{50} values of **1** against recombinant Src V284C, JNK2 V40C/M108T, EphA2 V627C and PAK1 V286C/M346T, and wild-type Src, JNK2, EphA2 and PAK1. IC_{50} values shown are mean ± SEM, $n = 3$. (B) **1-TCO** selectively enriches drug-sensitized EphA2 (V627C; residue 590 - 876) from cell lysates. HEK293 cell lysate containing either N-terminal His-tagged EphA2 V627C or

EphA2 WT were treated with **1-TCO** (10 ∝M), incubated with tetrazine-conjugated sepharose beads (Tz-beads), and captured proteins were eluted under reducing and denaturing conditions. An anti-His Tag immunoblot of the flow through (FT) and elution (EL) are shown. (C) **1-TCO** selectively enriches drug-sensitized JNK2 (V40C/M108T) from cell lysates. HEK293 cell lysate containing either JNK2 V40C/M108T or JNK2 WT were treated with **1-TCO** (10 ∝M), incubated with Tz-beads, and captured proteins were eluted under reducing and denaturing conditions. An anti-JNK2 immunoblot of the flow through (FT) and elution (EL) are shown. (D) **1-TCO** selectively enriches drug-sensitized BTK (V416C) from cells. HEK293 cells transiently expressing either N-terminal Flag-tagged BTK (V416C) or BTK WT were treated with **1-TCO** (2.5 ∝M), lysed, and then incubated with Tz-beads. Captured proteins were eluted under reducing and denaturing conditions. An anti-DYKDDDDK Tag (Flag Tag) immunoblot of the flow through (FT) and elution (EL) are shown.

2.2.2 Conformation-selective TCO conjugates

We and others have demonstrated that there is an allosteric, bi-directional relationship between the ATP-binding sites and regulatory domains of protein kinases.[3, 11, 17-18, 20] Intramolecular engagement of kinase regulatory domains can stabilize ATP-binding site conformations that either inhibit or enhance phosphotransferase activity. Conversely, small molecule inhibitors that stabilize different ATP-binding site conformations can divergently modulate the regulatory domains of multidomain protein kinases, which can greatly influence intracellular protein-protein interactions.[18] To facilitate studies of how ATP-binding site conformation and regulatory domain engagement influence the intracellular functions of kinases, we developed analogs of

CystIMATIK probe **1** that stabilize different ATP-binding site conformations. Inhibitor **2** stabilizes an ATP-binding site conformation that involves displacement of a catalytically important helix–helix αC–in the N-terminal lobe of the catalytic domain from an active position (**Figure 2-6A**, *top left*). Stabilizing this inactive conformation, which is often referred to as the helix αC-out conformation, with ATP-competitive inhibitors leads to enhanced intramolecular engagement of Src's regulatory domains and a closed, auto-inhibited global conformation. CystIMATIK probe **3** stabilizes an ATP-binding site conformation that involves flipping of the DFG-motif in the activation loop of the catalytic domain to an inactive conformation–often referred to as the DFG-out conformation (**Figure 2-6A**, *bottom left*). We have demonstrated that the stabilization of the DFG-out conformation of Src leads to intramolecular disengagement of its regulatory domains and an open global conformation. TCO-conjugated versions of **2** and **3**–**2-TCO** and **3-TCO** (**Figure 2-6A**)–were generated in an analogous manner as **1-TCO**.

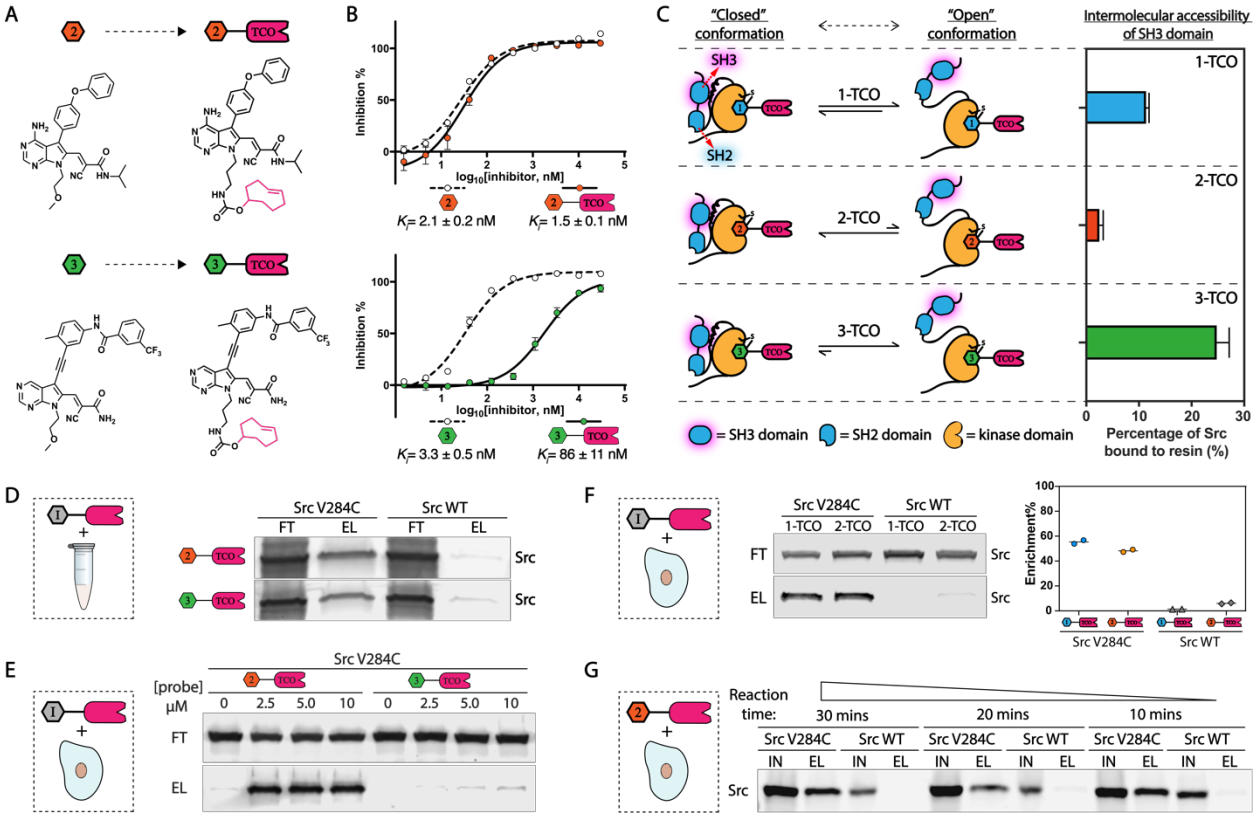

Figure 2-6**.** Conformation-selective versions of TCO-conjugated probes.

(A) Schematic for conversion of **2** and **3** (*left*) into **2-TCO** and **3-TCO** (*right*), respectively. (B) Inhibition curves and K_i values of **2**, **2-TCO**, **3**, and **3-TCO** against recombinant Src V284C activity. Values shown are mean ± SEM, $n = 3$. (C) **1-TCO**, **2-TCO** and **3-TCO** promote expected levels of intermolecular SH3 domain accessibility of Src V284C. Schematic of how conformation-selective probes are predicted to modulate the intramolecular regulatory interactions and global confomrational state of Src (*left*). Percentage retained Src in an SH3 pulldown assay with recombinant Src V284C treated with **1-TCO**, **2-TCO** or **3-TCO** (*right*). Values shown are mean ± SEM, $n = 3$. (D) **2-TCO** and **3-TCO** selectively enrich Src V284C from cell lysates. Cell lysates containing either Src V284C or Src WT were treated with **2-TCO** or **3-TCO** (5 µM), incubated with Tz-beads, and captured proteins were eluted under reducing and denaturing conditions. A Src

immunoblot of the flow through (FT) and elution (EL) are shown. (E) **2-TCO**–but not **3-TCO**–selectively enriches Src V284C from cells. HEK293 cells expressing either Src V284C or Src WT were treated with the indicated concentrations of **2-TCO** or **3-TCO**, lysed, and then incubated with Tz-beads. Captured proteins were eluted under reducing and denaturing conditions. A Src immunoblot of the flow through (FT) and elution (EL) are shown. (F) **1-TCO** and **2-TCO** selectively enrich Src V284C from HeLa cells. HeLa cells expressing either Src V284C or Src WT were treated with **1-TCO** (5 μM) or **2-TCO** (2.5 μM), lysed, and then incubated with Tz-beads. Captured proteins were eluted under reducing and denaturing conditions. A Src immunoblot (*left*) and qunatification (*right*) of the flow through (FT) and elution (EL) are shown. (G) Kinetics of probe-bound target capture with Tz-beads. HeLa cells expressing either Src V284C or Src WT were treated with **2-TCO** (2.5 μM), lysed, and then incubated with Tz-beads at 4 ˚C for the reaction time indicated. Immunoblots of the total lysate input (IN) and eluted proteins (EL) are shown.

We tested **2-TCO** and **3-TCO** for the inhibition of Src V284C and found that both probes potently inhibited this drug-sensitized kinase (**Figure 2-6B**), though conjugation of probe **3** to TCO led to a significant decrease in potency. Next, we validated that each TCO-conjugated probe biochemically modulated intramolecular SH3 domain engagement like their underivatized counterparts by performing pulldown assays of probe-bound Src V284C complexes with an immobilized SH3 domain ligand (**Figure 2-6C**). As expected, we found that the SH3 domain of the Src V284C/**2-TCO** complex was largely inaccessible to intermolecular ligand engagement, which is consistent with **2-TCO** promoting a closed, autoinhibited global conformation of Src. In contrast, the Src V284C/**3-TCO** complex was efficiently pulled down by the immobilized SH3 domain ligand, which is consistent with **3-TCO** promoting a regulatory domain disengaged

conformation of Src. Finally, we observed an intermediate amount of pulldown of the Src V284C/**1-TCO** complex, which is consistent with the pharmacophore of **1** minimally influencing the ATP-binding site conformation of Src, resulting in a moderately open global conformation.[17-18, 25]

Next, we validated that **2-TCO** and **3-TCO** were also capable of enriching Src V284C from complex proteomes. Like **1-TCO**, **2-TCO** and **3-TCO** significantly enriched recombinant Src V284C but not Src WT from a HEK293 lysate (**Figure 2-6D**). Treatment of HEK293 cells expressing Src V284C with **2-TCO** followed by lysis and incubation with Tz-beads led to efficient Src V284C enrichment. Unfortunately, very little Src V284C was captured with Tz-beads following lysis of **3-TCO**-treated HEK293 cells expressing this mutant. The low level of captured Src V284C observed with **3-TCO** is likely due to its poor cell permeability, as this probe worked efficiently in lysates (**Figure 2-6D,2-6E**).

Next, we investigated whether our conformation-selective CystIMATIK probes are compatible with the diverse set of kinases that can be sensitized to **1** and **1-TCO**. Like **1**, we found that probes **2** and **3** inhibited drug-sensitized BTK, EphA2, and JNK2 selectively over their WT variants (**Figure 2-7A,2-7B**). The V286C/M346T variant of PAK1 was inhibited by probe **2** but was almost completely insensitive to probe **3**. The inability to sensitize PAK1 to DFG-out-stabilizing probe **3** reflects the fact that some kinases may be incompatible with certain conformation-selective probes. We also observed that **2-TCO** and **3-TCO** were similarly efficient as **1-TCO** in enriching drug-sensitized kinases from lysates (**Figure 2-7C**), while only **2-TCO** was effective in mammalian cells (**Figure 2-7D**). The ability to sensitize diverse kinases to one or more conformation-selective

TCO conjugates will allow broader interrogation of how ATP-binding site conformation influences the interactomes of kinases.

A

		Src	JNK2	EphA2	PAK1
Drug -sensitized	IC_{50} [nM]	28 ± 3	180 ± 10	300 ± 30	151 ± 4
WT	IC_{50} [nM]	> 12,000	> 10,000	> 30,000	> 30,000

B

		Src	JNK2	EphA2	PAK1
Drug -sensitized	IC_{50} [nM]	39 ± 3	6.2 ± 0.2	32 ± 2	> 30,000
WT	IC_{50} [nM]	> 12,000	> 10,000	890 ± 60	> 30,000

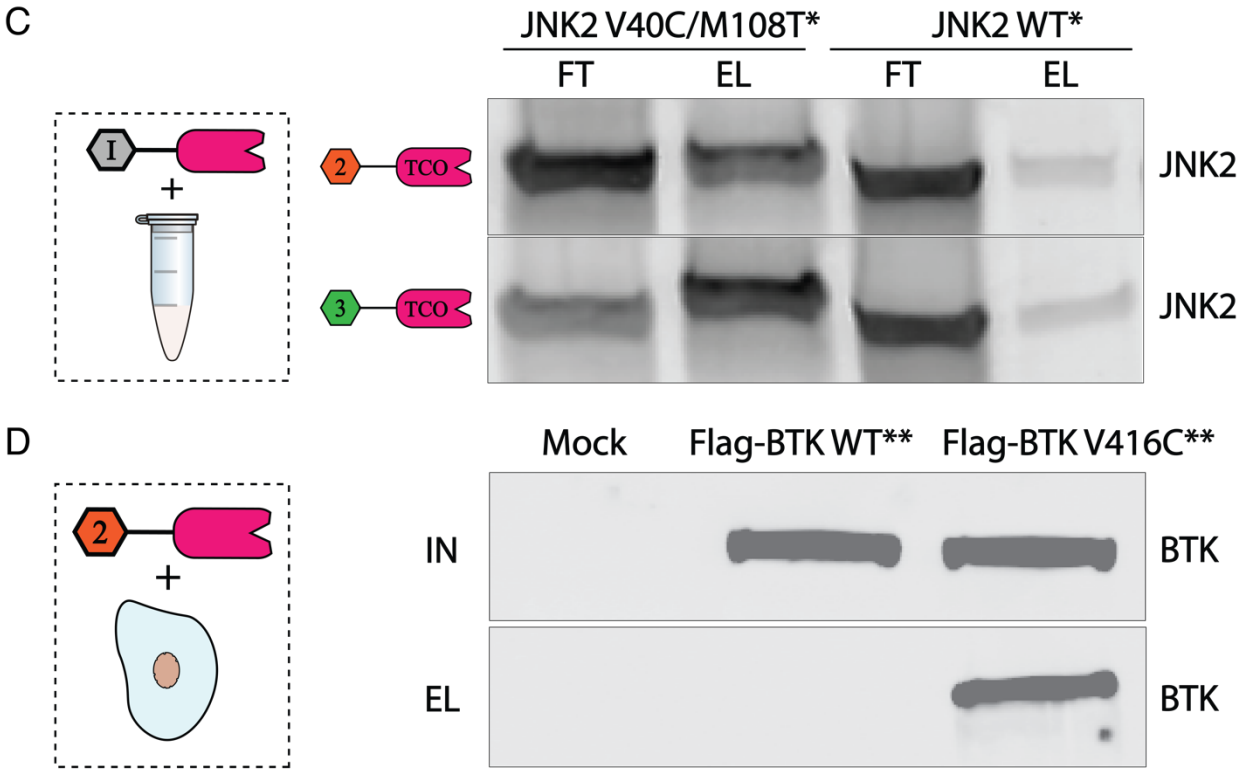

Notes: ** Full-length recombinant JNK2; ** N-terminal Flag-tagged full-length BTK*

Figure 2-7. Sensitization of diverse kinases to conformation-selective CystIMATIK probes.

(A) IC_{50} values of **2** against recombinant Src V284C, JNK2 V40C/M108T, EphA2 V627C and PAK1 V286C/M346T, and WT Src, JNK2, EphA2 and PAK1. Values shown are mean ± SEM, *n* = 3. (B) IC_{50} values of **3** against recombinant Src V284C, JNK2 V40C/M108T, EphA2 V627C and PAK1 V286C/M346T, and wild-type Src, JNK2, EphA2 and PAK1. Values shown are mean ± SEM, *n* = 3. (C) **2-TCO** and **3-TCO** selectively enrich drug-sensitized JNK2 (V40C/M108T) from cell lysates. HEK293 cell lysate containing either JNK2 (V40C/M108T) or JNK2 WT were treated with **2-TCO** (10 ∝M) or **3-TCO** (10 ∝M), incubated with Tz-beads, and captured proteins were eluted under reducing and denaturing conditions. An anti-JNK2 immunoblot of the flow through (FT) and elution (EL) are shown. (D) **2-TCO** selectively enriches drug-sensitized BTK (V416C) from cells. HEK293 cells transiently expressing either N-terminal Flag-tagged BTK (V416C) or BTK WT were treated with **2-TCO** (2.5 ∝M), lysed, and then incubated with Tz-beads. Captured proteins were eluted under reducing and denaturing conditions. An anti-DYKDDDDK Tag (Flag Tag) immunoblot of the flow through (FT) and elution (EL) are shown.

2.2.3 Clickable precipitation for interrogating Src's interactome

Having demonstrated that the TCO/tetrazine reaction is suitable for capturing inhibitor-bound kinase targets, we next developed cell lines suitable for studying Src's interactome under different signaling conditions. To do this, we generated HeLa cells lines stably expressing either exogenous Src WT or Src V284C. Development of HeLa lines that express equal amounts of a Src variant–Src V284C–that is sensitive to our TCO probes and a probe-resistant variant–Src WT–are valuable for performing com-parative proteomics of proteins that are enriched through their interactions with Src. Like in HEK293 cells, treat-ment of Src V284C-expressing HeLas with **1-TCO** or **2-**

TCO followed by lysis and Tz-beads capture led to a significant amount of captured Src (**Figure 2-6F**). We observed almost no enrichment of Src WT when HeLa cells expressing this variant were treated with either probe. Prior to performing co-clickable precipitation experiments to study Src's cellular interactome, we determined the mildest conditions that could be used for capturing probe-bound Src after lysis, while maintaining sufficiently stringent washing conditions for removing proteins non-specifically bound to the sepharose matrix. A time-course experiment revealed that the click reaction between probe-bound Src and Tz-beads was almost complete within 10 mins at 4 ˚C (**Figure 2-6G**). We felt that these fast and mild capture kinetics would be advantageous for enriching protein complexes with minimal dissociation following cell lysis.

2.2.4 Clickable precipitation for mapping Src's cellular interactome

Prior to performing proteomic experiments, we verified that our co-clickable precipitation method was capable of co-enriching proteins that are likely to be associated with Src in growth factor-stimulated cells, such as tyrosine-phosphorylated signaling proteins. To do this, HeLa cells expressing Src V284C or WT were pre-incubated with either **1-TCO** or **2-TCO**, stimulated with growth factor for 15 minutes, and subsequently lysed (**Figure 2-8A**). Lysates were immediately incubated with Tz-beads and subjected to Western blot analysis with an anti-phosphotyrosine antibody following elution. Consistent with **1-TCO** stabilizing a global conformation with an SH2 domain accessible to intermolecular interactions, we observed that treatment of Src V284C-expressing HeLas with this probe resulted in capture of several phosphotyrosine-containing proteins (**Figure 2-8B**).[45] In contrast, treatment of Src V284C-expressing HeLas with **2-TCO**, which stabilizes a closed global conformation with an inaccessible SH2 domain, led to capture of only tyrosine-phosphorylated Src. Thus, our co-clickable precipitation method is capable of co-

enriching proteins interacting with Src and TCO-conjugated probes are able to differentially modulate the accessibility of Src's SH2 domain through its ATP-binding site.

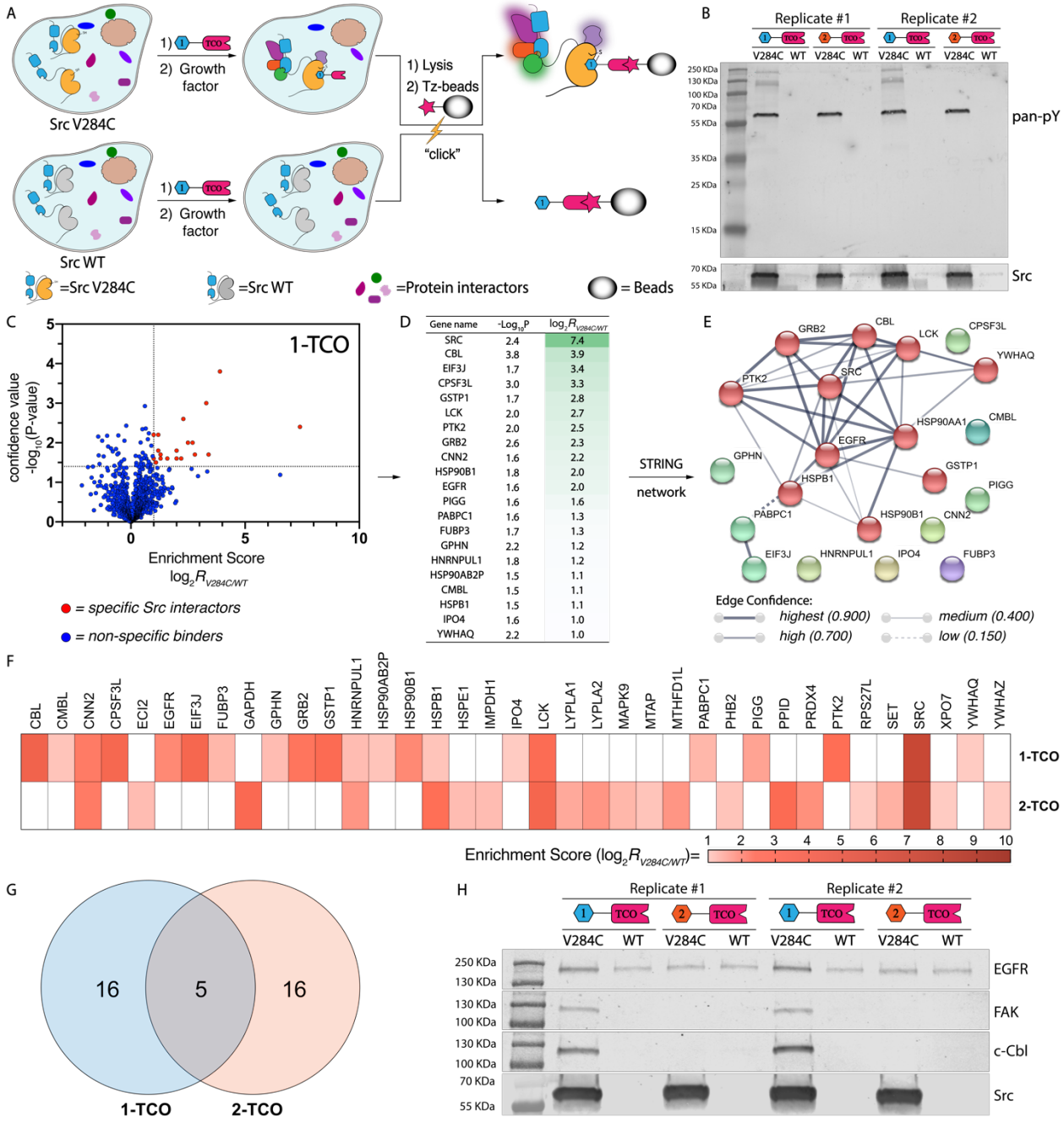

Figure 2-8. Interrogation of Src's interactome with co-clickable precipitation.

(A) A schematic representation of the co-clickable precipitation strategy for identifying Src's interactome. Cells stably expressing drug-sensitized Src V284C or drug-resistant Src WT are treated with a TCO-conjugated probe. Cells are then lysed, incubated with Tz-beads, and captured proteins are analyzed by Western blot or LC-MS/MS. Proteins that are enriched from cells expressing drug-sensitized Src V284C and not Src WT are classified as specific Src interactors. (B) Phosphotyrosine immunoblot of proteins enriched from growth factor-stimulated HeLa cells with TCO-conjugated probes. Cells expressing either Src V284C or Src WT were treated with **1-TCO** or **2-TCO**, lysed, and then incubated with Tz-beads. Captured proteins were eluted under reducing and denaturing conditions. Replicates of phosphotyrsosine (*top*) and Src (*bottom*) immunoblots of elutions are shown. (**C**-**E**) Interactome of **1**-**TCO**-bound Src V284C in growth factor-stimulated HeLa cells. (C) Volcano plot showing the $\log_2$ transformed MaxQuant intensities of the label-free comparison of **1**-**TCO**-treated, growth factor-stimulated HeLa cells expressing Src V284C and Src WT (n=3). Statistically significant interactors for drug-sensitized Src were defined as protein hits with an enrichment score = $\log_2$[intensity (drug-sensitized target)/intensity (WT target)] $\geq$ 1.0 and a confidence value = $-\log_{10}$(P-value) $\geq$ 1.4. The calculation was based on intensity values computed by MaxQuant. Missing protein intensity values were imputed by Perseus with a distribution downshift of 1.3 and a width of 0.2.[46] Proteins that fit the classification as statistically significant Src V284C interactors are shown in red. (D) Proteins that show statistically significant enrichment with **1**-**TCO** from Src V284C-expressing, growth factor-stimulated HeLa cells. The second column shows confidence values ($-\log_{10}$(P-value)) and the third column shows enrichment scores. (E) STRING network of the interactome of **1**-**TCO**-bound Src V284C. The STRING database was used to generate a network with significant interactors. Each circle (node) represents a member of the interactome. Each line between the nodes (edge)

represents a detected protein-protein interaction (PPI) in the STRING database.[47] The edge weight denotes the confidence of the PPI.[48] (**F**-**H**) Comparison of the interactomes between **1-TCO**- and **2-TCO**-bound Src V284C. (**F**) Heat map showing the enrichment score for each statistically significant interactor with **1-TCO**- and **2-TCO**-bound Src V284C (*n*=3). The panel's color scale indicates the mean enrichment score from three biological replicates. Cells colored in white represent proteins that are not classified as significant interactors for the Src V284C-probe complex shown. (**G**) Venn diagram[49] of common interactors between **1-TCO**- and **2-TCO**-bound Src V284C complexes. (**H**) Western blot confirmation of probe-bound Src V284C complex interactions.

Next, we established a quantitative proteomic analysis protocol to identify Src's intracellular interactome. To differentiate proteins that were co-enriched with Src V284C from non-specific interactors, we performed quantitative label free comparisons of TCO probe-enriched proteins from HeLa cells expressing Src V284C to HeLa cells expressing Src WT. Proteomic experiments were performed like the Western blot analysis experiments described in **Figure 2-8B**, except Tz-bead-captured proteins were subjected to on-bead tryptic digestion and resultant peptides were identified and quantified by tandem mass spectrometry. Raw MS data were processed with MaxQuant[50] across three biological replicates and analyzed with Perseus[46] (See Supporting Table 1-2 of *J. Am. Chem. Soc.* 2019, 141, 30, 11912-11922 for raw MS data). Enrichment scores (log2[intensity (Src V284C-expressing)/intensity (Src WT-expressing)]) were calculated using the relative intensity values from Src V284C- and WT-expressing cells with confidence values (-log10(P-value)) for each identified protein. We defined significant interactors as protein hits with an enrichment score ≥ 1.0 and a confi-dence value ≥ 1.4.

We first applied our quantitative proteomic analysis protocol to growth factor-stimulated HeLa cells. Our analysis showed that 21 high-confidence proteins are more than 2-fold enriched by **1-TCO** from Src V284C-expressing cells relative to Src WT-expressing cells (**Figure 2-8C,D**). Consistent with the orthogonality of the **1-TCO** probe, Src was the most highly enriched protein. The 20 putative Src interactors were enriched in the expected Gene Ontology (GO) terms[51-52] "EGFR signaling pathway" (Biological Process), "SH2 domain binding" (Molecular Function), and "cell junction" (Cellular Component). Among the 20 identified Src interactions, 11 (55%) have not been previously reported in GO and Kegg repositories. Highly co-enriched proteins include the tyrosine kinase PTK2 (FAK) and the E3 ligase c-Cbl, which have previously been demonstrated to interact with the SH2 and SH3 domain of Src,[53-54] respectively. These interactions are consistent with **1-TCO** stabilizing a moderately open global conformation of Src with intermolecularly accessible regulatory domains. Another notably co-enriched protein includes the receptor tyrosine kinase EGFR, which has been demonstrated to be a substrate of Src in growth factor-stimulated cells.[55] To better visualize Src's interactome in growth factor-stimulated cells, we generated a STRING interaction network of co-enriched proteins (**Figure 2-8E**). Overall, these results are consistent with Src participating in signaling complexes directly downstream of activated EGFR.

We observed that a similar number of proteins were selectively enriched from growth factor-stimulated, Src V284C-expressing HeLa cells treated with **2-TCO** (**Figure 2-8F** and **Figure 2-9**). Like **1-TCO**, the most highly enriched protein by **2-TCO** was Src. Of the 20 putative interactors with the Src/**2-TCO** complex, five have previously been described in GO and Kegg repositories.

Consistent with **2-TCO** promoting intramolecular SH2 and SH3 engagement, most co-enriched proteins are different than those enriched from **1-TCO**-treated cells (**Figure. 2-8F,2-8G**). The small heat shock protein HSPB1 and the SFK Lck are the only two proteins that are enriched by both **1-TCO** and **2-TCO**. Proteins that have been characterized to interact with the SH2 or SH3 domains of Src are notably absent in the list of proteins enriched by **2-TCO**, which further confirms that stabilizing the helix αC-out conformation prevents intermolecular interactions with these domains. Therefore, modulating the global conformational state of Src with conformation-selective, ATP-competitive inhibitors has a dramatic effect on its intracellular interactome. Prior to performing more expansive proteomic studies, we validated the enrichment of several representative protein targets with Western blot analysis. We found that only **1-TCO** enriched EGFR, FAK and c-Cbl, three key players in the EGFR pathway (GO:0007173),[51-52] from HeLa cells expressing the Src V284C mutant relative to HeLa cells expressing drug-resistant Src WT (**Figure 2-8H**). Only **2-TCO** detectably enriched PPID and PRDX4 from cells expressing drug-sensitized Src V284C relative to drug-resistant Src WT (**Figure 2-9**).

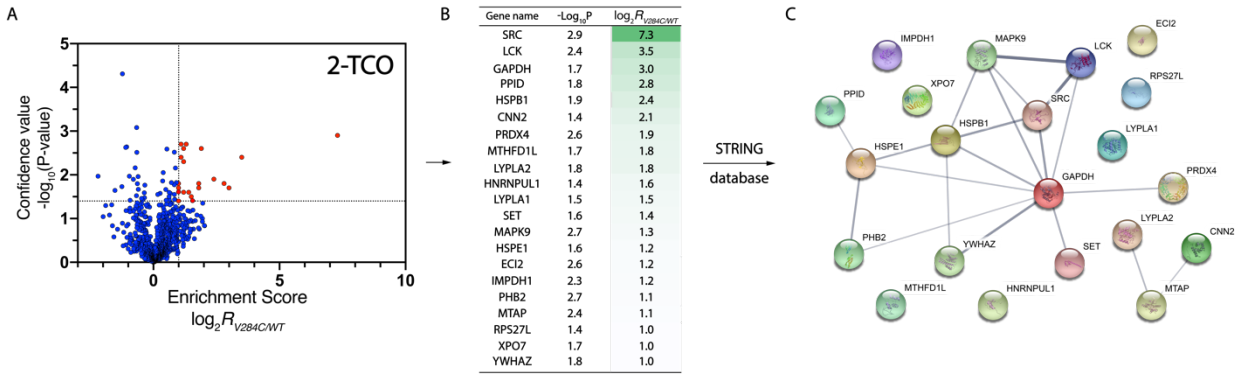

Gene name	-Log10P	log2RV284C/WT
SRC	2.9	7.3
LCK	2.4	3.5
GAPDH	1.7	3.0
PPID	1.8	2.8
HSPB1	1.9	2.4
CNN2	1.4	2.1
PRDX4	2.6	1.9
MTHFD1L	1.7	1.8
LYPLA2	1.8	1.8
HNRNPUL1	1.4	1.6
LYPLA1	1.5	1.5
SET	1.6	1.4
MAPK9	2.7	1.3
HSPE1	1.6	1.2
ECI2	2.6	1.2
IMPDH1	2.3	1.2
PHB2	2.7	1.1
MTAP	2.4	1.1
RPS27L	1.4	1.0
XPO7	1.7	1.0
YWHAZ	1.8	1.0

Figure 2-9**.** Interrogation of growth-factor-stimulated **2-TCO**-bound Src's interactome with co-clickable precipitation.

(A) Volcano plot showing the $\log_2$ transformed MaxQuant intensities of the label-free comparison of **2-TCO**-treated, growth factor-stimulated HeLa cells expressing Src V284C or Src WT (*n*=3). Statistically significant interactors for drug-sensitized Src were defined as protein hits with enrichment scores = $\log_2$[Intensity (drug-sensitized target)/Intensity (WT target)] ≥ 1.0 and confidence values = $-\log_{10}$(P-value) ≥ 1.4. The calculation was based on intensity values computed by MaxQuant. Missing protein intensity values were imputed by Perseus with a distribution downshift of 1.3 and a width of 0.2. Specific Src interactors are highlighted in red and non-specific binders are marked in blue. (B) Proteins that show statistically significant enrichment with **2-TCO** from Src V284C-expressing, growth factor-stimulated HeLa cells. The second column shows confidence values ($-\log_{10}$(P-value)) and the third column shows enrichment scores. (C) STRING network of the interactome of **2-TCO**-bound Src V284C. Significant interactors were visualized using the STRING database.[47-48] Each circle (node) represents a member of the interactome. Each line between the nodes (edge) represents a detected protein-protein interaction (PPI) according to the STRING database.

2.2.5 Interrogation of Src's interactome under diverse cellular conditions

We next subjected HeLa cells to a number of conditions to assess how cellular state affects the interactome of inhibitor-bound Src (**Figure 2-10**). Src V284C- and Src WT-expressing Hela cells were first treated with **1-TCO** or **2-TCO** and then either serum-starved, incubated in complete medium (DMEM), or plated on fibronectin. Cells were then lysed, and lysates were subjected to the same proteomic workflow as growth-factor-stimulated HeLas described in **Figure 2-8C**. Heatmaps showing the proteins that were specifically enriched by **1-TCO** and **2-TCO** under the four cellular states, which includes growth factor stimulated HeLas, that were probed are shown

in **Figures 2-10B, C**. For all four conditions, Src was the most highly enriched cellular target and a total of 94 and 37 co-enriched proteins were identified for **1-TCO** and **2-TCO**, respectively. Consistent with **1-TCO**-bound Src promoting a global conformation that is more capable of interacting with intra-cellular targets, more total proteins were enriched under all conditions with this probe than with **2-TCO**.

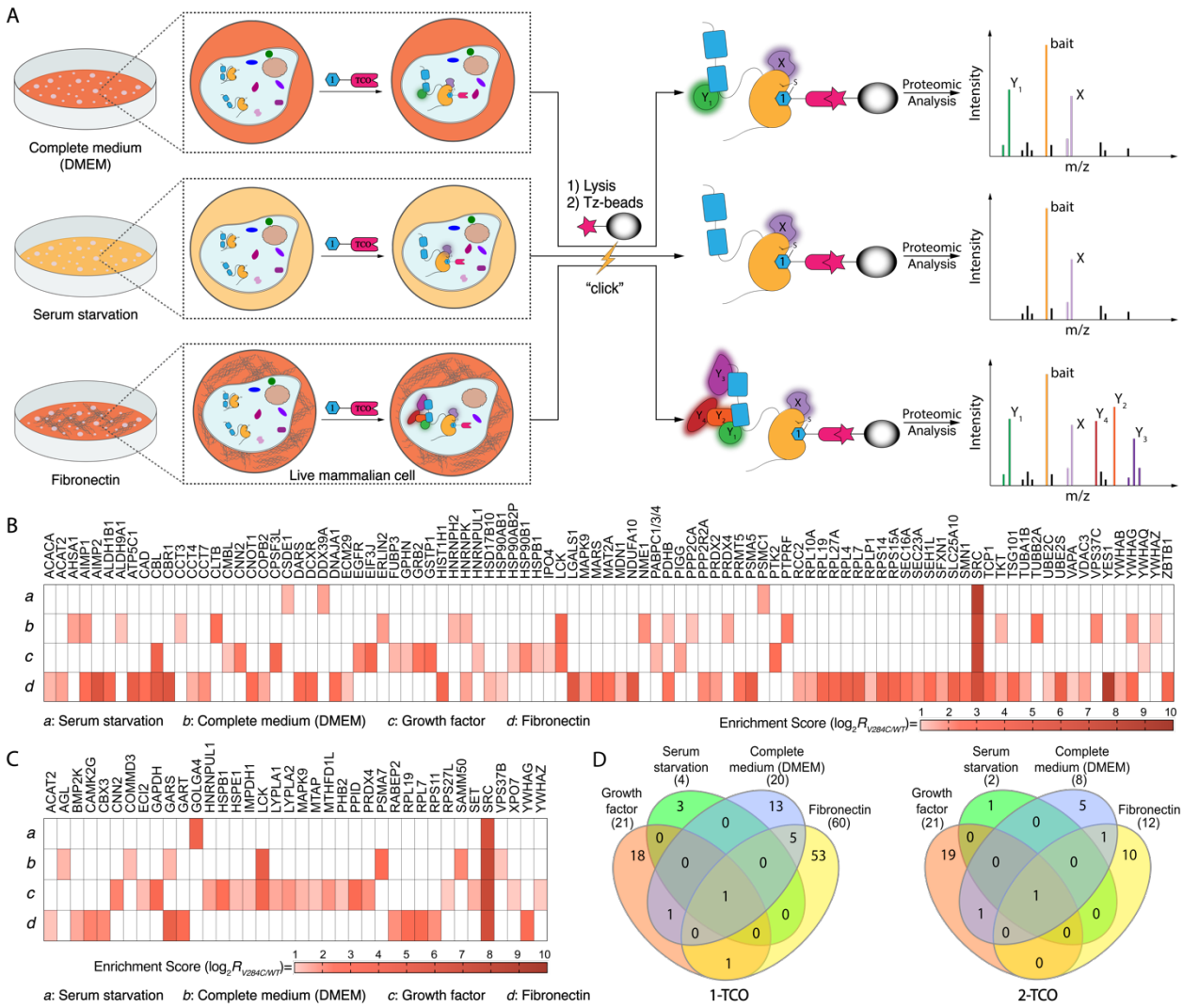

Figure 2-10. Src's interactome in different cellular states.

(A) A schematic representation of co-clickable precipitation experiments performed in three distinct cellular contexts. Hela cells stably overexpressing Src V284C or Src WT were serum-

starved, cultured in complete medium (DMEM) or plated on fibronectin. Prior to lysis, cells were incubated with **1-TCO** or **2-TCO**. Probe-bound Src complexes were enriched with Tz-beads and captured proteins were analyzed using LC-MS/MS. (B, C) Heat maps showing the enrichment score for each statistically significant interactor with **1-TCO**- and **2-TCO**-bound Src V284C under four different cellular conditions: (*a*) serum-starvation, (*b*) complete medium (DMEM), (*c*) growth factor stimulation, or (*d*) plating on fibronectin. The panel's color scale indicates the mean enrichment score from three biological replicates. Cells colored in white are proteins that were not classified as significant interactors with the Src V284C-probe complex shown. (D) Venn diagrams representing common interactors in four cellular states for **1-TCO-** (*left*) and **2-TCO**-bound (*right*) Src.

Our proteomic data with **1-TCO** shows that the cellular state of a cell can dramatically affect Src's interactome (**Figure 2-10B**). Consistent with serum starvation inactivating basal signaling pathways that Src participates in, only three proteins were co-enriched under this condition (**Figure 2-11A-C**). These three proteins have not previously been reported to interact with Src and no significant functional enrichments were detected in GO terms. Culturing cells in complete medium (DMEM) activates basal cell signaling and increases the number of interactions with **1-TCO**-bound Src (**Figure 2-12A-C**). 19 proteins co-enriched with **1-TCO**-bound Src from HeLa cells cultured in complete medium, with the GO terms "cellular metabolic process" (Biological process) and "SH2 domain binding" (Molecular function) being the most enriched. Growth factor stimulation further enhances the complexity of Src's interactome. Despite resulting in a similar number of Src interactors, growth factor stimulation led to 3.0-fold, 2.0-fold and 2.4-fold increases in involvement of GO terms "Biological Process", "Cellular Component" and "Molecular

Function", respectively. Finally, we observed that activation of integrin signaling by plating cells on fibronectin led to by far the most complex Src interactome (**Figure 2-13A-C**). In total, 59 proteins were co-enriched by **1-TCO**-bound Src V284C under this condition. This interconnected interaction network displayed a high degree of complexity, highly enriching in several GO terms (104 of "Biological Process" terms, 22 of "Molecular Function" terms, and 29 of "Cellular Component" terms).

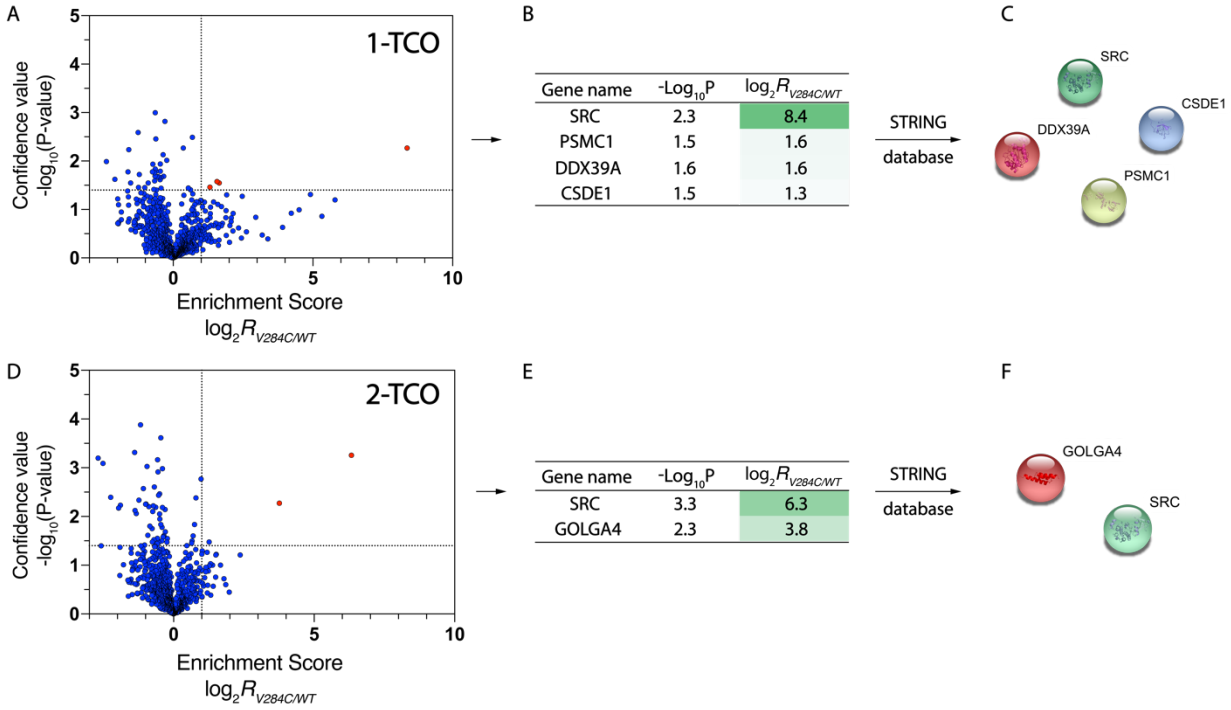

Figure 2-11. Characterization of **1-TCO**-bound and **2-TCO**-bound Src's interactome in serum-starved HeLa cells.

(A, D) Volcano plot showing the $\log_2$ transformed MaxQuant intensities of the label-free comparison of **1-TCO**-treated (A, *top*) or **2-TCO**-treated (D, *bottom*), serum-starved HeLa cells expressing Src V284C or Src WT (n=3). Statistically significant interactors for drug-sensitized Src were defined as protein hits with enrichment scores = $\log_2$[Intensity (drug-sensitized

target)/Intensity (WT target)] ≥ 1.0 and confidence values = -$\log_{10}$(P-value) ≥ 1.4. The calculation was based on intensity values computed by MaxQuant. Missing protein intensity values were imputed by Perseus with a distribution downshift of 1.3 and a width of 0.2. Specific Src interactors are highlighted in red and non-specific binders are marked in blue. (B, E) Proteins that significantly co-enriched with **1-TCO** (B, *top*) or **2-TCO** (E, *bottom*) from Src V284C-expressing, serum-starved HeLa cells. The second column shows confidence values (-$\log_{10}$(P-value)) and the third column shows enrichment scores. (C, F) STRING network of the interactome of **1-TCO**-bound (C, *top*) or **2-TCO**-bound (F, *bottom*) Src V284C. Significant interactors were visualized using the STRING database. Each circle (node) represents a member of the interactome.

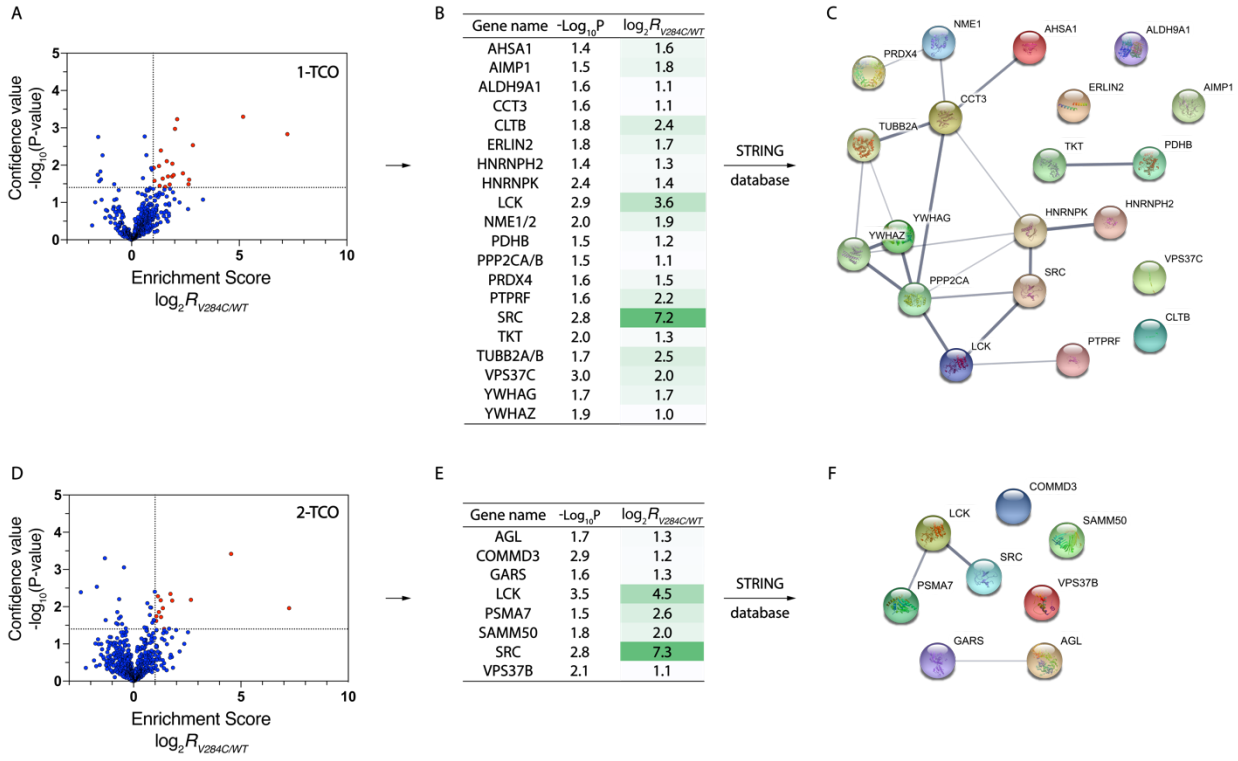

Gene name	-Log$_{10}$P	log$_2$R$_{V284C/WT}$
AHSA1	1.4	1.6
AIMP1	1.5	1.8
ALDH9A1	1.6	1.1
CCT3	1.6	1.1
CLTB	1.8	2.4
ERLIN2	1.8	1.7
HNRNPH2	1.4	1.3
HNRNPK	2.4	1.4
LCK	2.9	3.6
NME1/2	2.0	1.9
PDHB	1.5	1.2
PPP2CA/B	1.5	1.1
PRDX4	1.6	1.5
PTPRF	1.6	2.2
SRC	2.8	7.2
TKT	2.0	1.3
TUBB2A/B	1.7	2.5
VPS37C	3.0	2.0
YWHAG	1.7	1.7
YWHAZ	1.9	1.0

Gene name	-Log$_{10}$P	log$_2$R$_{V284C/WT}$
AGL	1.7	1.3
COMMD3	2.9	1.2
GARS	1.6	1.3
LCK	3.5	4.5
PSMA7	1.5	2.6
SAMM50	1.8	2.0
SRC	2.8	7.3
VPS37B	2.1	1.1

Figure 2-12**.** Characterization of **1-TCO**-bound and **2-TCO**-bound Src's interactome in Hela cells cultured in complete medium (DMEM).

(A, D) Volcano plot showing the $\log_2$ transformed MaxQuant intensities of the label-free comparison of **1-TCO**-treated (A, *top*) or **2-TCO**-treated (D, *bottom*) HeLa cells expressing Src V284C or Src WT (n=3) cultured in complete medium (DMEM). Statistically significant interactors for drug-sensitized Src were defined as protein hits with enrichment scores = $\log_2$[Intensity (drug-sensitized target)/Intensity (WT target)] ≥ 1.0 and confidence values = -$\log_{10}$(P-value) ≥ 1.4. The calculation was based on intensity values computed by MaxQuant. Missing protein intensity values were imputed by Perseus with a distribution downshift of 1.3 and a width of 0.2. Specific Src interactors are highlighted in red and non-specific binders are marked in blue. (B, E) Proteins that significantly co-enriched with **1-TCO** (B, *top*) or **2-TCO** (E, *bottom*) from Src V284C-expressing HeLa cells cultured in complete medium (DMEM). The second column shows confidence values (-$\log_{10}$(P-value)) and the third column shows enrichment scores. (C, F) STRING network of the interactome of **1-TCO**-bound (C, *top*) or **2-TCO**-bound (F, *bottom*) Src V284C. Significant interactors were visualized using the STRING database. Each circle (node) represents a member of the interactome. Each line between the nodes (edge) represents a detected protein-protein interaction (PPI) according to the STRING database.

A

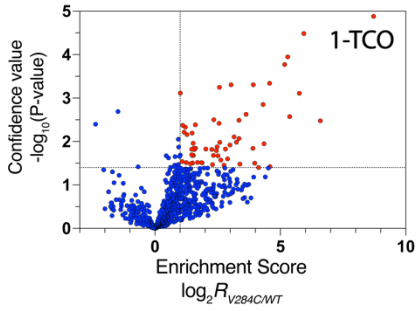

D

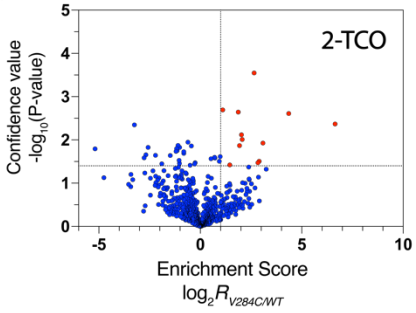

B

Gene name	-Log$_{10}$P	log$_2$R$_{V284C/WT}$
ACACA	1.5	1.3
ACAT2	1.8	1.6
AIMP1	2.4	2.6
AIMP2	4.5	5.9
ALDH1B1	1.5	3.4
ATP5C1	1.4	4.6
CAD	1.9	2.5
CBL	3.9	5.3
CBR1	3.1	5.8
CCT4	1.5	1.4
CCT7	1.5	1.9
CNOT1	2.0	2.6
COPB2	1.7	1.5
DARS	1.8	2.8
DCXR	3.3	3.0
DNAJA1	1.7	2.5
ECM29	2.4	1.1
HIST1H1	2.1	3.4
HNRNPK	1.8	1.6
HSD17B10	2.2	1.3

Gene name	-Log$_{10}$P	log$_2$R$_{V284C/WT}$
LGALS1	2.6	5.4
MAPK9	2.0	1.5
MARS	3.2	2.6
MAT2A	1.8	2.4
MDN1	2.2	1.2
NDUFA10	3.8	5.2
PDHB	1.8	2.3
PPP2R2A	1.8	2.0
PRDX2	1.5	1.7
PRMT5	1.5	2.3
PSMA5	3.3	4.6
RCC2	1.7	1.5
RPL10A	1.8	1.5
RPL19	2.5	3.4
RPL27A	2.1	3.2
RPL4	1.4	4.1
RPL7	1.9	4.4
RPLP1	2.3	1.2
RPL14	1.8	3.9
RPS15A	2.6	3.6

Gene name	-Log$_{10}$P	log$_2$R$_{V284C/WT}$
SEC16A	1.7	2.3
SEC23A	1.5	1.9
SEH1L	1.6	2.6
SFXN1	2.4	1.6
SLC25A10	1.5	4.0
SMN1	2.5	2.3
SRC	2.5	6.6
SUB1	3.3	3.9
TCP1	1.5	2.8
TKT	2.2	1.5
TSG101	1.9	3.0
TUBA1B	1.5	1.5
UBE2C	1.5	1.1
UBE2S	2.9	4.3
VAPA	3.1	1.0
VDAC3	1.8	1.6
YES1	4.9	8.7
YWHAB	1.7	1.5
YWHAG	1.6	2.9
ZBTB1	2.0	3.3

E

Gene name	-Log$_{10}$P	Difference
ACAT2	2.7	1.1
BMP2K	1.4	1.5
CAMK2G	2.0	2.1
CBX3	2.1	2.0
GARS	2.6	4.4
GART	1.5	2.9
RABEP2	1.9	1.9
RPL19	1.5	2.8
RPL7	1.9	3.1
RPS11	2.6	1.9
SRC	2.4	6.6
YWHAG	3.5	2.7

STRING database

STRING database

C

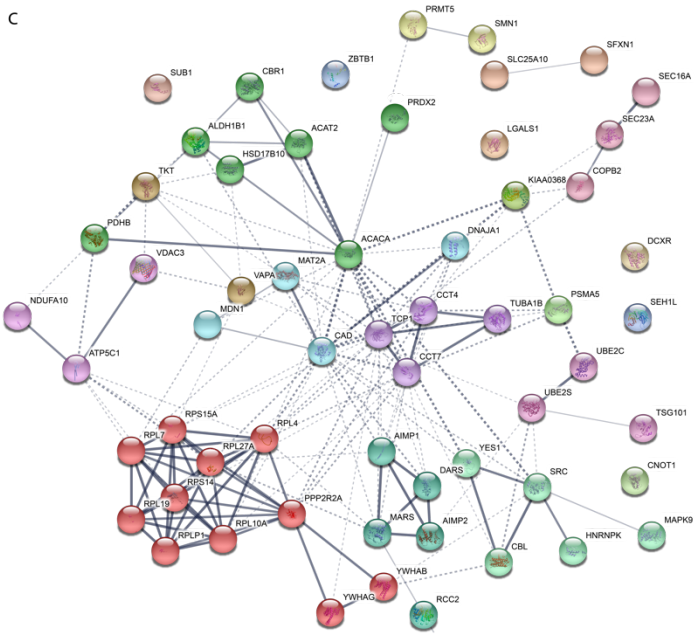

F

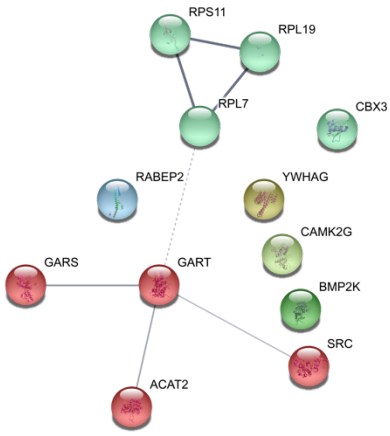

Figure 2-13**.** Characterization of **1-TCO**-bound and **2-TCO**-bound Src's interactome in HeLa cells plated on fibronectin.

(A, D) Volcano plot showing the $\log_2$ transformed MaxQuant intensities of the label-free comparison of **1-TCO**-treated (A, *left*) or **2-TCO**-treated (D, *right*) HeLa cells expressing Src V284C or Src WT (n=3) plated on fibronectin. Statistically significant interactors for drug-sensitized Src were defined as protein hits with enrichment scores = $\log_2$[Intensity (drug-sensitized target)/Intensity (WT target)] ≥ 1.0 and confidence values = $-\log_{10}$(P-value) ≥ 1.4. The calculation was based on intensity values computed by MaxQuant. Missing protein intensity values were imputed by Perseus with a distribution downshift of 1.3 and a width of 0.2. Specific Src interactors are highlighted in red and non-specific binders are marked in blue. (B, E) Proteins that significantly co-enriched with **1-TCO** (B, *left*) or **2-TCO** (E, *right*) from Src V284C-expressing HeLa cells plated on fibronectin. The second column shows confidence values ($-\log_{10}$(P-value)) and the third column shows enrichment scores. (C, F) Significant interactors were visualized using the STRING database. Each circle (node) represents a member of the interactome. Each line between the nodes (edge) represents a detected protein-protein interaction (PPI) according to the STRING database.

Similar to **1-TCO**, our proteomic data with **2-TCO** shows significant differences in Src's interactome in different cellular states (**Figure 2-10C**). In serum starved HeLa cells, only one protein was significantly co-enriched with **2-TCO**-bound Src V284C (**Figure 2-11D-F**). In HeLa cells with basal signaling activated by culturing in complete medium (DMEM), 7 proteins were enriched by 2-TCO-bound Src V284C, only 1 of which, Lck, was a mutual interactor shared with **1-TCO**-bound Src V284C (**Figure 2-12D-F**). Consistent with growth factor stimulation further activating cellular signaling, the **2-TCO**/Src V284C complex interacts with 1.6-fold more proteins

under this condition than in HeLas cultured in complete medium (**Figure 2-10D**). Notably, activation of integrin signaling by plating cells on fibronectin didn't further enhance the size and complexity of the **2-TCO**/Src V284C complex interactome (**Figure 2-13D-F**). Only 11 proteins were significantly co-enriched with **2-TCO**-bound Src V284C. This loss of sensitivity towards stimulation with fibronectin is likely due to **2-TCO**'s promotion of a closed global conformation of Src with reduced intermolecular accessibility of regulatory SH2 and SH3 domains. While **2-TCO** reduced the number of Src interactors compared to **1-TCO** under all of the cellular states tested, the largest difference between the two probes was in cells plated on fibronectin. Src forms 48 more interactions when bound to **1-TCO** compared to **2-TCO** under integrin stimulation, with only YWHAG–a 14-3-3 protein–commonly co-enriched. Thus, stabilizing a closed global conformation of Src has the most dramatic effect on Src's interactome in cells.

2.2.6 TCO-conjugated probes for performing in situ proximity ligation assays

Beyond allowing the proteomic interrogation of drug-bound kinase complexes, we reasoned that our TCO conjugates could be used to characterize the in *situ* localization and interactions of probe-bound kinases. To do this, we developed a click chemistry-mediated proximity ligation assay with TCO probe-bound cellular targets (Figure 6A).[56-59] In this method, cells are treated with a TCO-conjugated probe and then fixed and detergent-permeabilized. The TCO moiety is used to deliver a tetrazine-containing Oregon Green488 (OG488) dye, which allows visualization and serves as an exogenous epitope for an anti-OG488 antibody, to an inhibitor-bound target. Cells are then incubated with primary antibodies for OG488 and potential interactors or cellular organelle markers, which are recognized by secondary antibodies conjugated to single-stranded oligonucleotides that only template the formation of a circular DNA when two binding epitopes

are <40 nm in proximity.[56, 60] A rolling circle amplification (RCA) is then performed, followed by hybridization with complementary oligonucleotides labeled with fluorophores, which are imaged using confocal microscopy.

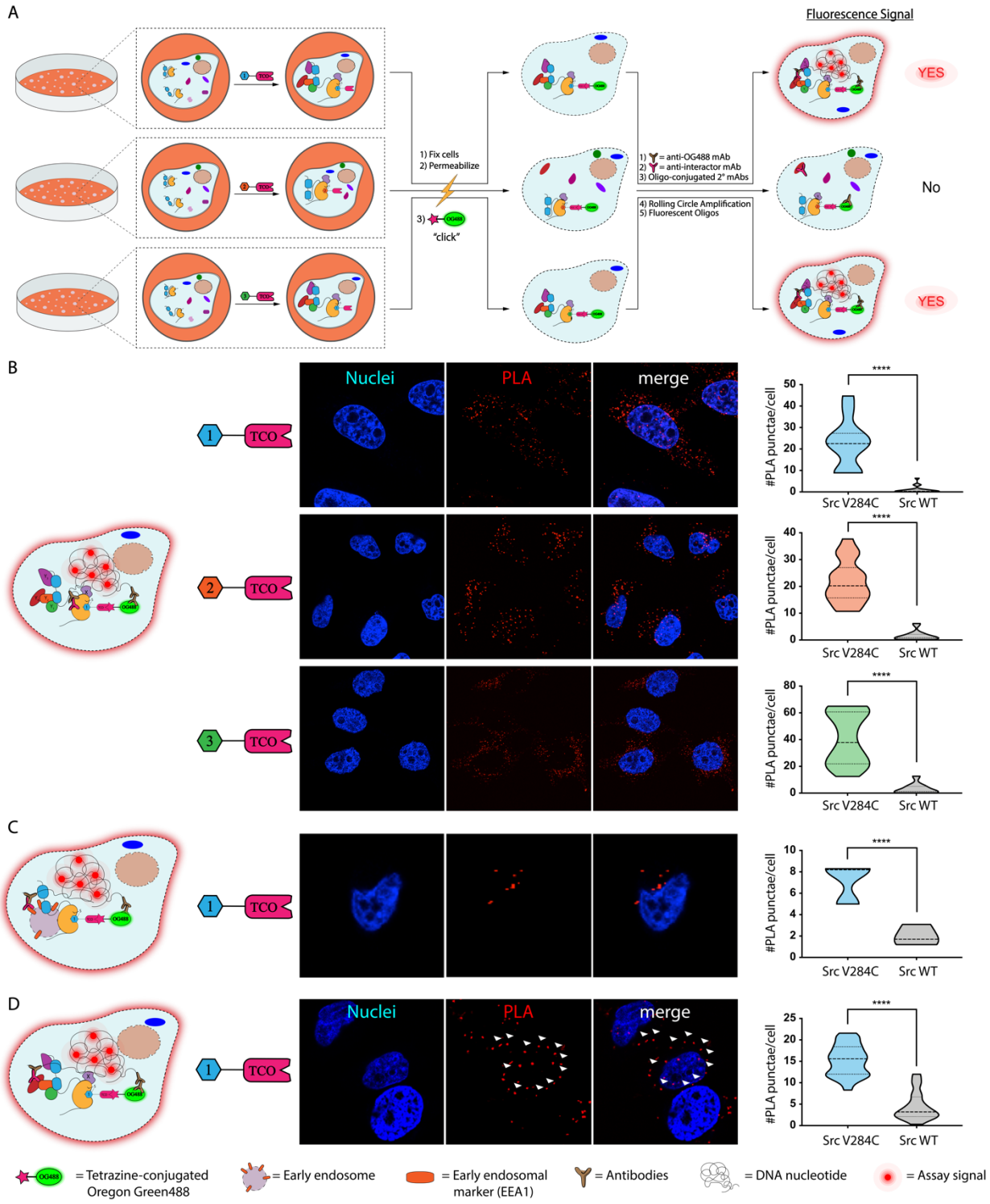

Figure 2-14**.** Clickable proximity ligation assays (PLAs) with TCO-conjugated probes.

(A) A schematic representation of PLAs performed with TCO-conjugated probes. Cells are treated with a TCO-conjugated probe, fixed, permeabilized, and then treated with a tetrazine-containing Oregon Green488 (OG488) dye. Fixed cells are then subjected to a standard proximity ligation assay protocol. (B) PLA for visualization of a probe-bound target. Representative images (nuclei in blue and PLA signal in red) of cells from three biological replicates are shown (*middle*). Quantified signals for the number of PLA-mediated fluorescent puncta observed per cell are shown in the violin plot (*right*). Values shown are the means of fluorescent puncta per cell from three biological replicates. (number of total cells quantified: *n*=97 for **1-TCO**/Src V284C, and *n*=215 for **1-TCO**/Src WT; *n*=148 for **2-TCO**/Src V284C, and *n*=171 for **2-TCO**/Src WT; *n*=142 for **3-TCO**/Src V284C, and *n*=179 for **3-TCO**/Src WT). (C) Clickable PLA for visualizing the cellular localization of TCO probe-bound Src in HeLa cells incubated in complete medium (DMEM). Representative images (nuclei in blue and PLA signal in red) of TCO probe-treated Src V284C-expressing HeLa cells are shown (*middle*). Quantified signals for the number of PLA-mediated fluoscent puncta observed per cell are shown in the violin plot (*right*). Values shown are the means of fluorescent puncta per cell from three biological replicates (number of total cells quantified: *n*=66 for Src V284C, and *n*=39 for Src WT). (D) Clcikable PLA for visualizing the interaction between Src and FAK. Representative images (nuclei in blue and PLA signal in red) of TCO probe-treated Src V284C-expressing HeLa cells plated on fibronectin are shown. The arrows (white) indicated examples of plasma membrane localization. Quantified signals for the number of PLA-mediated fluoscent puncta observed per cell are shown in the violin plot (*right*). Values shown are

means of PLA puncta per cell from three biological replicates (number of total cells quantified: *n*= 375 for Src V284C, and *n*=314 for Src WT).

Prior to performing PLA experiments, we validated that Src V284C and Src WT have the same overall expression level (**Figure 2-15**) and cellular localization in HeLa cells (**Figure 2-16** and **Figure 2-17**). Next, we confirmed that probe-bound Src V284C could selectively be visualized with an in situ PLA (**Figure 2-14**). Src V284C- and Src WT-expressing HeLa cells were treated with TCO probes, fixed, detergent-permeabilized and reacted with tetrazine-conjugated Oregon Green488 dye. Primary antibodies for Oregon Green488 and Src were then added prior to performing RCA with single-strand oligonucleotide-conjugated secondary antibodies and hybridization with complementary oligonucleotides (**Figure 2-14B**, *left*). We observed that fluorescent puncta formation required the presence of both the OG488 and Src antibodies (**Figure 2-18**). Consistent with our probes only selectively engaging drug-sensitized Src V284C in *situ*, significantly more fluorescent puncta were detected in Src V284C-expressing Hela cells versus cells expressing Src WT. Similar to the **1-TCO** probe, significantly more signal was observed in Src V284C-expressing HeLa cells treated with **2-TCO** and **3-TCO** than in cells expressing Src WT.

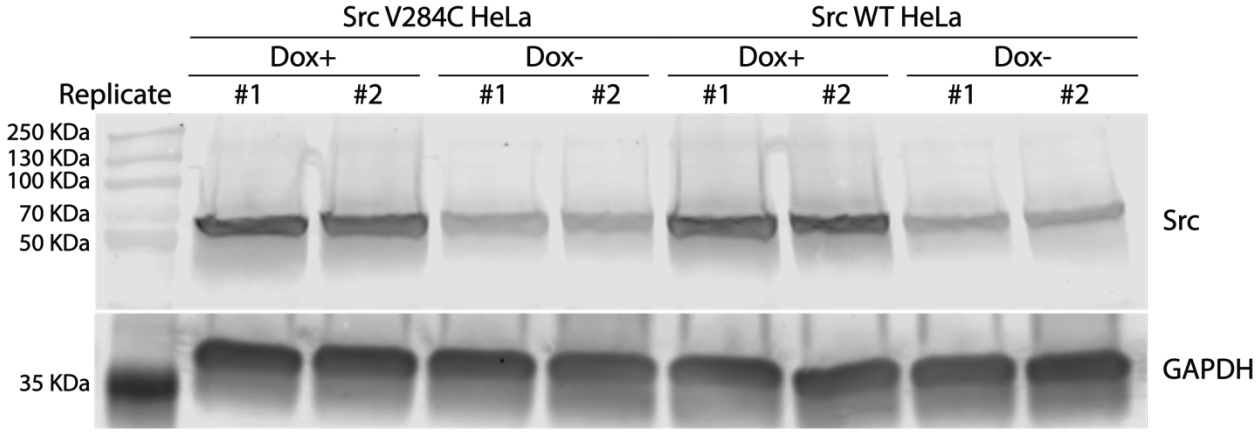

Figure 2-15. Anti-Src immunoblots of HeLa cells stably expressing Src V284C or Src WT (*n=2*). Src V284C and Src WT expression was induced with 1 µg/mL of doxycycline for 24 hours prior to performing PLA studies.

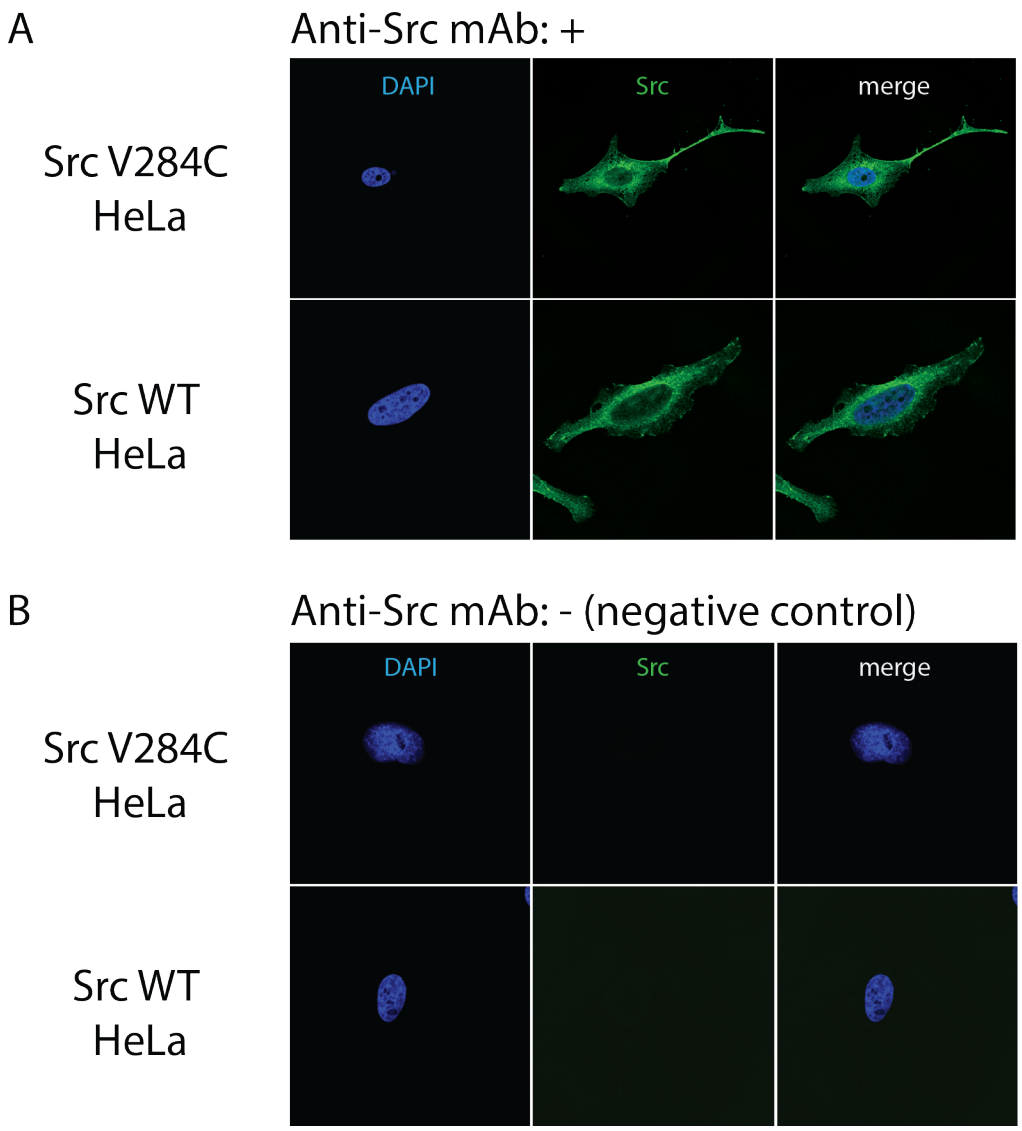

Figure 2-16. Cellular localization of Src V284C and Src WT in HeLa cells prior to treatment with TCO probes.

(A) Immunofluorescent analysis of Src V284C (*top*) and Src WT (*bottom*) in HeLa cells. HeLa cells stably expressing Src V284C (*top*) or Src WT (*bottom*) were fixed and incubated with an anti-Src antibody, followed by a Mega 485-conjugated secondary antibody. The nucleus was visualized using DAPI. (B) Negative control of immunofluorescent analysis. HeLa cells stably expressing Src V284C (*top*) or Src WT (*bottom*) were fixed and incubated with only a Mega 485-conjugated secondary antibody. The nucleus was visualized using DAPI.

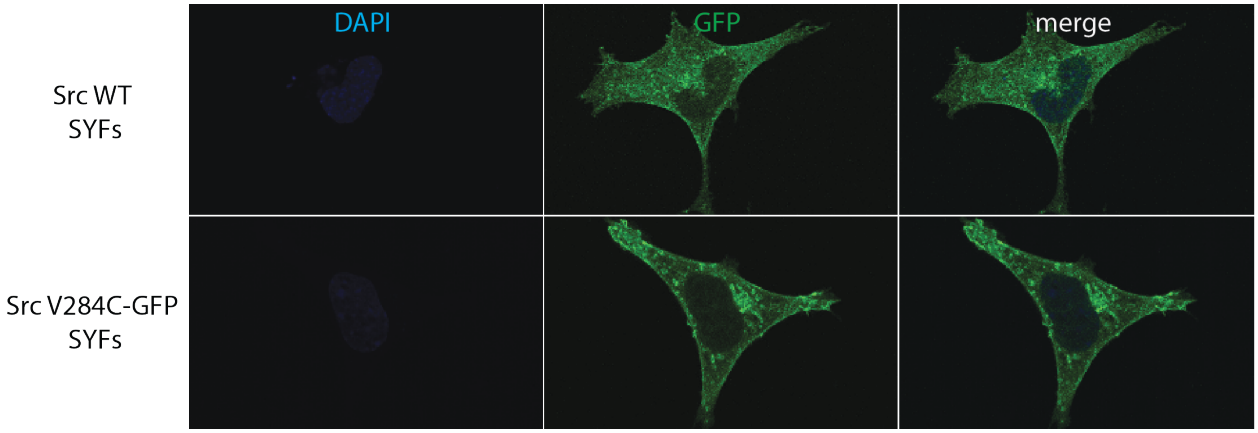

Figure 2-17**.** Cellular localization of C-terminal GFP-tagged full-length Src WT (*top*) and Src V284C (*bottom*) in Src/Yes/Fyn (-/-/-) fibroblast cells (SYFs). SYFs cells that transiently express Src WT-GFP (*top*) or Src V284C-GFP (*bottom*) were fixed with 4% para-formaldehyde. The nucleus was visualized using DAPI. GFP-tagged Src constructs were visualized under GFP channel (excitation: 488 nm; emission: 510 nm).

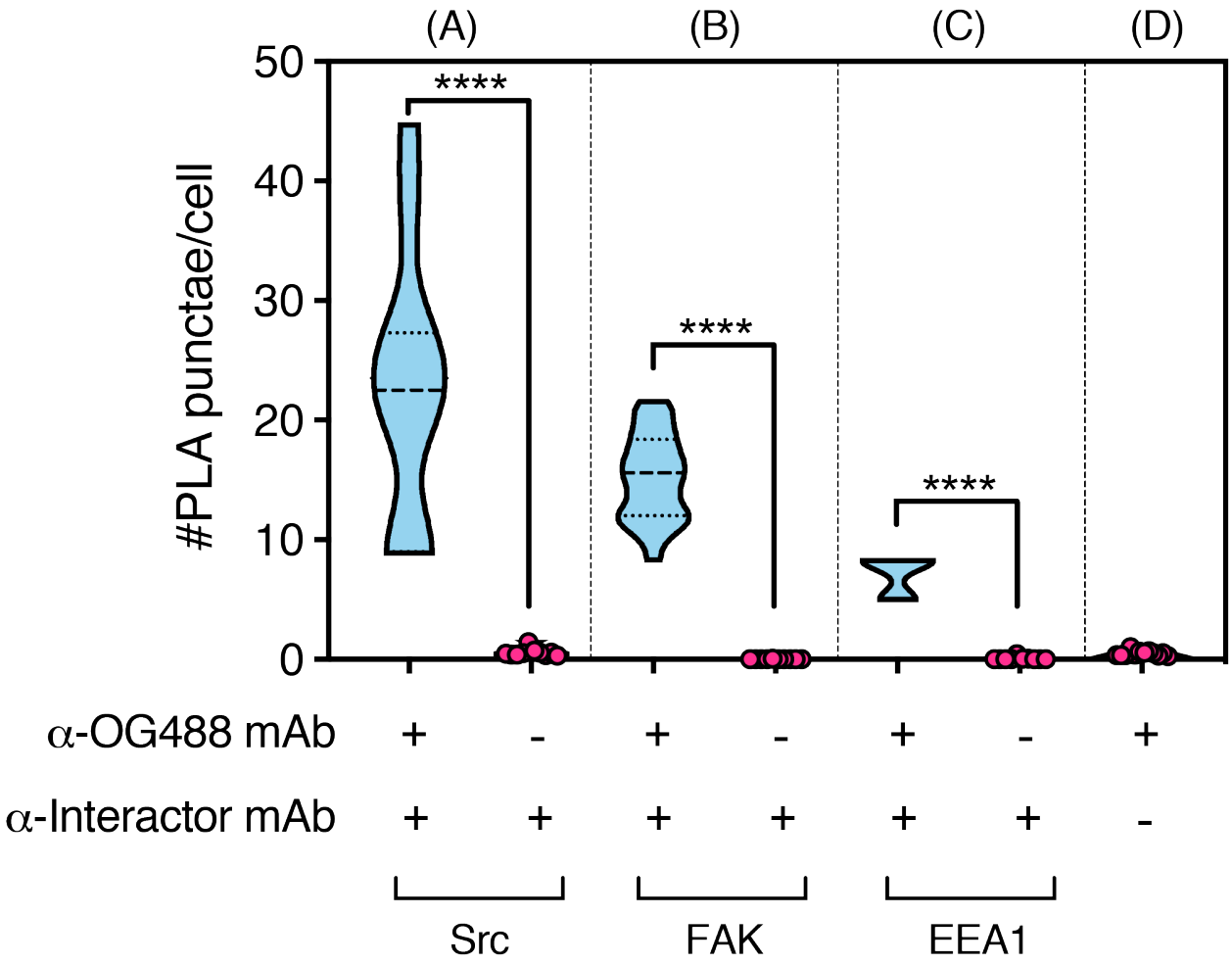

Figure 2-18**.** Technical negative controls of proximity ligation assays (PLAs) in HeLa cells treated by **1-TCO**.

(A) Technical negative control of PLA for visualization of the probe-bound target. Quantified signals for the number of PLA-mediated fluorescent puncta observed per cell are shown in the violin plot. Values shown are the means of fluorescent puncta per cell from at least three independent experiments (number of total cells quantified for control experiments: *n*=308). (B) Technical negative control of the Src/FAK interaction PLA. Quantified signals for the number of PLA-mediated fluorescent puncta observed per cell are shown in the violin plot. Values shown are the means of fluorescent puncta per cell from at least three independent experiments. (number of

total cells quantified for control experiments: *n*=464). (C) Technical negative control of the cellular organelle localization PLA. Quantified signals for the number of PLA-mediated fluorescent puncta observed per cell are shown in the violin plot. Values shown are the means of fluorescent puncta per cell from at least three independent experiments. (number of total cells quantified for control experiments: *n*=209). (D) Technical negative control of PLA with the anti-Oregon Green488 antibody. Quantified signals for the number of PLA-mediated fluorescent puncta observed per cell are shown in the violin plot. Values shown are the means of fluorescent puncta per cell from at least three independent experiments. (number of total cells quantified for control experiments: *n*=263).

Next, we used an organelle marker to determine if PLA can be used to provide information on the localization of probe-bound Src complexes (**Figure 2-14C**). Specifically, we determined if probe-bound Src is localized to early endosomes in Src V284C-expressing Hela cells cultured in complete medium (DMEM). Src has been shown to traffic through early endosomes during specific signaling events.[61] Anti-bodies for the early endosomal marker EEA1[62] and OG488 were added to fixed and detergent-permeabilized cells following treatment with **1-TCO**. Consistent with **1-TCO** bound Src V284C localizing to early endosomes, fluorescent puncta were observed in the perinuclear region of Src V284C-expressing HeLas only with the presence of both primary antibodies (**Figure 2-14C** and **Figure 2-18**).

Finally, we used PLA to validate kinase interactors in situ (**Figure 2-14D**). To do this, we probed the well-characterized interaction between FAK and Src in HeLa cells plated on fibronectin. As expected, fluorescent puncta were specifically observed at the plasma membrane—the site of focal

adhesions—in Src V284C-expressing HeLa cells that were treated with **1-TCO** followed by FAK and OG488 antibodies after fixation and cell permeabilization (**Figure 2-14D**, *left*). Interestingly, fluorescent signal was also observed in the peri-nuclear region, suggesting that Src and FAK interact in this subcellular region as well. Thus PLA, can validate probe-bound kinase interactions in situ and provide information on where these events occur.

2.3 CONCLUSION

In sum, we have explored the utility of click handle-conjugated probes for studying the interactomes and cellular localization of inhibitor-bound targets. We found that the rapid kinetics and mild reaction conditions of the iEDDA click reaction are well suited for capturing transient protein complexes associated with inhibitor-bound Src kinase. While click handle-conjugated probes have become important reagents for profiling and enriching direct cellular targets, our study, to the best of our knowledge, is the first to use this strategy to identify the proteins complexed to an inhibitor-bound cellular target. By developing TCO-conjugated probes that are able to stabilize different ATP-binding site conformations and divergently modulate the regulatory domains of Src, we are able to interrogate the cellular interactome of Src in various global conformations. We find that when the regulatory domains of Src are intra-molecularly disengaged that its binding partners are dominated by SH2 and SH3 domain interactors. In contrast, when the regulatory domains of Src are fully intramolecularly engaged it interacts with a complementary set of proteins. We also find that cellular context has a dramatic effect on probe-bound Src's interactome. As expected, Src interacts with very few proteins in cells with low basal signaling. As the number of active signaling pathways in-creases, the number of proteins comprising Src's

interactome expands. Our observation that Src forms the largest number of intermolecular interactions under prolonged integrin activation with fibronectin is consistent with the centrality of Src in downstream signaling events. More generally, our studies demonstrate that both kinase global conformation and cellular context greatly influence the interactions that kinases form within the cell.

In our study, we used a drug-sensitized kinase mutant to obtain selectivity for our TCO-conjugated probes. We demonstrate that an advantage of this strategy is that the same TCO-conjugated probes can be used to target multiple drug-sensitized kinases. While the overall generality of our drug-sensitization strategy throughout the kinome remains to be determined, our chemical proteomic strategy should be applicable to any WT kinase or druggable protein target for which a selective inhibitor that contains a suitable site of chemical derivatization is available. Our chemoproteomic method is an alternative to the co-immunoprecipitation of proteins from inhibitor-treated cells. We feel that the rapid capture of inhibitor-bound targets that our method facilitates will likely provide a better representation of protein complexes present upon cell lysis. Furthermore, our strategy does not require the introduction of an epitope tag into a protein target, which can interfere with the regulation of proteins like Src that contain regulatory interactions at both termini, or the use of a target-specific antibody that can potentially disrupt the protein-protein interactions of an inhibitor-bound target. Finally, the ability to perform direct on-bead digestion of inhibitor-bound targets decreases the number of MS runs that need to be performed and increases the diversity of conditions that can be profiled. Going forward, we envision that our chemoproteomic strategy can be applied to a number of kinases and other druggable protein targets.

2.4 MATERIALS AND METHODS

Materials and reagents

Lysis Buffer and Washing Buffer 1: [Tris]= 50 mM, pH= 7.8; [NaCl]= 120 mM; [NaF]= 10 mM; [Na_3VO_4]= 1 mM; [EDTA]= 1 mM; [IGEPAL CA-630]= 1% (by volume); Protease Inhibitor Tablet (Pierce)

Washing Buffer 2: [Tris]= 50 mM, pH= 7.8; [NaCl]= 120 mM; [EDTA]= 1 mM.

Denaturing Buffer: [Tris]= 50 mM, pH= 8.5; [Guanidinium Chloride]= 6 M; [TCEP]= 5 mM (add freshly); [CAM]= 10 mM (add freshly).

Pierce Protease Inhibitor Tablets (Thermo Scientific; Catalog number: A32963)

NHS-Activated Sepharose 4 Fast Flow (GE Healthcare; Catalog number: 17090601)

Pierce 660 nm Protein Assay (Thermo Scientific)

Lys-c Lysyl Endopeptidase, MS Grade (Wako)

MS Grade Trypsin (Pierce)

Grace Bio-labs CultureWell chambered coverglass (8 wells, well diam. × thickness 6 mm × 1 mm, well volume 15-30 µL; Sigma-Aldrich, cat. no. GBL103380)

Anti-Src antibody (Cell Signaling Technology, cat. no. #2109)

Anti-FAK antibody (Cell Signaling Technology, cat. no. #71433)

Anti-c-Cbl antibody (Cell Signaling Technology, cat. no. #2747)

Anti-EGFR antibody (Cell Signaling Technology, cat. no. #4267)

Anti-EEA1 antibody (Cell Signaling Technology, cat. no. #3288)

Anti-Oregon Green488 antibody (Thermo Fisher, cat. no. A-11095)

Anti-His Tag antibody (Abcam, cat. no. G020)

Anti-DYKDDDDK Tag antibody (Cell Signaling Technology, cat. no. #2368)

Anti-SAPK/JNK antibody (Cell Signaling Technology, cat. no. #9252)

Anti-PPID antibody (ABclonal, cat. no. #A6949)

Anti-PRDX4 antibody (ABclonal, cat.no. #A1486)

Anti-GAPDH antibody (Abcam, cat. no. 9485)

Duolink *in situ* mounting medium with DAPI (Sigma-Aldrich, cat. no. DUO82040)

Duolink *in situ* PLA probe anti-rabbit PLUS (Sigma-Aldrich, cat. no. DUO92002)

Duolink *in situ* PLA probe anti-goat MINUS (Sigma-Aldrich, cat. no. DUO92006)

Duolink *in situ* detection reagents orange (Sigma-Aldrich, cat. no. DUO92007)

Duolink *in situ* wash buffers, Fluorescence (Sigma-Aldrich, cat. no. DUO82049)

Generation of stable HeLa cell line

Doxycycline-inducible HeLa cells expressing Src V284C or Src WT were generated using Flp-In T-REx HeLa cells (a generous gift from Stephen S. Taylor, University of Manchester). Flp-In T-REx HeLa cells were co-transfected with Src V284C-pcDNA5/FRT/TO or Src WT-pcDNA5/FRT/TO vector, and pOG44 Flp recombinase vector (Thermo) (1:2= pcDNA5/FRT/TO:pOG) using Lipofectamine (1 ∝g of DNA: 3 ∝L of Lipofectamine). Stably transfected HeLa cells were selected with 200 ∝g/mL of hygromycin for 7–10 d. After induction with 1 ∝g/mL of doxycycline, expression of the desired transgenes was verified using Western blot analysis.

Inserted gene of Src V284C:

MGSNKSKPKDASQRRRSLEPAENVHGAGGGAFPASQTPSKPASADGHRGPSAAFAPAA

AEPKLFGGFNSSDTVTSPQRAGPLAGGVTTFVALYDYESRTETDLSFKKGERLQIVNNTE

GDWWLAHSLSTGQTGYIPSNYVAPSDSIQAEEWYFGKITRRESERLLLNAENPRGTFLV
RESETTKGAYCLSVSDFDNAKGLNVKHYKIRKLDSGGFYITSRTQFNSLQQLVAYYSKH
ADGLCHRLTTVCPTSKPQTQGLAKDAWEIPRESLRLEVKLGQGCFGECWMGTWNGTTR
VAIKTLKPGTMSPEAFLQEAQVMKKLRHEKLVQLYAVVSEEPIYIVTEYMSKGSLLDFL
KGETGKYLRLPQLVDMAAQIASGMAYVERMNYVHRDLRAANILVGENLVCKVADFGL
ARLIEDNEYTARQGAKFPIKWTAPEAALYGRFTIKSDVWSFGILLTELTTKGRVPYPGMV
NREVLDQVERGYRMPCPPECPESLHDLMCQCWRKEPEERPTFEYLQAFLEDYFTSTEPQ
YQPGENL*

Inserted gene of Src WT:

MGSNKSKPKDASQRRRSLEPAENVHGAGGGAFPASQTPSKPASADGHRGPSAAFAPAA
AEPKLFGGFNSSDTVTSPQRAGPLAGGVTTFVALYDYESRTETDLSFKKGERLQIVNNTE
GDWWLAHSLSTGQTGYIPSNYVAPSDSIQAEEWYFGKITRRESERLLLNAENPRGTFLV
RESETTKGAYCLSVSDFDNAKGLNVKHYKIRKLDSGGFYITSRTQFNSLQQLVAYYSKH
ADGLCHRLTTVCPTSKPQTQGLAKDAWEIPRESLRLEVKLGQGCFGEVWMGTWNGTT
RVAIKTLKPGTMSPEAFLQEAQVMKKLRHEKLVQLYAVVSEEPIYIVTEYMSKGSLLDF
LKGETGKYLRLPQLVDMAAQIASGMAYVERMNYVHRDLRAANILVGENLVCKVADFG
LARLIEDNEYTARQGAKFPIKWTAPEAALYGRFTIKSDVWSFGILLTELTTKGRVPYPGM
VNREVLDQVERGYRMPCPPECPESLHDLMCQCWRKEPEERPTFEYLQAFLEDYFTSTEP
QYQPGENL*

Synthesis of TCO probes (1-TCO, 2-TCO, and 3-TCO)

All chemicals purchased from commercial suppliers were used without further purification unless otherwise stated. Reactions were monitored with thin-layer chromatography (TLC) using silica gel 60 F254 coated glass plates (EM Sciences). Compound purification was performed with an IntelliFlash 280 automated flash chromatography system using pre-packed Varian SuperFlash silica gel columns (Hexane/EtOAc or CH_2Cl_2/MeOH gradient solvent). A Varian Dynamax Microsorb 100-5 C18 column (250 mm x 21.4 mm), eluting with H_2O/CH_3CN or H_2O/ MeOH gradient solvent (+0.05% TFA), was used for preparatory HPLC purification. The purity of all final compounds was determined by analytical HPLC with an Agilent ZORBAX SB-C18 (2.1 mm x 150 mm) or Varian Microsorb-MV 100-5 C18 column (4.6 mm x 150 mm), eluting with either H_2O/CH_3CN or H_2O/MeOH gradient solvent (+0.05% TFA). Elution was monitored by a UV detector at λ= 220 nm and λ= 254 nm, with all final compounds displaying >95% purity. Nuclear magnetic resonance (NMR) spectra were recorded on Bruker 300 or 500 MHz NMR spectrometers at ambient temperature. Chemical shifts were reported in parts per million (ppm) and coupling constants in hertz (Hz). ^{1}H-NMR spectra were referenced to the residual solvent peaks as internal standards (7.26 ppm for $CDCl_3$, 2.50 ppm for d6-DMSO, and 3.34 ppm for CD_3OD). Mass spectra were recorded with a Bruker Esquire Liquid Chromatograph - Ion Trap Mass Spectrometer.

Synthesis of 1-TCO

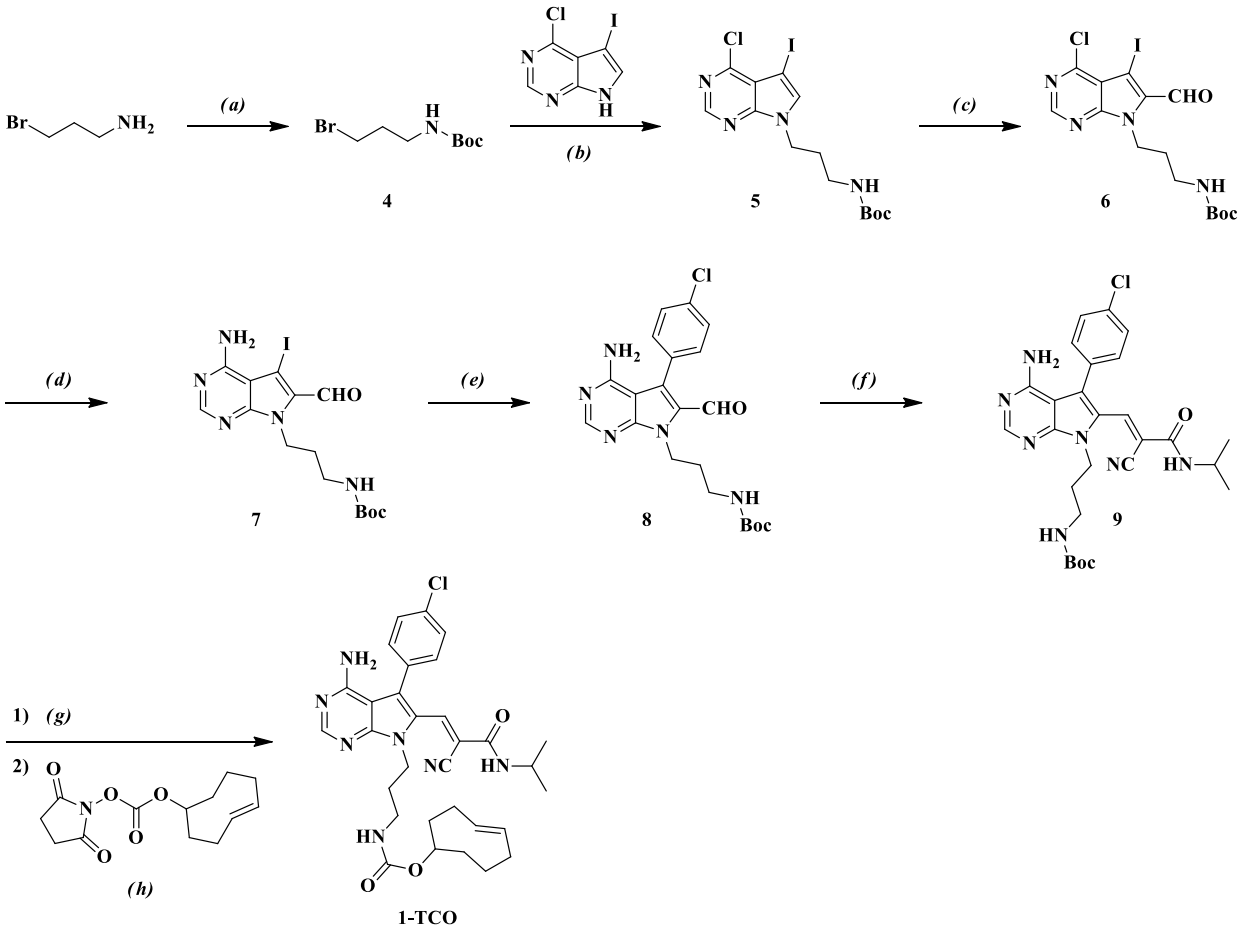

Reaction scheme for **1-TCO**: (a) Boc_2O, Et_3N, DCM, 0 °C-rt, 95%; (b) Cs_2CO_3, DMF, 50 °C, 14 hours, 59%; (c) Diisopropylamine, *n*-BuLi, ethyl formate, THF, -78 °C-rt, overnight, 22%; (d) Ammonium hydroxide, 1,4-Dioxane, 40 °C, 3 hours, 43%; (e) 4-Chlorophenylboronic acid, K_3PO_4, $Pd(dppf)_2Cl_2$, 1,4-Dioxane, H_2O, 90 °C, 130 mins (microwave), 74%; (f) 2-Cyano-*N*-isopropylacetamide, DBU, THF, rt, 6 hours, 50%; (g) TFA, DCM, rt, 30 mins; (h) DIPEA, THF, rt, overnight, 60%.

***Tert*-butyl (3-bromopropyl)carbamate (4)**

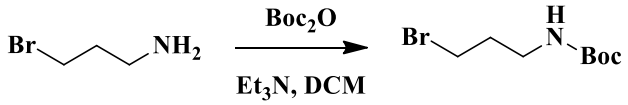

3-Bromopropylamine hydrobromide (5.3 g, 24 mmol, 1.0 equiv.) and triethylamine (2.7 g, 26 mmol, 3.6 mL, 1.1 equiv.) were dissolved in anhydrous dichloromethane (50 mL) and cooled to 0˚C in a 250-mL round bottom flask under nitrogen. A solution of di-*tert*-butyl dicarbonate (5.3 g, 24 mmol, 1.0 equiv.) in dichloromethane (40 mL) was added dropwise to the above solution over 30 minutes. The resulting reaction mixture was allowed to warm to room temperature overnight. The reaction was then quenched with aqueous sodium hydroxide solution (20 mL, 5% by weight). The organic phase was washed with water (20 mL), brine (20 mL) and then dried over anhydrous sodium sulfate. The solvent was removed in vacuo and afforded *tert*-butyl (3-bromopropyl)carbamate as a white solid (5.4 g, 95%). The crude product was used in further steps without purification. ^{1}H-NMR (300 MHz, $CDCl_3$) δ= 4.64 (s, 1H), 3.44 (t, J = 6.5 Hz, 2H), 3.33 – 3.22 (m, 2H), 2.12 – 1.99 (m, 2H), 1.45 (s, 9H); MS (ESI, m/z) calculated for $C_8H_{16}BrNO_2$ 237.0, $[M+H]^+$ found 238.8.

***Tert*-butyl (3-(4-chloro-5-iodo-7*H*-pyrrolo[2,3-*d*]pyrimidin-7-yl)propyl)carbamate (5)**

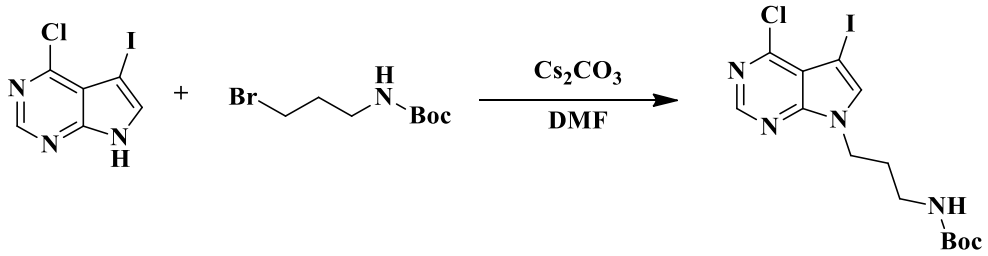

4-Chloro-5-iodo-7H-pyrrolo[2,3-d]pyrimidine (1.7 g, 6.2 mmol, 1.0 equiv.), *tert*-butyl (3-bromopropyl)carbamate (2.0 g, 8.4 mmol, 1.4 equiv.) and cesium carbonate (6.7 g, 12.4 mmol, 2.0

equiv.) were dissolved in dimethylformamide (20 mL) in a 100-mL round bottom flask under nitrogen. The reaction mixture was heated at 50 ˚C for 14 hours. The solvent was then removed in *vacuo* and the resulting solid residue was redissolved in ethyl acetate (200 mL). The organic phase was washed with aqueous ammonium chloride solution (40 mL), aqueous sodium bicarbonate solution (40 mL), brine (40 mL), dried over anhydrous sodium sulfate and concentrated in *vacuo*. Purification with Flash chromatography afforded *tert*-butyl (3-(4-chloro-5-iodo-7*H*-pyrrolo[2,3-*d*]pyrimidin-7-yl)propyl)carbamate as a pale yellow solid (1.6 g, 59%). ^{1}H-NMR (500 MHz, $CDCl_3$) δ= 8.62 (s, 1H), 7.45 (d, J = 14.2 Hz, 1H), 5.01 (s, 1H), 4.33 (t, J = 6.6 Hz, 2H), 3.11 – 3.03 (m, 2H), 2.06 – 1.97 (m, 2H), 1.45 (s, 9H); MS (ESI, m/z) calculated for $C_{14}H_{18}ClIN_4O_2$ 436.0, $[M+H]^+$ found 437.1.

Tert-butyl (3-(4-chloro-6-formyl-5-iodo-7*H*-pyrrolo[2,3-*d*]pyrimidin-7-yl)propyl)carbamate (6)

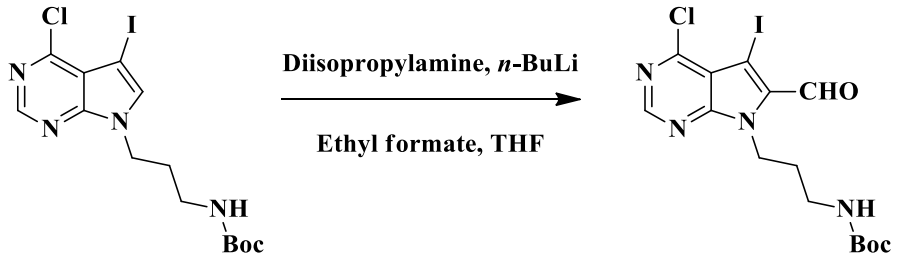

In a flame-dried 100-mL round bottom flask, diisopropylamine (228 mg, 316 ∝L, 2.25 mmol, 1.75 equiv.) was dissolved in dry THF (10 mL) and cooled to -78˚C under nitrogen. *n*-BuLi solution (2.5 M in hexane, 901 ∝L, 2.25 mmol, 1.75 equiv.) was added dropwise to the above solution at -78 ˚C. The reaction was stirred at 0 ˚C for 1 hour and then cooled to -78 ˚C. A solution of *tert*-butyl (3-(4-chloro-5-iodo-7*H*-pyrrolo[2,3-*d*]pyrimidin-7-yl)propyl)carbamate (562 mg, 1.29 mmol, 1.00 equiv.) in dry THF (5 mL) was added dropwise at -78 ˚C. After 1 hour, ethyl formate

(200 mg, 218 ∝L, 2.70 mmol, 2.10 equiv.) was added dropwise at -78 ˚C. The reaction mixture was allowed to warm up to room temperature overnight. The reaction was quenched by adding aqueous ammonium chloride solution (2 mL) and diluted with ethyl acetate (150 mL). The organic phase was washed with aqueous sodium bicarbonate solution (20 mL), brine (20 mL), dried over anhydrous sodium sulfate and concentrated in *vacuo*. Purification by flash chromatography on silica gel (EtOAc:Hexane= 0:100 to EtOAc: Hexane= 1:2) afforded *tert*-butyl (3-(4-chloro-6-formyl-5-iodo-7*H*-pyrrolo[2,3-*d*]pyrimidin-7-yl)propyl)carbamate as a pale brown powder (130 mg, 22%; R_f= 0.57 in EtOAc:Hexane= 3:2). ^{1}H -NMR (300 MHz, $CDCl_3$) δ= 10.08 (s, 1H), 8.77 (s, 1H), 5.12 (s, 1H), 4.72 (t, *J* = 6.6 Hz, 2H), 3.14 – 2.96 (m, 2H), 2.03 – 1.89 (m, 2H), 1.45 (s, 9H); MS (ESI, m/z) calculated for $C_{15}H_{18}ClIN_4O_3$ 464.0, $[M+H]^+$ found 465.0.

***Tert*-butyl (3-(4-amino-6-formyl-5-iodo-7*H*-pyrrolo[2,3-*d*]pyrimidin-7-yl)propyl)carbamate (7)**

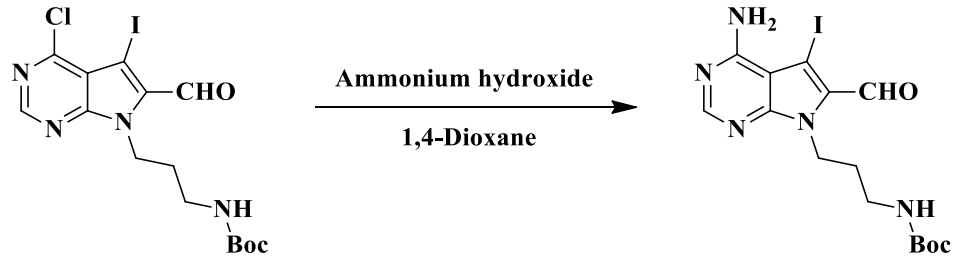

In a 10-mL pressure tube, *tert*-butyl (3-(4-chloro-6-formyl-5-iodo-7*H*-pyrrolo[2,3-*d*]pyrimidin-7-yl)propyl)carbamate (130 mg, 0.28 mmol, 1.0 equiv.) was dissovled in 1,4-Dioxane (1.2 mL). To it was added aqueous ammonium hydroxide solution (1.2 mL, 28.0 %- 30.0 % NH_3 basis). The resulting solution was heated at 40 ˚C for 3 hours and then diluted with ethyl acetate (40 mL). The organic phase was washed with 1 M hydrochloride aqueous solution, sodium bicarbonate, brine and dried over anhydrous sodium sulfate. Purification on silica gel using a gradiant of MeOH:

DCM= 0:100 to MeOH: DCM= 10:90 afforded *tert*-butyl (3-(4-amino-6-formyl-5-iodo-7*H*-pyrrolo[2,3-*d*]pyrimidin-7-yl)propyl)carbamate as a pale brown solid (54 mg, 43%; R_f= 0.51 in MeOH:DCM= 1:9). ^{1}H-NMR (300 MHz, $CDCl_3$) δ= 9.82 (s, 1H), 8.38 (s, 1H), 6.04 (s, 2H), 5.50 (s, 1H), 4.63 (t, J = 6.4 Hz, 2H), 3.07 – 2.91 (m, 2H), 2.01 – 1.86 (m, 2H), 1.45 (s, 9H); MS (ESI, m/z) calculated for $C_{15}H_{20}IN_5O_3$ 445.1, $[M+H]^+$ found 446.3.

Tert-butyl(3-(4-amino-5-(4-chlorophenyl)-6-formyl-7*H*-pyrrolo[2,3-*d*]pyrimidin-7-yl)propyl)carbamate (8)

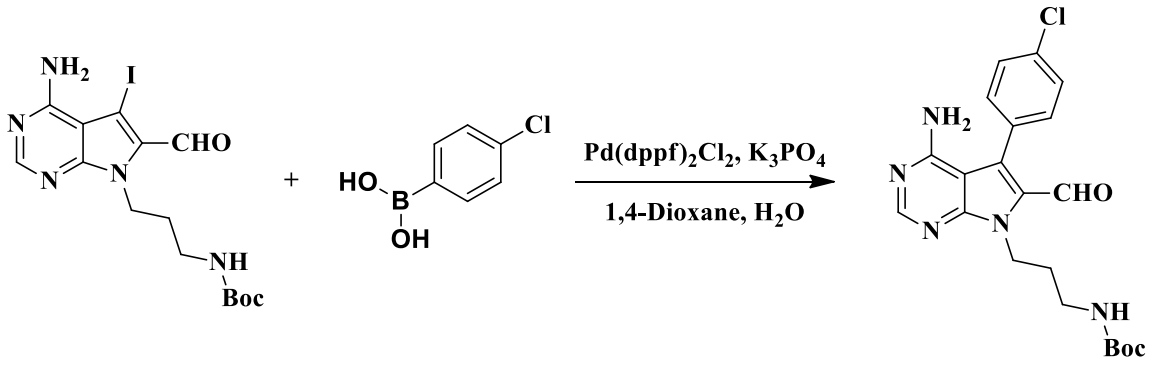

In a 10-mL microwave reaction tube, tert-butyl (3-(4-amino-6-formyl-5-iodo-7*H*-pyrrolo[2,3-*d*]pyrimidin-7-yl)propyl)carbamate (54 mg, 0.12 mmol, 1.0 equiv.), 4-chlorophenylboronic acid (28 mg, 0.18 mmol, 1.5 equiv.), potassium phosphate (77 mg, 0.36 mmol, 3.0 equiv.) and [1,1′-Bis(diphenylphosphino)ferrocene]dichloropalladium(II) (9.9 mg, 0.012 mmol, 0.1 equiv.) were dissolved in a mixture of 1,4-Dioxane (1.0 mL) and water (0.25 mL). The resulting mixture was heated in a microwave reactor at 90 ˚C for 130 mins. The reaction was then quenched with saturated NH_4Cl solution (1 mL) and diluted with ethyl acetate (30 mL). The organic phase was washed with saturated NaHCO3 solution (5 mL), brine (5 mL), dried over anhydrous Na_2SO_4 and concentrated in *vacuo*. Purification using flash chromatography on silica gel with a EtOAc/Hexane gradient (0:100 to 90:10) afforded *tert*-butyl (3-(4-amino-5-(4-chlorophenyl)-6-formyl-7*H*-

pyrrolo[2,3-*d*]pyrimidin-7-yl)propyl)carbamate as a pale yellow solid (39 mg, 74%; Rf= 0.31 in EtOAc:Hexane= 9:1).^{1}H-NMR (300 MHz, $CDCl_3$) δ= 9.60 (s, 1H), 8.41 (s, 1H), 7.58 – 7.42 (m, 4H), 5.62 (s, 1H), 5.32 (s, 2H), 4.70 (t, *J* = 6.3 Hz, 2H), 3.19 – 2.94 (m, 2H), 2.06 – 1.96 (m, 2H), 1.46 (s, 9H); MS (ESI, m/z) calculated for $C_{21}H_{24}ClN_5O_3$ 429.2, $[M+H]^+$ found 430.1.

(*Z*)- or (*E*)-*tert*-butyl (3-(4-amino-5-(4-chlorophenyl)-6-(2-cyano-3-(isopropylamino)-3-oxoprop-1-en-1-yl)-7*H*-pyrrolo[2,3-*d*]pyrimidin-7-yl)propyl)carbamate (9)

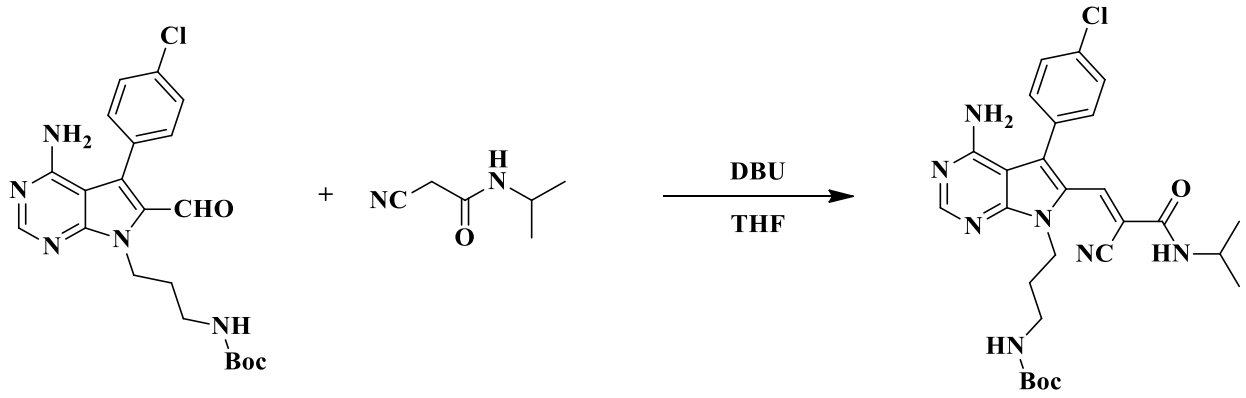

Tert-butyl (3-(4-amino-5-(4-chlorophenyl)-6-formyl-7*H*-pyrrolo[2,3-*d*]pyrimidin-7-yl)propyl)carbamate (20 mg, 0.048 mmol, 1.0 equiv.) and 2-cyano-*N*-isopropylacetamide (9.2 mg, 0.072 mmol, 1.5 equiv.) were dissolved in tetrahydrofuran (300 ∝L). To the above solution was added 1,8-diazabicyclo[5.4.0]undec-7-ene (15 mg, 14 ∝L, 0.096 mmol, 2.0 equiv). The reaction mixture was stirred at room temperature for 6 hours. The reaction was then quenched with saturated NH_4Cl solution (1 mL) and diluted with ethyl acetate (30 mL). The organic layer was washed with saturated NaHCO3 solution (5 mL), brine (5 mL), dried over anhydrous Na_2SO_4 and concentrated in *vacuo*. Purification using preparative thin-layer chromatography developed by pure EtOAc rendered (*Z*)- or (*E*)-*tert*-butyl (3-(4-amino-5-(4-chlorophenyl)-6-(2-cyano-3-(isopropylamino)-3-oxoprop-1-en-1-yl)-7*H*-pyrrolo[2,3-*d*]pyrimidin-7-yl)propyl)carbamate as a

bright yellow powder (13 mg, 50%; Rf [(E)- and (Z)-isomers)]= 0.25 in EtOAc:Hexane= 9:1). ^{1}H-NMR (300 MHz, MeOD) δ= 8.30 – 8.18 (m, 3H), 7.70 (s, 1H), 7.64 – 7.36 (m, 8H), 6.68 (s, 2H), 5.53 (s, 2H), 5.16 (s, 4H), 4.43 (t, *J* = 6.9 Hz, 2H), 4.34 (t, *J* = 7.0 Hz, 2H), 4.19 – 4.04 (m, 1H), 3.71 – 3.54 (m, 1H), 3.15 – 2.97 (m, 4H), 2.06 – 1.92 (m, 4H), 1.46 (s, 9H), 1.33 (s, 9H), 1.24 (d, *J* = 6.6 Hz, 6H), 1.05 (d, *J* = 6.6 Hz, 6H); MS (ESI, m/z) calculated for $C_{27}H_{32}ClN_7O_3$ 537.2, $[M+H]^+$ found 538.1.

(*E*)-cyclooct-4-en-1-yl (3-(4-amino-5-(4-chlorophenyl)-6-((*E*)-2-cyano-3-(isopropylamino)-3-oxoprop-1-en-1-yl)-7*H*-pyrrolo[2,3-*d*]pyrimidin-7-yl)propyl)carbamate or (*E*)-cyclooct-4-en-1-yl (3-(4-amino-5-(4-chlorophenyl)-6-((*Z*)-2-cyano-3-(isopropylamino)-3-oxoprop-1-en-1-yl)-7*H*-pyrrolo[2,3-*d*]pyrimidin-7-yl)propyl)carbamate (1-TCO)

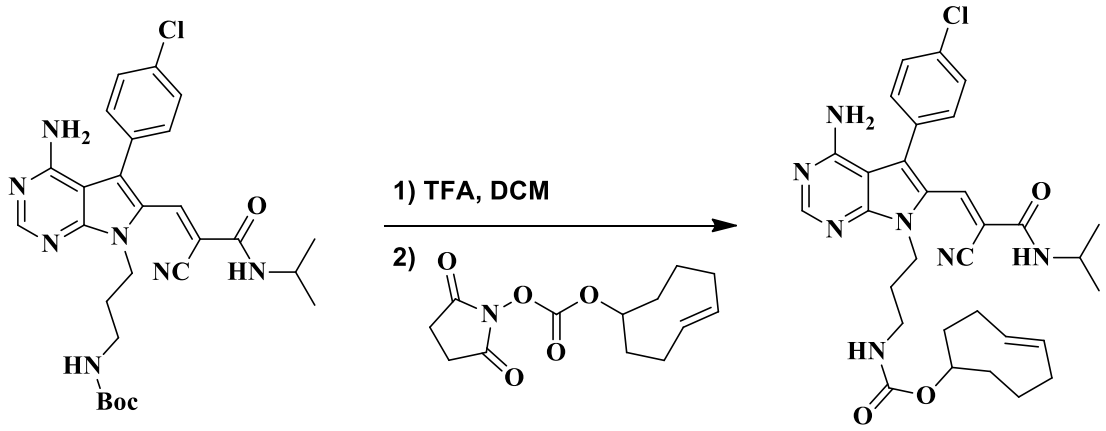

(*Z*)- or (*E*)-*tert*-butyl (3-(4-amino-5-(4-chlorophenyl)-6-(2-cyano-3-(isopropylamino)-3-oxoprop-1-en-1-yl)-7*H*-pyrrolo[2,3-*d*]pyrimidin-7-yl)propyl)carbamate (13 mg, 0.024 mmol, 1.0 equiv.) was dissolved in a mixture of trifluoacetic acid (0.30 mL) and dichloromethane (0.70 mL). The reaction solution was stirred at room temperature for 30 mins and concentrated in *vacuo*. The solid residue was dissolved in anhydrous tetrahydrofuran (400 ∝L). Then diisopropylethylamine (7.8 mg, 11 μL, 0.060 mmol, 2.5 equiv.) and (*E*)-cyclooct-4-en-1-yl (2,5-dioxopyrrolidin-1-yl)

carbonate (8.4 mg, 0.031 mmol, 1.3 equiv.) were added to the above solution sequentially. The resulting mixture was stirred at room temperature overnight and quenched with water (1 mL) and diluted with ethyl acetate (30 mL). The organic layer was washed with saturated $NaHCO_3$ solution (5 mL), brine (5 mL), dried over anhydrous Na_2SO_4 and concentrated in *vacuo*. Purification using flash chromatography with a EtOAc/Hexane gradient (0:100 to 90:10) afforded a mixture of (*E*)-cyclooct-4-en-1-yl (3-(4-amino-5-(4-chlorophenyl)-6-((*E*)-2-cyano-3-(isopropylamino)-3-oxoprop-1-en-1-yl)-7*H*-pyrrolo[2,3-*d*]pyrimidin-7-yl)propyl)carbamate or (*E*)-cyclooct-4-en-1-yl (3-(4-amino-5-(4-chlorophenyl)-6-((*Z*)-2-cyano-3-(isopropylamino)-3-oxoprop-1-en-1-yl)-7*H*-pyrrolo[2,3-*d*]pyrimidin-7-yl)propyl)carbamate as a bright yellow powder (8.6 mg, 60% for 2 steps; R_f [(*E*)- and (*Z*)-isomers)]= 0.33 or 0.26 in EtOAc:Hexane= 9:1) ^{1}H-NMR (300 MHz, MeOD) δ= 8.26 – 8.16 (m, 3H), 7.66 (s, 1H), 7.60 – 7.34 (m, 8H), 6.77 (s, 2H), 5.76 – 5.36 (m, 4H), 5.13 (s, 4H), 4.45 – 4.21 (m, 4H), 4.18 – 4.00 (m, 1H), 3.70 – 3.49 (m, 1H), 3.17 – 2.92 (m, 4H), 2.43 – 2.27 (m, 4H), 2.27 – 0.94 (m, 32H), 1.00 – 0.82 (m, 4H); MS (ESI, m/z) calculated for $C_{31}H_{36}ClN_7O_3H$ (M+H) 590.2641, $[M+H]^+$ (HRMS) found 590.2633; HPLC purity: 97.9% (UV detector wavelength: 254 nm).

2.4.1.1 Synthesis of 2-TCO

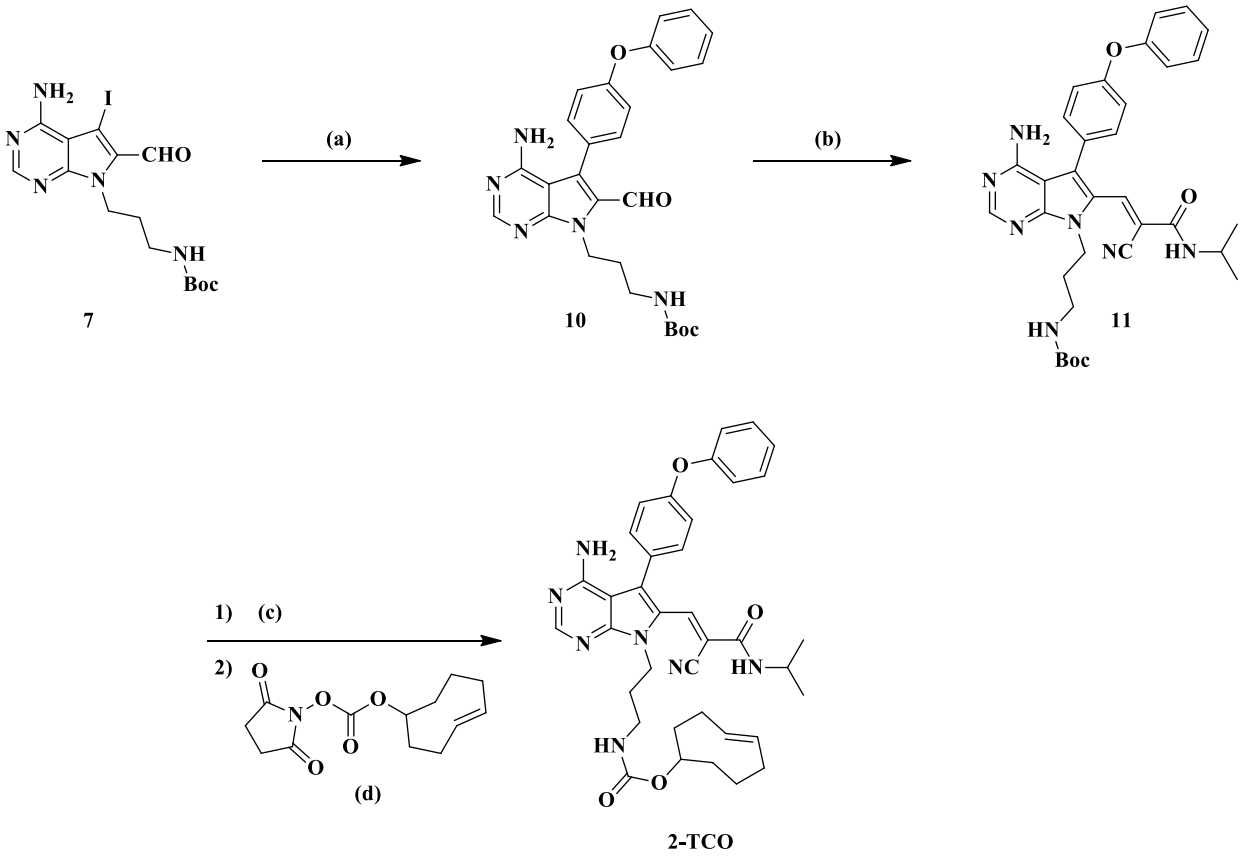

Reaction scheme for **2-TCO**: (a) 4-Phenoxyphenylboronic acid, K_3PO_4, $Pd(dppf)_2Cl_2$, 1,4-Dioxane, H_2O, 90 °C, 150 mins (microwave), 72%; (b) 2-Cyano-*N*-isopropylacetamide, DBU, THF, rt, 80 mins, 57%; (c) TFA, DCM, rt, 30 mins; (d) DIPEA, THF, rt, overnight, 44%.

***Tert*-butyl (3-(4-amino-6-formyl-5-(4-phenoxyphenyl)-7*H*-pyrrolo[2,3-*d*]pyrimidin-7-yl)propyl)carbamate (10)**

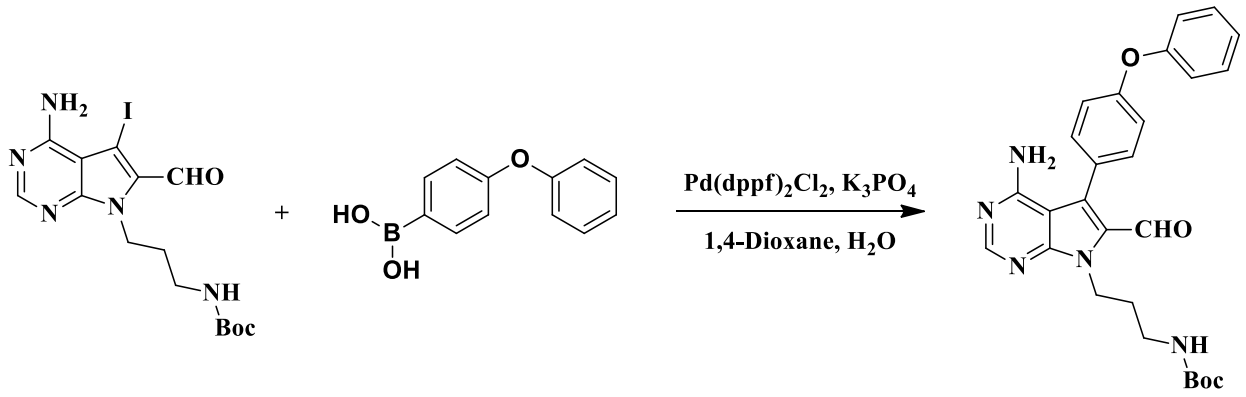

In a 10-mL microwave reaction tube, *tert*-butyl (3-(4-amino-6-formyl-5-iodo-7*H*-pyrrolo[2,3-*d*]pyrimidin-7-yl)propyl)carbamate (72 mg, 0.16 mmol, 1.0 equiv.), 4-phenoxyphenylboronic acid (52 mg, 0.24 mmol, 1.5 equiv.), potassium phosphate (100 mg, 0.49 mmol, 3.0 equiv.) and [1,1′-Bis(diphenylphosphino)ferrocene]dichloropalladium(II) (13 mg, 0.016 mmol, 0.1 equiv.) were dissolved in a mixture of 1,4-Dioxane (1.3 mL) and water (0.33 mL). The resulting mixture was heated in a microwave reactor at 90 ˚C for 150 mins. The reaction was quenched with saturated NH_4Cl solution (1 mL) and diluted with ethyl acetate (30 mL). The organic phase was washed with saturated NaHCO3 solution (5 mL), brine (5 mL), dried over anhydrous Na_2SO_4 and concentrated in *vacuo*. Purification using flash chromatography on silica gel with a EtOAc/Hexane gradient (0:100 to 90:10) afforded *tert*-butyl (3-(4-amino-6-formyl-5-(4-phenoxyphenyl)-7*H*-pyrrolo[2,3-*d*]pyrimidin-7-yl)propyl)carbamate as a pale yellow solid (57 mg, 72%; R_f= 0.87 in EtOAc:Hexane= 9:1). ^{1}H-NMR (500 MHz, $CDCl_3$) δ= 9.64 (s, 1H), 8.42 (s, 1H), 7.48 – 7.38 (m, 4H), 7.21 (t, J = 7.4 Hz, 1H), 7.16 – 7.09 (m, 4H), 5.68 (s, 1H), 5.35 (s, 2H), 4.69 (t, J = 6.3 Hz, 2H), 3.10 – 2.98 (m, 2H), 2.05 – 1.96 (m, 2H), 1.46 (s, 9H); MS (ESI, m/z) calculated for $C_{27}H_{29}N_5O_4$ 487.2, $[M+H]^+$ found 488.5.

(*Z*)- or (*E*)-tert-butyl (3-(4-amino-6-(2-cyano-3-(isopropylamino)-3-oxoprop-1-en-1-yl)-5-(4-phenoxyphenyl)-7*H*-pyrrolo[2,3-*d*]pyrimidin-7-yl)propyl)carbamate (11)

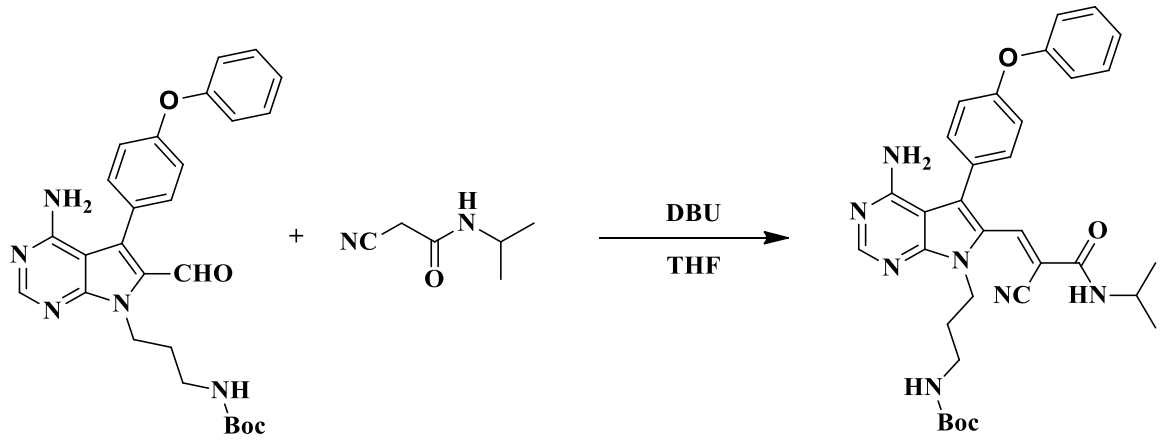

Tert-butyl (3-(4-amino-6-formyl-5-(4-phenoxyphenyl)-7*H*-pyrrolo[2,3-*d*]pyrimidin-7-yl)propyl)carbamate (57 mg, 0.095 mmol, 1.0 equiv.) and 2-cyano-*N*-isopropylacetamide (18 mg, 0.14 mmol, 1.5 equiv.) were dissolved in dry THF (600 ∝L mL). 1,8-Diazabicyclo[5.4.0]undec-7-ene (29 mg, 28 μL, 0.19 mmol, 2.0 equiv.) was added and the resulting solution was stirred at room temperature for 80 mins. The reaction mixture was then diluted with EtOAc (30 mL) and quenched with saturated aqueous NH_4Cl solution. The organic phase was washed with saturated $NaHCO_3$ solution (5 mL), brine (5 mL), dried over anhydrous Na_2SO_4. Purification with preparative thin-layer chromatography afforded a mixture of (*Z*)- or (*E*)-tert-butyl (3-(4-amino-6-(2-cyano-3-(isopropylamino)-3-oxoprop-1-en-1-yl)-5-(4-phenoxyphenyl)-7*H*-pyrrolo[2,3-*d*]pyrimidin-7-yl)propyl)carbamate as a bright yellow powder (32 mg, 57%; Rf [(E) and (Z)-isomers)]= 0.26 in EtOAc:Hexane= 9:1). ^{1}H-NMR (300 MHz, MeOD) δ= 8.25 – 8.19 (m, 3H), 7.65 (s, 1H), 7.51 – 7.34 (m, 8H), 7.24 – 7.05 (m, 10H), 5.14 (s, 2H), 4.48 – 4.38 (m, 2H), 4.31 (t, *J* = 7.0 Hz, 2H), 4.15 – 4.07 (m, 1H), 3.74 – 3.62 (m, 1H), 3.13 – 2.94 (m, 4H), 2.04 – 1.85 (m, 4H), 1.44 (s, 18H), 1.23 (d, *J* = 6.6 Hz, 6H), 1.07 (d, *J* = 6.5 Hz, 6H); MS (ESI, m/z) calculated for $C_{33}H_{37}N_7O_4$ 595.3, $[M+H]^+$ found 597.4.

(*E*)-cyclooct-4-en-1-yl (3-(4-amino-6-((*E*)-2-cyano-3-(isopropylamino)-3-oxoprop-1-en-1-yl)-5-(4-phenoxyphenyl)-7*H*-pyrrolo[2,3-*d*]pyrimidin-7-yl)propyl)carbamate or (*E*)-cyclooct-4-en-1-yl (3-(4-amino-6-((*Z*)-2-cyano-3-(isopropylamino)-3-oxoprop-1-en-1-yl)-5-(4-phenoxyphenyl)-7*H*-pyrrolo[2,3-*d*]pyrimidin-7-yl)propyl)carbamate (2-TCO)

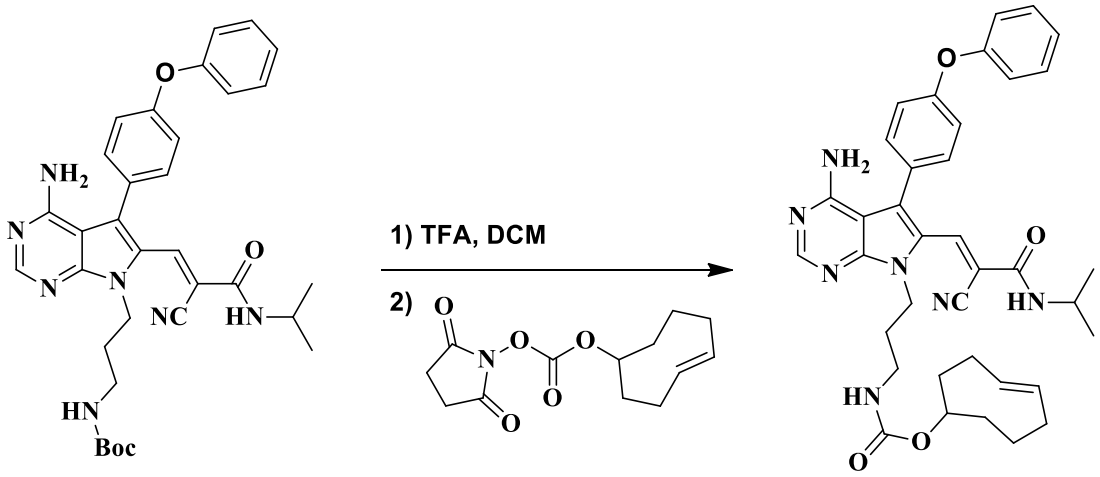

A mixture of (*Z*)- or (*E*)-tert-butyl (3-(4-amino-6-(2-cyano-3-(isopropylamino)-3-oxoprop-1-en-1-yl)-5-(4-phenoxyphenyl)-7*H*-pyrrolo[2,3-*d*]pyrimidin-7-yl)propyl)carbamate (24 mg, 0.034 mmol, 1.0 equiv.) was dissolved in a mixture of trifluoacetic acid (0.60 mL) and dichloromethane (1.4 mL). The resulting soluting was stirred at room temperature for 30 mins and concentrated in vacuo. The solid residue was dissolved in anhydrous tetrahydrofuran (2 mL), and to it was added diisopropylethylamine (22 mg, 30 μL, 0.17 mmol, 5.0 equiv.) and (*E*)-cyclooct-4-en-1-yl (2,5-dioxopyrrolidin-1-yl) carbonate (12 mg, 0.044 mmol, 1.3 equiv.) sequentially. The resulting mixture was stirred at room temperature overnight and quenched with water (1 mL) and diluted with ethyl acetate (30 mL). The organic layer was washed with saturated NaHCO3 solution (5 mL), brine (5 mL), dried over anhydrous Na2SO4. The crude product was purified using flash chromatography with a MeOH/EtOAc gradient (0:100 to 10:90). A mixture of isomers of (*E*)-cyclooct-4-en-1-yl (3-(4-amino-6-((*E*)-2-cyano-3-(isopropylamino)-3-oxoprop-1-en-1-yl)-5-(4-

phenoxyphenyl)-7*H*-pyrrolo[2,3-*d*]pyrimidin-7-yl)propyl)carbamate or (*E*)-cyclooct-4-en-1-yl (3-(4-amino-6-((*Z*)-2-cyano-3-(isopropylamino)-3-oxoprop-1-en-1-yl)-5-(4-phenoxyphenyl)-7*H*-pyrrolo[2,3-*d*]pyrimidin-7-yl)propyl)carbamate was rendered as a bright yellow powder (9.6 mg, 44% for 2 steps; Rf [(E) and (Z)-isomers)]= 0.27 in EtOAc:Hexane= 3:2) ^{1}H-NMR (300 MHz, MeOD) δ= 8.26 – 8.13 (m, 3H), 7.60 (s, 1H), 7.50 – 7.32 (m, 8H), 7.23 – 7.05 (m, 10H), 5.52 (t, 4H), 4.40 (t, J = 6.8 Hz, 2H), 4.27 (t, J = 6.8 Hz, 2H), 4.19 – 4.02 (m, 1H), 3.77 – 3.59 (m, 1H), 3.27 – 3.14 (m, 2H), 3.14 – 2.93 (m, 4H), 2.42 – 2.22 (m, 4H), 2.22 – 0.97 (m, 32H), 0.97 – 0.81 (m, 4H); MS (ESI, m/z) calculated for $C_{37}H_{41}N_7O_4H$ (M+H) 648.3293, $[M+H]^+$ (HRMS) found 648.3279; HPLC purity: 99.0% (UV detector wavelength: 254 nm)

2.4.1.2 Synthesis of 3-TCO

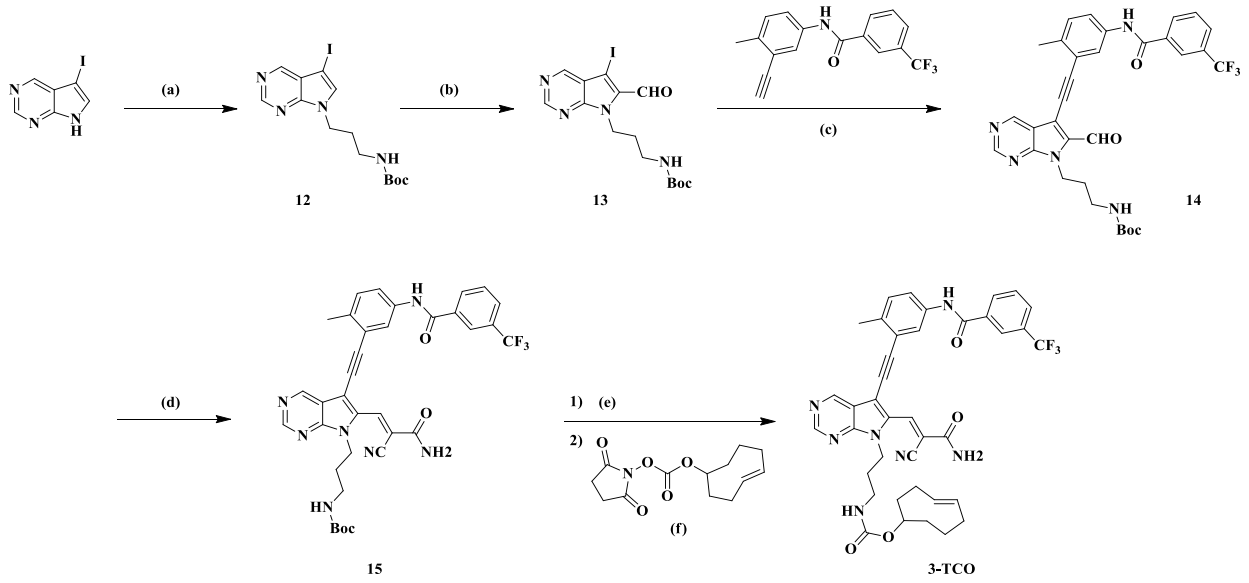

Reaction scheme for **3-TCO**: (a) Cs_2CO_3, DMF, 50 °C, overnight, 73%; (b) Diisopropylamine, *n*-BuLi, ethyl formate, THF, -78 °C-rt, overnight, 32%; (c) *N*-(3-ethynyl-4-methylphenyl)-3-(trifluoromethyl)-benzamide, $Pd(PPh_3)_2Cl_2$, CuI, DMF, 50 °C, overnight, 39%; (f)

Cyanoacetamide, DBU, THF, rt, 25 mins, 44%; (g) TFA, DCM, rt, 30 mins; (h) DIPEA, THF, rt, 30 mins, 59%.

***Tert*-butyl (3-(5-iodo-7*H*-pyrrolo[2,3-*d*]pyrimidin-7-yl)propyl)carbamate (12)**

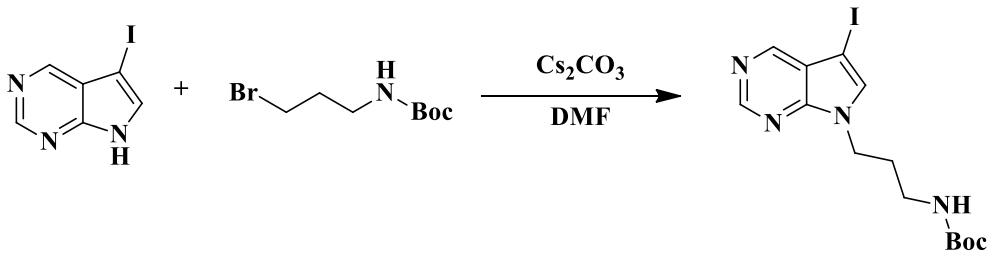

5-Iodo-7*H*-pyrrolo[2,3-*d*]pyrimidine (2.0 g, 8.2 mmol, 1.0 equiv.), *tert*-butyl (3-bromopropyl)carbamate (2.5 g, 11 mmol, 1.3 equiv.) and cesium carbonate (8.8 g, 16 mmol, 2.0 equiv.) were dissolved in dimethylformamide (20 mL) in a 100-mL round bottom flask. The reaction mixture was heated at 50 ˚C overnight. The solvent was then removed in *vacuo*. The crude compound was redissolved in ethyl acetate (200 mL) and washed with saturated NH_4Cl solution (40 mL), aqueous $NaHCO_3$ solution (40 mL), brine (40 mL), dried over anhydrous Na_2SO_4. Purification with Flash chromatography afforded *tert*-butyl (3-(5-iodo-7*H*-pyrrolo[2,3-*d*]pyrimidin-7-yl)propyl)carbamate as a pale brown solid (2.4 g, 73%; Rf= 0.20 in EtOAc:Hexane= 1:2). ^{1}H-NMR (300 MHz, $CDCl_3$) δ= 8.81 (s, 1H), 8.66 (s, 1H), 7.16 (s, 1H), 5.02 (s, 1H), 4.25 (t, J = 6.5 Hz, 2H), 3.13 – 2.82 (m, 2H), 2.09 – 1.82 (m, 2H), 1.36 (s, 9H); MS (ESI, m/z) calculated for $C_{14}H_{19}IN_4O_2$ 402.1, $[M+H]^+$ found 403.1.

***Tert*-butyl (3-(6-formyl-5-iodo-7*H*-pyrrolo[2,3-*d*]pyrimidin-7-yl)propyl)carbamate (13)**

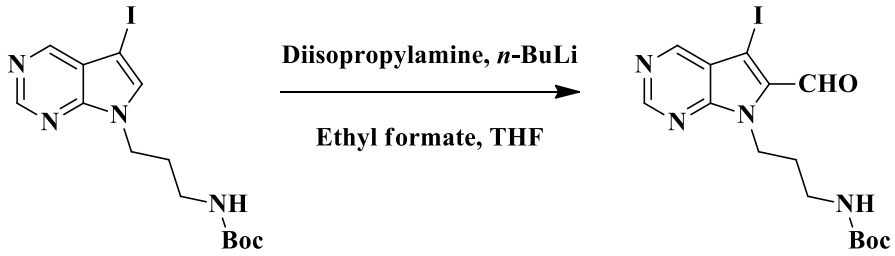

Diisopropylamine (490 mg, 680 µL, 4.9 mmol, 2.7 equiv.) was dissolved in dry THF (6 mL) and cooled to -78°C. A solution of *n*-BuLi (2.5 M in hexane, 1.8 mL, 4.5 mmol, 2.5 equiv.) was added dropwise to the above solution at -78 ˚C. The solution was stirred at 0 °C for 1 hour and then cooled to -78 °C. A solution of *tert*-butyl (3-(5-iodo-7*H*-pyrrolo[2,3-*d*]pyrimidin-7-yl)propyl)carbamate (730 mg, 1.8 mmol, 1.0 equiv., dissolved in 3 mL dry THF) was added dropwise and the reaction mixture was then stirred at -78 °C for 1 hour. A solution of ethyl formate (536 mg, 580 ∝L, 7.2 mmol, 4.0 equiv., dissolved in 3 mL dry THF) was then added dropwise at -78°C. The reaction was allowed to warm to room temperature overnight. After reaction, saturated NH4Cl solution (2 mL) was added and the resulting mixture was diluted with ethyl acetate (200 mL). The organic layer was washed with saturated aqueous NaHCO3 solution, brine and dried over anhydrous Na2SO4. Purification by flash chromatography on silica gel (EtOAc: Hexane= 0:100 to EtOAc: Hexane= 3:2) afforded *tert*-butyl (3-(6-formyl-5-iodo-7*H*-pyrrolo[2,3-*d*]pyrimidin-7-yl)propyl)carbamate as a pale brown solid (250 mg, 32%). ^{1}H-NMR (300 MHz, $CDCl_3$) δ= 10.02 (s, 1H), 9.07 (s, 1H), 8.98 (s, 1H), 5.22 (s, 1H), 4.73 (t, *J* = 6.6 Hz, 2H), 3.13 – 2.96 (m, 2H), 2.10 – 1.91 (m, 2H), 1.45 (s, 9H). MS (ESI, m/z) calculated for $C_{15}H_{19}IN_4O_3$ 430.1, $[M+H]^+$ found 431.0.

***Tert*-butyl (3-(6-formyl-5-((2-methyl-5-(3-(trifluoromethyl)benzamido)phenyl)ethynyl)-7*H*-pyrrolo[2,3-*d*]pyrimidin-7-yl)propyl)carbamate (14)**

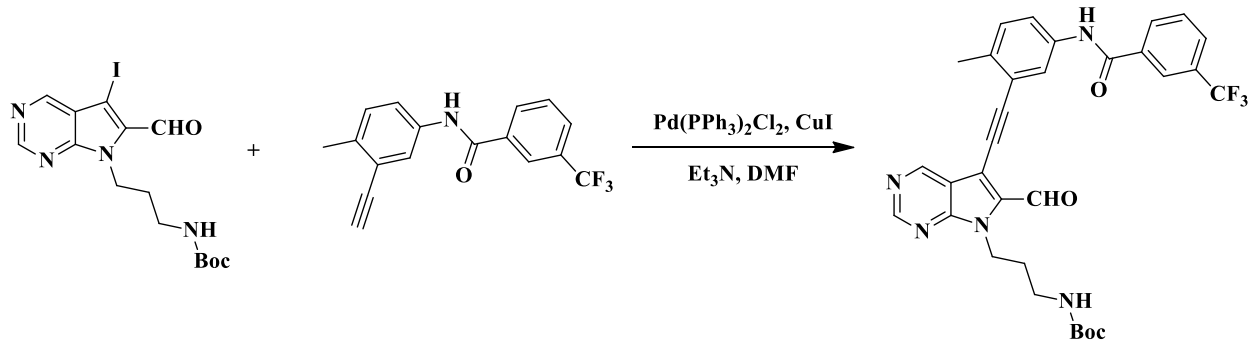

N-(3-ethynyl-4-methylphenyl)-3-(trifluoromethyl)-benzamide was synthesized according to previous reported (ref. SFK paper). *Tert*-butyl (3-(6-formyl-5-iodo-7*H*-pyrrolo[2,3-*d*]pyrimidin-7-yl)propyl)carbamate (120 mg, 0.28 mmol, 1.0 equiv.) was dissovled in anhydrous DMF (3.5 mL) under nitrogen. Triethylamine (110 mg, 153 ∝L, 1.1 mmol, 4.0 equiv.), N-(3-ethynyl-4-methylphenyl)-3-(trifluoromethyl)benzamide (130 mg, 0.42 mmol, 1.5 equiv.), bis(triphenylphosphine)palladium(II) dichloride (9.8 mg, 0.014 mmol, 0.05 equiv.) and copper (I) iodide (5.3 mg, 0.028 mmol, 0.1 equiv.) were added to the above solution sequentially. The reaction was heated at 50 ˚C for overnight and then quenched with saturated NH4Cl (1 mL). The resulting mixture was diluted with ethyl acetate (200 mL) and the organic phase was washed with saturated NaHCO3 (30 mL), brine (30 mL) and then dried over anhydrous Na2SO4. Purification by flash chromatography on silica gel using a gradient of EtOAc/Hexane (0:100 to 60:40) afforded *tert*-butyl (3-(6-formyl-5-((2-methyl-5-(3-(trifluoromethyl)benzamido)phenyl) ethynyl)-7*H*-pyrrolo[2,3-*d*]pyrimidin-7-yl)propyl)carbamate as a pale brown solid (65 mg, 39%; Rf= 0.42 in EtOAc:Hexane= 3:2). ^{1}H-NMR (500 MHz, $CDCl_3$) δ= 10.26 (s, 1H), 9.19 (s, 1H), 9.02 (s, 1H), 8.72 (s, 1H), 8.16 (s, 1H), 8.10 (d, *J* = 7.8 Hz, 1H), 7.92 (s, 1H), 7.76 (d, *J* = 7.7 Hz, 1H), 7.58 (d, *J* = 6.6 Hz, 1H), 7.21 (d, *J* = 8.3 Hz, 1H), 5.33 (s, 1H), 4.68 (t, *J* = 6.0 Hz, 2H), 3.12 – 2.95 (m,

2H), 2.48 (s, 3H), 2.02 – 1.91 (m, 2H), 1.43 (s, 9H). MS (ESI, m/z) calculated for $C_{32}H_{30}F_3N_5O_4$ 605.2, $[M+H]^+$ found 606.2.

(*Z*)- or (*E*)-*tert*-butyl (3-(6-(3-amino-2-cyano-3-oxoprop-1-en-1-yl)-5-((2-methyl-5-(3-(trifluoromethyl)benzamido)phenyl)ethynyl)-7*H*-pyrrolo[2,3-*d*]pyrimidin-7-yl)propyl)carbamate (15)

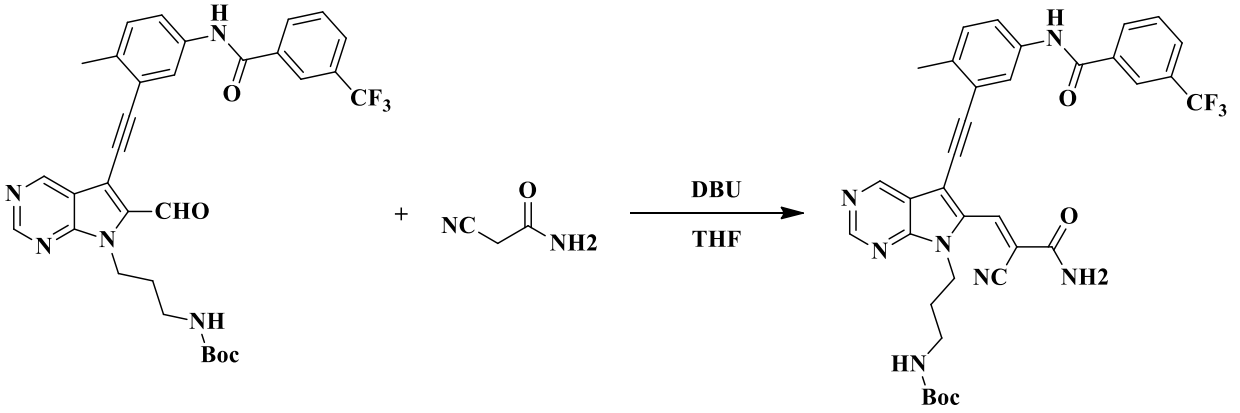

Tert-butyl (3-(6-formyl-5-((2-methyl-5-(3-(trifluoromethyl)benzamido)phenyl)ethynyl)-7*H*-pyrrolo[2,3-*d*]pyrimidin-7-yl)propyl)carbamate (33 mg, 0.054 mmol, 1.0 equiv.) and cyanoacetamide (5.4 mg, 0.065 mmol, 1.2 equiv.) were dissolved in anhydrous THF (1.0 mL). 1,8-Diazabicyclo[5.4.0]undec-7-ene (16 mg, 16 μL, 0.11 mmol, 2.0 equiv.) was added and the resulting mixture was stirred at room temperature for 25 mins. The reaction was quenched with saturated NH_4Cl solution and diluted with EtOAc (20 mL). The organic phase was washed with saturated $NaHCO_3$ (4 mL), brine (4 mL) and dried over anhydrous Na_2SO_4. Purification using preparative thin-layer chromatography developed with pure ethyl acetate afforded a mixture of (*Z*)- or (*E*)-*tert*-butyl (3-(6-(3-amino-2-cyano-3-oxoprop-1-en-1-yl)-5-((2-methyl-5-(3-(trifluoromethyl)benzamido)phenyl)ethynyl)-7*H*-pyrrolo[2,3-*d*]pyrimidin-7-yl)propyl)carbamate as a bright yellow solid powder (16 mg, 44%; R_f [(*E*) and (*Z*)-isomers)]= 0.48 in MeOH:DCM=

1:9).^{1}H-NMR (300 MHz, MeOD) δ= 9.18 (s, 1H), 9.06 (s, 1H), 8.96 (s, 1H), 8.90 (s, 1H), 8.42 (s, 2H), 8.28 (s, 2H), 8.22 (d, *J* = 7.8 Hz, 2H), 8.07 (s, 1H), 8.06 (s, 1H), 7.92 (d, *J* = 6.7 Hz, 1H), 7.89 (d, *J* = 6.7 Hz, 1H), 7.79 – 7.69 (m, 2H), 7.68 – 7.59 (m, 2H), 7.29 (d, *J* = 8.4 Hz, 2H), 5.12 (s, 2H), 4.58 – 4.38 (m, 4H), 3.13 – 2.98 (m, 4H), 2.54 (s, 6H), 2.11 – 1.91 (m, 4H), 1.42 (s, 18H); MS (ESI, m/z) calculated for $C_{35}H_{32}F_3N_7O_4$ 671.3, $[M+H]^+$ found 672.2.

(*E*)-cyclooct-4-en-1-yl (3-(6-((*E*)-3-amino-2-cyano-3-oxoprop-1-en-1-yl)-5-((2-methyl-5-(3-(trifluoromethyl)benzamido)phenyl)ethynyl)-7*H*-pyrrolo[2,3-*d*]pyrimidin-7-yl)propyl)carbamate or (*E*)-cyclooct-4-en-1-yl (3-(6-((*Z*)-3-amino-2-cyano-3-oxoprop-1-en-1-yl)-5-((2-methyl-5-(3-(trifluoromethyl)benzamido)phenyl)ethynyl)-7*H*-pyrrolo[2,3-*d*]pyrimidin-7-yl)propyl)carbamate (3-TCO)

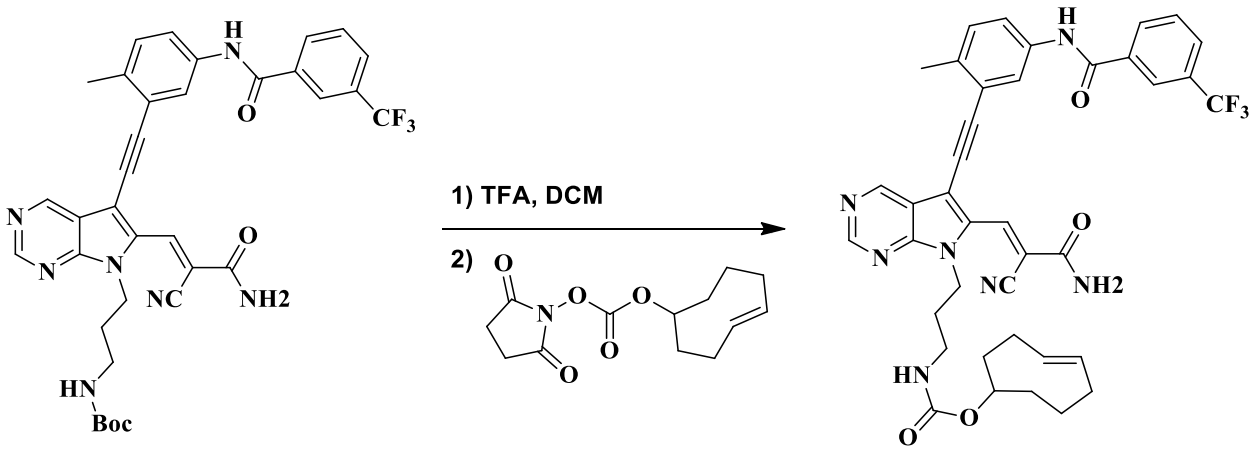

A mixture of (*Z*)- or (*E*)-*tert*-butyl (3-(6-(3-amino-2-cyano-3-oxoprop-1-en-1-yl)-5-((2-methyl-5-(3-(trifluoromethyl)benzamido)phenyl)ethynyl)-7*H*-pyrrolo[2,3-*d*]pyrimidin-7-yl)propyl)carbamate (16 mg, 0.024 mmol, 1.0 equiv.) was dissolved in a mixture of trifluoacetic acid (0.3 mL) and dichloromethane (0.7 mL). The reaction solution was stirred at room temperature for 30 mins and the solvent was removed in *vacuo*. The solid residue was dissolved in anhydrous tetrahydrofuran (1 mL). To the above solution was added diisopropylethylamine (22

mg, 30 μL, 0.17 mmol, 5.0 equiv.) and (*E*)-cyclooct-4-en-1-yl (2,5-dioxopyrrolidin-1-yl) carbonate (12 mg, 0.044 mmol, 1.3 equiv.) sequentially. The reaction was quenched with water (1 mL) after maintaining at room temperature overnight. The resulting mixture was then diluted with ethyl acetate (30 mL). The organic phase washed with saturated $NaHCO_3$ solution (5 mL), brine (5 mL), dried over anhydrous Na_2SO_4. Purification using flash chromatography on silica gel with a EtOAc/Hexane gradient (0:100 to 100:0) afforded a mixture of (*E*)-cyclooct-4-en-1-yl (3-(6-((*E*)-3-amino-2-cyano-3-oxoprop-1-en-1-yl)-5-((2-methyl-5-(3-(trifluoromethyl)benzamido)phenyl)ethynyl)-7*H*-pyrrolo[2,3-*d*]pyrimidin-7-yl)propyl)carbamate or (*E*)-cyclooct-4-en-1-yl (3-(6-((*Z*)-3-amino-2-cyano-3-oxoprop-1-en-1-yl)-5-((2-methyl-5-(3-(trifluoromethyl)benzamido)phenyl)ethynyl)-7*H*-pyrrolo[2,3-*d*]pyrimidin-7-yl)propyl)carbamate as a bright yellow powder (10 mg, 59% for 2 steps; Rf [(E) and (Z)-isomers)]= 0.50 in pure EtOAc) ^{1}H-NMR (500 MHz, MeOD) δ= 9.22 (s, 1H), 9.10 (s, 1H), 8.99 (s, 1H), 8.94 (s, 1H), 8.45 (s, 2H), 8.32 (s, 2H), 8.26 (d, *J* = 6.9 Hz, 2H), 8.13 (s, 1H), 7.99 (s, 1H), 7.94 (d, *J* = 6.0 Hz, 2H), 7.85 – 7.73 (m, 2H), 7.67 (d, *J* = 7.7 Hz, 2H), 7.34 (d, *J* = 8.0 Hz, 2H), 5.70 – 5.56 (m, 2H), 5.55 – 5.44 (m, 2H), 5.25 (s, 4H), 5.16 (s, 2H), 4.52 (s, 4H), 4.30 (s, 2H), 3.60 – 3.45 (m, 2H), 3.29 – 3.20 (m, 2H), 3.17 – 3.10 (m, 2H), 2.58 (s, 6H), 2.43 – 0.72 (m, 20H); MS (ESI, m/z) calculated for $C_{39}H_{36}F_3N_7O_4H$ (M+H) 724.2854, $[M+H]^+$ (HRMS) found 724.2842; HPLC purity: 98.2% (UV detector wavelength: 254 nm)

Expression and Purification of recombinant proteins

Recombinant Src expresssion

N-terminal His-tagged Src V284C and Src WT (residue 87-536) were expressed and purified accordingly to the Supplementary Information of *Mol. Cell* **2019**, *74*, p. 393-408 for primary profiling data.

Recombinant JNK2 expression

His-TEV+LIC-JNK2α2 WT and His-TEV+LIC-JNK2α2 V40C/M108T were expressed in *Escherichia coli* BL21(DE3) cells in LB Miller broth. JNK2α2 constructs were expressed in their inactive forms. Cells were grown to OD600 ~0.5 at 37 °C. The temperature was reduced to 18 °C and cells were induced 30 min after temperature reduction with 0.4 M isopropyl β-D-thiogalactoside. Expression occurred at 18 °C overnight. All purification steps were carried out at 4 °C. Cells were pelleted in 1L bottles via centrifugation at 6000 rpm. Cells were lysed with sonication in 2 mL/gram pellet weight of wash/lysis buffer consisting of 50 mM HEPES (pH = 7.5), 300 mM NaCl, 20 mM imidazole, 10% glycerol and 1 mM phenylmethylsulfonyl fluoride. The lysate was centrifuged at 10000 g for 20 min and the supernatant was allowed to batch bind for 60 min with 0.4 ml/L cell culture of Ni-NTA (Ni-nitrilotriacetate) resin. The resin was collected by centrifugation at 500 g for 5 min and washed with 20 mL of wash/lysis buffer per liter of culture. The wash step was repeated three times. The protein was eluted using ~5 mL of elution buffer (50 mM HEPES (pH 7.5), 300 mM NaCl, 200 mM imidazole and 10% glycerol) per liter of culture. Then, the eluate was dialyzed against 50 mM HEPES (pH = 7.5), 200 mM NaCl, 5% glycerol and 1 mM dithiothreitol (DTT) overnight. WT His-TEV+LIC-JNK2α2 was treated with TEV during

O.N. dialysis (2:25 wt:wt TEV:JNK2). The next day, the TEV cleaved WT JNK2α2 was allowed to bind to 1 mL of Ni-NTA slurry for 1 hr to remove the cleaved Hig tag and TEV. Cleaved JNK2α2 was rinsed from the resin with wash/lysis buffer. Constructs were dialyzed two additional times. The aliquoted proteins were flash-frozen and stored at −80 °C. Protein concentrations were determined using in-gel BSA standards.

Recombinant PAK1 expression

PAK1 V286C/M346T (residues 250-547) was cloned into the bacterial expression plasmid pMCSG7 as a N-terminal His-SUMO-tagged construct. The construct was transformed in *Escherichia coli* BL21(DE3) cells and plated on ampicillin selective plates. A single colony was picked and grown in an overnight culture of 50 mL of LB broth containing ampicillin. An 1 L culture was inoculated with the starter culture, grown to an OD600 of 0.8. The protein expression was then induced with 0.2 M IPTG at 18 ˚C. The next day, cells were harvested by centrifugation, lysed by sonication in lysis buffer (50 mM HEPES, pH = 8.0, 300 mM NaCl, 1 mM PMSF, 0.1% Triton-X, 20 mM imidazole), and centrifuged for 45 minutes at 10,000 rpm. Cleared lysates were incubated with 0.5 mL Ni-NTA resin (Thermo) for 1 h. The supernatant was then discarded, and beads were washed with 20 mL lysis buffer before bound protein was eluted with lysis buffer containing 300 mM imidazole. The eluted PAK1 V286C/M346T protein was dialyzed overnight at 4 ºC in dialysis buffer (50 mM Tris, pH = 8.0, 150 mM NaCl, 5% glycerol, 1 mM DTT). PAK1 WT was purchased from SignalChem (cat. no. P02-10BG-05).

Recombinant EphA2 expression

The genes of N-terminal His-tagged EphA2 V627C and EphA2 WT (residue 590-876) were cloned into the bacterial expression plasmid pMCSG7. The construct was transformed in *Escherichia coli* BL21(DE3) cells and plated on ampicillin selective plates. A single colony was picked and grown in an overnight culture of 50 mL of LB broth containing ampicillin. The starting culture was then transferred to an one liter LB corth, grown to an OD600 of 1.2. Next, protein expression was induced with 0.2 M IPTG at 18 ˚C. The next day, cells were harvested by centrifugation, lysed by sonication in lysis buffer (50 mM HEPES, 300 mM NaCl, 1 mM PMSF, 0.1% Triton-X, 20 mM imidazole, pH 8.0), and centrifuged for 45 min at 10,000 rpm. Cleared lysates were incubated with 0.5 mL Ni-NTA resin (Thermo) for 1 h. The supernatant was then discarded, and beads were washed with 20 mL lysis buffer before the bound protein was eluted with lysis buffer containing 300 mM imidazole. The Eluted His-tagged recombinant EphA2 proteins were dialyzed overnight at 4 ºC in dialysis buffer (50 mM Tris, pH = 8.0, 150 mM NaCl, 5% glycerol, 1 mM DTT).

Protocol of activity assays to determine Ki values of 1, 2, 3 and TCO probes.

Src activity assay

Enzyme inhibition of Src V284C-variant or wild-type recombinant Src constructs (residue 87-536) was determined using a fluorogenic assay using a self-reporting Src kinase substrate EEEIYGE-(DAP-Pyrene)-EA. **1**, **2**, **3**, or TCO-conjugated probes (3-fold dilution, initial concentration of probe in reaction= 30 ∝M) were assayed in triplicate against 12.5 nM of V284C-Src-3D or 7.5 nM of WT Src-3D in kinase reaction buffer ([HEPES]= 75 mM, pH= 8.0, [$MgCl_2$]= 15 mM, [EGTA]= 3.75 mM, [NaCl]= 150 mM, [BSA]= 0.2 mg/mL and [Na_3VO_4]= 750 nM). Src was incubated with inhibitors and ATP (1 mM) for 30 mins in a Corning® 384 well microplate (Low flange; product

number: CLS3573). Then 20 ∝M of fluorogenic substrate solution in kinase reaction buffer was added and incubated for 120 mins. Fluorescent emission readouts were measured at wavelength of 405 nm when excited at 344 nm using a Perkin Elmer Envision Plate Reader. Percentage of inhibition was calculated and IC50 values were determined using One site – Fit logIC_{50} model in GraphPad software Prism 7.

PAK1 activity assay

(*Pak1*) Pak1 WT and Pak1 V286C/M346T catalytic domains were catalytically active after expression in *E. coli* and purification. Pak1 WT (18 nM) and Pak1 V284C/M344T (35 nM) were incubated with **1**, **2** or **3** (initial concentration = 10 μM, 3-fold serial dilutions, 10 data points), 4 μM cold ATP, and 0.007 μCi/μL γ^{32}P-ATP for 30 min in assay buffer (76 mM HEPES, pH = 7.5, 5 mM $MgCl_2$, 150 mM NaCl, 3.8 mM EGTA, 0.2 mg/mL BSA, 150 uM Na_3VO_4, 1 mM BME) then PAKtide (sequence:RRRLSFAEPG) (final concentration = 0.2 mg/mL) was added. After incubating for 2-4 h, 4.6 ∝L of the reaction mixture were spotted onto phosphocellulose. Membranes were washed with 0.05% phosphoric acid (3x 10 min wash) and air-dried, and the radioactivity was determined by phosphor-imaging with a GE Typhoon FLA 9000 phosphor-scanner. Data was analyzed using GraphPad Prism software, and IC_{50} values were determined using "One-site fit logIC_{50}" option. All assays were performed in triplicate.

JNK2 activity assay

Activated JNKs were prepared and activated using purified, activated MKK4α. 2.5 μM JNK2 was pre-activated with 150 nM MKK4α for 1 hour at RT in (50 mM Tris/HCl, pH = 7.5, 0.01% (v/v) Tween 20, 10 mM MgCl2, 2 mM DTT, 1 mM EGTA, 0.1 mg/mL BSA) with 400 ∝M ATP.

To get an inhibitor dose response curve, an enzyme titration for JNK2 was first carried out in order to determine the linear working concentration of the enzyme. Inhibitors (initial concentration = 10 μM, 3-fold serial dilutions, 9 data points) were assayed in triplicate against kinases (JNK2 WT = 6.25 nM and JNK2 V40C/M108T = 0.5 nM; in assay buffer (50 mM Tris/HCl, pH = 7.5, 0.01% (v/v) Tween 20, 10 mM $MgCl_2$, 0.1 mM DTT, 1 mM EGTA, 0.1 mg/mL BSA). JNK2 was incubated with inhibitors 4 ∝M cold ATP, and 0.007 uCi/uL ATP-[γ^{32}P] for 30 mins in a 96-well plate. To initiate the reaction, myelin basic protein (MBP) was added, at a final concentration of 0.2 mg/mL. The reaction mixture was incubated in a volume of 30.2 μL per well, at room temperature, for 2 hours for JNK2 WT and 4 h for JNK2 V40C/M108T. To quench the reaction, 4.6 ∝l of the reaction mixture were spotted onto nitrocellulose, the membranes washed 3 times with 0.5% phosphoric acid and dried with acetone. Membranes were wrapped in plastic wrap and placed in a phosphor screen for autoradiography and exposed overnight. Phospho imaging was performed using a Typhoon FL 9000 instrument (GE Healthcare, Pittsburgh, PA). Data was analyzed using GraphPad Prism software, and IC_{50} values were determined using "One-site fit logIC_{50}" option. All assays were performed in triplicate.

EphA2 activity assay

2.5 nM of recombinant EphA2 (residue 590-876) was incubated with inhibitors (initial concentration = 30 μM, 3-fold serial dilutions, 10 data points) for 30 minutes at room temperature in reaction buffer ([HEPES]= 50 mM, pH= 7.5, [$MgCl_2$]= 10 mM, [EGTA]= 1 mM, Tween-20= 0.1%, [DTT]= 1mM, BSA= 0.5 mg/mL). The reaction mixture was then incubated with 0.0067 mCi/mL of $^{32}\gamma$-ATP and 2 mM of cold ATP at room temperature for 30 minutes. EphA2 substrate Poly Glu:Tyr= 4:1 (0.5 mg/mL) was added and the reaction was incubated at room temperature

for 4 hours. The reaction was terminated by spotting 4.6 ∝L of the reaction mixture onto a phosphocellulose membrane. The membrane was washed with 0.05% phosphor5ic acid three times (10 mins each) and dried by air. The concentration of radioactively labeled EphA2 substrate was determined by phosphor-imaging with a GE Typhoon FLA 9000 phosphor-scanner. The image was processed and quantified with Image StudioLite software, and data were analyzed using GraphPad Prism, and IC_{50} values were determined using "One-site fit logIC_{50}" option. All assays were performed in triplicate.

SH3 domain pulldown assay

10 ∝L of a 50% slurry (by volume) of O^6-benzylguanine-containing sepharose beads were washed with immobilization buffer ([Tris]= 50 mM, pH= 7.5, [NaCl]= 100 mM, [DTT]= 1 mM, [BSA]=0.2 mg/mL) (10 bed volumes for 3 times). The washed beads were incubated with 50 ∝L of SNAP-tagged-polyproline peptide (VSLARRPLPPLP) (8 ∝M) on an end-to-end rotator at ambient temperature for 1 hour. After immobilization of the polyproline peptide, the beads were washed with immobilization buffer (10-bed volumes for 3 times).

Meanwhile, a saturating amount of **1-TCO**, **2-TCO**, or **3-TCO** (3 ∝M or 5 ∝M) was added to 50 ∝L of a solution in immobilization buffer containing 25 nM of recombinant TAMRA-conjugated Src V284C.[63-64] The solution was incubated at ambient temperature for 30 mins before being added to the polyproline peptide beads. After incubating at ambient temperature for 1 hour, the flow-through was collected and the beads were washed with immobilization buffer (10-bed volumes for 3 times). The bead-bound Src was eluted by boiling the beads in 50 ∝L of 1x SDS loading buffer at 95 ˚C for 10 mins. Input (IN) and elution (EL) were processed using SDS-PAGE electrophoresis

and imaged on GE-Typhoon FLA 9000. Intensities of rhodamine fluorescence for each band was quantified using ImageStudio™ Lite. Percentage of Src bound to the polyproline-containing beads= Intensity(EL)/[Intensity(IN)+Intensity(EL)] × 100% was plotted using GraphPad software Prism 7.

Generation of Tetrazine-Beads

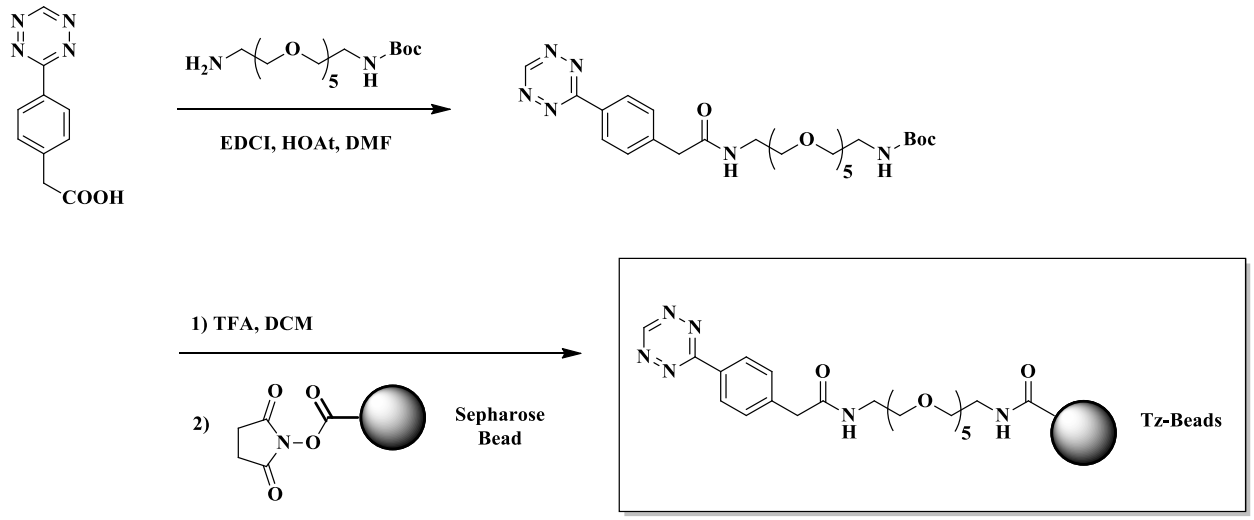

***Tert*-butyl (1-(4-(1,2,4,5-tetrazin-3-yl)phenyl)-2-oxo-6,9,12,15,18-pentaoxa-3-azaicosan-20-yl)carbamate**

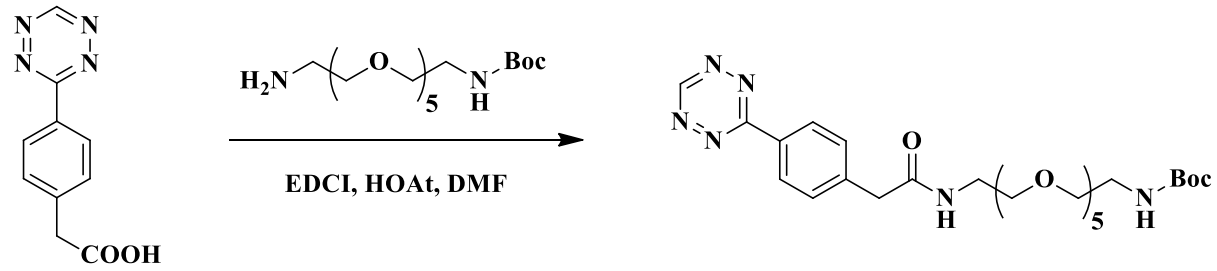

2-(4-(1,2,4,5-tetrazin-3-yl)phenyl)acetic acid (50 mg, 0.23 mmol, 1.0 equiv.), *tert*-butyl (17-amino-3,6,9,12,15-pentaoxaheptadecyl)carbamate (114 mg, 0.30 mmol, 1.3 equiv.) and 1-Hydroxy-7-azabenzotriazole (41 mg, 0.30 mmol, 1.3 equiv.) were dissolved in anhydrous DMF (3

mL). The solution was cooled to 0 ˚C and to it was added *N*-(3-Dimethylaminopropyl)-*N'*-ethylcarbodiimide hydrochloride (58 mg, 0.30 mmol, 1.3 equiv.). The reaction was allowed to warm to room temperature overnight. The solvent was removed in *vacuo* and the solid residue was dissolved in ethyl acetate (200 mL). The organic phase was washed with saturated KH_2PO_4 solution (30 mL), saturated $NaHCO_3$ solution (30 mL), brine (30 mL) and dried over anhydrous Na_2SO_4. Purification by flash chromatography on silica gel with a MeOH/EtOAc gradient (0:100 to 20:80) afforded *tert*-butyl (1-(4-(1,2,4,5-tetrazin-3-yl)phenyl)-2-oxo-6,9,12,15,18-pentaoxa-3-azaicosan-20-yl)carbamate as a bright pink solid (103 mg, 77%). ^{1}H-NMR (500 MHz, $CDCl_3$) δ= 10.22 (s, 1H), 8.59 (d, *J* = 7.9 Hz, 2H), 7.56 (d, *J* = 7.8 Hz, 2H), 6.69 (s, 1H), 5.12 (s, 1H), 3.68 (s, 2H), 3.67 – 3.43 (m, 22H), 3.32 – 3.26 (m, 2H), 1.43 (s, 9H); MS (ESI, m/z) calculated for $C_{27}H_{42}N_6O_8$ 578.3, $[M+H]^+$ found 479.5 (cleavage product of Boc-protection group - $COOC(CH_3)_3$); HPLC purity: 99.0% (UV detector wavelength: 254 nm)

Immobilization of tetrazine

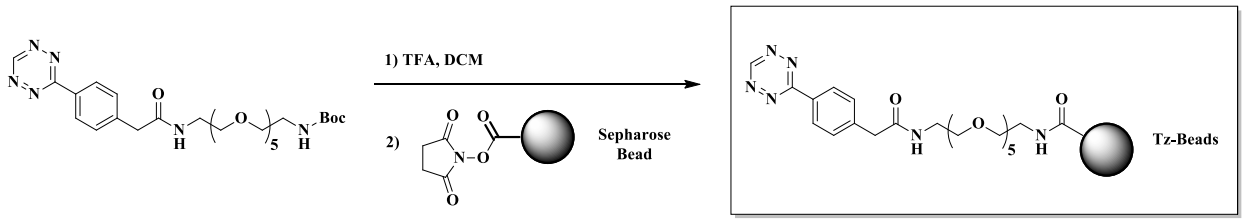

Tert-butyl (1-(4-(1,2,4,5-tetrazin-3-yl)phenyl)-2-oxo-6,9,12,15,18-pentaoxa-3-azaicosan-20-yl)carbamate (22 mg, 0.037 mmol, 1.0 equiv.) was dissolved in a mixture of trifluoroacetic acid (0.60 mL) and dichloromethane (1.4 mL). The solution was maintained at room temperature for 30 mins. After reaction, the solvent was removed in *vacuo* and the residue was dissolved in a mixture of EtOH (1.0 mL) and DMF (1.0 mL) as coupling solution. Meanwhile, a 50% slurry of NHS-activated Fast Flow sepharose beads (1.0 mL) were quickly washed three times with a mixed

solvent consisting of EtOH and DMF (EtOH:DMF=1:1; use 1.0 mL for each wash) in 2-mL Pierce Centrifuge Columns (Thermo Scientific). The drained beads were resuspended in the coupling solution (2 mL) and to it was added triethylamine (50 ∝L). The pH was of the supernatant was tested and adjusted to 7-8 with triethylamine if necessary. The reaction was agitated on a tube rotator at 4 ˚C overnight. On the second day, the beads were drained and washed three times with a mixed solvent consisting of EtOH and DMF (EtOH:DMF=1:1; use 1.0 mL for each wash), followed by three quick washes with an acid solution ([total CH3COOH/NaOOCCH3]= 0.1 M, [NaCl]= 0.5 M, pH=4.0) and a basic solution ([Tris-HCl]= 0.1 M, [NaCl]= 0.5 M, pH= 8.0) (1 mL for each wash). The beads were then washed three times with 20% EtOH in water (1 mL for each wash) and stored as 50% slurry in 20% EtOH in water.

Generation of sepharose beads for pre-clearing lysates

1 mL of 50% slurry of NHS-activated Fast Flow sepharose beads were quickly washed three times with a mixed solvent consisting of EtOH and DMF (EtOH:DMF=1:1; use 1.0 mL for each wash) in 2-mL Pierce Centrifuge Columns (Thermo Scientific). The washed beads were resuspended in a mixture of EtOH (1 mL) and DMF (1 mL) containing 150 mM ethanolamine. The reaction mixture was agitated on a tube rotator at 4˚C overnight. The reaction was agitated on a tube rotator at 4 ˚C overnight. On the second day, the beads were drained and washed three times with a mixed solvent consisting of EtOH and DMF (EtOH:DMF=1:1; use 1.0 mL for each wash), followed by three quick washes with an acid solution ([total CH3COOH/NaOOCCH3]= 0.1 M, [NaCl]= 0.5 M, pH=4.0) and a basic solution ([Tris-HCl]= 0.1 M, [NaCl]= 0.5 M, pH= 8.0) (1 mL for each wash). The beads were then washed three times with 20% EtOH in water (1 mL for each wash) and stored as 50% slurry in 20% EtOH in water.

Procedure for Enriching Probe-Bound Target in Cell Lysates

Cell culture and generation of cell lysates: HEK293 cells were grown on 10-cm plates in Dulbecco's Modified Eagle's Medium (DMEM) supplemented with 10% (by volume) Fetal Bovine Serum (FBS) at 37 ˚C in a humidified incubator containing 5% CO_2 until 90% confluence. Cells were washed with ice-cold DPBS once and lysed with 500 ∝L of ice-cold lysis buffer. Cell lysates were centrifuged at 17,000 × g for 10 minutes at 4 ˚C and were quantified using Pierce™ 660nm Protein Assay Reagent and diluted to 1.5 mg/mL with ice-cold lysis buffer.

TCO probe treatment: Recombinant 3D construct of Src V284C or Src WT were added to the diluted HEK293 cell lysates to a final concentration of 100 nM. 1 ∝L of **1-TCO**, **2-TCO**, or **3-TCO** solution (100× solution in DMSO) was added to 100 ∝L of the lysate (DMSO%= 1% in final solution). Lysates mixture was incubated with **TCO** probe for 30 minutes at 4 ˚C on an end-to-end rotator.

Capture probe-bound target using Tz-Beads: 5 ∝L (volume of drained beads) of Tz-Beads were added to a 200 ∝L tube and washed with ice-cold lysis buffer (three times; 100 ∝L for each wash). 100 ∝L of TCO probe-treated lysates mixture was added to the washed Tz-Beads and was gently incubated on an end-to-end rotator for 30 mins (or the indicated amount of time in Figure 3G) at 4 ˚C. After incubation with Tz-Beads, the flow-through was quickly removed by aspiration. The beads were then washed for three times with ice-cold Washing Buffer **1** (100 ∝L for each wash) by gently inverting the tube for four times. The probe-bound target should be bound to Tz-Beads by the end of this step.

Elute enriched probe-bound target and Western blot analysis: The sepharose matrix was incubated with 100 ∝L of Lysis Buffer containing 2% SDS (by weight) for 20 mins at 25 ˚C with agitation. The eluted proteins were separated using SDS-PAGE gel electrophoresis, transferred onto nitrocellulose membranes and immunoblotted with corresponding primary antibodies. The nitrocellulose membranes were imaged on LI-COR Odyssey IR imager.

Enrichment of probe-bound Src kinase complex from live mammalian cell

Cell culture and TCO probe treatment:

(***Condition a: Serum starvation***) Hela cells that stably overexpressed full-length wild-type Src and V284C variant of Src were grown on 10-cm plates in Dulbecco's Modified Eagle's Medium (DMEM) supplemented with 10% (by volume) Fetal Bovine Serum (FBS) at 37 ˚C in a humidified incubator containing 5% CO_2 until 90% confluence, and was serum-starved for 24 hours prior to the assay. Expression of Src WT and Src V284C was induced by addition of Doxycycline (1 ∝g/mL) 24 hours prior to the assay. Click probes were added to the cells by replacing medium with fresh DMEM (5 mL) containing **1-TCO** (5 ∝M; DMSO%= 0.1% in final medium) or **2-TCO** (2.5 ∝M; DMSO%= 0.1% in final medium). Cells were incubated with **1-TCO** or **2-TCO** for 30 minutes at 37 ˚C in the incubator and the medium was removed immediately after incubation. The cells were quickly washed with ice-cold Dulbecco's Phosphate-Buffered Saline (DPBS) (5 mL, one time) and immediately lysed with ice-cold Lysis Buffer (500 ∝L). Cells were scrapped into pre-chilled 1.5-mL Eppendorf tubes and were centrifuged at 17,000 × g for 20 minutes at 4 ˚C. The supernatant of lysates was collected, and protein concentration was measured using Pierce 660 nm Protein Assay. The protein concentration of lysates was diluted to 1.5 mg/mL with ice-cold lysis buffer.

(***Condition b: Complete medium (DMEM)***) Hela cells that stably overexpressed full-length wild-type Src and V284C variant of Src were grown on 10-cm plates in Dulbecco's Modified Eagle's Medium (DMEM) supplemented with 10% (by volume) Fetal Bovine Serum (FBS) at 37 ˚C in a humidified incubator containing 5% CO_2 until 90% confluence. Expression of Src WT and Src V284C was induced by addition of Doxycycline (1 ∝g/mL) 24 hours prior to the assay. Click probes were added to the cells by replacing medium with fresh DMEM (5 mL) containing 10% FBS and **1-TCO** (5 ∝M; DMSO%= 0.1% in final medium) or **2-TCO** (2.5 ∝M; DMSO%= 0.1% in final medium). Cells were incubated with **1-TCO** or **2-TCO** for 30 minutes at 37 ˚C in the incubator and the medium was removed immediately after incubation. The cells were quickly washed with ice-cold Dulbecco's Phosphate-Buffered Saline (DPBS) (5 mL, one time) and immediately lysed with ice-cold Lysis Buffer (500 ∝L). Cells were scrapped into pre-chilled 1.5-mL Eppendorf tubes and were centrifuged at 17,000 × g for 20 minutes at 4 ˚C. The supernatant of lysates was collected, and protein concentration was measured using Pierce 660 nm Protein Assay. The protein concentration of lysates was diluted to 1.5 mg/mL with ice-cold lysis buffer.

(***Condition c: Growth factor***) Hela cells that stably overexpressed full-length wild-type Src and V284C variant of Src were grown on 10-cm plates in Dulbecco's Modified Eagle's Medium (DMEM) supplemented with 10% (by volume) Fetal Bovine Serum (FBS) at 37 ˚C in a humidified incubator containing 5% CO_2 until 90% confluence, and was serum-starved for 24 hours prior to the assay. Expression of Src WT and Src V284C was induced by addition of Doxycycline (1 ∝g/mL) 24 hours prior to the assay. Click probes were added to the cells by replacing medium with fresh DMEM (5 mL) containing 10% FBS and **1-TCO** (5 ∝M; DMSO%= 0.1% in final medium) or **2-TCO** (2.5 ∝M; DMSO%= 0.1% in final medium). Cells were incubated with **1-TCO** or **2-TCO** for 30 minutes at 37 ˚C in the incubator. The medium was then immediately

replaced with 5 mL of DMEM containing 10% FBS and EGF (100 ng/mL). After 10 minutes, the medium was removed immediately. The cells were quickly washed with ice-cold Dulbecco's Phosphate-Buffered Saline (DPBS) (5 mL, one time) and immediately lysed with ice-cold Lysis Buffer (500 ∝L). Cells were scrapped into pre-chilled 1.5-mL Eppendorf tubes and were centrifuged at 17,000 × g for 20 minutes at 4 ˚C. The supernatant of lysates was collected, and protein concentration was measured using Pierce 660 nm Protein Assay. The protein concentration of lysates was diluted to 1.5 mg/mL with ice-cold lysis buffer.

(***Condition d: Fibronectin***) 10-cm petri dish plates (Petri Dishes with Clear Lid. Thermo Fisher, catalog No. FB0875712) were treated with 5 mL of 10 ∝g/mL of Fibronectin solution in DPBS for 1 hour at 37 ˚C. The plates were washed with DPBS once before usage. Hela cells that stably overexpressed full-length wild-type Src and V284C variant of Src were grown on 10-cm fibronectin-coated plates in Dulbecco's Modified Eagle's Medium (DMEM) supplemented with 10% (by volume) Fetal Bovine Serum (FBS) at 37 ˚C in a humidified incubator containing 5% CO_2 until 90% confluence. Expression of Src WT and Src V284C was induced by addition of Doxycycline (1 ∝g/mL) 24 hours prior to the assay. Click probes were added to the cells by replacing medium with fresh DMEM (5 mL) containing 10% FBS and **1-TCO** (5 ∝M; DMSO%= 0.1% in final medium) or **2-TCO** (2.5 ∝M; DMSO%= 0.1% in final medium). Cells were incubated with click probes for 30 minutes at 37 ˚C in the incubator. The cells were quickly washed with ice-cold Dulbecco's Phosphate-Buffered Saline (DPBS) (5 mL, one time) and immediately lysed with ice-cold Lysis Buffer (500 ∝L). Cells were scrapped into pre-chilled 1.5-mL Eppendorf tubes and were centrifuged at 17,000 × g for 20 minutes at 4 ˚C. The supernatant of lysates was collected, and protein concentration was measured using Pierce 660 nm Protein Assay. The protein concentration of lysates was diluted to 1.5 mg/mL with ice-cold lysis buffer.

Capture probe-bound kinase complexes using Tz-Beads: For each co-clickable precipitation experiment, 15 ∝L (volume of drained beads) of Tz-Beads were added to a 1.5-mL Eppendorf tube and were washed with ice-cold lysis buffer (three times; 400 ∝L for each wash). 750 ∝g of protein lysates (1.5 mg/mL) was added to Tz-Beads (500 ∝L) and was gently incubated on an end-to-end rotator for 30 mins at 4 ˚C. To reduce background contaminants, lysates were pre-cleared by incubating with 15 ∝L (volume of drained beads) of sepharose beads coupled to ethanolamine for 1 hour at 4 ˚C prior to incubation with Tz-beads. After incubation with Tz-Beads, the flow-through was quickly removed by aspiration. The beads were then washed with ice-cold Washing Buffer **1** by gently inverting the tube for four times (three times; 400 ∝L for each wash), followed by washing with Washing Buffer **2** by gently inverting the tube for four times (three times; 400 ∝L for each wash). The bait protein and its interactors should be enriched and bound to the Tz-Beads by the end of this step.

***Characterization of kinase complex using Western-blot analysis*:** To detect the components of proteins enriched by Tz-Beads using Western-blot analysis, the beads were incubated with Lysis Buffer containing 2% SDS (by weight) for 20 mins (three times; 40 ∝L for each elution) at 25 ˚C with frequent agitation. The elutions were collected. The eluted proteins were processed using SDS-PAGE gel electrophoresis, transferred onto nitrocellulose membranes and immunoblotted with corresponding primary antibodies. The western-blots were imaged on LI-COR Odyssey IR imager.

***On-bead tryptic digestion of kinase complexes for tandem mass spectrometry analysis*:** To detect enriched bait and interactors using LC/MS, the washed beads were resuspended in 50 ∝L of Denaturing Buffer and were boiled at 95 ˚C for 5 minutes. After cooling down, 100 mM TEAB (50 ∝L) was added. The pH value was adjusted to 8 to 9 by adding NaOH (1 M). Lys-c Lysyl

Endopeptidase (1 ∝g) was then added and incubated with the beads at 37 ˚C for 2 hours in a thermal mixer agitating at 1,400 rpm. After incubation, the suspension was diluted with 100 mM TEAB (100 ∝L) and MS Grade Trypsin (1 ∝g) was added. pH was adjusted to 8 to 9. The beads were incubated with Trypsin overnight at 37 ˚C in a thermal mixer agitating at 1,400 rpm. After incubation, Buffer A (200 ∝L) was added to the beads and trypsin was quenched by adjusting the pH to 2 to 3 using formic acid. The resulting supernatant was desalted on C18 StageTip and washed once by buffer A (50 ∝L). The tryptic peptides were eluted off the C18 StageTip using buffer B (50 ∝L). The eluted solution was dried in speed-vac and then reconstituted with buffer A (20 ∝L) for LC/MS analysis.

Proteomic Data Acquisition, Process and Visualization of Target Interactome.

Proteomic Data Acquisition: Peptides were separated on a nanoAcquity UPLC instrument with 12 cm long fused silica capillary column (Polymicro Technologies Flexible Fused Silica Capillary Tubing, Inner Diameter 75 ∝m, Outer Diameter 375 ∝m, cat. no. 1068150019) made in-house with a laser puller and packed with 5 ∝m 120 Å reversed phase C18 beads (ReproSil-Pur 120 C18-AQ, Dr. Maisch GmbH HPLC, cat. no. r15.aq.). The LC gradient was 90 min long with 10-35% B at 200 nL/min. LC solvent A was 0.1% acetic acid and LC solvent B was 0.1% acetic acid, 99.9% acetonitrile. MS data were collected with a Thermo Scientific Orbitrap Fusion Tribrid mass spectrometer.

Proteomic Data Process: Raw data were analyzed using MaxQuant and search engine Andromeda using the following default settings: Multiplicity was set to 1; Digestion was set to trypsin/P; Variable modifications were set to Oxidation (M) and Acetyl (Protein N-term); LFQ minimal ratio count was set to 2; LFQ minimal number of neighbors set to 3; LFQ average number of neighbors set to 6; MS/MS spectra were searched against the UniProt human database (updated July 22nd, 2015); False discovery rate (FDR) was set to 0.01; First search and MS/MS search mass tolerance was set to 10 ppm; The data in the Protein Groups result table was processed with Perseus software. MaxQuant intensity values of identified proteins were used for all downstream analysis. We only consider proteins identified if MaxQuant was able to compute corresponding protein intensity values. Identified proteins that were classified as “only identified by site”, “reverse”, or “contaminant” were filtered and removed from the table. Proteins with 1 or fewer peptide counts

were filtered and removed. All intensity values were transformed based on log2 algorithm. Missing protein intensity values for identified proteins were imputed using Perseus by sampling from a distribution downshifted by 1.3 and having a width of 0.2[46, 65]. Imputed values are reported in the SI-Excel file 1. P-value was calculated using two-tailed, two-sample T-test. Enrichment scores ($\log_2$[intensity (Src V284C-expressing)/intensity (Src WT-expressing)]) were calculated using the relative intensity values from Src V284C- and WT-expressing cells with confidence values (-$\log_{10}$(P-value)) for each identified protein. We defined significant interactors as protein hits with an enrichment score ≥ 1.0 and a confidence value ≥ 1.4.

Visualization of Target Interactome: The list of gene names for significant Src interactors were uploaded to STRING: functional protein association networks database (version 10.5). The organism was set to *Homo sapiens*. The meaning of network edges was set to the confidence of the interaction, where the line thickness indicates the strength of data support as calculated by the STRING network database.[47] The edge confidence was indicated in Figure 4E. The minimum required interaction score is 0.400. The colored nodes represent query proteins. Each node represents all the proteins produced by a single, protein-coding gene locus. The splice isoforms or post-translational modifications are collapsed into the same node.

Clickable Proximity Ligation Assays (PLA).

Cell seeding: 40 ∝L of 0.8×10^5 cells/mL of Hela cells expressing Src-V284C or Src-WT were plated in Grace Bio-labs CultureWell chambered coverglass (8 wells, well diam. × thickness 6 mm × 1 mm, well volume 15-30 μL; Sigma-Aldrich; Catalog number: GBL103380) in DMEM supplemented with 10% FBS. The cells were then incubated until reaching 30-40% confluency in a humidified incubator at 37 ˚C containing 5% CO_2; **(for Figure 6D)** Prior to cell seeding, chambered coverglass was incubated with 40 ∝L of 1 mg/mL Fibronectin solution for 30 minutes at 37 ˚C for 30 mins and then rinsed with DPBS once. 40 ∝L of 0.8×10^5 cells/mL of Hela cells expressing Src-V284C or Src-WT were plated in Grace Bio-labs CultureWell chambered coverglass (8 wells, well diam. × thickness 6 mm × 1 mm, well volume 15-30 ∝L; Sigma-Aldrich; Catalog number: GBL103380) in DMEM supplemented with 10% FBS. The cells were then incubated until reaching 30-40% confluency in a humidified incubator at 37 ˚C containing 5% CO_2

Probe treatment: Cells were treated with 50 ∝L of 1-TCO (5 ∝M), 2-TCO (2.5 ∝M) or 3-TCO (10 ∝M) in DMEM supplemented with 10% FBS for 30 minutes.

Cell fixation and permeabilization: After incubation, the cells were gently washed with warm DPBS (40 ∝L) once and fixed with 40 ∝L of 4% paraformaldehyde for 15 minutes at room temperature. To quench the remaining para-formaldehyde, cells were then incubated with 40 ∝L of 125 mM of Glycine in DPBS for 5 mins. After washing with DBPS once, the cells were permeabilized using DPBS containing 0.75% Tween-20 and 0.75% Igepal CA-630 for 60 minutes at room temperature in a coplin jar on a shaker. The cells were then washed with DBPS once for 5 minutes at room temperature.

Click chemistry: Cells were treated with 40 ∝L of 500 nM Tetrazine-conjugated OregonGreen488 in DPBS for 10 minutes at room temperature. After the click chemistry reaction, the reaction

solution was removed from chambered coverglass and the cells were washed with DPBS for 5 minutes. The washing step was repeated for six times in total.

Blocking and treatment with primary antibodies: Cells were blocked with blocking buffer (Sigma Duolink buffer) at 37 ˚C for 1 hour. After blocking, blocking buffer was aspirated and cells were then treated with 40 ∝L of a solution consisted of primary antibodies in Antibody Dilution Buffer (Sigma Duolink) for OregonGreen488 (anti-fluorescein/OregonGreen goat IgG fraction; Life technologies; Catalog number: A11095) and Src(anti-Src (36D10) Rabbit mAb; Cell Signaling Technology; Catalog #: 2109), EEA1 (anti-EEA1 (C45B10) Rabbit mAb; Cell Signaling Technology; Catalog #: 3288) or FAK (anti-FAK (D5O7U) XP Rabbit mAb; Cell Signaling Technology; Catalog #: 71433) at 4 ˚C overnight. After incubation, the cells were washed with Wash Buffer A (Sigma Duolink) for 5 minutes twice in a coplin jar on a shaker.

Treatment with secondary antibodies and proximity ligation: Cells were then treated with 40 ∝L of a solution containing Duolink in situ rabbit PLUS probes and Duolink in situ goat MINUS probes in Antibody Dilution Buffer at 37 ˚C for 1 hour. After incubation, the cells were washed with Wash Buffer A for 5 minutes for three times. 40 ∝L of Ligation solution containing DNA ligase in ligation buffer was added to the cells. Cells were incubated with ligase for 30 minutes at 37 ˚C. After DNA ligation, cells were washed with Wash Buffer A for 5 minutes twice. For rolling cycle amplification, cells were treated with 40 ∝L of amplification buffer consisted of Polymerase and polymerase buffer (Sigma Duolink In Situ Detection Reagents Orange; Catalog #: DUO92007) for exactly 100 minutes at 37 ˚C. After incubation, the cells were washed with Wash Buffer B for 10 minutes twice at room temperature in a coplin jar on a shaker. The excess wash solution was removed. To stain nuclei, one drop of the Duolink In Situ mounting media containing DAPI was added to each well and the coverglass was mounted to a glass coverslip.

Imaging, data acquisition, and analysis: Cells were imaged using a Leica SP8X Confocal microscope equipped with a 63X objective (oil objective). Nuclei were imaged using laser excitation at 405 nm with 5% laser power. PLA puncta were imaged using laser excitation at 554 nm with 10% laser power. The number of PLA punctae was quantified using ImageJ software as following: Firstly, images were smoothened. Secondly, threshold was manually selected to discriminate PLA puncta from background fluorescence. Once selected, the threshold was applied uniformly to all images in the same sample set. The number of PLA puncta in each image was quantified using "Analyze Particles" function with the particle size of "0.75 $\propto m^2$-200 $\propto m^2$". The number of cells in each image was quantified using the number of nucleus. As an assay readout, the number of PLA puncta per cell was calculated. All data were visualized in violin plots using GraphPad Prism software.

3 How ATP-Competitive Inhibitors Allosterically Modulate Tyrosine Kinases That Contain a Src-like Regulatory Architecture (Chapter III)

3.1 Introduction

The human genome encodes ~540 eukaryotic protein kinases, an indication of the vast number of kinase-mediated cellular functions.[1] All kinases contain at least one highly homologous catalytic domain (CD) that is of similar overall architecture. Almost half of all protein kinases contain at least one auxiliary domain outside of the CD.[12] Precise regulation of these multidomain kinases often relies on intramolecular interactions between the CD and auxiliary domains. Intramolecular regulation of kinase phosphotransferase activity is pervasive—regulatory domains can allosterically modulate phosphotransferase activity by engaging and suppressing the CD intramolecularly.[66-67] In many cases, the global conformational changes within these regulatory domains also facilitate important phosphotransferase-independent functions in cells, including regulating protein scaffolding, localization, and gene transcription.[3, 68-69]

Src-family kinases (SFKs) are one of the best-characterized multidomain kinase families.[70-73] SFKs contain a membrane-interacting SH4 domain, a unique domain, and regulatory SH2 and SH3

domains that modulate the phosphotransferase activities of their CDs. Domains outside of the CD also provide additional binding surfaces for facilitating protein-protein interactions (**Figure 3-1A**).[74-75] In the inactive form, SFKs adopt a closed global conformation, where the phosphotransferase activity of the CD is allosterically suppressed by multiple intramolecular interactions: the SH3 domain's interaction with the SH2-CD linker, the SH2 domain's interaction with the phosphorylated C-terminal tail, and the SH4 domain's interaction with the C-lobe of the CD. Upon activation, these autoinhibitory, intramolecular interactions are released and SFKs adopt a more open global conformation with enhanced phosphotransferase activity.[76-77]

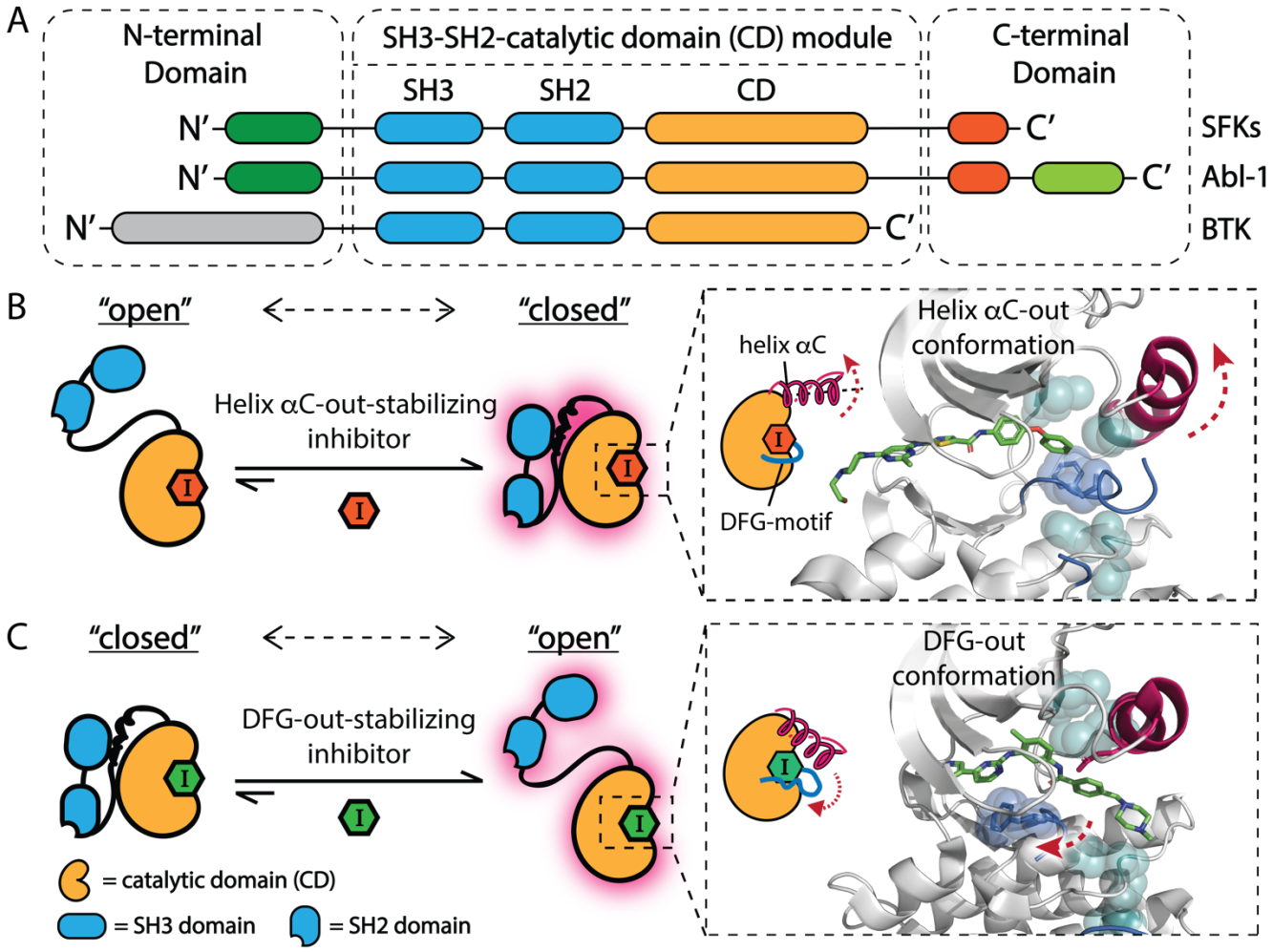

Figure 3-1**.** Allosteric modulation of tyrosine kinases that contain an SH3-SH2-catalytic domain (CD) module.

(A) Domain arrangement of Src-family kinases (SFKs), Abl-1, and BTK. (B-C) ATP-competitive, conformation-selective inhibitors can modulate the global conformation of SFKs. (B) Helix αC-out-stabilizing inhibitors promote a closed global conformation of Src's SH3-SH2-CD module by stabilizing the ATP-binding site in the helix αC-out form (PDB: 4YBK).[78] Shown are the catalytic spine (cyan), helix αC (magenta), and the activation loop (blue). (C) DFG-out-stabilizing inhibitors promote an open global conformation of Src's SH3-SH2-CD module by stabilizing the ATP-binding site in the DFG-out conformation (PDB: 2OIQ).[79]

Interdomain regulatory interactions suppress the phosphotransferase activity of SFKs by allosteric stabilization of an inactive conformation of the ATP-binding site, which misaligns the key catalytic residues for catalysis.[69, 80] We and others have shown that ATP-competitive inhibitors that stabilize different ATP-binding site conformations can exploit these allosteric networks to modulate the regulatory interactions of the SH3-SH2-CD module of SFKs.[17-19, 76, 78, 81-83] Inhibitors that stabilize the helix αC-out inactive conformation of the ATP-binding site, which involves outward movement of the catalytically important helix αC (**Figure 3-1B**), promote an autoinhibited, closed global conformation of the SH3-SH2-CD module of SFKs. The presence of an extended substituent that occupies the hydrophobic pocket formed by the displacement of helix αC is necessary for inhibitors to stabilize this inactive conformation. In contrast, inhibitors that stabilize the DFG-out inactive ATP-binding site conformation, which involves the displacement of the DFG-motif in the activation loop, promote an open, regulatory domain disengaged conformation of the SH3-SH2-CD module (**Figure 3-1C**). Despite extensive biochemical and structural

characterization, the ATP-binding site contacts that are directly responsible for the divergent effects that helix αC-out- and DFG-out-stabilizing inhibitors have on the global conformations of SFKs are not completely known.

It is also unclear how general the effects of conformation-selective inhibitors are on kinase conformation beyond the SFKs. Structural analysis of the Abelson tyrosine kinase 1 (Abl-1), which contains a Src-like SH3-SH2-CD module, have demonstrated that ATP-competitive inhibitors can also modulate the global conformation of Abl-1.[84-87] Specifically, the ability of inhibitors to flip the DFG-motif in the activation loop correlates with their abilities to promote an open global conformation of Abl-1's SH3-SH2-CD module.[88] Beyond the SFKs and Abl-1/Arg, there are at least 10 additional tyrosine kinases that contain an SH3-SH2-CD module (**Figure 3-2**).[89] It is currently unknown whether inhibitors that stabilize the DFG-out and helix αC-out inactive ATP-binding site conformations can also allosterically modulate the global conformation of SH3-SH2-CD modules of tyrosine kinases beyond the SFKs.

In this study, we describe the development of chemical probes that allow us to deconvolute which features in the ATP-binding site are responsible for the allosteric modulation of the SH3-SH2-CD module of Src. With these probes, we found that the ability of an inhibitor to allosterically modulate the global conformation of Src's SH3-SH2-CD module depends mainly on its influence on the conformation of helix αC. Thus, the observed ability of DFG-out-stabilizing inhibitors to promote an open global conformation of Src is not due to their influence on the DFG-motif in the activation loop but rather their ability to stabilize an active conformation of helix αC. Using these design principles, we developed a new probe that can be used with a drug-sensitized Src variant to

specifically stabilize Src's helix αC in the active conformation without perturbing its activation loop. Using this chemical genetic approach, we found that stabilizing Src's helix αC in an active conformation was sufficient to promote a Src-dependent phosphotransferase-independent alteration in cell morphology. Finally, we report that ATP-competitive, conformation-selective inhibitors can divergently modulate the global conformation of the SH3-SH2-CD module of tyrosine kinases beyond the SFKs. Taken together, our biochemical and cellular data strongly suggest that the ability of inhibitors to influence the conformation of helix αC is the main molecular determinant for allosterically modulating the global conformation of tyrosine kinases that contain an SH3-SH2-CD module.

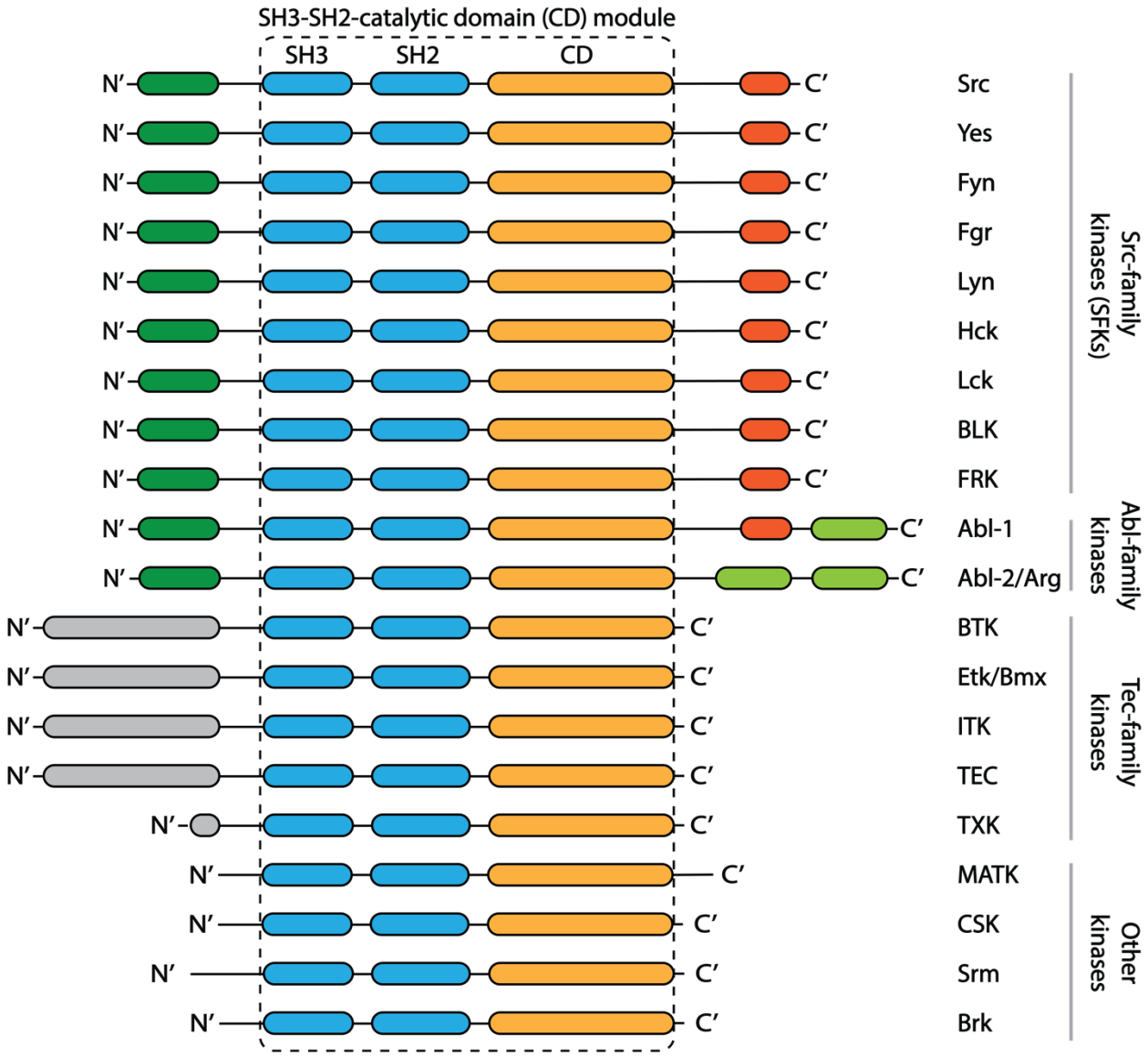

Figure 3-2. Domain organization of multidomain tyrosine kinases that contain Src-like SH3-SH2-CD modules.

3.2 Results and Discussion

3.2.1 Inhibitors divergently modulate the global conformation of tyrosine kinases that contain an SH3-SH2-CD module.

Prior to exploring the molecular details of how inhibitors influence the global conformation of the SH3-SH2-CD module, we first explored whether the divergent allosteric modulation we observed with the SFKs extended beyond this kinase family. To explore the pervasiveness of this effect, we characterized how stabilizing the DFG-out and helix αC-out ATP-binding site conformations affect the regulatory domains of Abl-1, the best-characterized member of Abl family kinases, and BTK, a Tec family kinase.

To modulate the ATP-binding sites of tyrosine kinases, we generated two inhibitors that stabilize the helix αC-out and DFG-out inactive conformations, respectively. Inhibitor **1** contains an extended 4-phenoxyphenyl substituent at the C-3 position on the pyrazolopyrimidine scaffold that occupies a hydrophobic pocket created by the outward movement of helix αC (**Figure 3-3**, *left*).[17-18, 76, 90] Inhibitor **2** stabilizes the DFG-out inactive conformation of tyrosine kinases (**Figure 3-3**, *right*). Inhibitor **2** contains a 3-trifluoromethylbenzamide substituent that occupies the hydrophobic pocket formed by the displacement of the DFG-motif.[76, 91] The conformationally rigid alkynylphenyl linker of **2** is most likely only compatible with DFG-out inactive conformation. Since **1** and **2** only differ at their C-3 substituents, the effects on the regulatory domains of tyrosine kinases should be due to each inhibitor stabilizing the desired inactive ATP-binding site conformation.

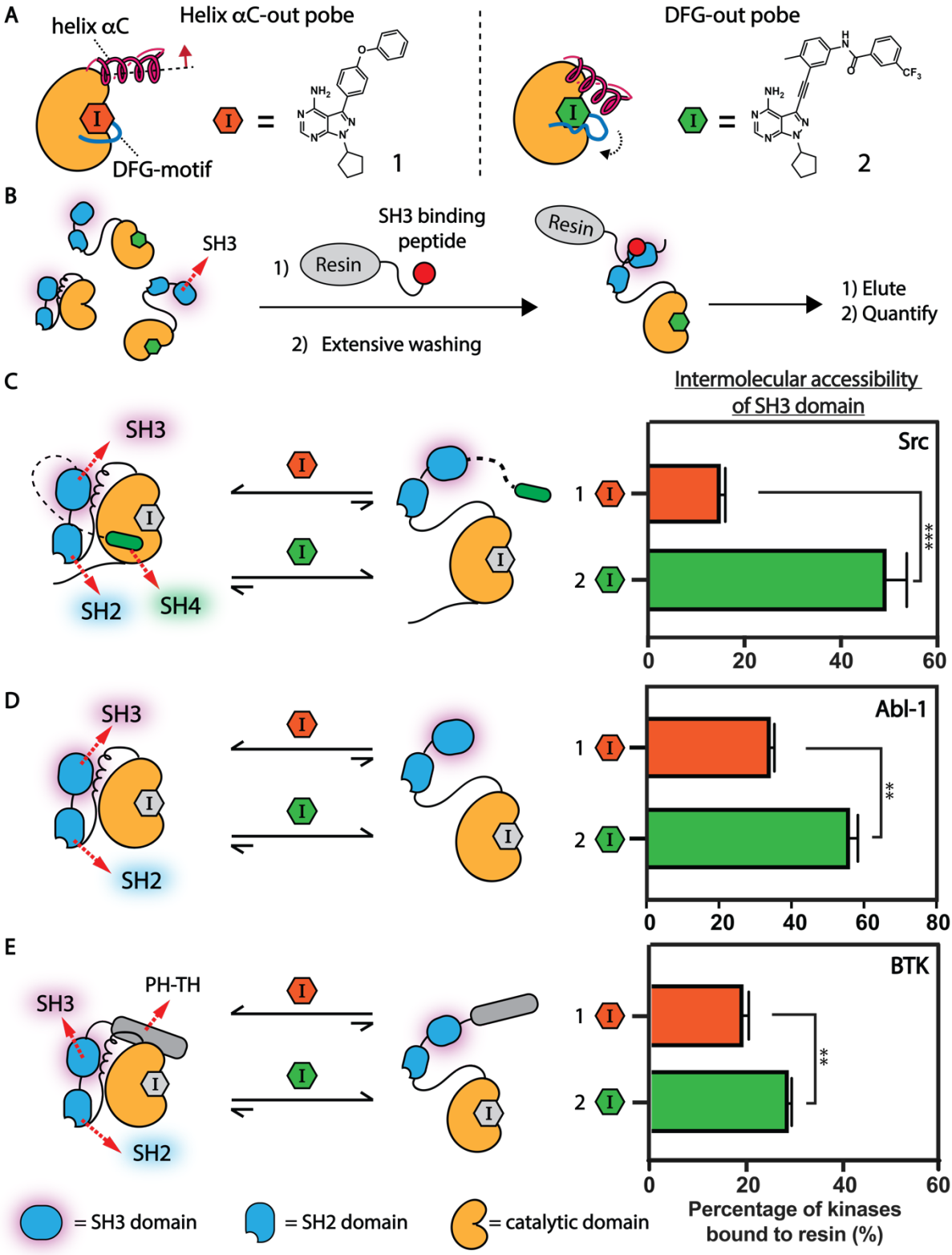
A
helix αC
Helix αC-out pobe
DFG-out pobe
DFG-motif
1
2
B
SH3
SH3 binding peptide
1) Resin
2) Extensive washing
Resin
1) Elute
2) Quantify
C
Intermolecular accessibility of SH3 domain
SH3
SH2
SH4
Src
***
0 20 40 60
D
SH3
SH2
Abl-1
**
0 20 40 60 80
E
SH3
PH-TH
SH2
BTK
**
0 20 40 60
= SH3 domain
= SH2 domain
= catalytic domain
Percentage of kinases bound to resin (%)

Figure 3-3**.** Conformation-selective inhibitors divergently modulate the global conformation of multidomain tyrosine kinases that contain an SH3-SH2-CD module.

(A) Helix αC-out-stabilizing inhibitor **1** (*left*) and DFG-out-stabilizing inhibitor **2** (*right*). (B) An illustration of the SH3 domain pull-down assay. (C-E) Determination of the global conformation of inhibitor-bound tyrosine kinases that contain the SH3-SH2-CD modules. (C) Allosteric modulation of Src's SH3-SH2-CD module by conformation-selective inhibitors. Inhibitor **1** promotes a closed SH3-SH2-CD module of Src. Inhibitor **2** promotes an open SH3-SH2-CD module of Src. (D) Allosteric modulation of Abl-1's SH3-SH2-CD module by conformation-selective inhibitors. Inhibitor **2** promotes a more open conformation of Abl-1's SH3-SH2-CD module than inhibitor **1**. (E) Allosteric modulation of BTK's SH3-SH2-CD module by conformation-selective inhibitors. Inhibitor **1** promotes a more closed conformation of BTK's SH3-SH2-CD module than inhibitor **2**. All values shown are mean ± SEM (n=3). P-values are calculated using a two-tailed t-test (* < 0.05, ** < 0.01, *** < 0.001).

We first validated that each inhibitor biochemically modulates Src's SH3-SH2-CD module as expected by performing SH3 domain pull-down assays with an immobilized SH3 domain ligand and inhibitor-bound Src complexes (**Figure 3-3B**). As expected, we found that the SH3 domain of the Src/**1** complex was inaccessible to intermolecular engagement with the SH3 domain ligand, consistent with helix αC-out-stabilizing inhibitors promoting a closed, autoinhibited SH3-SH2-CD module (**Figure 3-3C**). Conversely, the Src/**2** complex was significantly enriched by the immobilized SH3 domain ligand, which is consistent with **2** promoting a regulatory domain disengaged conformation of Src's SH3-SH2-CD module. Thus, inhibitors **1** and **2** can divergently

modulate the Src SH3-SH2-CD module by stabilizing two distinct inactive ATP-binding site conformations.

We then investigated how our conformation-selective inhibitors affect Abl-1's SH3-SH2-CD module. We first compared the SH3 domain accessibility of the Abl-1/**1** and Abl-1/**2** complexes. Like Src, Abl-1/**2** complex adopts a more open global conformation within the SH3-SH2-CD module, with a more intermolecularly accessible SH3 domain, relative to the Abl-1/**1** complex (**Figure 3-3D**). To further validate how stabilization of Abl-1 in both the helix αC-out and DFG-out conformations affects the global conformation of its SH3-SH2-CD module, we utilized electrophile-containing analogs of **1** and **2**—**1a** and **2a**, respectively—that potently inhibit a drug-sensitized cysteine mutant of Abl-1 (Abl-1 V256C) (**Figure 3-4A**). As expected, we found that the SH3 domain of the Abl-1 V256C/**1a** complex was largely inaccessible to intermolecular SH3 ligand engagement, which is consistent with helix αC-out-stabilizing **1a** promoting a closed conformation of Abl-1 V256C's SH3-SH2-CD module (**Figure 3-4B,3-4C**). Conversely, the SH3 domain of Abl-1 V256C/**2a** complex was efficiently enriched by the immobilized SH3 ligand, consistent with DFG-out stabilizing inhibitor **2a** promoting an open, intramolecularly disengaged Abl-1 SH3-SH2-CD module, like its underivatized counterpart. Thus, consistent with previous observations,[84, 88] an inhibitor that stabilizes the DFG-out inactive ATP-binding site conformation significantly promotes a regulatory domain-disengaged conformation of Abl-1's SH3-SH2-CD module. Inhibitors that stabilize the helix αC-out inactive ATP-binding site conformation promote a closed Abl-1's SH3-SH2-CD module, which further highlights the Src-like allosteric communication between Abl-1's regulatory domains and its ATP-binding site.

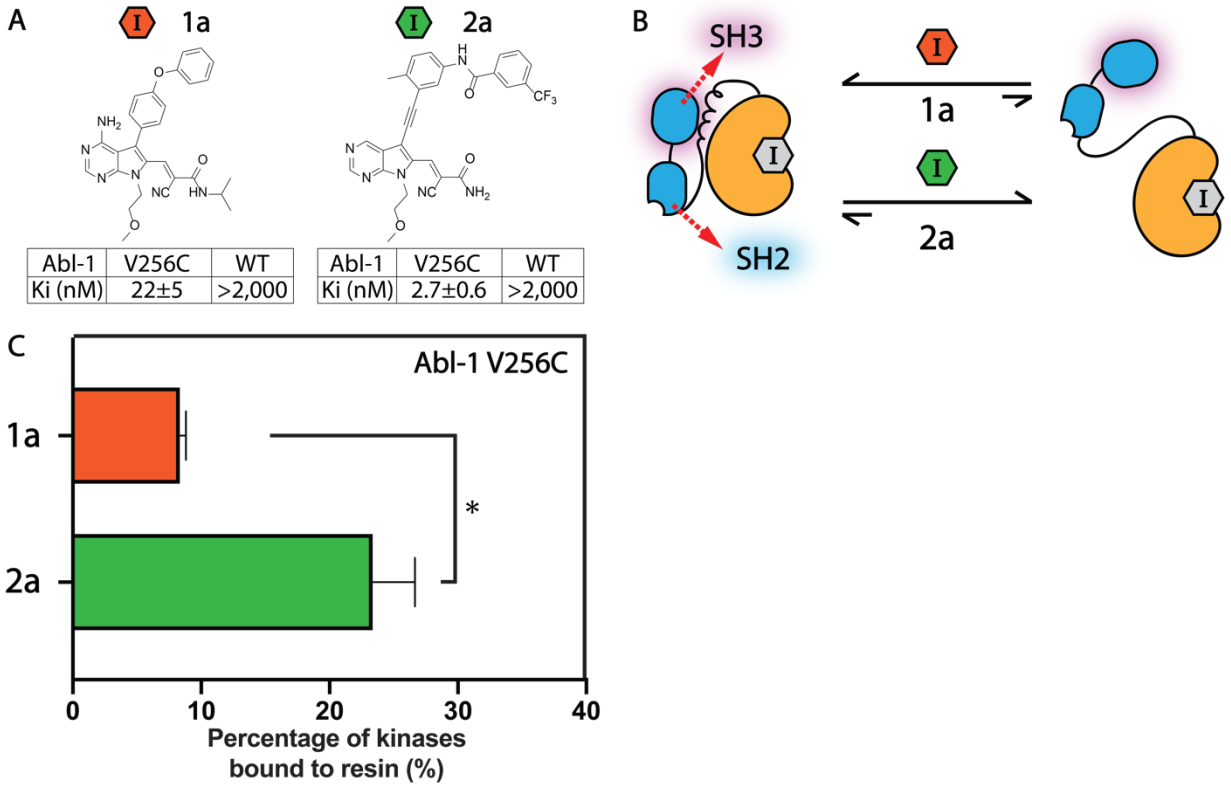

Figure 3-4. SH3 domain pull-down experiment with inhibitor-bound Abl-1 V256C complexes. (A) Inhibitor **1a** and **2a** provide potent inhibition of drug-sensitized Abl-1 V256C. Mean ± SEM of the Ki values are shown (n=3). (B) Allosteric modulation of Abl-1 V256C's SH3-SH2-CD module by conformation-selective inhibitors **1a** and **2a**. The DFG-out stabilizing inhibitor **2a** promotes a more open global conformation of Abl-1 V256C's SH3-SH2-CD module compared to the helix αC-out stabilizing inhibitor **1a**. (C) Quantification of SH3 pull-down experiments. The percentages of inhibitor-bound Abl-1 V256C retained on the SH3 ligand beads are the mean ± SEM (n=2). Shown are the mean ± SEM. P-values: * < 0.05, ** < 0.01, *** < 0.001.

Next, we explored whether conformation-selective, ATP-competitive inhibitors can also divergently modulate BTK's SH3-SH2-CD module. We first evaluated how the SH3 domain

accessibility of the BTK/**1** complex compared to the BTK/**2** complex. Like Src and Abl-1, helix αC-out-stabilizing inhibitor **1** resulted in a closed global conformation of BTK's SH3-SH2-CD module, with a largely intermolecularly inaccessible SH3 domain relative to the BTK/**2** complex (**Figure 3-3E**). To further validate how stabilization of BTK in both inactive ATP-binding site conformations affects the global conformation of its SH3-SH2-CD module, we used a drug-sensitized variant of BTK (BTK V416C) with inhibitors **1a** and **2a**.[75-76] Like wild-type BTK, we found that the SH3-SH2-CD module of the BTK V416C/**1a** complex adopted a more closed global conformation compared to the BTK/**2a** complex (**Figure 3-5**). Thus, conformation-selective inhibitors are capable of divergently modulating BTK's SH3-SH2-CD module, based on the ATP-binding site conformation they stabilize.

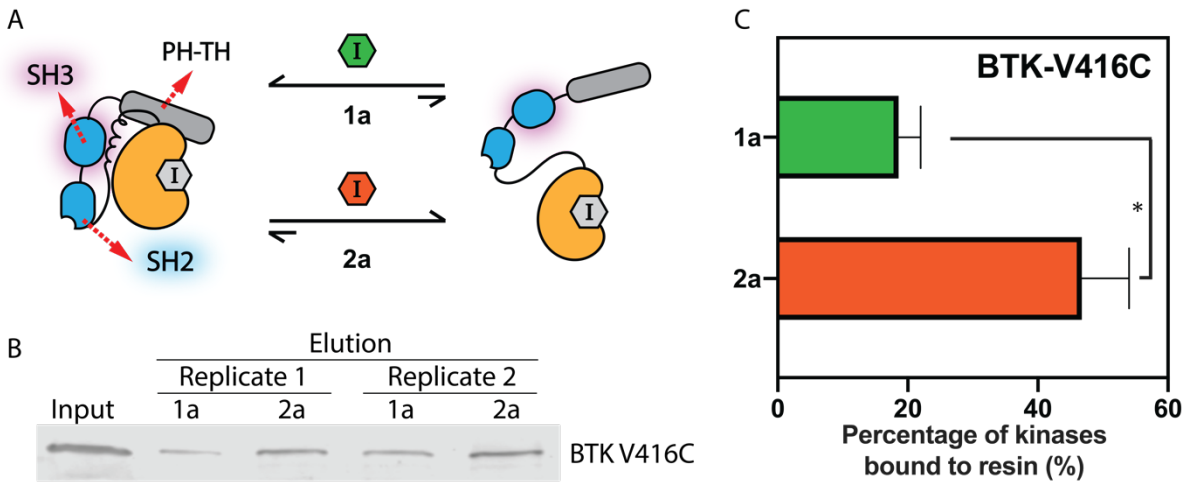

Figure 3-5**.** SH3 domain pull-down experiment with inhibitor-bound BTK V416C complexes. (A) Conformation-selective inhibitors **1a** and **2a** promote distinct global conformation of BTK V416C's SH3-SH2-CD module. The helix αC-out inhibitor **1a** promotes a closed global conformation of BTK V416C (*top*). The DFG-out inhibitor **2a** promotes an open global conformation of BTK V416C (*bottom*). (B) Western blot analysis of N-terminal Flag-tagged BTK

V416C in the input and elution samples of SH3 pull-down assays. An anti-BTK immunoblot is shown. (C) Quantification of SH3 pull-down experiments. The percentages of inhibitor-bound N-terminal Flag-tagged BTK V416C retained on the SH3 ligand beads are the mean ± SEM (n=2). P-values: * < 0.05, ** < 0.01, *** < 0.001.

3.2.2 Binding features of inhibitors that promote an open global conformation of Src.

While inhibitors that stabilizes the DFG-out inactive conformation promote an open global conformation of tyrosine kinases that contain an SH3-SH2-CD architecture,[22,23] we have found that other classes of ATP-competitive inhibitors are also capable of promoting allosteric disengagement of regulatory SH2 and SH3 domains.[18] To better understand the common features of inhibitors that promote an open global conformation of the SH3-SH2-CD regulatory module, we assembled a panel of 13 inhibitors that contain structurally diversified substituents that make varied ATP-binding site contacts and tested them in biochemical assays for the global conformational state of Src (**Figure 3-6A**). Inhibitors **1**, **3**, and **4** contain pharmacophores that should stabilize the helix αC-out inactive conformation of Src,[76, 81] while **2** and **5** contain substituents that stabilize the DFG-out form.[76, 91] The other eight inhibitors in our panel (**6**-**13**) contain various substituents that project into the ATP-binding pocket but are predicted to not stabilize either inactive conformation of the ATP-binding site.

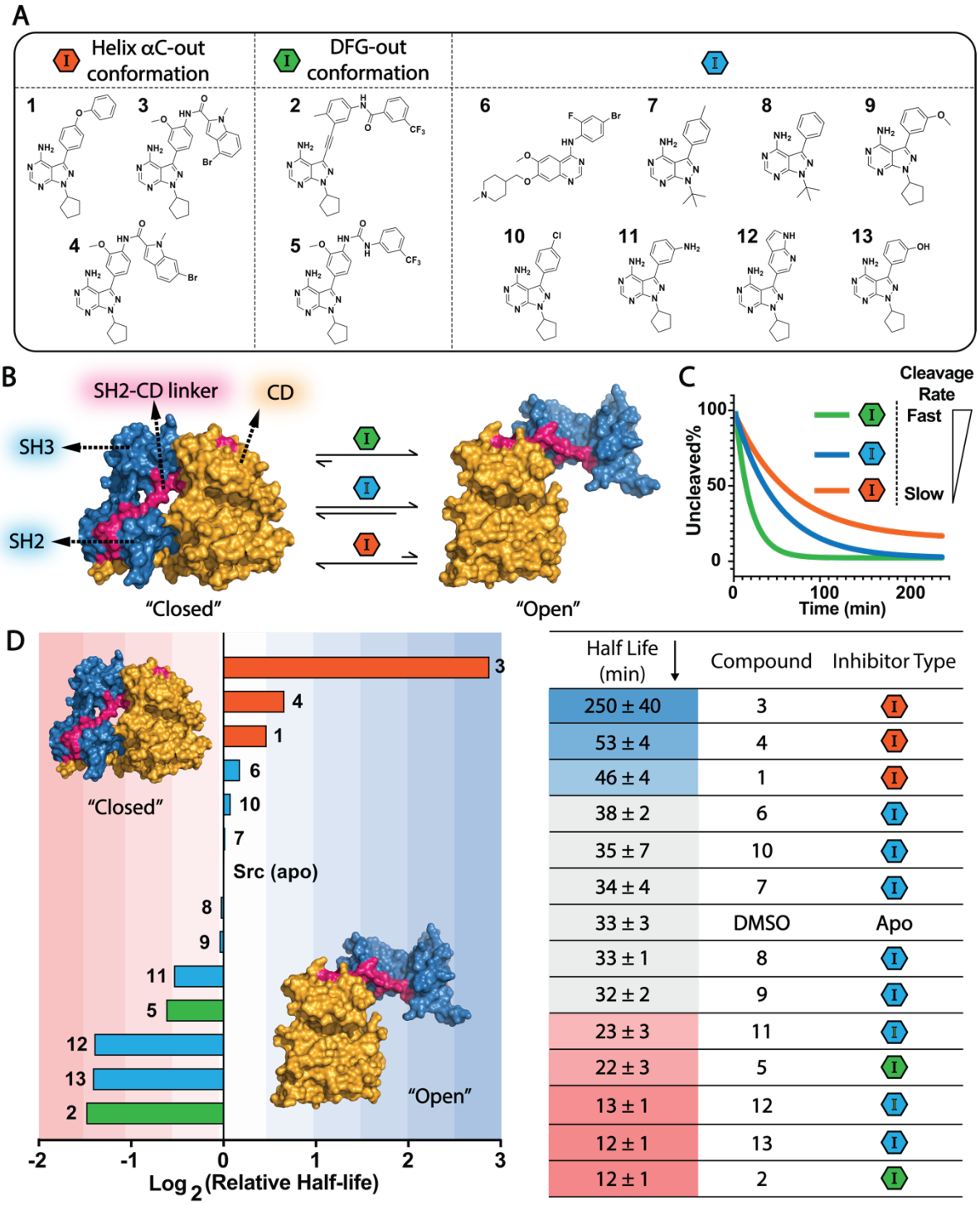

Half Life (min) ↓	Compound	Inhibitor Type
250 ± 40	3	I
53 ± 4	4	I
46 ± 4	1	I
38 ± 2	6	I
35 ± 7	10	I
34 ± 4	7	I
33 ± 3	DMSO	Apo
33 ± 1	8	I
32 ± 2	9	I
23 ± 3	11	I
22 ± 3	5	I
13 ± 1	12	I
12 ± 1	13	I
12 ± 1	2	I

Figure 3-6. Binding features of inhibitors that promote an open global conformation of Src.

(A) A panel of 13 ATP-competitive Src inhibitors. (B) Allosteric modulation of Src's global conformation with ATP-competitive inhibitors. (C) Thermolysin assay. The rate for proteolytic cleavage of the SH2-CD linker is sensitive to the global conformation of inhibitor-bound Src complexes. Thermolysin cleaves the SH2-CD linker (magenta) of inhibitor-bound Src in the open global conformation more quickly relative to the closed global conformation. The catalytic domain (CD) is colored in yellow and regulatory domains in blue. (D) (*Left*) Ranking of the log2-based relative half-life values of proteolytic cleavage rates of Src's SH2-CD linker. Relative ratio=$\log_2$[Half-life(Inhibitor-bound Src)/Half-life(*apo* Src)]. The means of the relative ratios are shown. (*Right*) The mean ± SEM of half-life values are shown (n=3).

To probe how our panel of inhibitors modulate the global conformation of Src's SH3-SH2-CD module, we performed limited proteolysis experiments with inhibitor-bound Src complexes (**Figure 3-6B**,**3-6C**).[83] It has previously been demonstrated that the metalloprotease thermolysin can selectively cleave the flexible linker that connects Src's SH2 domain to its CD (SH2-CD linker) and that the cleavage rate is sensitive to Src's global regulatory conformation (**Figure 3-6B**, colored in magenta).[83, 92] Therefore, we used half-life values for proteolytic cleavage as readouts for the global conformation of Src's SH3-SH2-CD module. We benchmarked the half-life for cleavage of *apo* Src as 33 ± 3 min. To assign a global conformation to inhibitor- bound Src complexes, we measured the half-life for their cleavage and used 5σ as the cutoff for significant deviation from *apo* Src (**Figure 3-6D**). Consistent with the ability of DFG-out-stabilizing inhibitors to disengage the regulatory SH2 and SH3 domains from Src's CD, the SH2-CD linkers of the Src/**2** and Src/**5** complexes are cleaved more rapidly than the *apo* Src. Conversely, consistent with helix αC-out-stabilizing inhibitors enhancing the regulatory SH2 and SH3 domain

engagement with Src's CD, the SH2-CD linkers of the Src/**1**, Src/**3**, and Src/**4** complexes are cleaved more slowly than the *apo* Src.

As expected, we found that the SH2-CD linker of Src bound to inhibitors **6**, **7**, **8**, **9**, or **10**, which all contain substituents that should make minimal interactions with helix αC or the activation loop, was cleaved at rates similar to Src's *apo* form (**Figure 3-6D**). However, although **11**, **12**, and **13** do not contain substituents that stabilize either inactive conformation of Src's ATP-binding site, the SH2-CD linker of Src bound to these inhibitors was cleaved at rates similar to the Src/**2** and Src/**5** complexes. Thus, **11**-**13** appear to promote a regulatory domain disengaged conformation of the SH3-SH2-CD module like DFG-out-stabilizing inhibitors. Despite lacking a substituent that promotes a flipped DFG-motif, like DFG-out stabilizing inhibitors **2** and **5**, **11**-**13** contain H-bond donors that we predicted are capable of forming a H-bonding interaction with the side-chain of Glu310 in Src's helix αC. As most inhibitors that stabilize the DFG-out conformation also contain H-bond donors that form a H-bonding interaction with the side-chain of Glu310 in Src's helix αC (**Figure 3-7A**), we further investigated whether this interaction is responsible for promoting an open global conformation of the SH3-SH2-CD module rather than their influence on the activation loop.

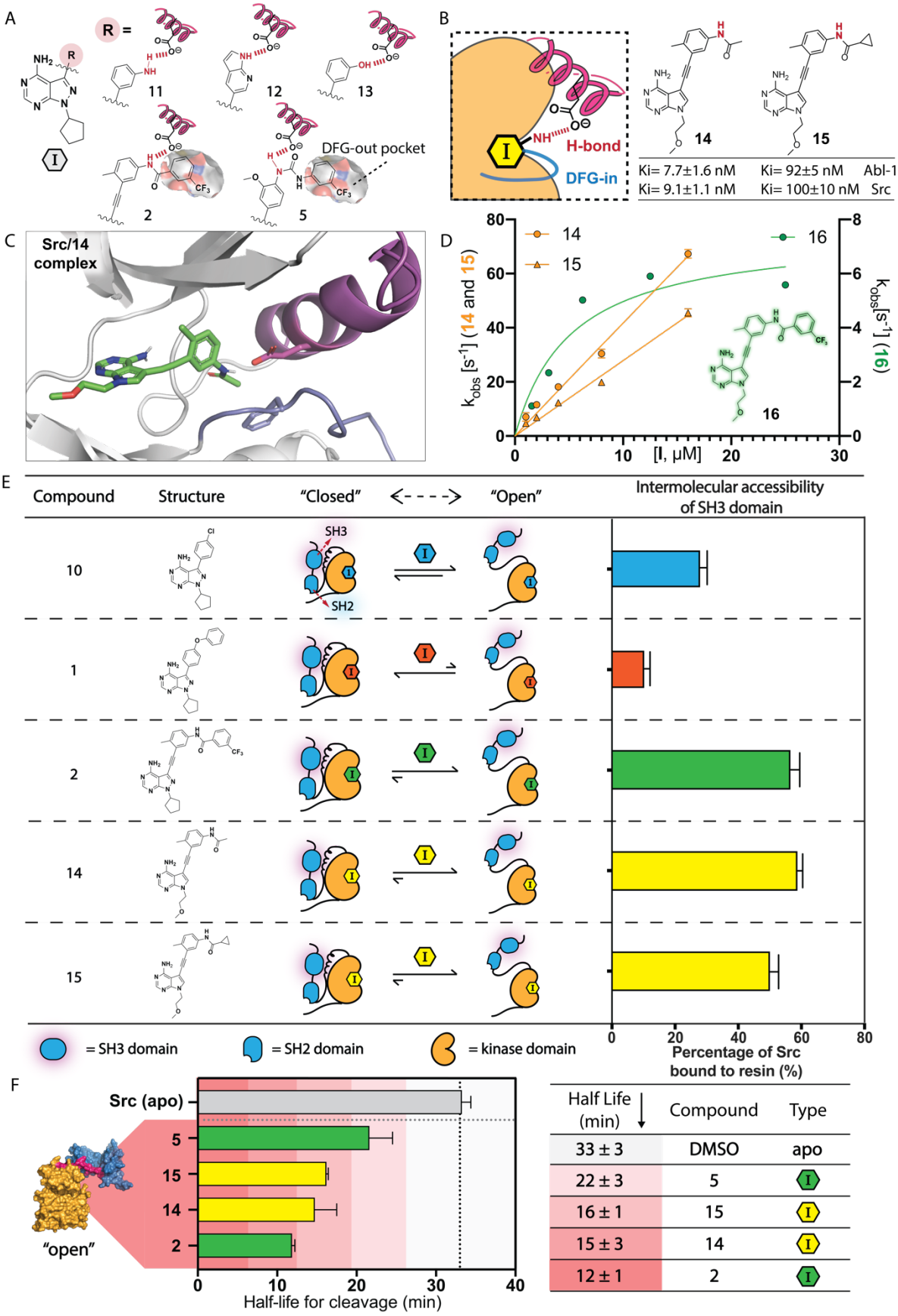
A
R =
11
12
13
2
5
DFG-out pocket
B
H-bond
DFG-in
14
15
Ki= 7.7±1.6 nM
Ki= 9.1±1.1 nM
Ki= 92±5 nM
Ki= 100±10 nM
Abl-1
Src
C
Src/14 complex
D
14
15
16
k_{obs} [s^{-1}] (14 and 15)
k_{obs}[s^{-1}] (16)
[I, μM]
E
Compound
Structure
"Closed"
"Open"
Intermolecular accessibility of SH3 domain
SH3
SH2
10
1
2
14
15
= SH3 domain
= SH2 domain
= kinase domain
Percentage of Src bound to resin (%)
F
Src (apo)
5
15
14
2
"open"
Half-life for cleavage (min)
Half Life (min)
Compound
Type
33 ± 3
DMSO
apo
22 ± 3
5
16 ± 1
15
15 ± 3
14
12 ± 1
2

Figure 3-7**.** Analysis of how helix αC interactions influence global conformation.

(A) ATP-binding site contacts of substituents that promote an open global conformation of Src. H-bonding interactions are colored in red. The hydrophobic DFG-out pocket is annotated. (B) Structures and the predicted binding features of inhibitors **14** and **15**. K_i values are shown as mean ± SEM (n=3). (C) X-ray cocrystal structure of the Src/**14** complex (PDB ID: 6WIW). Helix αC is colored in magenta. The activation loop is colored in blue. (D) The observed rate constants for Src binding to **14**, **15**, or **16** at pH 7.0. Mean ± SEM values are shown (n≥3). (E) SH3 domain intermolecular accessibility of Src bound to inhibitors **10**, **1**, **2**, **14**, or **15**. Mean ± SEM are shown (n=3). (F) Thermolysin assays with Src/**14** and Src/**15** complexes. The half-lives for cleavage of Src's SH2-CD linker are shown as the mean ± SEM (n=3).

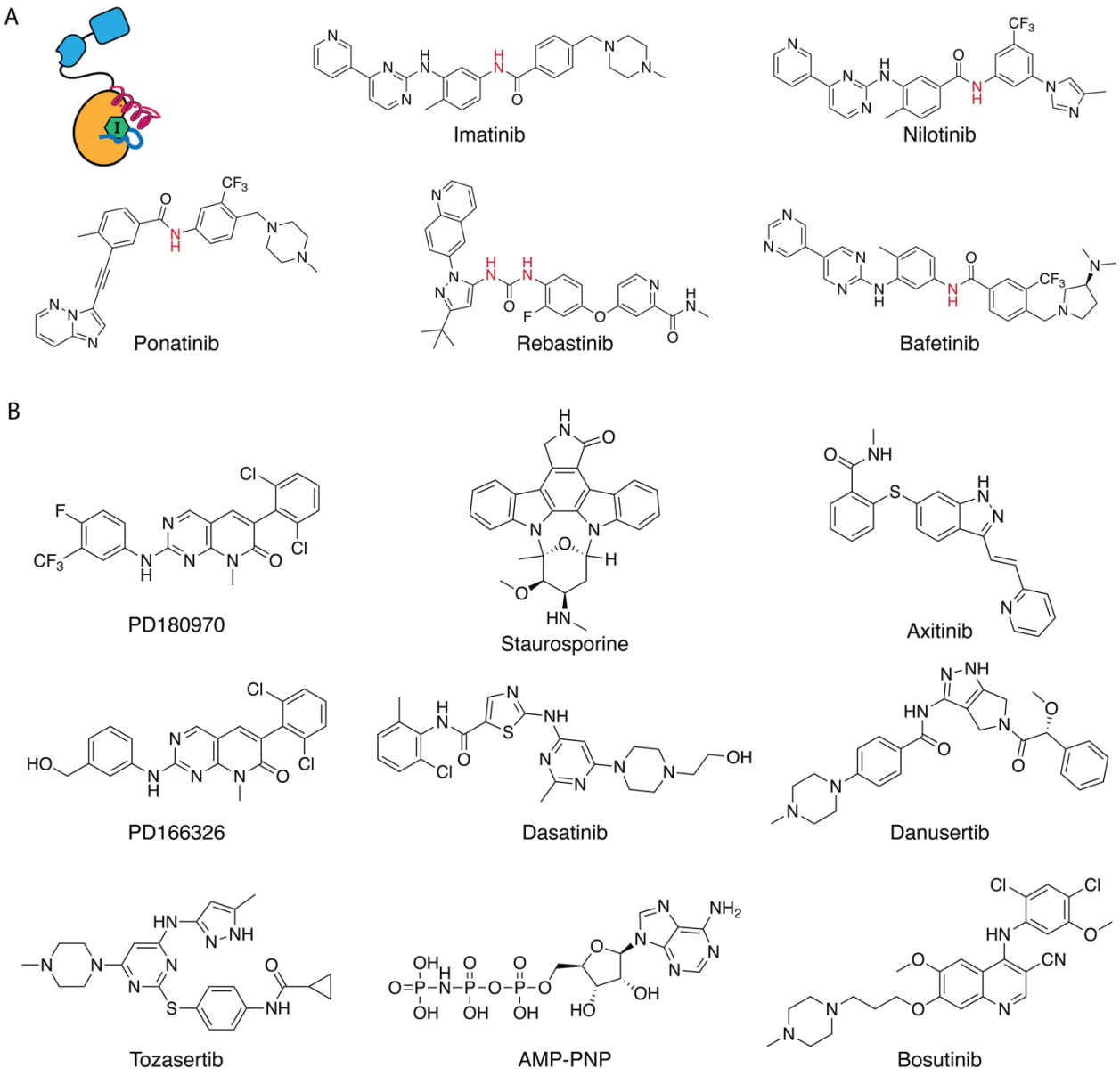

Figure 3-8. The global conformation of ligand-bound Abl-1's SH3-SH2-CD module is highly correlated with inhibitor's ability to form H-bond interaction with the Glu286 of helix αC.[88]

(A) Chemical structures of ligands that promote an open global conformation of Abl-1's SH3-SH2-CD module. The nitrogen atoms that can form H-bond interactions with Glu286 of the helix αC are colored in red. (B) Chemical structures of ligands that do not promote an open global conformation of Abl-1's SH3-SH2-CD module.

3.2.3 Analysis of how helix αC interactions influence global conformation.

Recent studies have shown that the ability of inhibitors to flip the DFG-motif of Abl-1's activation loop highly correlates with their promotion of an open global conformation of Abl-1's SH3-SH2-CD module.[88] Our observations in Src made us interested in revisiting the molecular binding features of 14 ligands that have previously been reported to promote an open global conformation of Abl-1, which was determined by characteristic NMR ^{1}H-^{15}N backbone chemical shifts within the SH3 and SH2 domains (**Figure 3-8**).[88] We found that all inhibitors—including imatinib, nilotinib, ponatinib, rebastinib, and bafetinib—that promote an open global conformation of Abl-1's SH3-SH2-CD module also form a H-bonding interaction with the side-chain of Abl-1's Glu286 that stabilize its helix αC in the active conformation (**Figure 3-9**). In contrast, inhibitors that lack the ability to form a H-bonding interaction with Glu286 do not promote an open global conformation of Abl-1 (**Figure 3-8B**). Taken together, an inhibitor's ability to hydrogen bond with the conserved Glu in helix αC highly correlates with the global conformation of Src's and Abl-1's SH3-SH2-CD modules. Therefore, we speculate that the influence of an inhibitor on the conformation of helix αC, and not on the DFG-motif, is responsible for its ability to promote an open global conformation of the SH3-SH2-CD module.

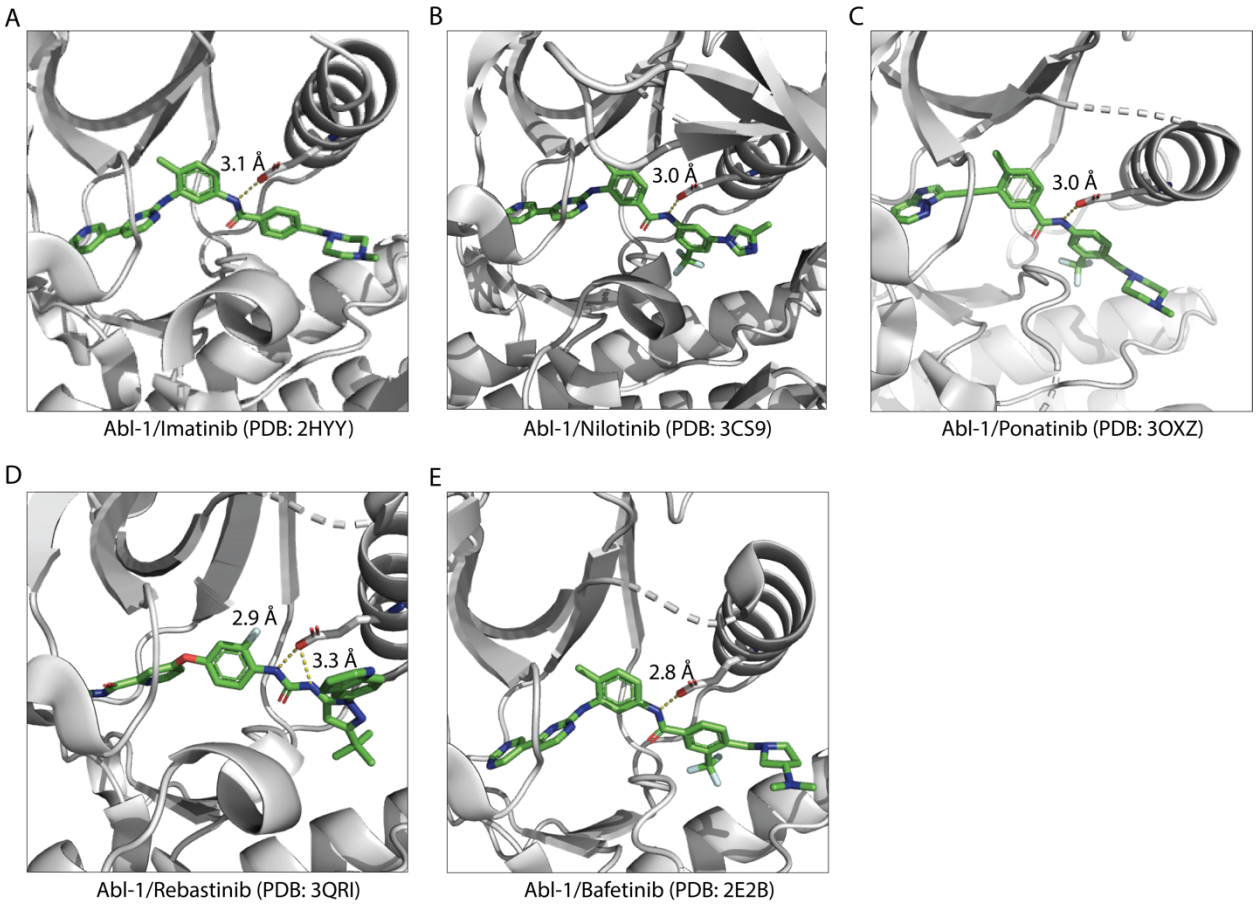

Figure 3-9. ATP-binding site contacts of five Abl-1 ligands that promotes open conformation of Abl-1's SH3-SH2-CD module.

(A) X-ray crystal structure of Imatinib-bound Abl-1 (PDB ID: 2HYY).[93] (B) X-ray crystal structure of Nilotinib-bound Abl-1 (PDB ID: 3CS9).[94] (C) X-ray crystal structure of Ponatinib-bound Abl-1 (PDB ID: 3OXZ).[95] (D) X-ray crystal structure of Rebastinib-bound Abl-1 (PDB ID: 3QRI).[96] (E) X-ray crystal structure of Bafetinib-bound Abl-1 (PDB ID: 2E2B).[97] The H-bonds are labeled with gray dotted lines, with their respective lengths. Inhibitors are colored based on atoms: carbon atoms are colored in green; oxygen atoms are colored in red; nitrogen atoms are colored in blue.

To test this notion, we designed inhibitors that possess the same H-bonding pattern as DFG-out-stabilizing inhibitors but lack bulky substituents that flip the DFG motif of the activation loop. We generated two analogs—**14** and **15** (**Figure 3-7B**)—of DFG-out stabilizing inhibitor **2**, which contains an amide linker that is predicted to hydrogen bond with Glu310 on helix □C and a bulky trifluoromethylphenyl group that is capable of occupying the hydrophobic pocket created by the displacement of the phenylalanine side-chain in the DFG-motif (**Figure 3-10**).[76, 91] **14** and **15** retain the same H-bonding pattern as **2** but contain less bulky alkyl substituents. While, unsurprisingly, **14** and **15** are less potent inhibitors than **2**, they both inhibit the phosphotransferase activity of Src and Abl-1 at reasonable concentrations.

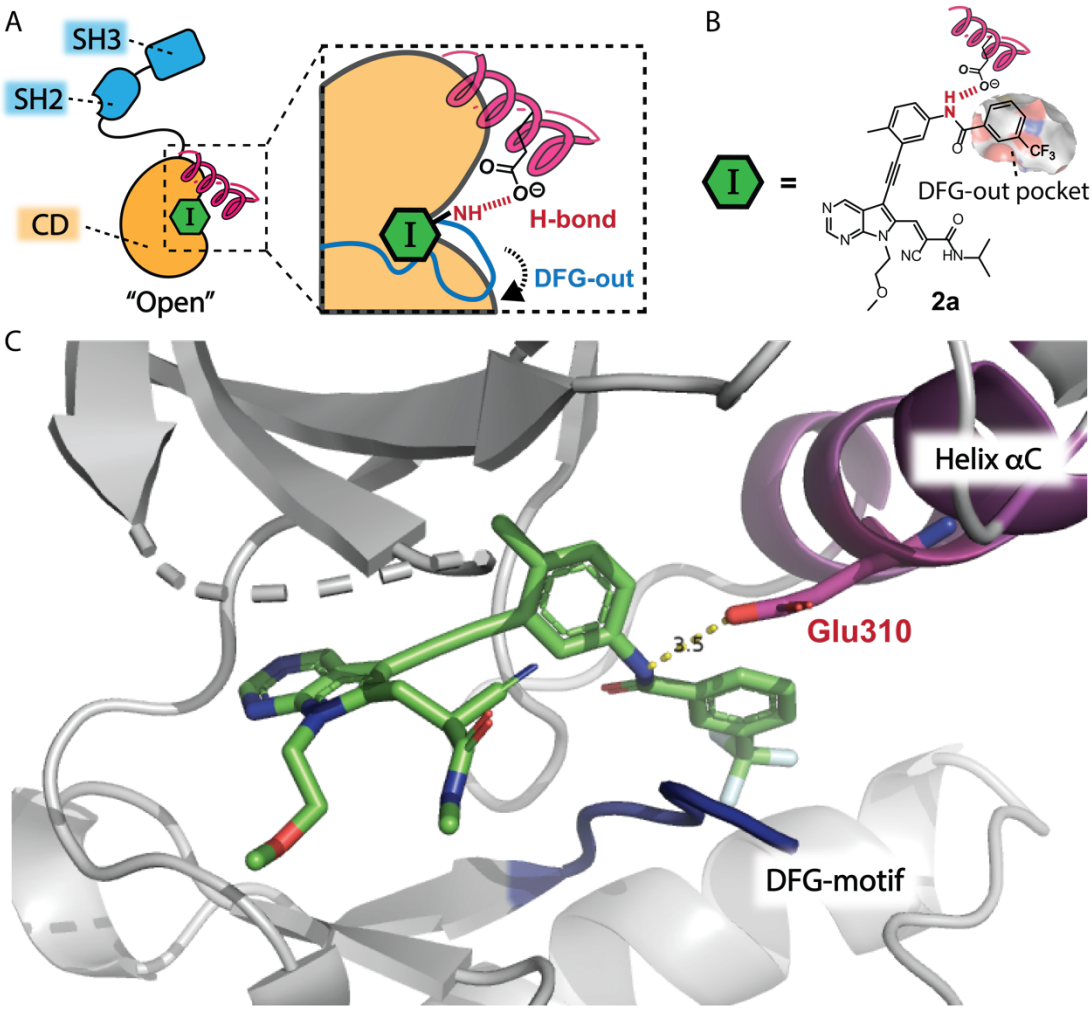

Figure 3-10. ATP-binding site contacts of a DFG-out-stabilizing inhibitor.

(A) An illustration of DFG-out-stabilizing inhibitors promotes an open global conformation of Src. The inhibitor contains an H-bond donor that interacts with Glu310 of Src (labeled in red dotted lines) and stabilizes an ATP-binding site conformation with flipped and displaced DFG-motif (colored in blue). (B) Chemical structure of an DFG-out-stabilizing inhibitor. C) Cocrystal structure of Src V284C bound to a DFG-out-stabilizing inhibitor (PDB ID: 5SYS).[76] H-bonds are labeled with yellow dotted lines, with their respective lengths (3.5 Å). The helix αC is colored in

magenta. The DFG-motif of the activation loop is colored in blue. A part of the protein structure is presented in a dotted line colored in gray.

To determine whether our new analogs interact with the ATP-binding site of Src as designed, we obtained a crystal structure of **14** bound to the CD of Src (**Figure 3-7C** and **Figure 3-10**). Two molecules of **14**-bound Src's CD were observed per crystallographic asymmetric unit. Inhibitor **14** occupies the ATP-binding site of Src and makes the same H-bonding interactions with the hinge region as similar pyrrolopyrimidine-based inhibitors.[76, 91, 98-100] Notably, the Src/**14** complex is in the active conformation, which is characterized by an inward position of the helix αC (helix αC-in) in the N-lobe and an unperturbed activation loop. Like a DFG-out stabilizing inhibitor, the amide linker that projects from the alkynylphenyl group of **14** forms a H-bond with Glu310 in the helix αC, presumably stabilizing the active conformation of this structural element (**Figure 3-10**). Although the acetamide group of **14** projects toward the activation loop, Src's DFG-motif is not flipped. An overlay of the Src/**14** complex with a crystal structure of Src in the DFG-out conformation shows that **14**'s acetamide group is not large enough to perturb the Phe405 residue of the DFG-motif in the activation loop from an active conformation.

To confirm that inhibitors **14** and **15** have a similar effect on Src's ATP-binding site in solution, we monitored their binding kinetics with Src using a previously reported stopped-flow tryptophan fluorescence assay (**Figure 3-7D**). For inhibitors that stabilize the DFG-out conformation, the rate-determining event for binding at high inhibitor concentrations is the flipping of the DFG-motif. This leads to an observed rate constant for binding (k_{obs}) that deviates from linearity of otherwise pseudo first-order kinetics.[101-102] Consistent with the flipping of the DFG-motif not being required

for **14** and **15** to interact with the ATP-binding site of Src, we found that the observed rate constants for both inhibitors increased linearly with concentration (**Figure 3-7D**, colored in yellow; **Figure 3-11A**,**3-11B**). In contrast, inhibitor **16**, which is a direct DFG-out-stabilizing analog of **14** and **15**, demonstrated a nonlinear k_{obs} with increasing inhibitor concentration, consistent with **16** requiring a flipped DFG-motif to be accommodated in Src's ATP-binding site (**Figure 3-7D**, colored in green). Additionally, because the flip of the DFG-motif necessitates protonation of the side-chain of its Asp residue, the kinetics of DFG-out-stabilizing inhibitors are pH-dependent.[101-102] We found that the observed rate constants for binding of **14** and **15** to Src were not dependent on pH, while the binding of **16** to Src was (**Figure 3-11C-F**). We also tested **14** and **15** for their binding kinetics with Abl-1 and found that both inhibitors demonstrate a kinetic profile that is similar to their interaction with Src (**Figure 3-12**). Taken together, we validated that inhibitor **14** and **15** retain the same H-bonding pattern as DFG-out-stabilizing inhibitors but do not require flipping of the DFG-motif in the activation loop of tyrosine kinases for binding.

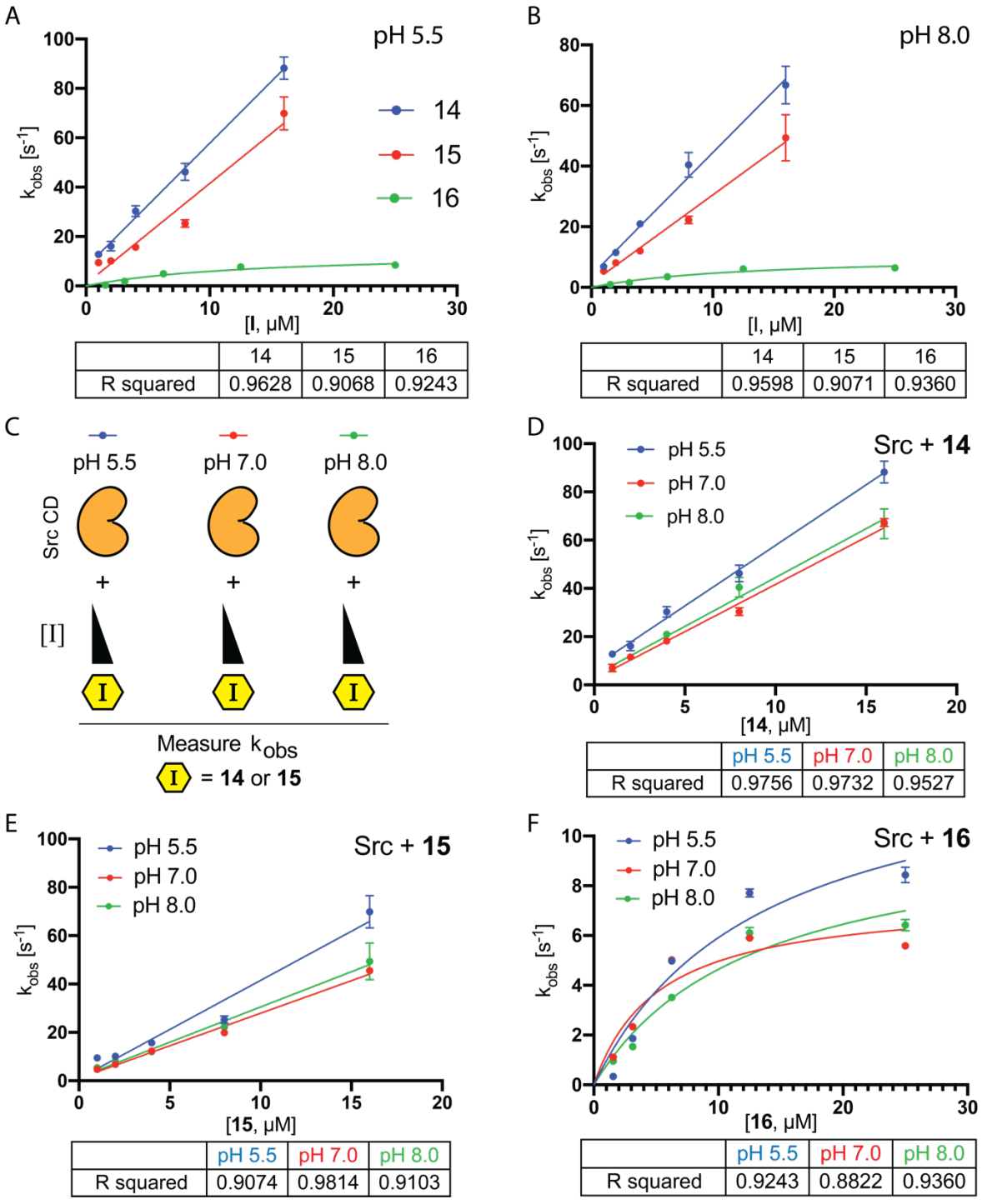

	14	15	16
R squared	0.9628	0.9068	0.9243

	14	15	16
R squared	0.9598	0.9071	0.9360

	pH 5.5	pH 7.0	pH 8.0
R squared	0.9756	0.9732	0.9527

	pH 5.5	pH 7.0	pH 8.0
R squared	0.9074	0.9814	0.9103

	pH 5.5	pH 7.0	pH 8.0
R squared	0.9243	0.8822	0.9360

Figure 3-11. Kinetics of inhibitors **14**, **15**, and **16** binding to the catalytic domains (CD) of Src. The observed rate constants (k_{obs}) of inhibitor binding are plotted against the final inhibitor concentration in the assay. See **Figure 4** for chemical structures of **14**-**16**.

(A-B) The observed rate constants (k_{obs}) of **14**, **15**, and **16** binding to Src's CD are plotted against the final concentration of each inhibitor. The observed rate constants of **14** and **15** were fitted to a linear regression model using GraphPad Prism8™ software. The observed rate constants of **16** were fitted to a nonlinear "One site-specific binding" model using GraphPad Prism8™ software. Experiments were performed at pH 5.5 (A) and pH 8.0 (B). (C) An illustration of stop-flow assay to determine the dependence of k_{obs} on pH. (D) Observed rate constants (k_{obs}) of **14** binding to Src's CD are plotted against the final concentration of **14**. Experiments were performed at pH 5.5 (blue), pH 7.0 (red) and pH 8.0 (green) in biological replicates ($n \geq 3$). The observed rate constants were fit to a linear regression model in GraphPad Prism8™ software. R squared was reported to indicate the fit with the designated model. (E) Observed rate constants (k_{obs}) of **15** binding to Src's CD are plotted against the final total inhibitor concentration of **15**. Experiments were performed at pH 5.5 (blue), pH 7.0 (red) and pH 8.0 (green) in biological replicates ($n \geq 3$). The observed rate constants were fit to a linear regression model in GraphPad Prism8™ software. R squared was reported to indicate the fit with the designated model. (F) Observed rate constants (k_{obs}) of **16** binding to Src's CD are plotted against the final concentration of **16**. Experiments were performed at pH 5.5 (blue), pH 7.0 (red) and pH 8.0 (green) in biological replicates ($n \geq 3$). The observed rate constants were fit to a nonlinear "One site-specific binding" model in GraphPad Prism8™ software. R squared was reported to indicate the fit with the designated model.

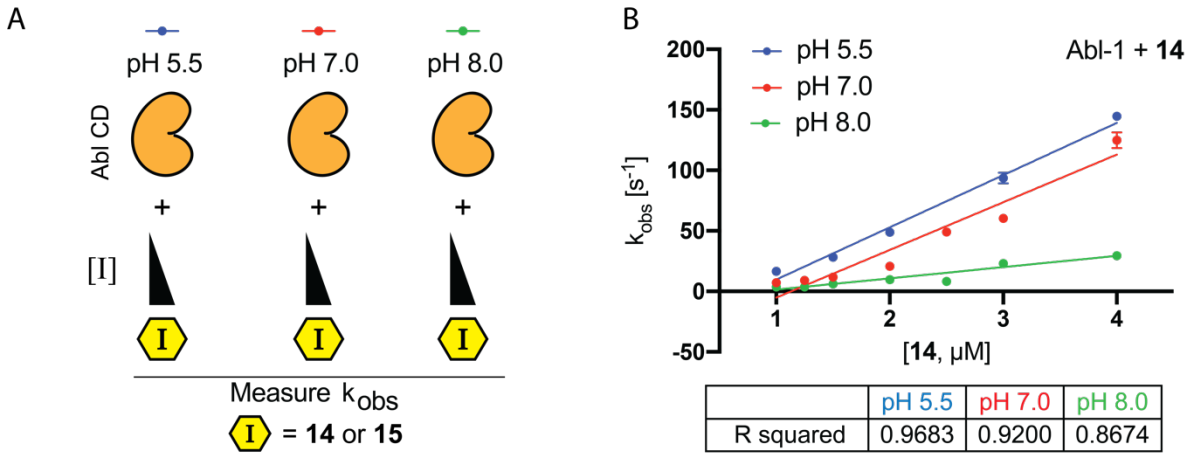

	pH 5.5	pH 7.0	pH 8.0
R squared	0.9683	0.9200	0.8674

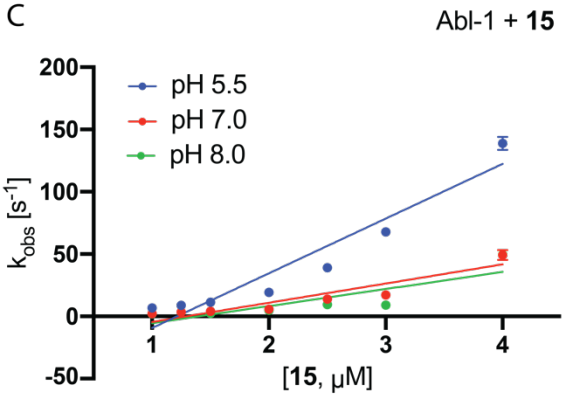

	pH 5.5	pH 7.0	pH 8.0
R squared	0.9044	0.8205	0.7046

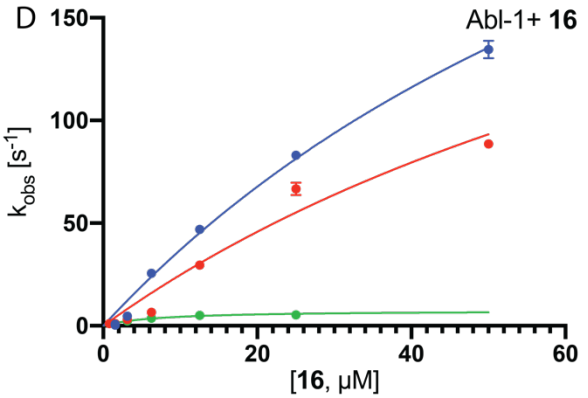

	pH 5.5	pH 7.0	pH 8.0
R squared	0.9870	0.9537	0.9534

Figure 3-12. Kinetics of inhibitors **14**, **15**, and **16** binding to the catalytic domain (CD) fo Abl-1. The observed rate constants (k_{obs}) of inhibitor binding to the CDs are plotted against the final concentration after mixing. See **Figure 4** for chemical structures of **14-16**.

(A) A schematic illustration of the stop-flow experiment to determine the dependence of k_{obs} on pH. The observed rate constants for inhibitor binding with the CD of Abl-1 were measured. (B) The observed rate constants (k_{obs}) of **14** binding to the Abl-1's CD are plotted against the final concentration of **14**. Experiments were performed at pH 5.5 (blue), pH 7.0 (red) and pH 8.0 (green) in biological replicates (n≥3). The observed rate constants were fit to a linear regression model in GraphPad Prism8™ software. R squared was reported to indicate the fit with the designated model.

(C) The observed rate constants (k_{obs}) of **15** binding to the Abl-1's CD are plotted against the final concentration of **15**. Experiments were performed at pH 5.5 (blue), pH 7.0 (red) and pH 8.0 (green) in biological replicates (n≥3). The observed rate constants were fit to a linear regression model in GraphPad Prism8™ software. R squared was reported to indicate the fit with the designated model. (D) The observed rate constants (k_{obs}) of **16** binding to the Abl-1's CD are plotted against the final total inhibitor concentration of **16**. Experiments were performed at pH 5.5 (blue), pH 7.0 (red) and pH 8.0 (green) in biological replicates (n≥3). The observed rate constants were fit to a nonlinear "One site-specific binding" model in GraphPad Prism8™ software. R squared was reported to indicate the fit with the designated model.

3.2.4 Inhibitors 14 and 15 promote an open global conformation of Src.

To determine whether our new helix αC-in-stabilizing inhibitors **14** and **15** promote an open global conformation of Src's SH3-SH2-CD module, we performed SH3 domain pull-down assays and limited proteolysis experiments with inhibitor-bound Src complexes. We found that both the Src/**14** and Src/**15** complexes were efficiently enriched by an immobilized SH3 ligand, consistent with **14** and **15** promoting an open, regulatory domain-disengaged conformation of Src (**Figure 3-7E**). Notably, the SH3 regulatory domains of both the Src/**14** and Src/**15** complexes had similar intermolecular accessibilities as the SH3 domain of Src bound to DFG-out stabilizing inhibitor **2**. We also found that the half-lives for cleavage of the SH2-CD linkers of the Src/**14** ($t_{1/2}$=15±3 min) and Src/**15** ($t_{1/2}$=16±1 min) complexes by thermolysin was within the range of Src bound to DFG-out-stabilizing inhibitors **2** and **5** (**Figure 3-7F**). Thus, the observed capability of DFG-out-

stabilizing inhibitors to promote an open global conformation of Src appears to rely on their ability to stabilize an active conformation of helix αC, rather than their ability to perturb the activation loop.

3.2.5 A chemical genetic strategy for investigating the effects of stabilizing the helix αC-in conformation in cells.

We have recently demonstrated that modulating Src's global conformation in cells with conformation-selective inhibitors can influence the phosphotransferase-independent functions of its regulatory domains.[75-76] To determine how stabilizing the helix αC-in conformation (characterized by an inward position of the helix αC in the N-lobe and an unperturbed activation loop) of Src affects its phosphotransferase-independent functions in cells compared to alternative ATP-binding site conformations, we pursued a chemical genetic strategy for sensitizing kinases to specific inhibtors.[99-100, 103-104] Our strategy, which we call Cystine Installation for Modulating Allostery and Target Inhibition of Kinases (CystIMATIK) (**Figure 3-13A**),[76] involves the introduction of a cysteine residue at the β2 strand of the N-terminal lobe of the catalytic domains of kinases that provides sensitivity to pyrrolopyrimidine-based inhibitors that contain a Michael acceptor at the C-6 position (**Figure 3-13B**). To implement the CystIMATIK strategy for Src, we generated electrophile-containing analogs of **14** and **15** (**14a** and **15a**, **Figure 3-13C**) and tested them for inhibition of drug-sensitized Src (Src V284C). We found that both **14a** and **15a** provided potent inhibition of Src V284C but not the wild-type kinase (**Figure 3-13C**).

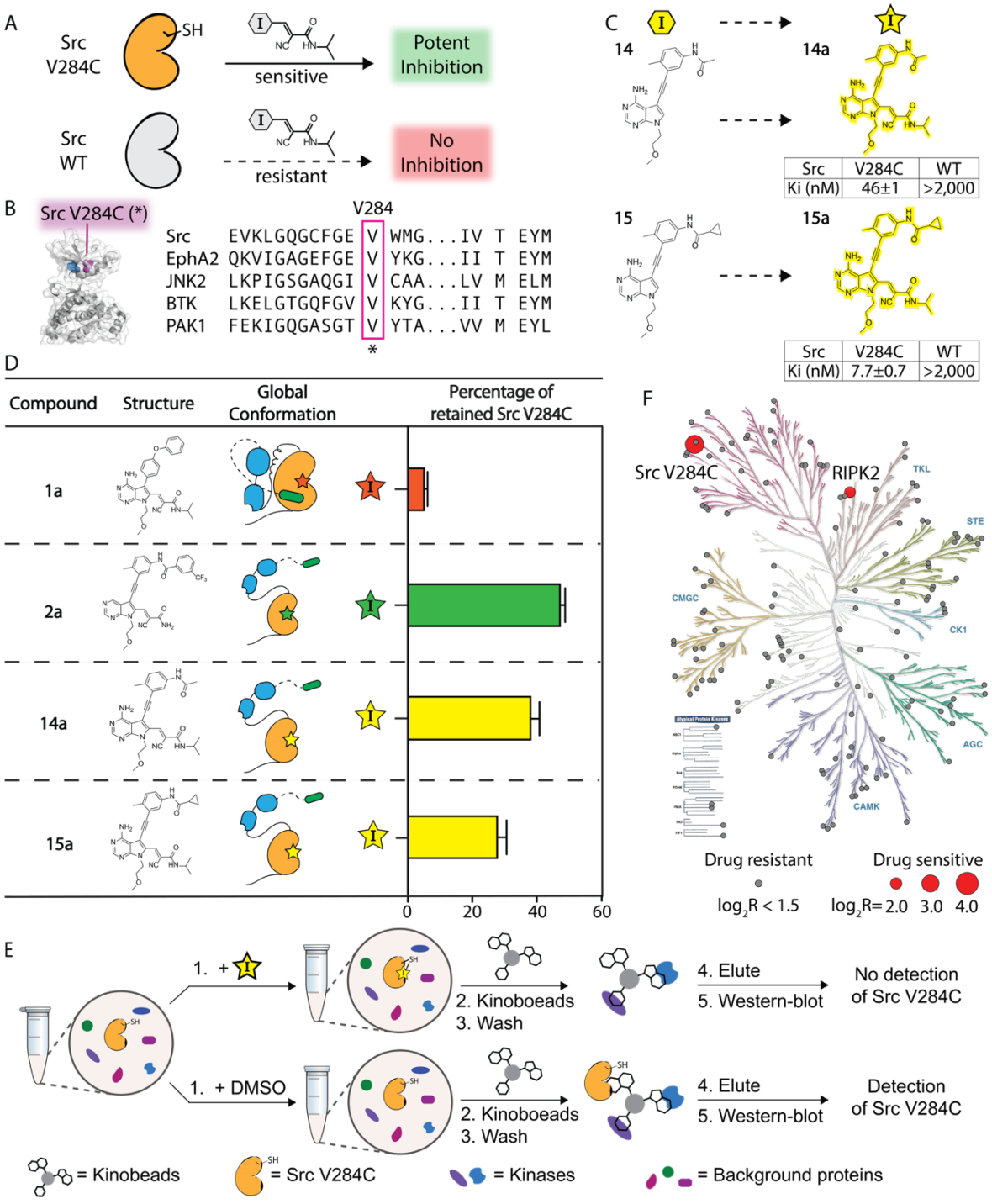

Figure 3-13. Chemical genetic strategy for investigating the effects of stabilizing the helix αC-in conformation of Src in cells.

(A) Cysteine Installation for Modulating Allostery and Targeted Inhibition of Kinases (CystIMATIK). CystIMATIK probes provide potent inhibition of drug-sensitized kinase variants, while wild type kinases are largely resistant to CystIMATIK probes. (B) Sensitization of Src to CystIMATIK probes through the introduction of a cysteine at V284. The sequence alignment shows a conserved valine at the position equivalent to V284 of Src. (C) Electrophile-containing analogs of **14** and **15**. The Ki values of **14a** (*top*) and **15a** (*bottom*) for wild-type Src and Src V284C are shown as mean ± SEM (n=3). (D) SH3 domain pull-down assays for characterizing the global conformation of the **14a**/Src V284C and **15a**/ Src V284C complexes. Values shown are the mean ± SEM (n=3). (E) Kinobead-based profiling method for determining the kinome-wide selectivity of **14a** and **15a**. Src V284C HeLa cell lysates were incubated with DMSO, **14a**, or **15a**, and an immobilized matrix of nonselective kinase inhibitors (kinobeads). Captured kinases were subjected to the proteomics workflow described in the supporting information. (F) Phylogenetic trees showing the selectivity of **14a**. All profiled kinases are represented by circles. Drug-sensitive kinases are shown as red circles, with the size corresponding to the level of competition (larger circle, more competed). Drug-resistant kinases are shown as gray circles. Kinases reported as being drug-sensitive ($Log_2R > 1.5$) were also required to show significance ($-Log_{10}P\text{-Value} > 1.5$) from a two-sample t-test with an FDR of 0.05 (n=3)

To validate that both **14a** and **15a** modulate the global conformation of Src like their non-electrophilic counterparts (**Figure 3-13D**), we performed SH3 domain pull-down assays with inhibitor-bound Src V284C complexes. As expected, we found that the SH3 domain of the Src V284C/**1a** complex was largely inaccessible to an immobilized SH3 ligand while the Src V284C/**2a** complex's SH3 domain readily participated in intermolecular interactions. Like the Src V284C/**2a** complex, we observed that both the Src V284C/**14a** and Src V284C/**15a** complexes were efficiently enriched by the immobilized SH3 ligand, which is consistent with their ability to promote an open global conformation of Src V284C's SH3-SH2-CD module.

Prior to studying how **14a** and **15a** affect Src's phosphotransferase-independent functions in cells, we determined their selectivity for Src V284C with a lysate profiling method (**Figure 3-13E**).[105-107] To do this, we measured the ability of **14a** and **15a** to compete for binding to a mixture of resin-immobilized nonselective ATP-competitive inhibitors (kinobeads) with lysate kinases. The binding of an inhibitor being profiled prevents enrichment of lysate kinases by kinobeads, which allows us to profile inhibitors against a large number of human kinases using quantitative mass spectrometry. Specifically, inhibitor selectivity can be determined by measuring the loss of relative enrichment of kinases in inhibitor-treated lysates versus lysate treated with a vehicle control (DMSO). **14a** and **15a** were both profiled at a single high concentration (20 ∝M) in Src V284C-expressing HeLa lysates and the relative enrichment of ~150 kinases was quantified. We found that Src V284C was the most competed target of **14a**, with Receptor Interacting Serine/Threonine Kinase 2 (RIPK2) being the only significant off-target kinase (**Figure 3-13F**). **15a** demonstrated a similar selectivity profile, except Src V284C and RIPK2 were competed at similar levels (**Figure 3-14**). Thus, our observation suggests that Src V284C is the primary target for **14a** and **15a**, with RIPK2 being the only off-target for both inhibitors in the Src V284C-expressing HeLa lysates.

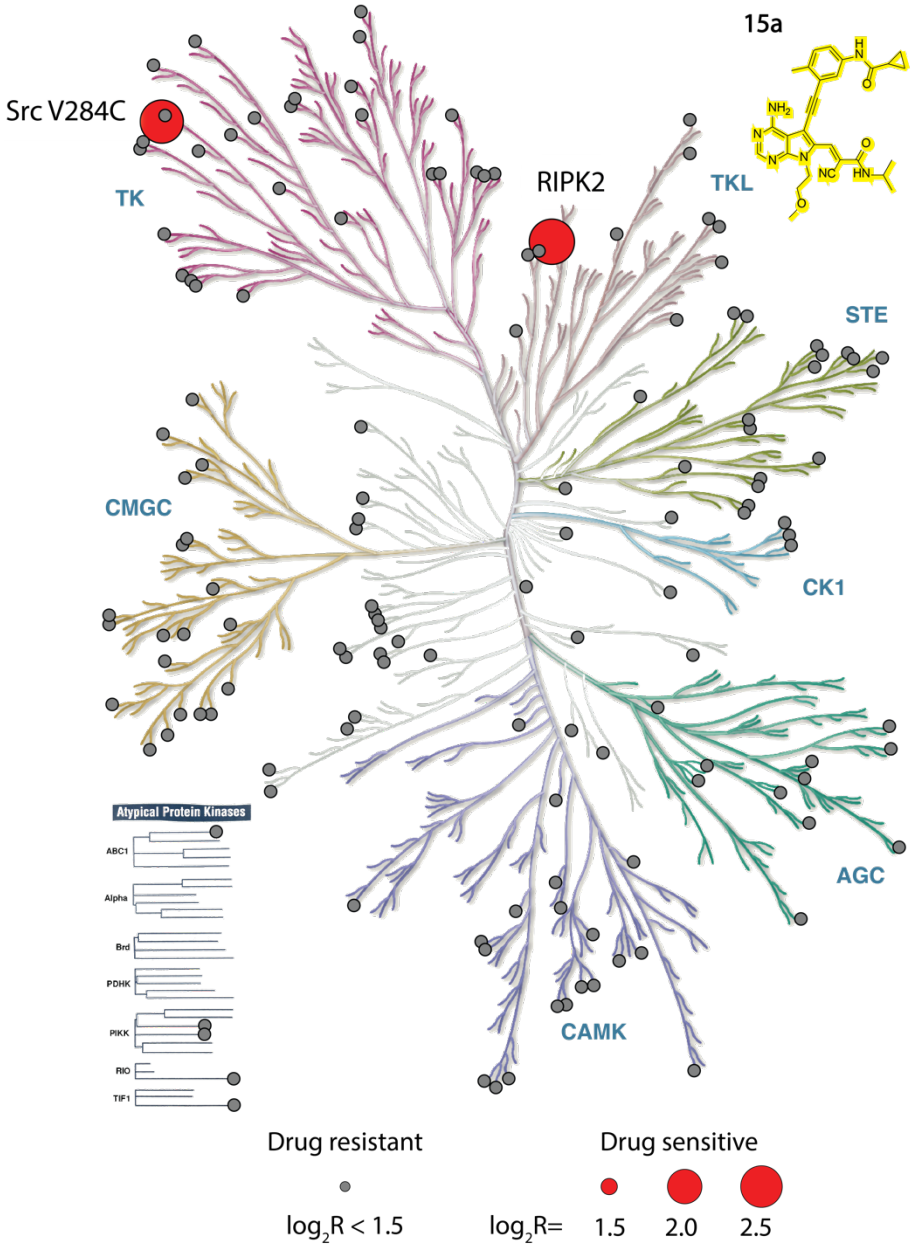

Figure 3-14**.** A phylogenetic tree showing the kinome selectivity of **15a**. All profiled lysate kinases are represented by circles. Drug-sensitive kinases are shown as red circles with the size corresponding to the level of competition (larger circle, more competed). Drug-resistant kinases are shown as gray circles. Kinases reported as being drug-sensitive ($Log_2R > 1.5$) were also

required to show significance ($-Log_{10}$P-Value > 1.5) from a two-sample t-test with FDR of 0.05 (n=3).

3.2.6 Stabilization of Src in the helix αC-in conformation is sufficient to promote a phosphotransferase-independent alteration in cell morphology.

We recently showed that Src can promote non-apoptotic membrane blebs, which are characterized by localized disruption of the actin-myosin cortex, through a phosphotransferase-independent mechanism and that conformation-selective inhibitors can differentially modulate this phenotype (**Figure 3-15A**).[76, 108] We found that the expression of drug-sensitive Src V284C and wild-type Src (WT) in HeLa cells yielded a basal number of cells with membrane blebs (~10%), which was negligibly influenced by treatment with helix αC-out-stabilizing **1a** (**Figure 3-15B**). In contrast, treatment with DFG-out-stabilizing inhibitor **2a** significantly induced membrane blebs in HeLas expressing Src V284C (~55%) but not in Src WT-expressing HeLa cells (**Figure 3-15B**).[76]

Our observations with **14** and **15** in *vitro* made us interested in investigating whether stabilizing Src in the helix αC-in conformation in cells is sufficient to mimic the phenotype promoted by DFG-out-stabilizing inhibitor **2a**. Therefore, we tested the influence of **14a** and **15a** on the cell morphology of Src V284C-expressing HeLas. We found that treatment of Src V284C-expressing HeLas with **14a** and **15a** yielded a significant increase in the percentage of cells with membrane blebs (~60%) (**Figure 3-15B**), while Src WT-expressing HeLas remained at the basal level when treated with these inhibitors (**Figure 3-16**). Notably, Src V284C-expressing HeLas that are treated with **14a** and **15a** showed levels of blebbing comparable to cells treated with **2a**. Thus, stabilization of Src in the helix αC-in conformation is sufficient to induce membrane blebs. Therefore, the

observed ability of a DFG-out-stabilizing inhibitor to promote membrane blebs is not due to its ability to perturb Src's activation loop but rather its ability to stabilize Src's helix αC in an active conformation.

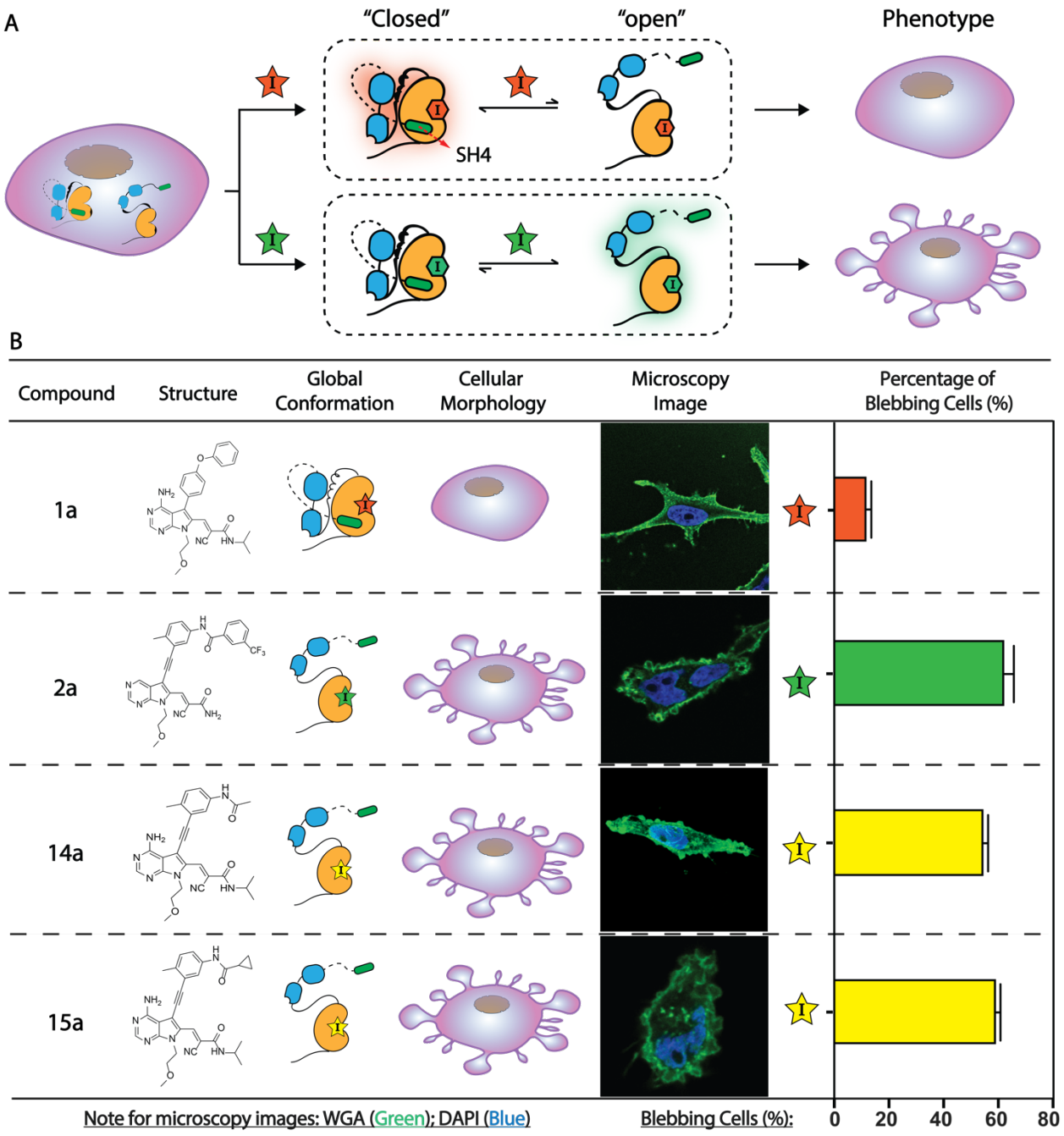

Figure 3-15. Stabilization of Src's helix □C in an active conformation (helix αC-in) is sufficient to promote a Src-mediated, phosphotransferase-independent alteration in cell morphology.

(A) CystIMATIK probes that enforce an open global conformation of Src V284C promote non-apoptotic membrane blebs in HeLas expressing drug-sensitized Src V284C. (B) Levels of membrane blebs in Src V284C-expressing HeLas that are treated with CystIMATIK probes. Percentages of blebbing cells are shown as mean ± SEM (n=3). Nuclei were stained with DAPI (blue) and membranes were stained with Wheat Germ Agglutinin (WGA)-Alexa488 (green). For each replicate, 17 to 32 images were taken and the percentage of blebbing cells from all imaged cells was quantified. Each image contained 1-3 stained cells. The number of blebbing cells was scored based on the criteria described in the supporting information.

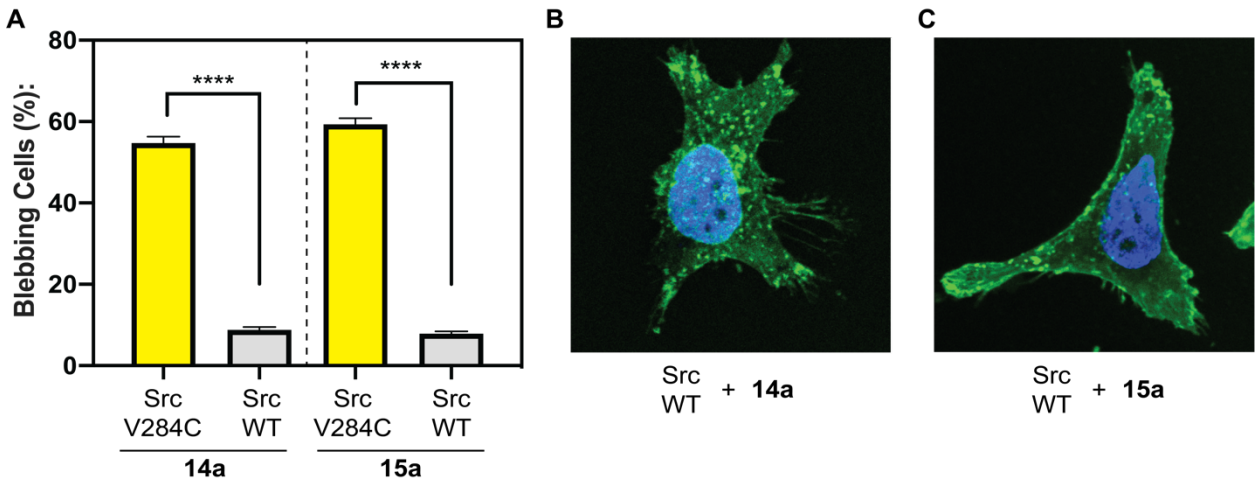

Figure 3-16. The level of blebbing in Src WT-expressing HeLas that are treated with 14a and 15a.

(A) Comparison of the level of membrane blebs in Src V284C- and Src WT-expressing HeLas that are treated with 14a or 15a. Percentages of blebbing cells are shown as mean ± SEM (n=3). P-values are calculated using a two-tailed t test (* < 0.05, ** < 0.01, *** < 0.001, ****<0.0001). (B) An example of confocal imaging of 14a-treated HeLas expressing Src WT. (C) An example of

confocal imaging of 15a-treated HeLas expressing Src WT. Nuclei were stained with DAPI (blue) and membranes were stained with Wheat Germ Agglutinin (WGA)-Alexa488 (green).

3.3 CONCLUSIONS

Interdomain regulation is a defining characteristic of multidomain kinases. Almost half of the human kinases contain at least one auxiliary domain, which, in many cases, are implicated in phosphotransferase-independent functions within cells.[3] Although a growing body of evidence strongly suggests that conformation-selective, ATP-competitive inhibitors can modulate regions distal to a kinase's CD, the overall generality and molecular determinants of this phenomenon are not completely known. In this study, we have demonstrated that inhibitors which stabilize two different inactive ATP-binding site conformations can divergently modulate the global conformation of multidomain tyrosine kinases that contain a Src-like regulatory SH3-SH2-CD module, including the SFKs, Abl-1, and the Tec family kinase BTK. Despite structural differences in the N- and C-termini of SFKs, Abl-1, and BTK, the allosteric communication between their ATP-binding sites and regulatory SH3 and SH2 domains remain conserved. This observation suggests that the effects of conformation-selective inhibitors on global conformation are likely conserved in other tyrosine kinases that contain a homologous SH3-SH2-CD module.

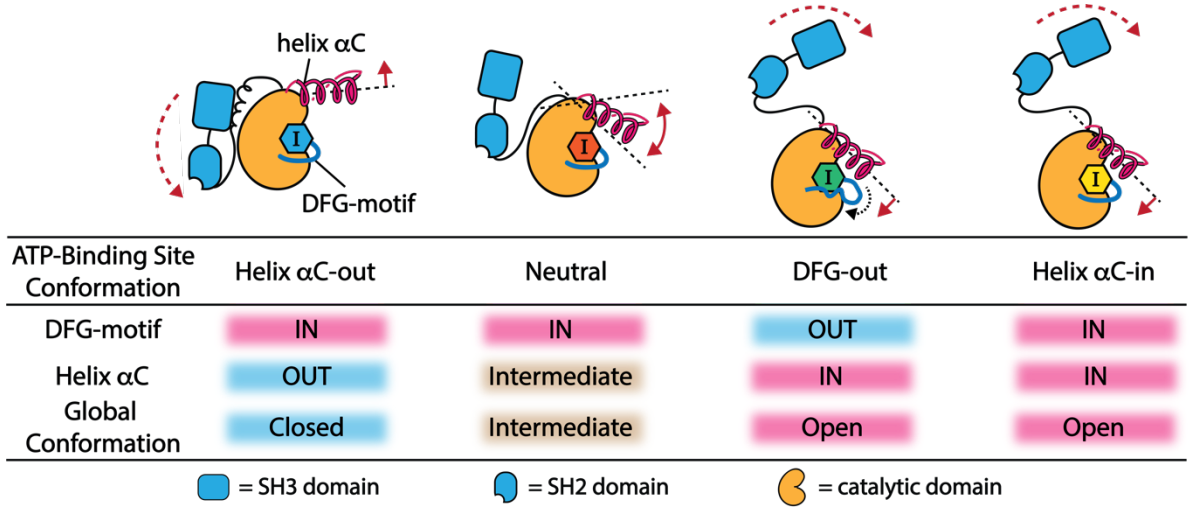

Figure 3-17**.** ATP binding site contacts of inhibitors that allosterically modulate the SH3-SH2-CD module. An inhibitor's ability to stabilize helix αC in an active conformation (helix αC-in) is the main determinant of its ability to promote an open global conformation of the SH3-SH2-CD module.

By systematically analyzing the common features of inhibitors that promote an open global conformation of Src, we were able to develop chemical probes that allowed us to isolate the effects of specific ATP-binding site interactions. With these probes, we found that an inhibitor's ability to promote an open global conformation of Src's SH3-SH2-CD module mainly relies on its ability to stabilize an active conformation of the helix αC. Thus, the noted ability of DFG-out-stabilizing inhibitors to promote an open global conformation in Src and Abl-1 is most likely due to their interactions with the helix αC, rather than perturbation of the DFG-motif in the activation loop (**Figure 3-17**). Furthermore, we have determined that stabilization of Src's helix αC in the active conformation (helix αC-in) is sufficient to promote a Src-mediated, phosphotransferase-independent alteration in cell morphology, a phenotypic effect consistent with releasing the

otherwise intramolecularly sequestered N-terminal SH4 domain of Src. Like Src's SH4 domain, Abl-1's N-terminal myristate and BTK's N-terminal PH-TH domain not only suppress phosphotransferase activity by interacting with their CDs[85-86, 109-110] but also interact with the plasma membrane and additional organelles when intermolecularly accessible.[86, 109, 111-113] Based on our observation with Src, inhibitors that stabilize or perturb the helix αCs of Abl-1 and BTK likely influence the localization and other phosphotransferase-independent functions of these kinases by allosterically modulating global conformation.[114-115] Taken together, our results have direct implications for targeting the helix αC in the ATP-binding site of multidomain tyrosine kinases with inhibitors to modulate kinase functional surfaces distal to their CDs. Although our results highlight the effects of conformation-selective inhibitors on the subset of tyrosine kinases that contain an SH3-SH2-CD module, it is likely that multidomain kinases with alternative regulatory architectures can also be allosterically modulated using similar principles. The conceptual framework and probes that we describe in this report may help facilitate these studies.

3.4 MATERIALS AND METHODS

REGENTS AND MATERIALS:

REAGENTS	SOURCE	NOTES
Antibodies and Reagents		
Rabbit monoclonal anti-Src (36D10)	Cell Signaling Technology	#2109
Btk (D6T2C) Mouse mAb	Cell Signaling Technology	#56044

c-Abl Antibody	Cell Signaling Technology	#2862
Goat anti-Rabbit IgG (H+L), Superclonal Recombinant Secondary Antibody	Thermo Fisher Scientific	#A27033
Goat anti-Mouse IgG (H+L), Superclonal Recombinant Secondary Antibody	Thermo Fisher Scientific	#A28174
Bacterial and Virus Strains		
Escherichia coli (BL21 DE3)	New England Biolabs	#C2527H
Escherichia coli (NEB 5α)	New England Biolabs	#C2987H
Chemicals, Peptides, and Recombinant Proteins		
Inhibitor **1**, **2**, **10**, **1a**, **2a**, and **10a**	/	See the Supplementary Information of *Mol. Cell 2019, 74, p. 393-408* for synthesis and primary profiling data.
Inhibitor **3**, **4**, **5**, and **13**	/	See the Supplementary Information of *ACS chemical biology 14 (6), 1249-1259* for synthesis and primary profiling data.
Inhibitor **6** (Vandetinib)	Chemietek	/
Inhibitor **7** (PP1)	Selleckchem	/
Inhibitor **8**	/	See the Supplementary Information of *European journal of medicinal chemistry 74 (2014): 562-573* for synthesis and primary profiling data.
Inhibitor **9**, **11**, **14**, **15**, **14a**, and **15a**	/	See the Supplementary Information for synthesis and primary profiling data.
Inhibitor **12** (PP121)	Selleckchem	/
Snap-VSL12	/	PMID: 2494627

Snap-NP40	/	This study
Turbofectin 8.0	Origene	#TF81001
Sortase A	Addgene	Plasmid #64973
Thermolysin	Promega Corp	#v4001
Paraformaldehyde (16%)	Electron Microscopy Sciences	#15710
Fluoromount-G mounting media	Southern Biotechnology	#0100-01
Wheat Germ Agglutinin, Alexa Fluor™ 488 Conjugate	Thermo Fisher Scientific	#W11261
NucBlue™ Fixed Cell ReadyProbes™ Reagent	Thermo Fisher Scientific	#R37606
NHS-sepharose beads Fast-flow (4B)	Millipore Sigma	#GE17-0906-01
SYPRO Ruby staining solution	BIO-RAD	#1703125
Pierce protease inhibitor	Thermo Fisher Scientific	#A32963
Pierce phosphatase inhibitor cocktail 2	Millipore Sigma	#P5726
Pierce phosphatase inhibitor cocktail 3	Millipore Sigma	#P0044
IGEPAL® CA-630	Millipore Sigma	#I8896
2-Mercaptoethanol	BIO-RAD	#1610710
Endoproteinase LysC	New England Biolabs	#P8109S
Pierce MS Grade Trypsin	Thermo Fisher Scientific	#PI90057
Critical Commercial Assays		

Library Quantification kit (Illumina)	KAPA Biosystems	KK4854
MiSeq Reagent Kit v2 (300 cycles)	Illumina	MS-102-2002
NextSeq 500/550 High Output v2 kit (75 cycles)	Illumina	FC-404-2005
Deposited Data		
Atomic coordinates, Src/**14** structure	Protein Data Bank	PDB: 6WIW
Experimental Models: Cell Lines		
Human: TREx™-FlpIN™-HeLa cells	/	A generous gift from Stephen S. Taylor, University of Manchester
Recombinant DNA		
all vectors	/	See **Table S3**
Software and Algorithms		
PyMOL	Schrödinger	https://pymol.org/
ImageJ	Schneider *et al*. 2012	https://imagej.nih.gov/ij/
GraphPad Prism 8	GraphPad Software	https://www.graphpad.com/
MaxQuant	Max Planck Institute of Biochemistry	https://www.maxquant.org/maxquant/
Perseus	Max Planck Institute of Biochemistry	https://www.maxquant.org/perseus/
Pro-Data SX20	Applied Photophysics Ltd.	https://www.photophysics.com/
PHENIX	NIH General Medical Sciences	https://www.phenix-online.org/

Coot	MRC Laboratory of Molecular Biology	https://www2.mrc-lmb.cam.ac.uk/personal/pemsley/coot/
XDS	MPI for Medical Research, Heidelberg	http://xds.mpimf-heidelberg.mpg.de/

Mammalian cell culture

TREx™-FlpIN™-HeLa cells were used for imaging experiments. All cells used in this study were maintained in DMEM (GIBCO) supplemented with 10% FBS (GIBCO) at 37 ˚C in a humidified incubator containing 5% CO_2. Transfections were performed with a 3:1 ratio of Turbofectin (Origene)/DNA according to the standard protocol.

Cloning: All enzymes were purchased from New England Biolabs and all chemicals purchased from Sigma unless otherwise specified. All mutants were generated using either QuickChange Site-Directed Mutagenesis (Agilent) following standard protocols. Mutations were verified with Sanger sequencing by Genewiz. All subcloning was achieved using Gibson assembly following standard protocols and validated by Sanger sequencing.

Generation of Stable HeLa Cell Line: The doxycycline-inducible HeLa cell lines expressing Src V284C and Src WT were previously generated using Flp-In T-REx HeLa cells (a generous gift from Stephen S. Taylor, University of Manchester) in our lab.[75-76] See the supporting information of *J. Am. Chem. Soc.* 2019, 141, 30, 11912-11922 for primary profiling data.

(*Inserted protein sequence of Src V284C*)

MGSNKSKPKDASQRRRSLEPAENVHGAGGGAFPASQTPSKPASADGHRGPSAAFAPAA
AEPKLFGGFNSSDTVTSPQRAGPLAGGVTTFVALYDYESRTETDLSFKKGERLQIVNNTE
GDWWLAHSLSTGQTGYIPSNYVAPSDSIQAEEWYFGKITRRESERLLLNAENPRGTFLV
RESETTKGAYCLSVSDFDNAKGLNVKHYKIRKLDSGGFYITSRTQFNSLQQLVAYYSKH
ADGLCHRLTTVCPTSKPQTQGLAKDAWEIPRESLRLEVKLGQGCFGECWMGTWNGTTR
VAIKTLKPGTMSPEAFLQEAQVMKKLRHEKLVQLYAVVSEEPIYIVTEYMSKGSLLDFL
KGETGKYLRLPQLVDMAAQIASGMAYVERMNYVHRDLRAANILVGENLVCKVADFGL
ARLIEDNEYTARQGAKFPIKWTAPEAALYGRFTIKSDVWSFGILLTELTTKGRVPYPGMV
NREVLDQVERGYRMPCPPECPESLHDLMCQCWRKEPEERPTFEYLQAFLEDYFTSTEPQ
YQPGENL*

(*Inserted protein sequence of Src WT*)

MGSNKSKPKDASQRRRSLEPAENVHGAGGGAFPASQTPSKPASADGHRGPSAAFAPAA
AEPKLFGGFNSSDTVTSPQRAGPLAGGVTTFVALYDYESRTETDLSFKKGERLQIVNNTE
GDWWLAHSLSTGQTGYIPSNYVAPSDSIQAEEWYFGKITRRESERLLLNAENPRGTFLV
RESETTKGAYCLSVSDFDNAKGLNVKHYKIRKLDSGGFYITSRTQFNSLQQLVAYYSKH
ADGLCHRLTTVCPTSKPQTQGLAKDAWEIPRESLRLEVKLGQGCFGEVWMGTWNGTT
RVAIKTLKPGTMSPEAFLQEAQVMKKLRHEKLVQLYAVVSEEPIYIVTEYMSKGSLLDF
LKGETGKYLRLPQLVDMAAQIASGMAYVERMNYVHRDLRAANILVGENLVCKVADFG
LARLIEDNEYTARQGAKFPIKWTAPEAALYGRFTIKSDVWSFGILLTELTTKGRVPYPGM
VNREVLDQVERGYRMPCPPECPESLHDLMCQCWRKEPEERPTFEYLQAFLEDYFTSTEP
QYQPGENL*

Cell lysis: HEK293 or HeLa cells were grown on 10-cm plates in Dulbecco's Modified Eagle's Medium (DMEM) supplemented with 10% (by volume) Fetal Bovine Serum (FBS) at 37 °C in a humidified incubator containing 5% CO2 until 90% confluence.

(For SH3 pull-down experiments) Cells were washed with ice-cold DPBS once and lysed with 500 µL of ice-cold lysis buffer ([Tris]=50 mM, pH=7.5, [NaCl]=150 mM, [EDTA]=1 mM, [BME]=1 mM, [Igepal-CA630]=1.0%(v/v), Pierce protease inhibitor, Pierce phosphatase inhibitor cocktail 2 and 3). Cell lysates were centrifuged at 17,000 × g for 10 minutes at 4 °C. The supernatant was collected and quantified using Pierce 660nm Protein Assay Reagent. The lysate protein concentration was adjusted to 1.0 mg/mL with ice-cold lysis buffer.

(For lysate kinase profiling experiments) Cells were washed with ice-cold DPBS three times and lysed with 500 µL of ice-cold Mod. RIPA buffer ([Tris]=50 mM, [NaCl]=150 mM, [NaF]=10 mM, [Igepal-CA630]=1.0% (by volume), [Sodium deoxycholate]=0.25%, [glycerol]=5%, pH=7.8 containing protease inhibitor, 1mM PMSF, and phosphatase inhibitor cocktail 2&3). Cell lysates were centrifuged at 17,000 × g for 10 minutes at 4 °C. The supernatant was collected and quantified using Pierce 660nm Protein Assay Reagent. The lysate protein concentration was adjusted to 2.0 mg/mL with ice-cold lysis buffer.

Protein expression and purification

(*Recombinant $Src^{TAMRA\text{-}3D}$ V284C*) TAMRA-labelled $Src^{TAMRA\text{-}3D}$ V284C (residue 87-536) were expressed and purified accordingly to the Supplementary Information of *Mol. Cell* 2019, *74*, p. 393-408.

(*Recombinant Src^{3D} V284C*) Src^{3D} V284C (residue 87-536) were expressed and purified accordingly to the Supplementary Information of *Mol. Cell* 2019, *74*, p. 393-408.

(*Recombinant Src^{3D} WT*) N-terminal His6-tagged Src^{3D} WT (residue 87-536) were expressed and purified accordingly to the Supplementary Information of *Mol. Cell* 2019, *74*, p. 393-408 and *ACS Chem. Biol. 2019, 14, 6, 1249-1259*.

(*Recombinant Src^{FL} WT*) Src^{FL} WT (residue 2-536) were expressed and purified accordingly to the Supplementary Information of *Mol. Cell* 2019, *74*, p. 393-408 and *ACS Chem. Biol. 2019, 14, 6, 1249-1259.*

(*Recombinant Abl-1^{3D} WT*) See the star method of *Cell metabolism, 25(4), 883-897* for expression and purification of Abl-1^{3D} WT. Briefly, Abl-1^{3D} WT (Residues 65-534) were cloned in a pET-28a vector. The plasmids for Abl-1^{3D} WT, YopH (pCDFDuet-1 plasmid), and GroEL (pGRO7 plasmid) were co-transformed into BL21 cells and plated onto triple selective (kanamycin, streptomycin, and chloramphenicol) LB agar plates and grown overnight at 37 ˚C. A single colony from the plate was grown in an overnight culture of 50 mL of Terrific Broth containing kanamycin/streptomycin/ chloramphenicol overnight at 37 ˚C. A large 2L culture was then inoculated with the overnight culture and grown to an OD600=1.2 at 37 ˚C. The culture was then cooled to 18 ˚C and the expression was induced with 0.2mM IPTG for 16 hr (overnight) at 18 ˚C and pelleted. The cell pellet was re-suspended in chilled lysis buffer (50mM HEPES pH 8.0, 20 mM Imidazole, 300 mM NaCl, 0.1% Triton-X, and 1 mM PMSF). Cells were lysed by sonication and cleared by spinning for 30-45 min at 10,000 x rcf. The clarified lysate was incubated with 1 mL 50% Ni-NTA slurry at 4 ˚C for 1 hr. The resin was then washed with cold lysis buffer (3 times of bead volume). Eluted protein was dialyzed overnight into 50 mM Tris pH 8.0, 150 mM NaCl, 5% Glycerol, and 1 mM DTT. Proteins were purified on an anion exchange column (QFF HiTrap; GE Healthcare) to yield pure Abl-1^{3D} WT.

(*Recombinant Abl-1^{3D} V256C*) Recombinant Abl-1^{3D} V256C (Residues 65-534) was expressed and purified using the same protocol as described for recombinant Abl-1^{3D} WT with plasmids for Abl-1^{3D} V256C (pET-28a plasmid), YopH (pCDFDuet-1 plasmid), and GroEL (pGRO7 plasmid).

(*Sequence for Abl-1^{3D} WT*)

MHHHHHHSSGVDLGTENLYFQSMARWNSKENLLAGPSENDPNLFVALYDFVASGDNT
LSITKGEKLRVLGYNHNGEWCEAQTKNGQGWVPSNYITPVNSLEKHSWYHGPVSRNA
AEYLLSSGINGSFLVRESESSPGQRSISLRYEGRVYHYRINTASDGKLYVSSESRFNTLAE
LVHHHSTVADGLITTLHYPAPKRNKPTVYGVSPNYDKWEMERTDITMKHKLGGGQYG
EVYEGVWKKYSLTVAVKTLKEDTMEVEEFLKEAAVMKEIKHPNLVQLLGVCTREPPFY
IITEFMTYGNLLDYLRECNRQEVNAVVLLYMATQISSAMEYLEKKNFIHRDLAARNCLV
GENHLVKVADFGLSRLMTGDTYTAHAGAKFPIKWTAPESLAYNKFSIKSDVWAFGVLL
WEIATYGMSPYPGIDLSQVYELLEKDYRMERPEGCPEKVYELMRACWQWNPSDRPSFA
EIHQAFETMFQESSISDEVEKELGKQGV*

(*Sequence for Abl-1^{3D} V256C*)

MHHHHHHSSGVDLGTENLYFQSMARWNSKENLLAGPSENDPNLFVALYDFVASGDNT
LSITKGEKLRVLGYNHNGEWCEAQTKNGQGWVPSNYITPVNSLEKHSWYHGPVSRNA
AEYLLSSGINGSFLVRESESSPGQRSISLRYEGRVYHYRINTASDGKLYVSSESRFNTLAE
LVHHHSTVADGLITTLHYPAPKRNKPTVYGVSPNYDKWEMERTDITMKHKLGGGQYG
EVYEGCWKKYSLTVAVKTLKEDTMEVEEFLKEAAVMKEIKHPNLVQLLGVCTREPPFY
IITEFMTYGNLLDYLRECNRQEVNAVVLLYMATQISSAMEYLEKKNFIHRDLAARNCLV
GENHLVKVADFGLSRLMTGDTYTAHAGAKFPIKWTAPESLAYNKFSIKSDVWAFGVLL
WEIATYGMSPYPGIDLSQVYELLEKDYRMERPEGCPEKVYELMRACWQWNPSDRPSFA
EIHQAFETMFQESSISDEVEKELGKQGV*

(*N-Flag-tagged BTK WT*) HEK293 cells were transfected with N-terminal Flag-tagged BTK WT construct. Cells were lysed in mod RIPA buffer buffer ([Tris]=50 mM, pH=7.5, [NaCl]=150 mM, [EDTA]=1 mM, [BME]=1 mM, [Igepal-CA630]=1.0% (by volume), Pierce protease inhibitor, Pierce phosphatase inhibitor cocktail 2 and 3) and the lysate protein concentration was normalized to 1.0 mg/mL.

(*N-Flag-tagged BTK V416C*) HEK293 cells were transfected with N-terminal Flag-tagged BTK V416C construct. Cells were lysed in mod RIPA buffer buffer ([Tris]= 50 mM, pH=7.5, [NaCl]=150 mM, [EDTA]=1 mM, [BME]=1 mM, [Igepal-CA630]=1.0% (by volume), Pierce protease inhibitor, Pierce phosphatase inhibitor cocktail 2 and 3) and the lysate protein concentration was normalized to 1.0 mg/mL.

(*Sequence for BTK^{FL} WT*)

MDYKDDDDKGMAAVILESIFLKRSQQKKKTSPLNFKKRLFLLTVHKLSYYEYDFERGR
RGSKKGSIDVEKITCVETVVPEKNPPPERQIPRRGEESSEMEQISIIERFPYPFQVVYDEGP
LYVFSPTEELRKRWIHQLKNVIRYNSDLVQKYHPCFWIDGQYLCCSQTAKNAMGCQILE
NRNGSLKPGSSHRKTKKPLPPTPEEDQILKKPLPPEPAAAPVSTSELKKVVALYDYMPM
NANDLQLRKGDEYFILEESNLPWWRARDKNGQEGYIPSNYVTEAEDSIEMYEWYSKHM
TRSQAEQLLKQEGKEGGFIVRDSSKAGKYTVSVFAKSTGDPQGVIRHYVVCSTPQSQYY
LAEKHLFSTIPELINYHQHNSAGLISRLKYPVSQQNKNAPSTAGLGYGSWEIDPKDLTFL
KELGTGQFGVVKYGKWRGQYDVAIKMIKEGSMSEDEFIEEAKVMMNLSHEKLVQLYG
VCTKQRPIFIITEYMANGCLLNYLREMRHRFQTQQLLEMCKDVCEAMEYLESKQFLHR
DLAARNCLVNDQGVVKVSDFGLSRYVLDDEYTSSVGSKFPVRWSPPEVLMYSKFSSKS

DIWAFGVLMWEIYSLGKMPYERFTNSETAEHIAQGLRLYRPHLASEKVYTIMYSCWHE
KADERPTFKILLSNILDVMDEES

(*Sequence for BTK^{FL} V416C*)

MDYKDDDDKGMAAVILESIFLKRSQQKKKTSPLNFKKRLFLLTVHKLSYYEYDFERGR
RGSKKGSIDVEKITCVETVVPEKNPPPERQIPRRGEESSEMEQISIIERFPYPFQVVYDEGP
LYVFSPTEELRKRWIHQLKNVIRYNSDLVQKYHPCFWIDGQYLCCSQTAKNAMGCQILE
NRNGSLKPGSSHRKTKKPLPPTPEEDQILKKPLPPEPAAAPVSTSELKKVVALYDYMPM
NANDLQLRKGDEYFILEESNLPWWRARDKNGQEGYIPSNYVTEAEDSIEMYEWYSKHM
TRSQAEQLLKQEGKEGGFIVRDSSKAGKYTVSVFAKSTGDPQGVIRHYVVCSTPQSQYY
LAEKHLFSTIPELINYHQHNSAGLISRLKYPVSQQNKNAPSTAGLGYGSWEIDPKDLTFL
KELGTGQFGVCKYGKWRGQYDVAIKMIKEGSMSEDEFIEEAKVMMNLSHEKLVQLYG
VCTKQRPIFIITEYMANGCLLNYLREMRHRFQTQQLLEMCKDVCEAMEYLESKQFLHR
DLAARNCLVNDQGVVKVSDFGLSRYVLDDEYTSSVGSKFPVRWSPPEVLMYSKFSSKS
DIWAFGVLMWEIYSLGKMPYERFTNSETAEHIAQGLRLYRPHLASEKVYTIMYSCWHE
KADERPTFKILLSNILDVMDEES

Western blot analysis of mammalian cell lysates and in *vitro* assays: All protein samples were boiled in 3x SDS buffer (240 mM Tris, pH 6.8, 30% glycerol, 3% SDS, 0.01% bromophenol blue, 15% 2-mercaptoethanol) unless stated otherwise. Samples were resolved on SDS-PAGE gels (150 V, 30-50 mins). Gels were transferred to a PVDF membrane using Trans-blot Turbo Transfer System (BIO-RAD) at 24V and room temperature for 14 minutes. Membrane was washed and blocked in 5% dry milk in 1xTBST buffer for 1 hour. The blocked membrane was incubated with primary antibodies at 4˚C overnight while shaking. All subsequent wash steps were performed

three times in 1xTBST buffer for 5 min while shaking. The probed membrane was washed and incubated with anti-Rabbit (1:10000) or anti-Mouse (1:10000) secondary antibodies (Invitrogen) for 1 hour. After three washes with 1xTBST, all immunoblots were imaged using a LI-COR Odyssey IR imager. Blots were quantified using ImageStudio Lite software.

SyproRuby staining for thermolysin assay: All protein samples were resolved using SDS-PAGE electrophoresis. SyproRuby staining was then performed using the standard protocol by the manufacturer.

Inhibitor IC_{50} and K_i determination by inhibitor titration: For IC_{50} determination experiments, a kinase enzyme titration was performed prior to inhibitor testing in order to ensure that the kinase concentration was in the linear range. Ki values were calculated using Cheng-Prusoff equation with previously reported Km [ATP].

(*Src V284C and Src WT*) Inhibitor IC_{50} against Src V284C or Src WT recombinant constructs (residue 87-536) was determined using a fluorogenic assay using a self-reporting fluorescent SFK peptide (EEEIYGE-(Dap-Pyrene)-EA). Inhibitors (3-fold dilution, initial concentration of inhibitor in reaction= 30 μM) were assayed in triplicate against 7.5 nM of Src^{3D} WT and 12.5 nM of Src^{3D} V284C in kinase reaction buffer ([HEPES]= 75 mM, pH= 8.0, [$MgCl_2$]= 15 mM, [EGTA]= 3.75 mM, [NaCl]= 150 mM, [BSA]= 0.2 mg/mL and [Na_3VO_4]= 750 nM). Src was incubated with inhibitors and ATP (1 mM) for 30 mins in a Corning® 384 well microplate (Low flange; product number: CLS3573). Then 20 μM of fluorogenic substrate solution in kinase

reaction buffer was added and incubated for 120 minutes. Raw fluorescence units were measured on an Envision plate reader (Perkin Elmer) with an excitation wavelength of 344 nm and an emission wavelength of 405 nm. Percentage of inhibition was calculated and IC_{50} values were determined using "One site – Fit logIC_{50}" model in GraphPad software Prism 8. All assays were performed in triplicate.

(*Abl-1 V256C and Abl-1 WT*) Inhibitor IC_{50} against Abl-1 V256C or Abl-1 WT recombinant was determined using a radiation assay using an Abl-1 Peptide Substrate (APS; EAIYAAPFAKK). Briefly, inhibitors (3-fold dilution, initial concentration of inhibitor in reaction= 30 μM) were assayed in triplicate against 38 nM of Abl-1^{3D} V256C and 7.5 nM of Abl-1^{3D} WT in kinase reaction buffer containing 75 mM HEPES (pH 8.0), 15 mM $MgCl_2$, 3.8 mM EGTA, 750 nM Na_3VO_4, 150 mM NaCl, 0.2 mg/mL BSA, and 40 μM Abl-1 Peptide Substrate (Ac-AEAIYAA(dap-pyrene)-LA-NH_2) at a total volume of 30 μL. The kinases were incubated with inhibitors and 1 mM of ATP for 30 minutes in a 384-black assay plate (Corning, #3573). 40 μM of self-report fluorescent Abl-1 peptide was then added to the plate and incubated for 2 hours. The raw fluorescence date was determined using Envision (Perkin Elmer) plate reader with an excitation wavelength of 344 nm and an emission wavelength of 405 nm. The Data was analyzed using GraphPad Prism 8 software and IC_{50} values were determined using "One-site fit log IC_{50}" model. All IC_{50} values were then converted to Ki values using Cheng-Prusoff's equation. All assays were performed in biological replicates (n=3).

SH3 domain pull-down experiments

(*Src^{FL} WT complexes*) The protocol was modified based on methods described in the supporting information of *J. Am. Chem. Soc. 2019, 141, 30, 11912-11922*. Briefly, 10 µL of a 50% slurry (by volume) of O^6-benzylguanine-containing sepharose beads were washed with immobilization buffer ([Tris]= 50 mM, pH= 7.5, [NaCl]= 100 mM, [DTT]= 1 mM, [BSA]=0.2 mg/mL) (10 bed volumes) for 3 times. The beads were then incubated with 50 µL of SNAP-tagged SH3 ligand (peptide sequence: VSLARRPLPPLP) (8 µM) on an end-to-end rotator at room temperature for 1 hour. After immobilization of the SNAP-tagged SH3 ligand, the beads were washed with immobilization buffer (10-bed volumes) for 3 times. Meanwhile, a saturating amount of inhibitor 1 or 2 (10 µM) was added to 50 µL of a solution in immobilization buffer containing 80 nM of recombinant Src^{FL} WT. The solution was incubated at ambient temperature for 30 minutes before being added to the immobilized SH3 ligand beads. After incubating at room temperature for 1 hour, the beads were washed with immobilization buffer (10-bed volumes) for 3 times. The captured Src^{FL} WT complex was eluted by boiling the beads in 50 µL of 1x SDS loading buffer at 95 ˚C for 10 minutes. The protein bands were immunoblotted using an anti-Src antibody and imaged on LI-COR Odyssey IR imager. Intensity value of each band was quantified using ImageStudio™Lite. Percentage of Src^{FL} WT bound to the polyproline-containing beads=Intensity(EL)/[Intensity(IN)+Intensity(EL)]×100% was plotted using GraphPad software Prism 8.

(*Src^{3D} WT complexes*) The protocol was modified based on methods described in the supporting information of *J. Am. Chem. Soc. 2019, 141, 30, 11912-11922*. Briefly, 10 µL of a 50% slurry (by volume) of O^6-benzylguanine-containing sepharose beads were washed with immobilization

buffer ([Tris]= 50 mM, pH= 7.5, [NaCl]= 100 mM, [DTT]= 1 mM, [BSA]=0.2 mg/mL) (10 bed volumes) for 3 times. The beads were then incubated with 50 µL of SNAP-tagged SH3 ligand (peptide sequence: VSLARRPLPPLP) (8 µM) on an end-to-end rotator at room temperature for 1 hour. After immobilization of the SNAP-tagged SH3 ligand, the beads were washed with immobilization buffer (10-bed volumes) for 3 times. Meanwhile, a saturating amount of inhibitor 1, 2, 10, 14, or 15 (10 µM) was added to 50 µL of a solution in immobilization buffer containing 80 nM of recombinant Src^{3D} WT. The solution was incubated at ambient temperature for 30 minutes before being added to the immobilized SH3 ligand beads. After incubating at room temperature for 1 hour, the beads were washed with immobilization buffer (10-bed volumes) for 3 times. The captured Src^{3D} WT complex was eluted by boiling the beads in 50 µL of 1x SDS loading buffer at 95 ˚C for 10 mins. The input (IN) and elution (EL) were immunoblotted using an anti-Src antibody and imaged on LI-COR Odyssey IR imager. Intensities of the bands for each band was quantified using ImageStudio™Lite. Percentage of Src bound to the polyproline-containing beads=Intensity(EL)/[Intensity(IN)+Intensity(EL)]×100% was plotted using GraphPad software Prism 8.

(*$Src^{TAMRA\text{-}3D}$ V284C complex*) 10 µL of a 50% slurry (by volume) of O^6-benzylguanine-containing sepharose beads were washed with immobilization buffer ([Tris]= 50 mM, pH= 7.5, [NaCl]= 100 mM, [DTT]= 1 mM, [BSA]=0.2 mg/mL) (10 bed volumes) for 3 times. The beads were then incubated with 50 µL of SNAP-tagged SH3 ligand (peptide sequence: VSLARRPLPPLP) (8 µM) on an end-to-end rotator at room temperature for 1 hour. After immobilization of the SNAP-tagged SH3 ligand, the beads were diluted by 16-fold with underivatized NHS-sepharose beads and washed with mod RIPA buffer (10-bed volumes) for 3 times. Meanwhile, a saturating amount of

inhibitors (10 μM) was added to 50 μL of immobilization buffer containing 25 nM of Src^{3D} V284C. The solution was incubated at room temperature for 30 minutes before being added to the immobilized SH3 ligand beads. After incubating at room temperature for 1 hour, the beads were washed with immobilization buffer (10-bed volumes) for 3 times. The captured $Src^{TAMRA\text{-}3D}$ V284C complex was eluted by boiling the beads in 50 μL of 1x SDS loading buffer at 95 ˚C for 10 mins. The input (IN) and elution (EL) were analyzed using SDS-PAGE electrophoresis and imaged on GE-Typhoon FLA 9000. Intensities of RITC fluorescence for each band was quantified using ImageStudio™Lite. Percentage of $Src^{TAMRA\text{-}3D}$ V284C bound to the polyproline-containing beads=Intensity(EL)/[Intensity(IN)+Intensity(EL)] × 100% was plotted using GraphPad software Prism 8.

(*Abl-1^{3D} WT complex*) 20 μL of a 50% slurry (by volume) of O^6-benzylguanine-containing sepharose beads were washed with mod RIPA buffer ([Tris]= 50 mM, pH= 7.5, [NaCl]= 150 mM, [EDTA]=1 mM, [BME]= 1 mM, Pierce protease inhibitor, Pierce phosphatase inhibitor cocktail 2 and 3) (10 bed volumes) for 3 times. The beads were then incubated with 50 μL of SNAP tag−polyproline peptide (APTYSPPPPP) (8 μM) on an end-to-end rotator at room temperature for 1 hour. After immobilization of the SNAP-tagged SH3 ligand, the beads were diluted by 256-fold with unmodified NHS-sepharose beads and washed with mod RIPA buffer (10-bed volumes) for 3 times. Meanwhile, a saturating amount of inhibitors (10 μM) was added to 50 μL of HeLa cell lysate containing 50 nM of recombinant Abl^{3D} WT. The solution was incubated at room temperature for 30 minutes before being added to the immobilized SH3 ligand beads. After incubating at room temperature for 1 hour, the beads were washed with mod RIPA buffer (10-bed volumes) for 4 times. The captured Abl^{3D} WT was eluted by boiling the beads in 50 μL of 1x SDS

loading buffer at 95 ˚C for 10 mins. The input (IN) and elution (EL) were analyzed using SDS-PAGE and Western-blot analysis. The protein bands were immunoblotted using an anti-Abl antibody and imaged on LI-COR Odyssey IR imager. Intensities of each band was quantified using ImageStudio™Lite. Percentage of Abl bound to the polyproline-containing beads= Intensity(EL)/[Intensity(IN)+Intensity(EL)] × 100% was plotted using GraphPad software Prism 8.

(*Abl-1^{3D} V256C complex*) 100 nM Abl-1^{3D} V256C (100 nM) and mammalian HEK293 lysate (0.2 mg/mL) were diluted in immobilization buffer [50 mM Tris, 100 mM NaCl, and 1 mM DTT (pH 7.5)]. A saturating amount of the 1a or 2a (10 μM) was added to this kinase solution. The mixture was allowed to incubate for 30 min at room temperature. Meanwhile, 40 μL of a 50% slurry of SNAPCapture Pull-Down Resin (NEB) was washed (twice, 10 bed volumes) with immobilization buffer. A SNAP tag−polyproline peptide (APTYSPPPPP) fusion (10 μM) was loaded onto the resin at a final volume of 100 μL in immobilization buffer. The resin was rotated on an end-to-end rotator at room temperature for 90 minutes. After polyproline peptide immobilization, the resin was washed (twice, 10 bed volumes), and 100 μL of the kinase−inhibitor complex was loaded. The resin was allowed to agitate on an end-to-end rotator at room temperature for 1 hour. After incubation, the flow-through was collected and the resin was washed (three times, 10 bed volumes). To elute the retained kinase, 100 μL of 1xSDS loading buffer was added, and the beads were boiled at 95 ˚C for 10 min. All samples were separated via SDS-PAGE electrophoresis and immunoblotted using a His6-specific antibody [1:5000 dilution]. The immunoblot was imaged with a LI-COR Odyssey imager. The bands were analyzed using ImageStudio software to determine the percentage of kinase retained on the resin on the basis of the loaded and eluted fractions.

(*BTK^{FL} WT complex*) HEK293 cells were transfected with N-terminal Flag-tagged BTK-WT construct. Cells were lysed in mod RIPA buffer buffer ([Tris]= 50 mM, pH= 7.5, [NaCl]= 150 mM, [EDTA]=1 mM, [BME]= 1 mM, [Igepal-CA630]= 1.0%, Pierce protease inhibitor, Pierce phosphatase inhibitor cocktail 2 and 3) and the protein concentration of lysates were normalized to 1.0 mg/mL. 20 µL of a 50% slurry (by volume) of O^6-benzylguanine-containing sepharose beads were washed with mod RIPA buffer (10 bed volumes) for three times. The beads were then incubated with 50 µL of SNAP-tagged SH3 ligand (BTK's SH3 ligand peptide sequence: VSLARRPLPPLP) (8 µM) on an end-to-end rotator at room temperature for 1 hour. After immobilization of the SNAP-tagged SH3 ligand, the beads were diluted with unmodified NHS-sepharose beads and washed with mod RIPA buffer (10-bed volumes) for 3 times. Meanwhile, a saturating amount of inhibitors (10 µM) was added to 50 µL of HeLa cell lysate containing BTK^{FL} WT. The solution was incubated at room temperature for 30 minutes before being added to the immobilized SH3 ligand beads. After incubating at room temperature for 1 hour, the beads were washed with mod RIPA buffer (10-bed volumes) for 4 times. The captured BTK^{FL} WT was eluted by boiling the beads in 50 µL of 1x SDS loading buffer at 95 ˚C for 10 minutes. The input (IN) and elution (EL) were analyzed using SDS-PAGE and Western-blot analysis. The protein bands were immunoblotted using an anti-BTK antibody and imaged on LI-COR Odyssey IR imager. Intensities of each protein band was quantified using ImageStudio™Lite. Percentage of BTK bound to the SH3 ligand-containing beads= Intensity(EL)/[Intensity(IN)+Intensity(EL)] × 100% was plotted using GraphPad software Prism 8.

(*BTK^{FL} V416C complex*) HEK293 cells were transfected with N-terminal Flag-tagged BTK-V416C construct. Cells were lysed in mod RIPA buffer buffer ([Tris]= 50 mM, pH= 7.5, [NaCl]= 150 mM, [EDTA]=1 mM, [BME]= 1 mM, [Igepal-CA630]= 1.0%, Pierce protease inhibitor, Pierce phosphatase inhibitor cocktail 2 and 3) and the protein concentration of lysates were normalized to 1.0 mg/mL. 20 µL of a 50% slurry (by volume) of O^6-benzylguanine-containing sepharose beads were washed with mod RIPA buffer ([Tris]= 50 mM, pH= 7.5, [NaCl]= 150 mM, [EDTA]=1 mM, [BME]= 1 mM, Pierce protease inhibitor, Pierce phosphatase inhibitor cocktail 2 and 3) (10 bed volumes) for 3 times. The beads were then incubated with 50 µL of SNAP-tagged SH3 ligand (BTK's SH3 ligand peptide sequence: VSLARRPLPPLP) (8 µM) on an end-to-end rotator at room temperature for 1 hour. After immobilization of the SNAP-tagged SH3 ligand, the beads were diluted with unmodified NHS-sepharose beads and washed with mod RIPA buffer (10-bed volumes) for 3 times. Meanwhile, a saturating amount of inhibitor 1a or 2a (10 µM) was added to 50 µL of HeLa cell lysate containing BTK^{FL} V416C. The solution was incubated at room temperature for 30 mins before being added to the immobilized SH3 ligand beads. After incubating at room temperature for 1 hour, the beads were washed with mod RIPA buffer (10-bed volumes) for 4 times. The captured BTK^{FL} V416C was eluted by boiling the beads in 50 µL of 1x SDS loading buffer at 95 ˚C for 10 minutes. The input (IN) and elution (EL) were analyzed using SDS-PAGE and Western-blot analysis. The protein bands were immunoblotted using an anti-BTK antibody and imaged on LI-COR Odyssey IR imager. Intensities of each protein band was quantified using ImageStudio™Lite. Percentage of BTK^{FL} V416C bound to the SH3 ligand-containing beads= Intensity(EL)/[Intensity(IN)+Intensity(EL)] × 100% was plotted using GraphPad software Prism 8.

Thermolysin assay for inhibitor-bound Src. This protocol was modified based on the methods described in *ACS Chem. Biol. 2019, 14, 1556−1563*. Recombinant Src^{FL} WT were diluted into proteolysis buffer ([Tris]=50 mM, pH=8.0, [NaCl]=100 mM, [$CaCl_2$]=0.5 mM) to generate a solution of Src^{FL} WT at 0.5 μM. In 200 μL low-retention PCR strips, 1.5 μL of inhibitor solution (60X) was added. 86 μL of the kinase solution was added to the inhibitor solution. The mixture was incubated at room temperature for 30 minutes. 2.5 μL of thermolysin solution (36X; 1.8 μM in proteolysis buffer; this solution was freshly made) was added to the above mixture. The resulting solution was incubated at 37 ˚C. 8 μL of the proteolysis reaction was added to 4 μL of SDS loading dye (3X) containing 50 mM EDTA to quench the reaction at multiple time points (0, 2, 5, 10, 30, 60, 120, 180, and 240 mins). The samples were then resolved by SDS-PAGE. The gels were stained with Sypro Ruby Gel Stain and imaged using GE Typhoon FLA 9000. The intensities of bands were quantified using ImageStudio™ Lite software. Percentage of Src WT that has not been cleaved at the SH2-CD linker was plotted against time and fit to the one phase decay equation (Y=(Y0 - Plateau)*exp(-K*X) + Plateau). [Y= Percentage of Src WT that has not been cleaved at the SH2-CD linker; X=time (mins)]. The mean ± SEM of the half-life values for decay were reported. Relates to Figure 3, 4F.

X-ray crystallography data acquisition and processing

(*Protein Purification of Src^{CD}*) The purification of the kinase domain of wild-type chicken Src (residues 251–533, Src^{CD}) from bacteria with extinction coefficient of 52,745 is described in detail elsewhere.[116]

(*Crystallization of the Src/14 Complex*) The concentration of recombinant Src^{CD} protein was determined by absorbance at 280 nm. The recombinant Src^{CD} was concentrated to 10 mg/mL (330 μM) in 20 mM Tris (pH 8.0), 100 mM NaCl, 5 mM DTT, and 5% DMSO. 14 was added to a final concentration of 500 μM. Crystals of the Src/14 complex grew via hanging drop vapor diffusion at 20 °C with a mother liquor of 0.1 M Bis-Tris (pH 5.5), 100 mM NaOAc, and 12% PEG 3350 with a drop size of 2 μL, where the protein and mother liquor were mixed at a 1:1 volumetric ratio. The crystal was cryoprotected in increasing glycerol concentration from 20% to 30% glycerol prior to being frozen in liquid nitrogen. X-ray diffraction data were collected at the FMX beamline of National Synchrotron Light Source II.

Structure Determination and Refinement: Data of Src^{CD}/14 crystals was processed using XDS[117] and Xtriage (Zwart, P. H., Grosse-Kunstleve, R. W. & Adams, P. D. (2005). CCP4 Newsl. 43, contribution 7.). Structures were solved by molecular replacement with Phaser[118], using a model of the catalytic domain of Src (PDB ID: 20IQ). Refinement was performed with PHENIX[119] and model building with Coot[120]. The coordinates and structure factors have been deposited in the protein databank with PDB ID: 6WIW.

Stop-flow kinetic experiment

Kinetics of inhibitor binding to bacterially expressed human Abl-1^{3D} (residues 248-531) and Src^{3D} (residues 251-533) were monitored by changes in protein fluorescence[101]. Equal volumes of kinase and inhibitor were mixed using an Applied Photophysics SX20 stopped flow at 298 K. Kinetics were recorded under pseudo first order conditions with final concentrations of kinase at indicated post-mixing concentrations of inhibitors. The binding of each inhibitor to the catalytic domain was measured at 5-6 different inhibitor concentrations in a buffer containing 50 mM Tris (pH range 7.0-9.0) or Bis-Tris (pH range 5.5-6.5), 100 mM NaCl, 1 mM DTT, 5% DMSO, and 5% Glycerol. Protein fluorescence was excited at 295 nm and decay in fluorescence was measured with a 360 nm bandpass filter for 10-20 half-lives of each transient, recorded by 1,000-2,000 data points. The highest concentration of inhibitor was chosen so that the inhibitor was soluble in 5% DMSO and k_{obs} was slower than 150 sec^{-1}. The time-dependent decrease in protein fluorescence was fit to a single exponential with slope to accommodate photobleaching using the Pro-Data SX software, $y=A*exp^{-kobs*t} + Bt + c$, where A is the amplitude of the fluorescence signal, B is the slope of the baseline, and k_{obs} is the observed rate constant. Binding kinetics at each inhibitor concentration were measured at least 3-times and averaged. Errors for k_{obs} were calculated as the standard error of the mean (SEM). The degree of curvature indicating the requirement for the flip of DFG-motif for binding was determined as the R square value of the curve fit to a linear equation (DFG-motif is unflipped), or a quadratic equation (DFG-motif is flipped) [102]. The data was fit to a curve derived from a pH dependent, two-step binding model previously used to fit inhibitor's binding curvature with the tested kinase. The kinetic scheme for kinase-inhibitor binding was as follows:

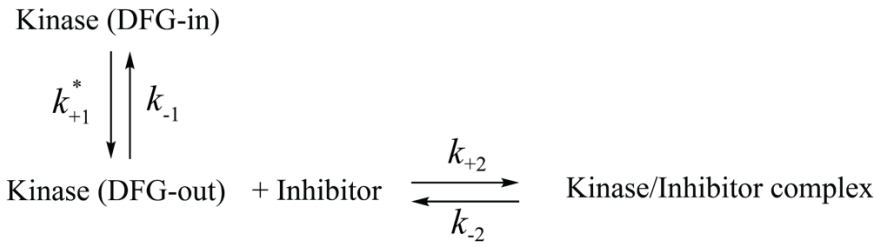

where $k^*_{+1} = P_{AspH,in}k_{+1}$, and $P_{AspH} = (1 + 10^{pH-pKa,in})^{-1}$ is the probability that Asp in the DFG-motif is protonated in a DGF-in conformation. This two-step kinetic model has a slow and a fast rate constant. The slower rate constant is derived as follows:

$$k_{obs} = \frac{k_{-1}k_{-2} + k^*_{+1}k_{-2} + k^*_{+1}k_{+2}L}{k^*_{+1} + k_{-1} + k_{+2}L + k_{-2}}, \quad \text{[Eq. 1]}$$

where L is the concentration of imatinib. For our purposes, we assume that k_{-1}, k^*_{+1}, and $k_{+2}L$ exceed k_{-2} to a significant extent. In this case, this equation simplifies to:

$$k_{obs} = k^*_{+1}\frac{L}{\zeta + L}, \quad \text{[Eq. 2]}$$

where $\zeta = (k^*_{+1} + k_{-1})/k_{+2}$. At each pH value, we independently perform 2-parameter fits of the rate constants as a function of inhibitor concentration. Therefore, we use Eq. 2 with the pH dependent ζ and k^*_{+1} as fitting parameters. This fitting was performed in GradPad Prism8 software.

Lysate profiling experiments with kinobeads matrix for 14a and 15a

(*Preparation of cell lysates*) In a 10-cm plate, HeLas that overexpress Src^{FL} V284C were washed with ice-cold DPBS for three times and lysed with 500 µL of ice-cold Mod. RIPA buffer ([Tris]=50 mM, [NaCl]=150 mM, [NaF]=10 mM, [Igepal-CA630]=1.0%, [Sodium deoxycholate]=0.25%, [glycerol]=5%, pH=7.8 containing protease inhibitor, 1mM PMSF, and phosphatase inhibitor cocktail 2&3). Cell lysates were centrifuged at 17,000 × g for 10 minutes at 4 °C. The supernatant was collected and quantified using Pierce 660nm Protein Assay Reagent and diluted to 2.0 mg/mL with ice-cold lysis buffer.

(*Inhibitor treatment and kinase enrichment with kinobeads*) The lysates (160 µL) were then incubated DMSO, or 20 µM of 14a or 15a for 30 minutes on an end-to-end rotator at 4˚C. Meanwhile, 10 µL of a 50% kinobeads slurry (prepared according to *J Proteome Res, 2017, 16 (3), 1216-1227)* washed with 500 µL of mod RIPA buffer twice. The inhibitor-treated lysates were then added to the drained kinobeads and incubated on an end-to-end rotator for 3 hours at 4˚C. After incubation, the beads were spun down and the supernatant was aspirated off. The beads were then washed with 500 µL of ice-cold mod RIPA buffer twice and three times with 500 µL of ice-cold TBS buffer ([Tris]=50 mM, pH= 7.8, [NaCl]=150 mM) to remove the detergent.

(*On-bead trypsinization and LC/MS sample preparation*) The washed beads were then resuspended in 25 µL of denaturing buffer ([TFE]=20%, [Tris]=5 mM, pH=8.5, [TCEP]=5 mM (add freshly), [CAM]=10 mM (add freshly)). The beads slurry was vortexed briefly and then boiled at 95 ˚C for 5 mins (release pressure occasionally). The beads slurry was diluted with 25 µL of 10% TFE in water. The pH of the resulting suspension was adjusted to 8-9 by adding 1 µL of 1N

NaOH at a time. 0.4 µg of LysC was added to the slurry and agitated on a thermo mixer at 37 ˚C for 2 hours at 1,400 rpm. The slurry was then diluted with 50 µL of 10% TFE. 0.4 µg of sequencing grade trypsin was added to the slurry and the sample was agitated overnight at 37 ˚C at 800 rpm on a thermo mixer. After trypsinization, the slurry was diluted with 100 µL of Buffer A (5% acetonitrile in water, 0.1% TFA) containing 1% formic acid. The resulting slurry was agitated at room temperature for 5 mins. The resulting supernatant was then loaded onto a C-18 column made in-house, washed with 50 µL of Buffer A, and eluted to a low-retention Eppendorf tube using 50 µL of Buffer B (80% acetonitrile in water, 0.1% TFA). The peptides were then resuspended in 20 µL of Buffer A to render the final samples.

(*Proteomic Data Acquisition*) Peptides were separated on a nanoAcquity UPLC instrument with a 12-cm long fused silica capillary column (Polymicro Technologies Flexible Fused Silica Capillary Tubing, Inner Diameter 75 µm, Outer Diameter 375 µm, cat. no. 1068150019) made in-house with a laser puller and packed with 5 µm 120 Å reversed phase C18 beads (ReproSil-Pur 120 C18-AQ, Dr. Maisch GmbH HPLC, cat. no. r15.aq.). The LC gradient was 90-minutes long with 10-35% solvent B at 200 nL/min. LC solvent A was 0.1% acetic acid and LC solvent B was 0.1% acetic acid, 99.9% acetonitrile. MS data were collected with a Thermo Scientific Orbitrap Fusion Tribrid mass spectrometer.

(*Proteomic Data Process and Analysis*) The protocol was modified based on the protocol previously described in the supporting information of *Journal of the American Chemical Society, 141(30), 11912-11922*. Raw data were analyzed using MaxQuant and search engine Andromeda using the following default settings: Multiplicity was set to 1; Digestion was set to trypsin/P;

Variable modifications were set to Oxidation (M) and Acetyl (Protein N-term); LFQ minimal ratio count was set to 2; LFQ minimal number of neighbors set to 3; LFQ average number of neighbors set to 6; MS/MS spectra were searched against the UniProt human database (updated July 22nd, 2015); False discovery rate (FDR) was set to 0.01; First search and MS/MS search mass tolerance was set to 10 ppm; The data in the Protein Groups result table was processed with Perseus software. The missing protein intensity values in LFQ analyses were imputed by sampling from a distribution downshifted by 1.3 with a width of 0.2. The imputed LFQ-intensity values of identified proteins were used for all downstream analyses. We only consider proteins as quantified if MaxQuant was able to compute corresponding protein intensity values in DMSO-treated samples. Identified proteins that were classified as "only identified by site", "reverse", or "contaminant" were filtered and removed from the table. Proteins with 1 or fewer peptide counts were filtered and removed. All intensity values were transformed based on log2 algorithm. P-value was calculated using two-tailed, two-sample T-test. Competition scores (log_2R)= (log2[Intensity(DMSO-treated)/Intensity(Inhibitor-treated)]) were calculated using the relative intensity values from DMSO- and inhibitor-treated lysates with confidence values=-log_{10}(P-value) for each identified protein. We defined significantly competed kinases as protein hits with a competition score ≥ 1.5 and a confidence value ≥ 1.5 from a two-sample t-test with an FDR of 0.05 (n=3).

Microscopy (Cellular assays for plasma membrane blebbing)

(*Cell plating*) Doxycycline-inducible HeLa cells that stably express full-length Src WT or Src V284C were plated on 18-mm round glass cover slips at $\mathbf{1 \times 10^4}$ cells in 12-well plate in Dulbecco's Modified Eagle's Medium (DMEM) supplemented with 10% (by volume) Fetal Bovine Serum (FBS). Expression of Src WT and Src V284C was induced by addition of Doxycycline (1.0 μg/mL) upon plating. The cells were incubated at 37 ˚C in a humidified incubator containing 5% CO_2.

(*Inhibitor treatment*) After 48 hours, the media was replaced with 1 mL warm DMEM containing 10% FBS and 10 μM of 14a or 15a. The cells were then incubated with the inhibitor solution at 37 ˚C in a humidified incubator containing 5% CO_2.

(*Cell fixation*) After 15 mins, medium was removed, and cells were washed with warm DPBS solution once. The cells were fixed with 4% paraformaldehyde (by volume) in DPBS for 15 mins at room temperature, and then washed with DPBS twice at room temperature.

(*Staining and sample preparation*) Cells were staining with 250 μL DPBS solution containing 2 drops of NucBlue Fixed Cell ReadyProbes Reagent (DAPI) staining solution and 1.5 μL of Wheat Germ Agglutinin-Alexa488 conjugate (WGA-Alexa488, 1.0 mg/mL in water) for 10 minutes at room temperature. The samples were then rinsed with water once. After removing excess water on the cover slip, one drop of Fluoromount-G mounting media was added onto the cover slip. The samples were then sealed with nail polisher.

(*Imaging, data acquisition, and data processing*) Cells were imaged using a Leica SP8X confocal microscope equipped with a 63X objective (oil objective). Nuclei were imaged using laser excitation at 405 nm with 5% laser power. WGA-Alexa488 were imaged using laser excitation at 490 nm with 10% laser power. The images were analyzed in ImageJ software. All microscopy

images were brightened for clarity. The number of cells that contain significant membrane blebs in each image was quantified as followed. Cells were scored if they contained a single nucleus, had an intact and continuous membrane, and the majority of the cell was in the image. A cell was considered to be blebbing if it contained three or more rounded membrane protrusions. As an assay readout, the percentage of blebbing cells out of all imaged cells was calculated. All data were visualized using GraphPad Prism 8 software.

QUANTIFICATION AND STATISTICAL ANALYSIS

For all statistical tests (unless otherwise noted), a two-tailed Student's t test was used to compare means between two samples. Significance is denoted as follows: * = $p < 0.05$, ** = $p < 0.01$, *** = $p < 0.001$, **** = $p < 0.0001$. Statistical tests were performed in GraphPad Prism8 software.

Synthesis of inhibitors

General Synthetic Procedures: All chemicals purchased from commercial suppliers were used without further purification unless otherwise stated. Reactions were monitored with thin-layer chromatography (TLC) using silica gel 60 F254 coated glass plates (EM Sciences). Compound purification was performed with an IntelliFlash 280 automated flash chromatography system using pre-packed Varian SuperFlash silica gel columns (Hexane/EtOAc or CH_2Cl_2/MeOH gradient solvent). A Varian Dynamax Microsorb 100-5 C18 column (250 mm x 21.4 mm), eluting with H_2O/CH_3CN or H_2O/ MeOH gradient solvent (+0.05% TFA), was used for preparatory HPLC purification. The purity of all final compounds was determined by analytical HPLC with an Agilent ZORBAX SB-C18 (2.1 mm x 150 mm) or Varian Microsorb-MV 100-5 C18 column (4.6 mm x 150 mm), eluting with either H_2O/CH_3CN or H_2O/MeOH gradient solvent (+0.05% TFA). Elution was monitored by a UV detector atλ= 220 nm andλ= 254 nm, with all final compounds displaying ≥95% purity. Nuclear magnetic resonance (NMR) spectra were recorded on Bruker 300 or 500 MHz NMR spectrometers at ambient temperature. Chemical shifts were reported in parts per million (ppm) and coupling constants in hertz (Hz). ^{1}H-NMR spectra were referenced to the residual solvent peaks as internal standards (7.26 ppm for $CDCl_3$, 2.50 ppm for d6-DMSO, and 3.34 ppm for CD_3OD). Mass spectra were recorded with a Bruker Esquire Liquid Chromatograph-Ion Trap Mass Spectrometer.

Synthesis of inhibitors 9 and 11

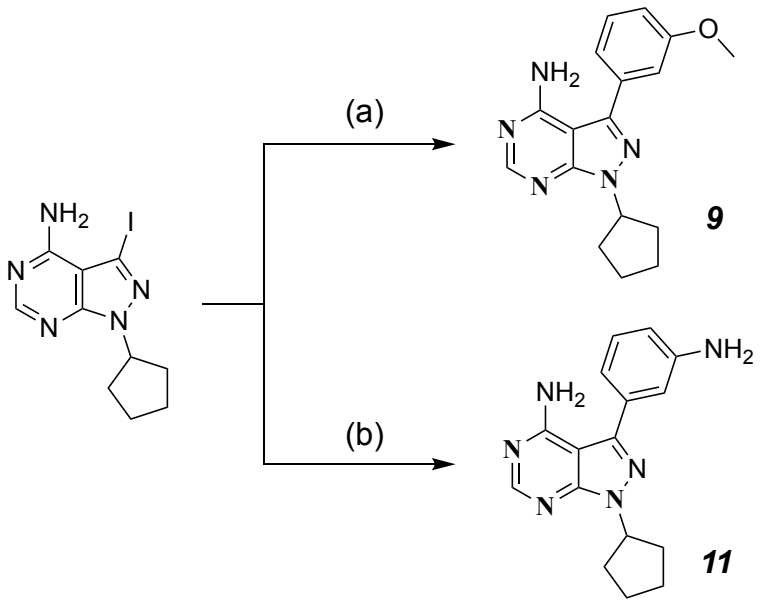

Scheme 1: a) K_3PO_4, $PdCl_2(dppf)_2$, 3-methoxyphenylboronic acid, 1,4-Dioxane/H_2O, 85˚C (microwave); b) K_3PO_4, $PdCl_2(dppf)_2$, 3-aminophenylboronic acid, 1,4-Dioxane/H_2O, 85˚C (microwave).

1-cyclopentyl-3-(3-methoxyphenyl)-1H-pyrazolo[3,4-d]pyrimidin-4-amine (Inhibitor 9)

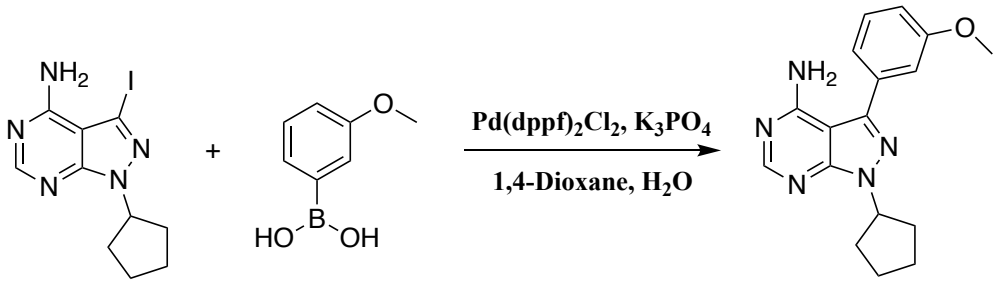

In a 10-mL microwave reaction tube, 1-cyclopentyl-3-iodo-1H-pyrazolo[3,4-d]pyrimidin-4-amine (15 mg, 0.046 mmol, 1.0 equiv.), 3-methoxyphenylboronic acid (10 mg, 0.068 mmol, 1.5 equiv.), potassium phosphate (24 mg, 0.11 mmol, 2.5 equiv.), and [1,1′-Bis(diphenylphosphino)ferrocene]dichloropalladium(II) (3.7 mg, 0.11 mmol, 0.10 equiv.) were

dissolved in a mixture of 1,4-Dioxane (0.8 mL) and water (0.2 mL). The resulting mixture was heated in a microwave reactor at 85 ˚C for 120 minutes. The reaction was then quenched with saturated NH_4Cl solution (5 mL) and diluted with ethyl acetate (30 mL). The organic phase was washed with saturated NaHCO3 solution (5 mL), brine (5 mL), dried over anhydrous Na_2SO_4 and concentrated in *vacuo*. Purification using flash chromatography on silica gel with a EtOAc/Hexane gradient (0:100 to 90:10) rendered 1-cyclopentyl-3-(3-methoxyphenyl)-1H-pyrazolo[3,4-d]pyrimidin-4-amine as a pale brown solid (9.0 mg, 64%; Rf= 0.31 in EtOAc:Hexane= 9:1). ^{1}H-NMR (500 MHz, $CDCl_3$) δ= 8.40 (s, 1H), 7.51 – 7.44 (m, 1H), 7.31 – 7.28 (m, 2H), 7.03 (d, *J* = 8.3 Hz, 1H), 5.69 (s, 2H), 5.34 (p, *J* = 7.5 Hz, 1H), 3.91 (s, 3H), 2.28 – 2.17 (m, 4H), 2.07 – 1.97 (m, 2H), 1.83 – 1.69 (m, 2H); MS (ESI, m/z) calculated for $C_{17}H_{19}N_5O$ 309.2, $[M+H]^+$ found 310.1. HPLC purity=94%.

3-(3-aminophenyl)-1-cyclopentyl-1H-pyrazolo[3,4-d]pyrimidin-4-amine (inhibitor 11)

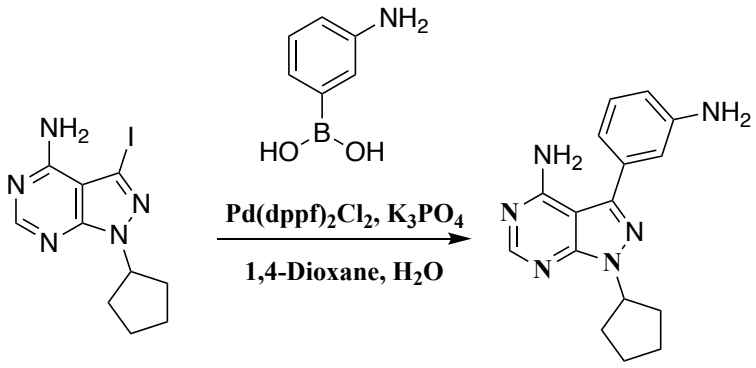

In a 10-mL microwave reaction tube, 1-cyclopentyl-3-iodo-1H-pyrazolo[3,4-d]pyrimidin-4-amine (15 mg, 0.046 mmol, 1.0 equiv.), 3-aminophenylboronic acid (9.4 mg, 0.068 mmol, 1.5 equiv.), potassium phosphate (24 mg, 0.11 mmol, 2.5 equiv.), and [1,1′-Bis(diphenylphosphino)ferrocene]dichloropalladium(II) (3.7 mg, 0.11 mmol, 0.1 equiv.) were dissolved in a mixture of 1,4-Dioxane (0.8 mL) and water (0.2 mL). The resulting mixture was heated in a microwave reactor at 85 ˚C for 120 minutes. The reaction was then quenched with

saturated NH_4Cl solution (5 mL) and diluted with ethyl acetate (30 mL). The organic phase was washed with saturated $NaHCO_3$ solution (5 mL), brine (5 mL), dried over anhydrous Na_2SO_4 and concentrated in *vacuo*. Purification using flash chromatography on silica gel with a EtOAc/Hexane gradient (0:100 to 90:10) afforded *3-(3-aminophenyl)-1-cyclopentyl-1H-pyrazolo[3,4-d]pyrimidin-4-amine* as a pale brown solid (10 mg, 91%; Rf= 0.38 in EtOAc:Hexane= 9:1). ^{1}H-NMR (300 MHz, CDCl3) δ= 8.33 (s, 1H), 7.31 (d, J = 7.7 Hz, 1H), 7.09 – 6.94 (m, 2H), 6.76 (d, J = 7.2 Hz, 1H), 5.88 (s, 2H), 5.30 (p, J = 7.6 Hz, 1H), 3.44 (s, 2H), 2.28 – 2.11 (m, 4H), 2.06 – 1.89 (m, 2H), 1.84 – 1.65 (m, 2H). MS (ESI, m/z) calculated for $C_{16}H_{18}N_6$ 294.2, $[M+H]^+$ found 295.1. HPLC purity=94%.

Synthesis of inhibitors 14 and 15

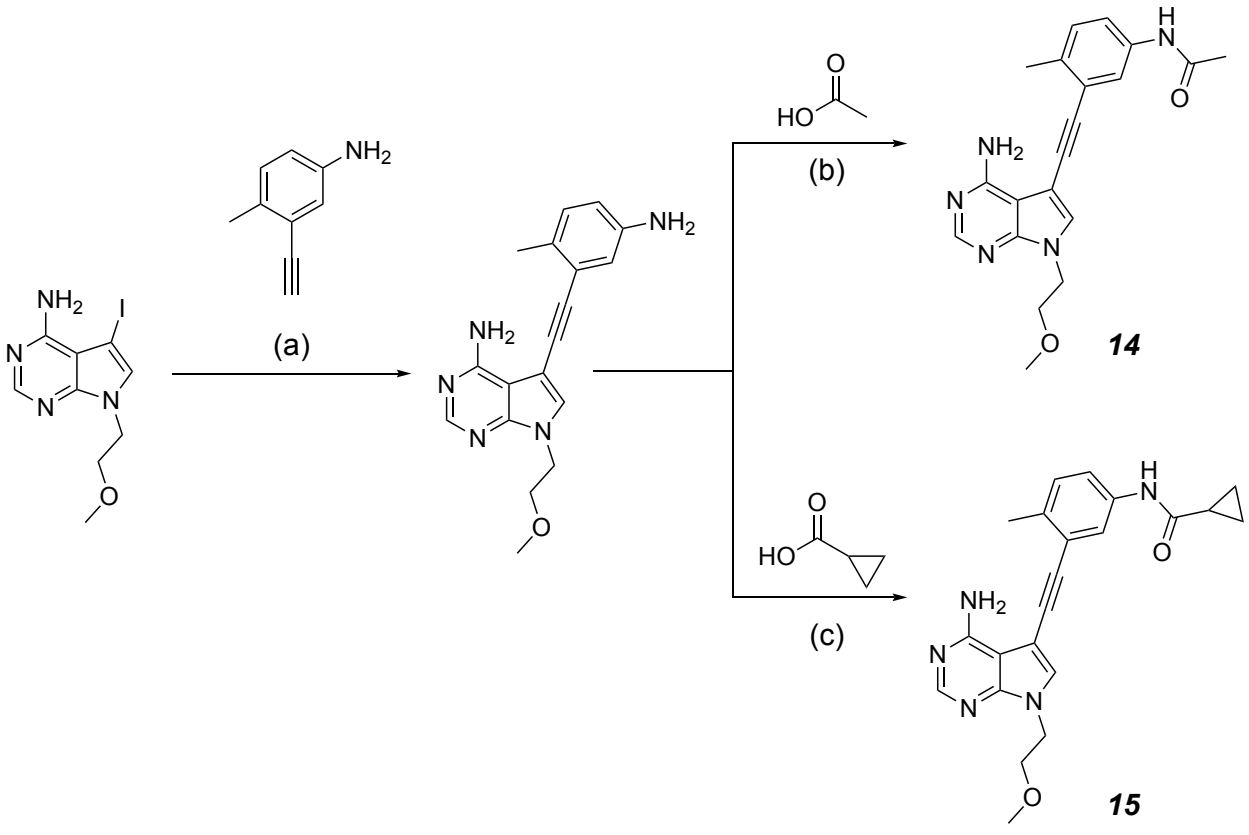

Scheme 2: a) $PdCl_2(PPh_3)_2$, CuI, Et_3N, DMF, 50˚C, overnight; b) EDCI, HOAt, DMF, RT, overnight; c) EDCI, HOAt, DMF, RT, overnight.

5-((5-Amino-2-methylphenyl)ethynyl)-7-(2-methoxyethyl)-7H-pyrrolo[2,3-d]pyrimidin-4-amine

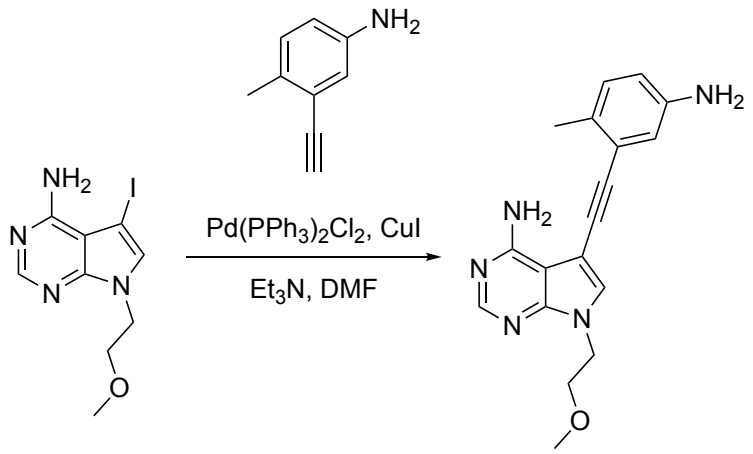

5-Iodo-7-(2-methoxyethyl)-7H-pyrrolo[2,3-d]pyrimidin-4-amine and 3-ethynyl-4-methylaniline were synthesized according to previous reports (PCT Int. Appl., 2014184069, 20 Nov 2014 and *J. Med. Chem.* 2012, 55, 11, 5270-5290). 3-Ethynyl-4-methylaniline (180 mg, 1.3mmol, 3.0 equiv.) was dissolved in DMF (2.3 mL) under nitrogen. Triethyl amine (180 mg, 1.8 mmol, 4.0 equiv.), 5-iodo-7-(2-methoxyethyl)-7H-pyrrolo[2,3-d]pyrimidin-4-amine (140 mg, 0.45mmol, 1.0 equiv.), bis(triphenylphosphine)palladium(II) dichloride (16 mg, 0.022 mmol, 0.050 equiv.), and copper (I) iodide (9.0 mg, 0.045 mmol, 0.10 equiv.) were added to the above solution sequentially. The reaction was heated to 50 ˚C and stirred overnight then quenched with saturated NH_4Cl (20 mL). The mixture was diluted with ethyl acetate (200 mL) and the organic phase was washed with saturated $NaHCO_3$ (50 mL), brine (50 mL) and then dried over anhydrous Na_2SO_4. 5-((5-Amino-2-methylphenyl)ethynyl)-7-(2-methoxyethyl)-7H-pyrrolo[2,3-d]pyrimidin-4-amine was purified as a yellow foam using flash chromatography on silica gel using a gradient of EtOAc/Hexane (0:100 to 60:40) (99 mg, 69%; Rf=0.55 in EtOAC:Hexane 30:70). ^{1}H-NMR (300 MHz, $CDCl_3$) δ= 8.30 (s, 1H), 7.32 (s, 1H), 7.02 (d, *J* = 8.1 Hz, 1H), 6.83 (s, 1H), 6.61 (d, *J* = 8.1 Hz, 1H), 5.66 (s, 2H), 4.36 (t, *J* = 4.8 Hz, 2H), 3.72 (t, *J* = 4.8 Hz, 2H), 3.35 (s, 3H), 2.39 (s, 3H), 1.67 (s, 2H). MS (ESI, m/z) calculated for $C_{18}H_{19}N_5O$ 321.4, [M+H] found 322.1.

N-(3-((4-amino-7-(2-methoxyethyl)-7H-pyrrolo[2,3-d]pyrimidin-5-yl)ethynyl)-4-methylphenyl)acetamide (Inhibitor 14)

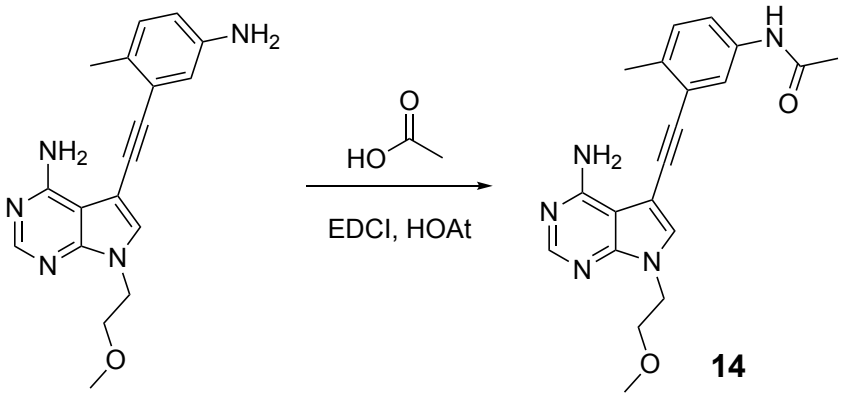

14

5-((5-Amino-2-methylphenyl)ethynyl)-7-(2-methoxyethyl)-7H-pyrrolo[2,3-d]pyrimidin-4-amine (16 mg, 0.050 mmol, 1.0 equiv.) was dissolved in DMF (0.50 mL) under nitrogen. EDCI (14 mg, 0.075 mmol, 1.5 equiv.), HOAt (10 mg, 0.075 mmol, 1.5 equiv.) and acetic acid (4.5 mg, 0.075mmol, 1.0 equiv.) were added sequentially on ice. Solution was stirred and allowed to warm to room temperature overnight. Reaction was diluted with EtOAc (50 mL), washed with NH_4Cl (5 mL), saturated $NaHCO_3$ (5 mL) and brine. The organic phase was dried over anhydrous Na_2SO_4. The N-(3-((4-amino-7-(2-methoxyethyl)-7H-pyrrolo[2,3-d]pyrimidin-5-yl)ethynyl)-4-methylphenyl)acetamide was purified as a brown solid using flash chromatography on silica gel using a gradient of MeOH/DCM (0:100 to 10:90) (11 mg, 58%). ^{1}H-NMR (300 MHz, $CDCl_3$) δ= 8.68 (s, 1H), 8.05 (d, *J* = 15.4 Hz, 1H), 7.92 (s, 1H), 7.81 (d, *J* = 12.9 Hz, 1H), 7.57 (d, *J* = 8.2 Hz, 1H), 6.70 (s, 1H), 4.78 (m, *J* = 5.0 Hz, 2H), 4.13 (t, *J* = 5.0 Hz, 2H), 3.76 (d, *J* = 7.3 Hz, 3H), 2.91 – 2.79 (m, 3H), 2.67 – 2.49 (m, 3H), 1.67 (s, 2H). MS (ESI, m/z) calculated for $C_{20}H_{21}N_5O_2$ 363.4, [M+H] found 364.4. HPLC purity=98%.

N-(3-((4-amino-7-(2-methoxyethyl)-7H-pyrrolo[2,3-d]pyrimidin-5-yl)ethynyl)-4-methylphenyl)cyclopropanecarboxamide (Inhibitor 15)

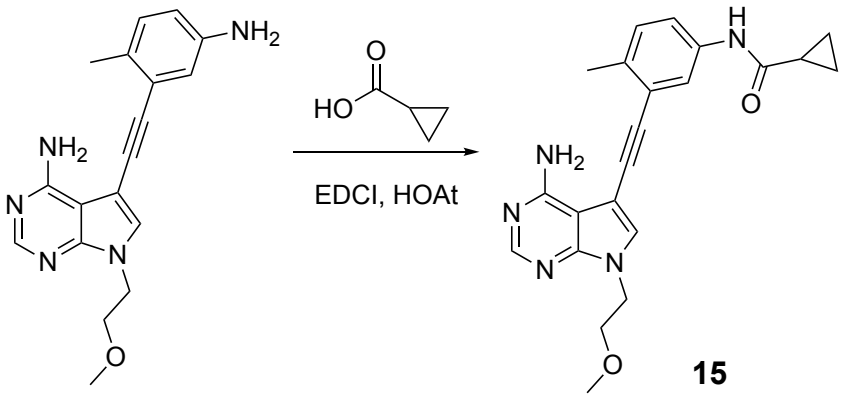

15

5-((5-Amino-2-methylphenyl)ethynyl)-7-(2-methoxyethyl)-7H-pyrrolo[2,3-d]pyrimidin-4-amine (16 mg, 0.050 mmol, 1.0 equiv.) was dissolved in DMF (0.50 mL) under nitrogen. EDCI (14 mg, 0.075 mmol, 1.5 equiv.), HOAt (10 mg, 0.075 mmol, 1.5 equiv.), and cyclopropanecarboxylic acid (6.4 mg, 0.075 mmol, 1.0 equiv.) were added sequentially on ice. Solution was stirred and allowed to warm to room temperature overnight. Reaction was diluted with EtOAc (50 mL), washed with NH_4Cl (5 mL), saturated $NaHCO_3$ (5 mL) and brine. The organic phase was dried over anhydrous Na_2SO_4. The N-(3-((4-amino-7-(2-methoxyethyl)-7H-pyrrolo[2,3-d]pyrimidin-5-yl)ethynyl)-4-methylphenyl)cyclopropanecarboxamide was purified as a brown solid using flash chromatography on silica gel using a gradient of MeOH/DCM (0:100 to 10:90) (11 mg, 59%). ^{1}H-NMR (300 MHz, $CDCl_3$) δ= 8.25 (s, 1H), 7.70 (s, 1H), 7.46 – 7.31 (m, 2H), 7.14 (d, *J* = 8.3 Hz, 1H), 6.39 (s, 1H), 4.36 (t, *J* = 5.0 Hz, 2H), 3.71 (t, *J* = 4.9 Hz, 2H), 3.36 (s, 3H), 2.73 (s, 2H), 2.50 – 2.31 (m, 3H), 1.25 (s, 1H), 1.16 – 0.97 (m, 2H), 0.95 – 0.73 (m, 2H). MS (ESI, m/z) calculated for $C_{22}H_{23}N_5O_2$ 389.5, [M+H] found 390.5. HPLC purity=93%.

Synthesis of inhibitor *14a* and *15a*

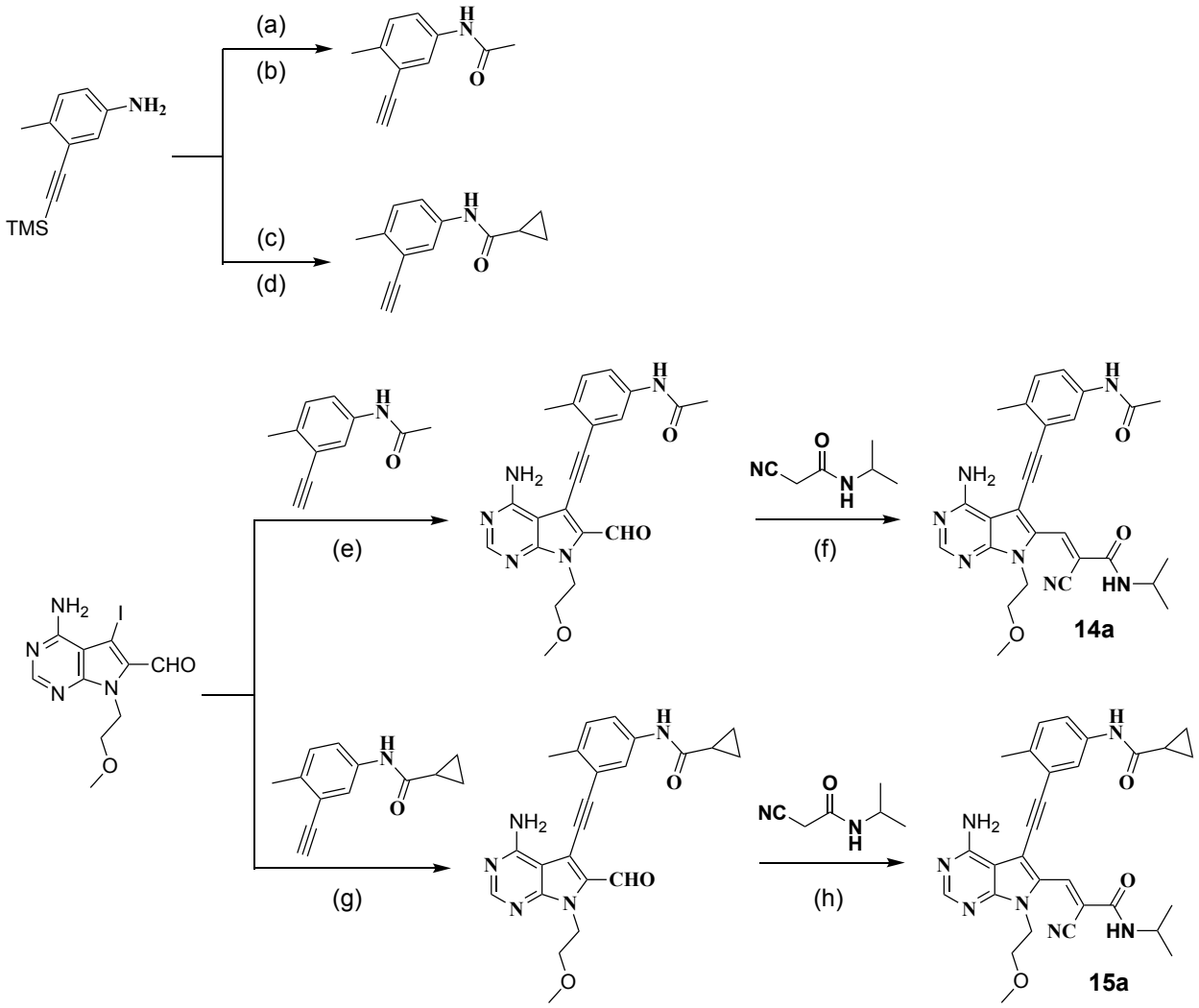

Scheme 3: a) EDCI, HOAt, DMF, RT, overnight; b) KF, MeOH, RT, 1 day; c) EDCI, HOAt, DMF, RT, overnight; d) KF, MeOH, RT, 1 day; e) $PdCl_2(PPh_3)_2$, CuI, Et_3N, DMF, 50˚C, overnight; f) DBU, THF, 17 hours; g) $PdCl_2(PPh_3)_2$, CuI, Et_3N, DMF, 50˚C, overnight; f) DBU, THF, 6 hours;

N-(3-ethynyl-4-methylphenyl)acetamide

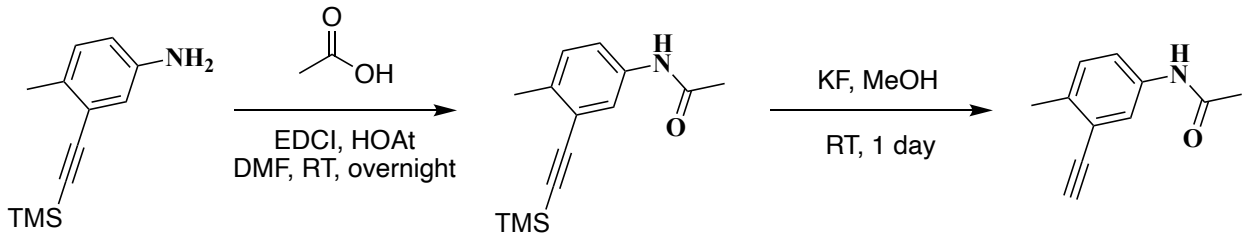

4-Methyl-3-((trimethylsilyl)ethynyl)aniline (110 mg, 0.54 mmol, 1.0 equiv.), acetic acid (49 mg, 0.81 mmol, 47 µL, 1.5 equiv.) and HOAt (110 mg, 0.81 mmol, 1.5 equiv.) were dissolved in dry DMF (5 mL). The solution was cooled to 0 ˚C and to it was added 1-Ethyl-3-(3-dimethylaminopropyl) carbodiimide (126 mg, 0.81 mmol, 1.5 equiv.). The reaction mixture was then allowed to warm to room temperature overnight. The solvent was removed in vacuo and the solid residue was dissolved in EtOAc (40 mL). The organic layer was washed with saturated aqueous KH_2PO_4 solution (10 mL), saturated aqueous $NaHCO_3$ solution (10 mL), brine (10 mL) and dried over anhydrous Na_2SO_4. The solvent was removed in vacuo and the solid residue was dissolved in dry MeOH (3.5 mL). Potassium fluoride (130 mg, 2.2 mmol, 3.6 equiv.) was added and the resulting mixture was stirred at room temperature for 1 day. The reaction mixture was then filtered and concentrated in vacuo. The solid residue was dissolved in EtOAc (40 mL) and washed with water (10 mL), brine (10 mL) and dried over anhydrous Na2SO4. Purification by flash chromatography with silica gel afforded N-(3-ethynyl-4-methylphenyl)acetamide as a pale brown solid (43 mg, 46% for two steps). ^{1}H-NMR (500 MHz, $CDCl_3$) δ= 7.54 (s, 1H), 7.43 (d, J = 8.2 Hz, 1H), 7.15 (d, J = 8.1 Hz, 1H), 7.09 (s, 1H), 3.26 (s, 1H), 2.40 (s, 3H), 2.16 (s, 3H); MS (ESI, m/z) calculated for $C_{11}H_{11}NO$ 173.1, $[M+H]^+$ found 173.9.

N-(3-((4-amino-6-formyl-7-(2-methoxyethyl)-7H-pyrrolo[2,3-d]pyrimidin-5-yl)ethynyl)-4-methylphenyl)acetamide

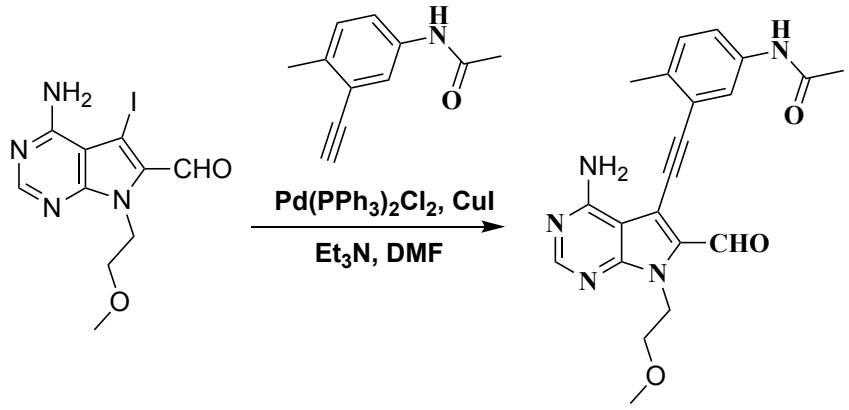

4-Amino-5-iodo-7-(2-methoxyethyl)-7H-pyrrolo[2,3-d]pyrimidine-6-carbaldehyde was synthesized according to previous reported[76]. 4-Amino-5-iodo-7-(2-methoxyethyl)-7H-pyrrolo[2,3-d]pyrimidine-6-carbaldehyde (25 mg, 0.072 mmol, 1.0 equiv.) was dissolved in anhydrous DMF (1 mL) under nitrogen. Triethylamine (30 mg, 40 µL, 0.29 mmol, 4.0 equiv.), N-(3-ethynyl-4-methylphenyl)acetamide (19 mg, 0.11 mmol, 1.5 equiv.), bis(triphenylphosphine)palladium(II) dichloride (2.5 mg, 0.0036 mmol, 0.05 equiv.), and copper (I) iodide (1.4 mg, 0.0072 mmol, 0.1 equiv.) were added to the above solution sequentially. The reaction was heated at 50 ˚C for overnight and then quenched with saturated NH_4Cl (1 mL). The resulting mixture was diluted with ethyl acetate (40 mL) and the organic phase was washed with saturated $NaHCO_3$ (10 mL), brine (10 mL) and then dried over anhydrous Na_2SO_4. Purification by flash chromatography on silica gel using a gradient of MeOH/DCM (0:100 to 10:90) afforded N-(3-((4-amino-6-formyl-7-(2-methoxyethyl)-7H-pyrrolo[2,3-d]pyrimidin-5-yl)ethynyl)-4-methylphenyl)acetamide as a pale brown solid (26 mg, 92%; Rf= 0.45 in MeOH:DCM= 10:90). ^{1}H-NMR (300 MHz, $CDCl_3$) δ= 10.16 (s, 1H), 8.41 (s, 1H), 7.77 (s, 1H), 7.41 (d, *J* = 8.0 Hz, 1H),

7.30 (s, 1H), 7.22 (d, *J* = 8.3 Hz, 1H), 6.49 (s, 2H), 4.82 (t, *J* = 5.3 Hz, 2H), 3.74 (t, *J* = 5.3 Hz, 2H), 3.31 (s, 3H), 2.47 (s, 3H), 2.20 (s, 3H); MS (ESI, m/z) calculated for $C_{21}H_{21}N_5O_3$ 391.2, $[M+H]^+$ found 392.2.

(Z)- or (E)-3-(5-((5-acetamido-2-methylphenyl)ethynyl)-4-amino-7-(2-methoxyethyl)-7H-pyrrolo[2,3-d]pyrimidin-6-yl)-2-cyano-N-isopropylacrylamide (Inhibitor 14a)

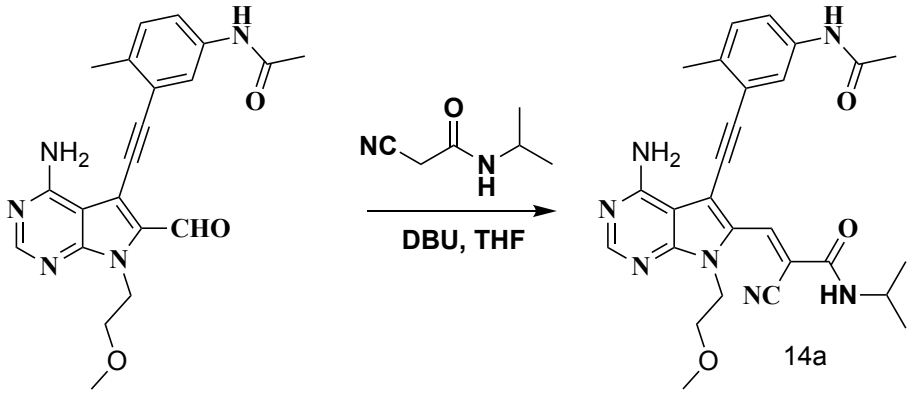

N-(3-((4-Amino-6-formyl-7-(2-methoxyethyl)-7H-pyrrolo[2,3-d]pyrimidin-5-yl)ethynyl)-4-methylphenyl)acetamide (26 mg, 0.066 mmol, 1.0 equiv.) and 2-cyano-N-isopropylacetamide (10 mg, 0.079 mmol, 1.2 equiv.) were dissolved in THF (2 mL). To the above solution was added 1,8-diazabicyclo[5.4.0]undec-7-ene (20 mg, 20 µL, 0.13 mmol, 2.0 equiv). The reaction mixture was stirred at room temperature for 17 hours. The reaction was then quenched with saturated NH_4Cl solution (1 mL) and diluted with ethyl acetate (30 mL). The organic layer was washed with saturated $NaHCO_3$ solution (10 mL), brine (10 mL), dried over anhydrous Na_2SO_4 and concentrated in *vacuo*. Purification using preparative thin-layer chromatography developed by pure EtOAc rendered (*Z*)- or (*E*)-3-(5-((5-acetamido-2-methylphenyl)ethynyl)-4-amino-7-(2-methoxyethyl)-7H-pyrrolo[2,3-d]pyrimidin-6-yl)-2-cyano-N-isopropylacrylamide as a bright yellow powder (5.0 mg, 15%; Rf [(E)- and (Z)-isomers)]= 0.53 in MeOH:DCM= 10:90). ^{1}H-NMR (300 MHz, MeOD) δ= 8.46 (s, 1H), 8.25 (s, 1H), 8.22 (s, 1H), 7.99 (s, 1H), 7.92 (s, 1H), 7.74 (s,

1H), 7.59 (d, *J* = 8.0 Hz, 1H), 7.41 (d, *J* = 8.3 Hz, 1H), 7.24 (d, *J* = 8.2 Hz, 2H), 5.14 (s, 1H), 4.54 – 4.43 (m, 4H), 4.04 – 3.95 (m, 1H), 3.82 – 3.50 (m, 6H), 3.36 (s, 6H), 2.48 (s, 6H), 2.16 (s, 3H), 2.15 (s, 3H), 1.05 – 0.82 (m, 12H); MS (ESI, m/z) calculated for $C_{27}H_{29}N_7O_3$ 499.2, $[M+H]^+$ found 500.3. HPLC purity (mixture of *E*- and *Z*-isomers)>99%.

N-(3-ethynyl-4-methylphenyl)cyclopropanecarboxamide

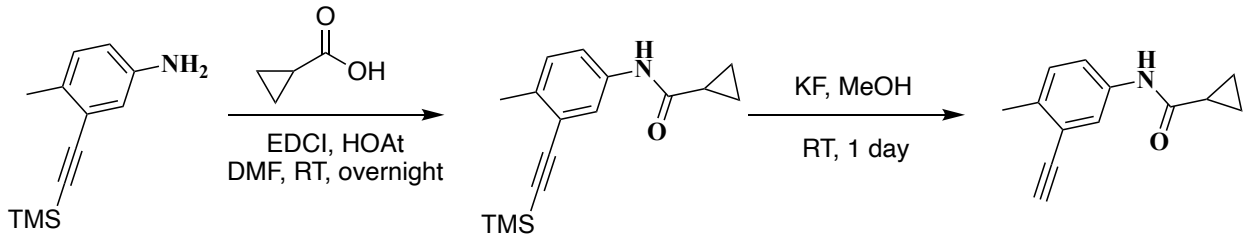

4-Methyl-3-((trimethylsilyl)ethynyl)aniline (126 mg, 0.62 mmol, 1.0 equiv.), cyclopropyl acid (80 mg, 0.93 mmol, 74 µL, 1.5 equiv.), and HOAt (127 mg, 0.93 mmol, 1.5 equiv.) were dissolved in dry DMF (5 mL). The solution was cooled to 0 ˚C and to it was added 1-Ethyl-3-(3-dimethylaminopropyl) carbodiimide (144 mg, 0.93 mmol, 1.5 equiv.). The reaction mixture was then allowed to warm to room temperature overnight. The solvent was removed in vacuo and the solid residue was dissolved in EtOAc (40 mL). The organic layer was washed with saturated aqueous KH_2PO_4 solution (10 mL), saturated aqueous $NaHCO_3$ solution (10 mL), brine (10 mL) and dried over anhydrous Na_2SO_4. The solvent was removed in vacuo and the solid residue was dissolved in dry MeOH (3.5 mL). Potassium fluoride (128 mg, 2.2 mmol, 3.6 equiv.) was added and the resulting mixture was stirred at room temperature for 1 day. The reaction mixture was then filtered and concentrated in vacuo. The solid residue was dissolved in EtOAc (40 mL) and washed with water (10 mL), brine (10 mL), and dried over anhydrous Na2SO4. Purification by flash chromatography with silica gel afforded N-(3-ethynyl-4-methylphenyl)cyclopropanecarboxamide as a pale brown solid (82 mg, 66% for two steps). ^{1}H-NMR (500 MHz, $CDCl_3$) δ= 7.57 (s, 1H), 7.45 (d, *J* = 8.1 Hz, 1H), 7.31 (s, 1H), 7.14 (d, *J* = 8.1 Hz, 1H), 3.25 (s, 1H), 2.40 (s, 3H), 1.47 (s,

1H), 1.13 – 1.05 (m, 2H), 0.88 – 0.78 (m, 2H); MS (ESI, m/z) calculated for $C_{13}H_{13}NO$ 199.1, [M+H]+ found 199.9.

N-(3-((4-amino-6-formyl-7-(2-methoxyethyl)-7H-pyrrolo[2,3-d]pyrimidin-5-yl)ethynyl)-4-methylphenyl)cyclopropanecarboxamide

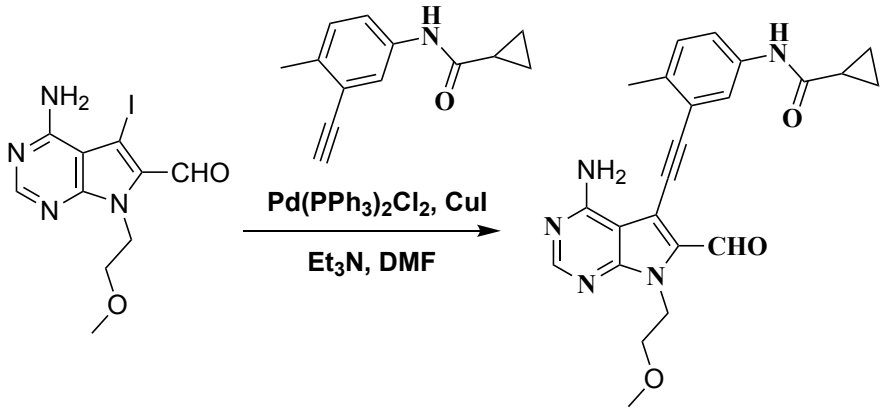

4-Amino-5-iodo-7-(2-methoxyethyl)-7H-pyrrolo[2,3-d]pyrimidine-6-carbaldehyde (25 mg, 0.072 mmol, 1.0 equiv.) was dissolved in anhydrous DMF (1 mL) under nitrogen. Triethylamine (30 mg, 40 µL, 0.29 mmol, 4.0 equiv.), N-(3-ethynyl-4-methylphenyl)cyclopropanecarboxamide (21.6 mg, 0.11 mmol, 1.5 equiv.), bis(triphenylphosphine)palladium(II) dichloride (2.5 mg, 0.0036 mmol, 0.05 equiv.), and copper (I) iodide (1.4 mg, 0.0072 mmol, 0.1 equiv.) were added to the above solution sequentially. The reaction was heated at 50 ˚C for overnight and then quenched with saturated NH_4Cl (1 mL). The resulting mixture was diluted with ethyl acetate (40 mL) and the organic phase was washed with saturated $NaHCO_3$ (10 mL), brine (10 mL), and then dried over anhydrous Na_2SO_4. Purification by flash chromatography on silica gel using a gradient of MeOH/DCM (0:100 to 10:90) afforded N-(3-((4-amino-6-formyl-7-(2-methoxyethyl)-7H-pyrrolo[2,3-d]pyrimidin-5-yl)ethynyl)-4-methylphenyl)cyclopropanecarboxamide as a pale brown solid (30 mg, 98%; Rf= 0.51 in EtOAc:Hexane= 60:40). ^{1}H-NMR (300 MHz, $CDCl_3$) δ=

10.15 (s, 1H), 8.41 (s, 1H), 7.80 (s, 1H), 7.52 (s, 1H), 7.38 (d, J = 7.6 Hz, 1H), 7.20 (d, J = 8.3 Hz, 1H), 6.16 (s, 2H), 4.81 (t, J = 5.4 Hz, 2H), 3.74 (t, J = 5.3 Hz, 2H), 3.31 (s, 3H), 2.47 (s, 3H), 1.59 – 1.45 (m, 1H), 1.15 – 1.04 (m, 2H), 0.95 – 0.79 (m, 2H). MS (ESI, m/z) calculated for $C_{23}H_{23}N_5O_3$ 417.2, $[M+H]^+$ found 418.3.

(Z)- or (E)-N-(3-((4-amino-6-(2-cyano-3-(isopropylamino)-3-oxoprop-1-en-1-yl)-7-(2-methoxyethyl)-7H-pyrrolo[2,3-d]pyrimidin-5-yl)ethynyl)-4-methylphenyl)cyclopropanecarboxamide (Inhibitor 15a)

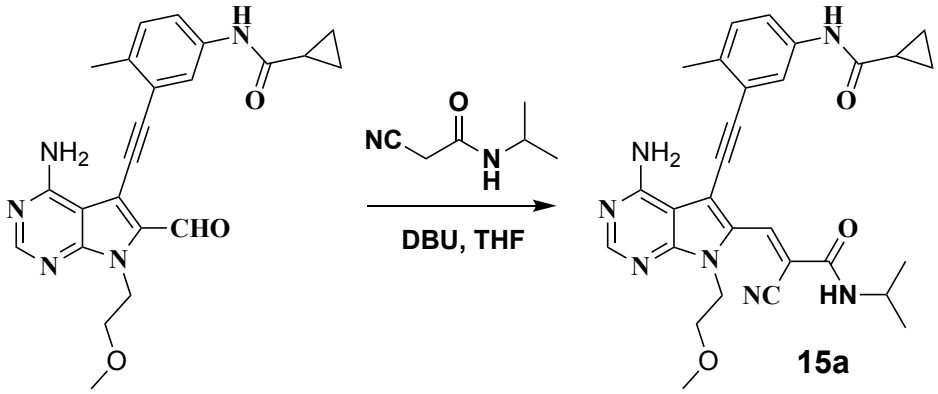

N-(3-ethynyl-4-methylphenyl)cyclopropanecarboxamide (30 mg, 0.071 mmol, 1.0 equiv.) and 2-cyano-*N*-isopropylacetamide (11 mg, 0.085 mmol, 1.2 equiv.) were dissolved in THF (3 mL). To the above solution was added 1,8-diazabicyclo[5.4.0]undec-7-ene (22 mg, 21 μL, 0.14 mmol, 2.0 equiv). The reaction mixture was stirred at room temperature for 6 hours. The reaction was then quenched with saturated NH_4Cl solution (1 mL) and diluted with ethyl acetate (30 mL). The organic layer was washed with saturated $NaHCO_3$ solution (5 mL), brine (5 mL), dried over anhydrous Na_2SO_4, and concentrated in vacuo. Purification using preparative thin-layer chromatography developed by pure EtOAc rendered (*Z*)- or (*E*)-N-(3-((4-amino-6-(2-cyano-3-(isopropylamino)-3-oxoprop-1-en-1-yl)-7-(2-methoxyethyl)-7H-pyrrolo[2,3-d]pyrimidin-5-yl)ethynyl)-4-methylphenyl)cyclopropanecarboxamide as a bright yellow powder (13 mg, 12%; Rf [(E)- and (Z)-isomers)]= 0.21 in EtOAc). ^{1}H-NMR (300 MHz, MeOD) δ= 8.44 (s, 1H), 8.24 (s,

1H), 8.21 (s, 1H), 7.95 (s, 1H), 7.90 (s, 1H), 7.73 (s, 1H), 7.56 (d, J = 8.2 Hz, 1H), 7.40 (d, J = 8.6 Hz, 1H), 7.22 (d, J = 8.3 Hz, 2H), 5.13 (s, 1H), 4.54 – 4.37 (m, 4H), 4.02 – 3.89 (m, 1H), 3.82 – 3.51 (m, 6H), 3.35 (s, 6H), 2.47 (s, 6H), 2.30 – 2.10 (m, 2H), 1.21 – 1.05 (m, 8H), 1.03 – 0.80 (m, 12H); MS (ESI, m/z) calculated for $C_{29}H_{31}N_7O_3$ 525.3, $[M+H]^+$ found 526.3. HPLC purity (mixture of *E*- and *Z*-isomers)>99%.

Synthesis of inhibitor 16

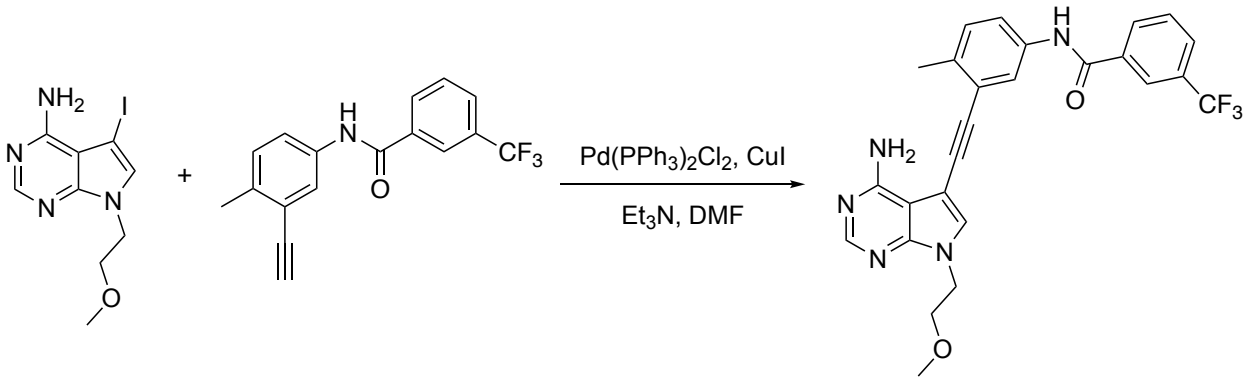

5-Iodo-7-(2-methoxyethyl)-7H-pyrrolo[2,3-d]pyrimidin-4-amine (20 mg, 0.066 mmol, 1.0 equiv.) was dissolved in anhydrous DMF (1 mL) under nitrogen. Triethylamine (27 mg, 36 µL, 0.26 mmol, 4.0 equiv.), N-(3-ethynyl-4-methylphenyl)-3-(trifluoromethyl)-benzamide (30 mg, 0.099 mmol, 1.5 equiv.), bis(triphenylphosphine)palladium(II) dichloride (2.3 mg, 0.0033 mmol, 0.05 equiv.), and copper (I) iodide (1.3 mg, 0.0066 mmol, 0.1 equiv.) were added to the above solution sequentially. The reaction was heated at 50 ˚C for overnight and then quenched with saturated NH_4Cl (1 mL). The resulting mixture was diluted with ethyl acetate (40 mL) and the organic phase was washed with saturated $NaHCO_3$ (10 mL), brine (10 mL), and then dried over anhydrous Na_2SO_4. Purification by flash chromatography on silica gel using a gradient of EtOAc/Hexane (0:100 to 100:0) afforded N-(3-((4-amino-7-(2-methoxyethyl)-7H-pyrrolo[2,3-d]pyrimidin-5-yl)ethynyl)-4-methylphenyl)-3-(trifluoromethyl)benzamide as a pale brown solid (23 mg, 71%). ^{1}H-NMR (300 MHz, $CDCl_3$) δ= 9.10 (s, 1H), 8.94 (s, 1H), 8.15 (s, 1H), 8.09 (d, J = 7.7 Hz, 1H),

7.95 – 7.77 (m, 3H), 7.72 – 7.39 (m, 4H), 7.28 (s, 1H), 4.50 (t, J = 4.9 Hz, 2H), 3.76 (t, J = 4.9 Hz, 2H), 3.37 (s, 3H), 2.54 (s, 3H); MS (ESI, m/z) calculated for $C_{26}H_{22}F_3N_5O_2$ 493.2, $[M+H]^+$ found 494.2. HPLC purity>99%.

Table S1. Data collection and refinement statistics for X-ray crystallography

Item	Src/14 complex (PDB ID: 6WIW)
Wavelength	
Resolution range	31.14 - 2.3 (2.382 - 2.3)
Space group	P 1
Unit cell	42.151 63.872 74.875 78.24 89.668 90.208
Total reflections	58130 (6169)
Unique reflections	30897 (3178)
Multiplicity	1.9 (1.9)
Completeness (%)	90.87 (93.36)
Mean I/sigma(I)	11.52 (3.30)
Wilson B-factor	30.18
R-merge	0.04921 (0.236)
R-meas	0.06698 (0.3195)
R-pim	0.04515 (0.2141)
CC1/2	0.997 (0.909)
CC*	0.999 (0.976)
Reflections used in refinement	30878 (3177)
Reflections used for R-free	1468 (152)

R-work	0.2040 (0.2463)
R-free	0.2351 (0.2962)
CC(work)	0.942 (0.879)
CC(free)	0.919 (0.808)
Number of non-hydrogen atoms	4453
macromolecules	4159
ligands	54
solvent	240
Protein residues	517
RMS(bonds)	0.015
RMS(angles)	1.42
Ramachandran favored (%)	98.82
Ramachandran allowed (%)	1.18
Ramachandran outliers (%)	0.00
Rotamer outliers (%)	1.11
Clashscore	8.61
Average B-factor	48.34
macromolecules	48.57
ligands	62.22
solvent	41.09

Note: Statistics for the highest-resolution shell are shown in parentheses.

Table S2. **List of Ki values of inhibitors** (*Note: All Ki values are reported in nM; NT: Not Tested; The IC50 and Ki values of inhibitors **1**-**8** have been reported elsewhere as described in the Materials and Reagents;* Km [ATP]= 68 ± 8 μM (Abl-1 WT). Km [ATP]= 55 ± 4 μM (Src WT). Km [ATP]= 62 ± 4 μM (Src V284C). Km [ATP]= 110 ± 20 μM (Abl-1 V256C))

Inhibitor	Src WT	Abl-1 WT	Src V284C	Abl-1 V256C
9	NT	/	/	/
10	2.3 ± 0.3	/	/	/
11	NT	/	/	/
13	4.0 ± 0.5	/	/	/
14	9.1 ± 1.1	7.7 ± 1.7	/	/
15	100 ± 10	92 ± 5	/	/
16	18 ± 2	48 ± 2	/	/
14a	> 2 μM	> 2 μM	46 ± 1	22 ± 5
15a	> 2 μM	> 2 μM	7.7 ± 0.7	2.7 ± 0.6

Table S3. **List of constructs and mutations used in manuscript.**

Construct	Expressed in	Residue numbers	Vectors used in	Notes	Citation
$Src^{TAMRA\text{-}FL}$ V284C	*E. coli*	2-536 (*E.coli*), 1-536 (mammalian)	pMCSG7 expressed as a His_6-SUMO construct, pEF1A	Used in Figure 2C	PMID: 30956043
Src^{FL} WT	*E. coli*	2-536 (*E.coli*), 1-536 (mammalian)	pMCSG7 expressed as a His_6-SUMO construct, pEF1A	Used in Figure 3 and 4F	PMID: 30956043
Src^{CD} WT	See citation	251–533	See citation	Used for X-ray crystallography	PMID: 16260764
Src^{3D} WT	*E. coli*	87-536	pMCSG7, pEF1A	Used in Figure 4E	PMID: 30956043
Src^{FL} V284C	*E. coli*, TRex-FlpIN-HeLa	1-536 (mammalian)	pMCSG7 expressed as a His_6-SUMO construct, pEF1A, pcDNA5	Used in Figure 5D and 5F	PMID: 30956043
Abl-1^{3D} WT	*E. coli*	65-534	pET-28a	Used in Figure 2D	PMID: 28380378
Abl-1^{3D} V256C	*E. coli*	65-534	pET-28a	Used in Figure S2	This study
BTK^{FL} WT	HEK293	full-length	pcDNA5	Used in Figure 2E	PMID: 31274292
BTK^{FL} V416C	HEK293	full-length	pcDNA5	Used in Figure S3	PMID: 31274292

Original gels:

SH3 pull-down assay: 1-bound and 2-bound Src WT (Note: The input samples were diluted by two-fold; The first lane on the left is the protein ladder (KDa); The unannotated lanes are for Src-WT complexes bound to inhibitor 13) (Replicate #1-3)

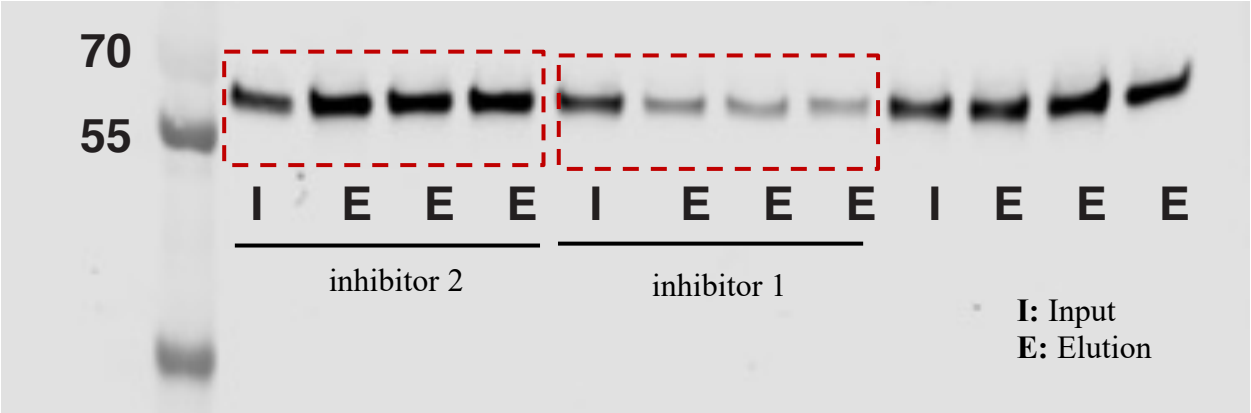

SH3 pull-down assay: 1-bound and 2-bound Abl-1 WT

Replicates #1-2:

Replicates #3: (Note: The following gel is from a trial SH3 pull-down experiment with inhibitor bound Abl-1 WT that used various concentration of immobilized Abl-1 SH3 ligands. The concentration of immobilized Abl-1 SH3 ligands in the highlighted lanes is consistent with the

Replicate #1-2. The unannotated lanes are for elutions from experiments performed with other concentrations of immobilized Abl-1 SH3 ligands.)

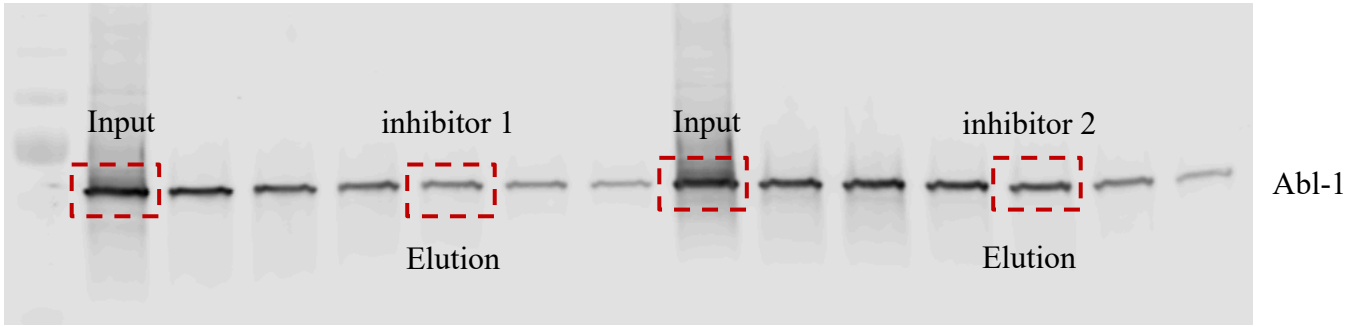

SH3 pull-down assay: 1-bound and 2-bound BTK WT (Replicate #1-3) (Note: The first lane to the left is for the protein ladder)

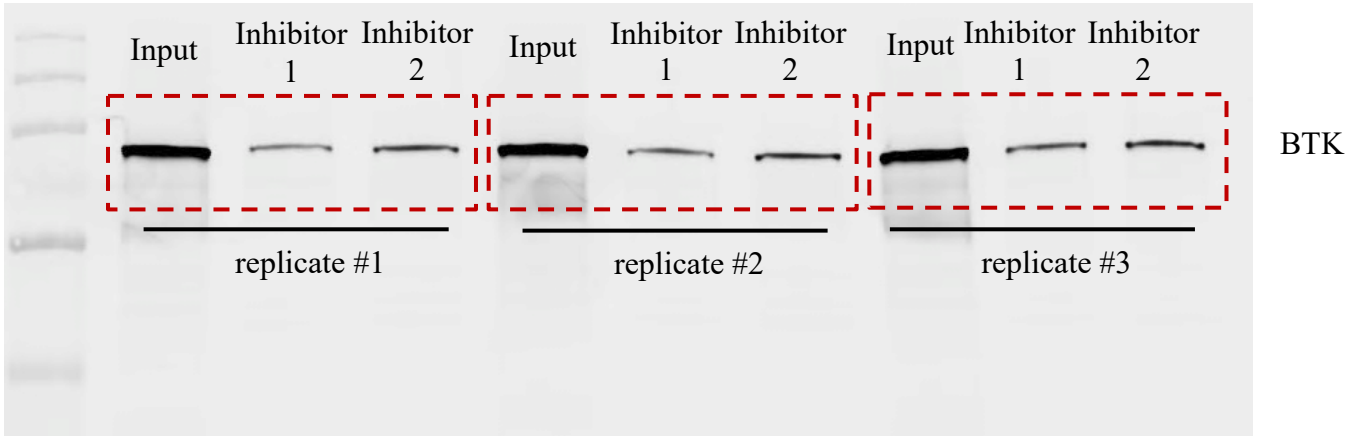

SH3 pull-down assay: 1a-bound and 2a-bound Abl-1 V256C (Replicate #1-2) (Note: The protein ladder was not added to the gel. The unannotated lanes are input and elution samples for experiments performed with other inhibitor-bound Abl-1 V256C complexes that are irrelevant to this study.)

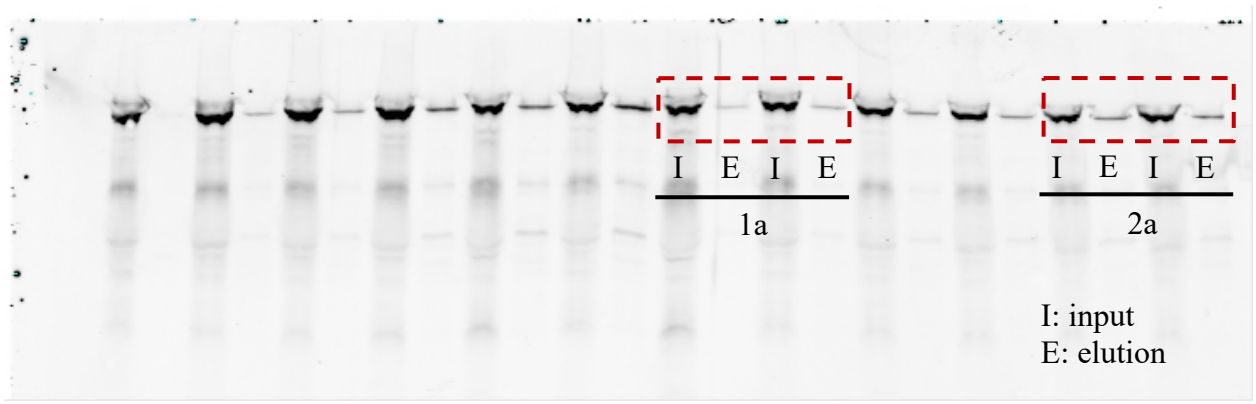

Abl-1

SH3 pull-down assay: 1a-bound and 2a-bound BTK V416C (Replicate #1-2) (The first lane on the left is for the protein ladder.)

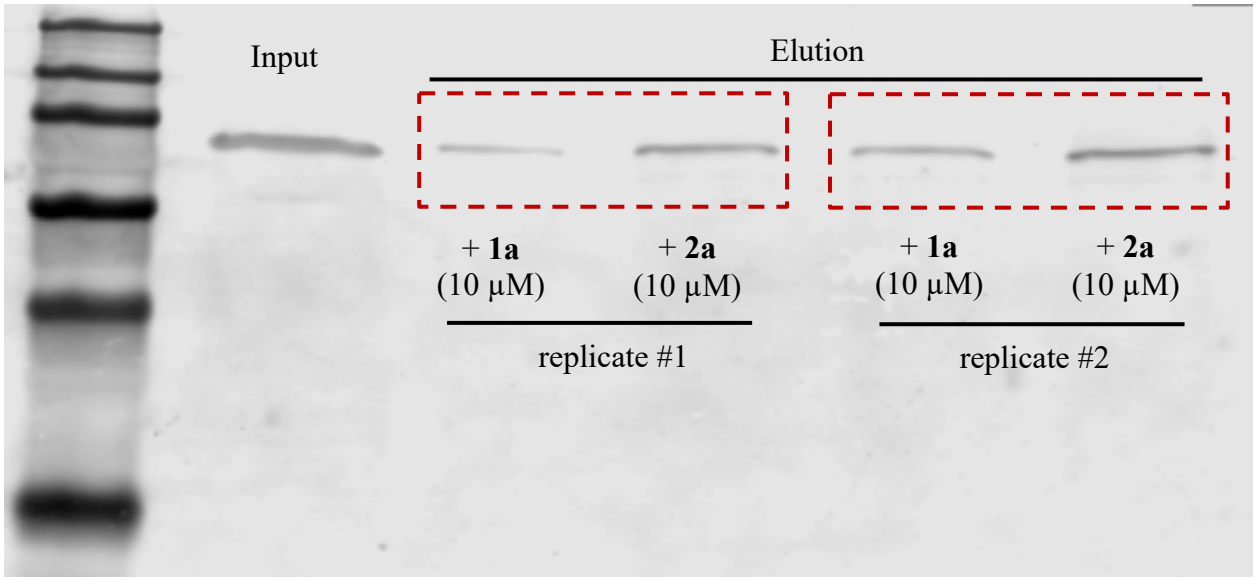

BTK

SH3 pull-down assay with inhibitor bound Src WT complexes. (Note: the input was diluted by two-fold; The last lane on the right is for the protein ladder.)

Replicate #1-2:

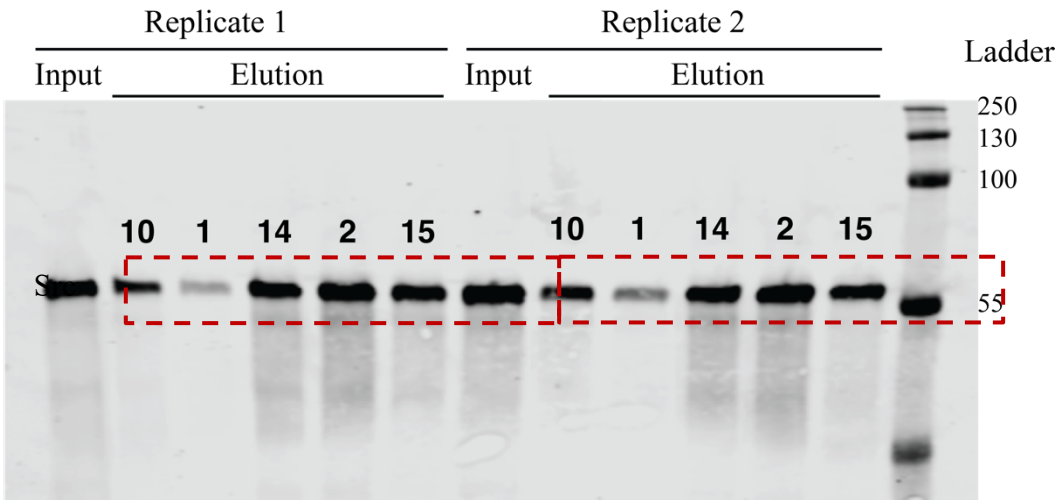

Replicate #3: (Note: The first lane on the left is for the protein ladder; The concentration of Src SH3 ligand used in the highlighted lanes are consistent with Replicate #1-2 above.)

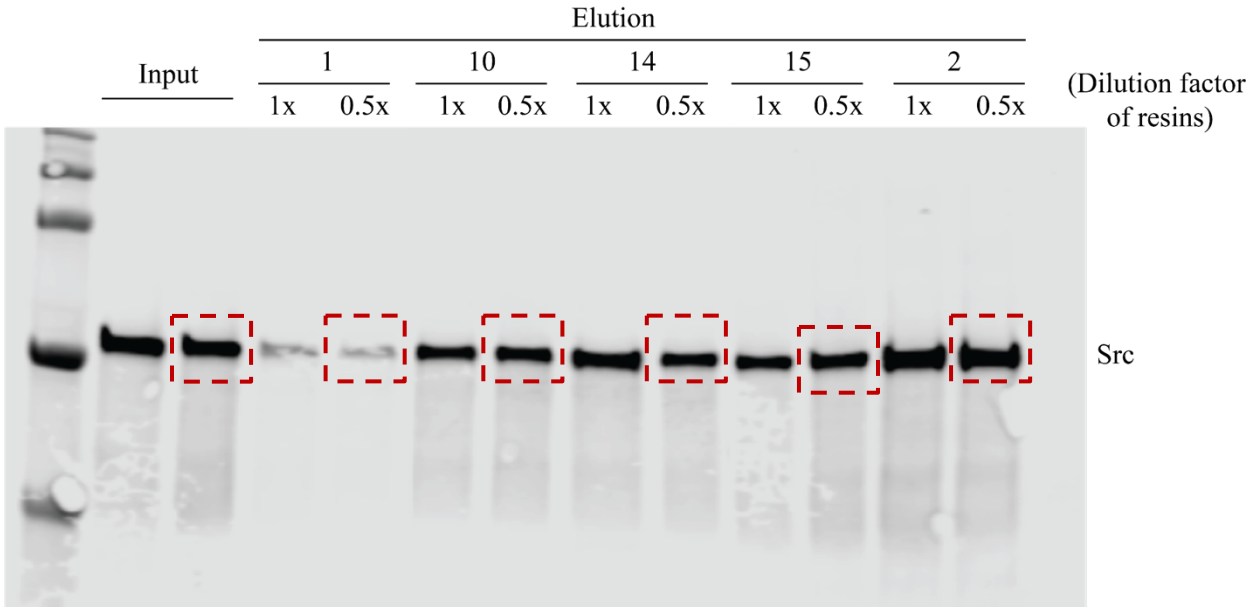

SH3 pull-down assay: Src$^{TAMRA-3D}$ V284C bound to 1a, 2a, 14a, and 15a. (Fluorescent imaging in TAMRA channel)

Replicate #1-2: (Note: Two gels were imaged at the same time. The gel on the left is for Replicate #1. The gel on the right is for Replicate #2. The first lane on the left of each gel is for the protein ladder.)

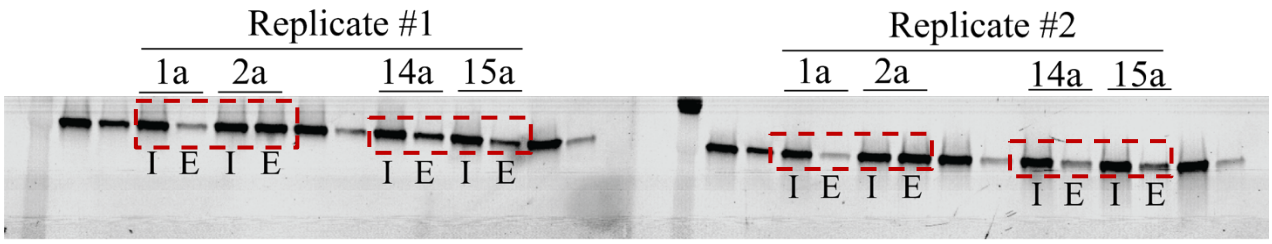

Replicate #3: (Note: The first lane on the left is for protein ladder. The unannotated lanes are input and elution samples for experiments performed with other inhibitor-bound Src V284C complexes that are irrelevant to this study.)

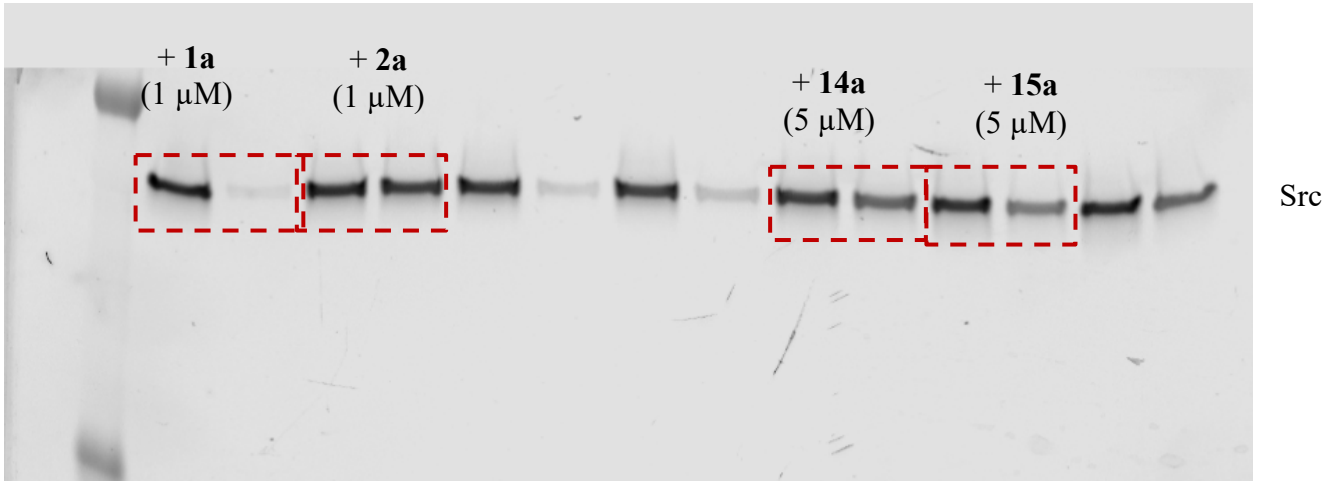

Half-life values for cleavage of *apo form of Src*.

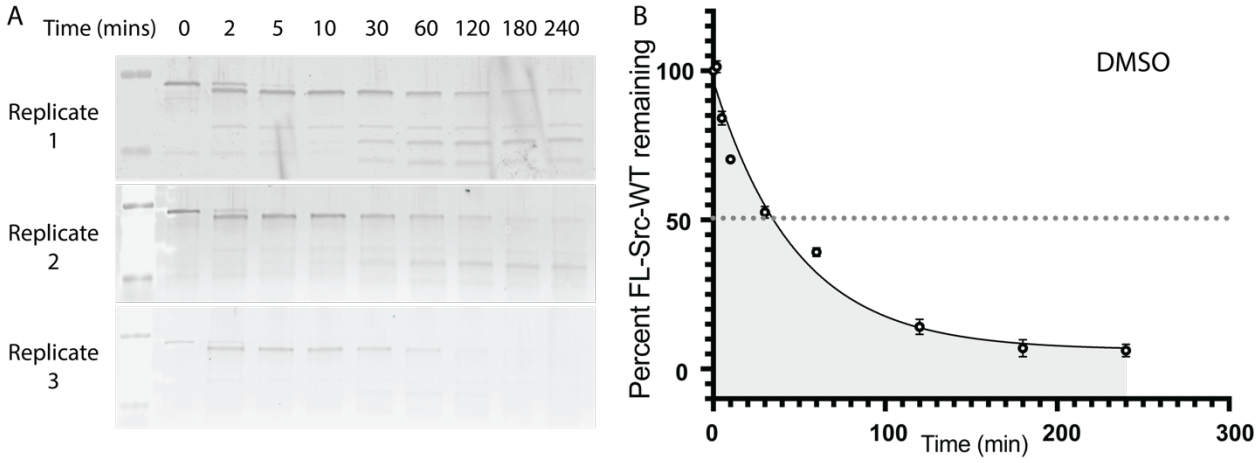

Half-life values for cleavage of Src bound to *DFG-out-stabilizing inhibitors.*

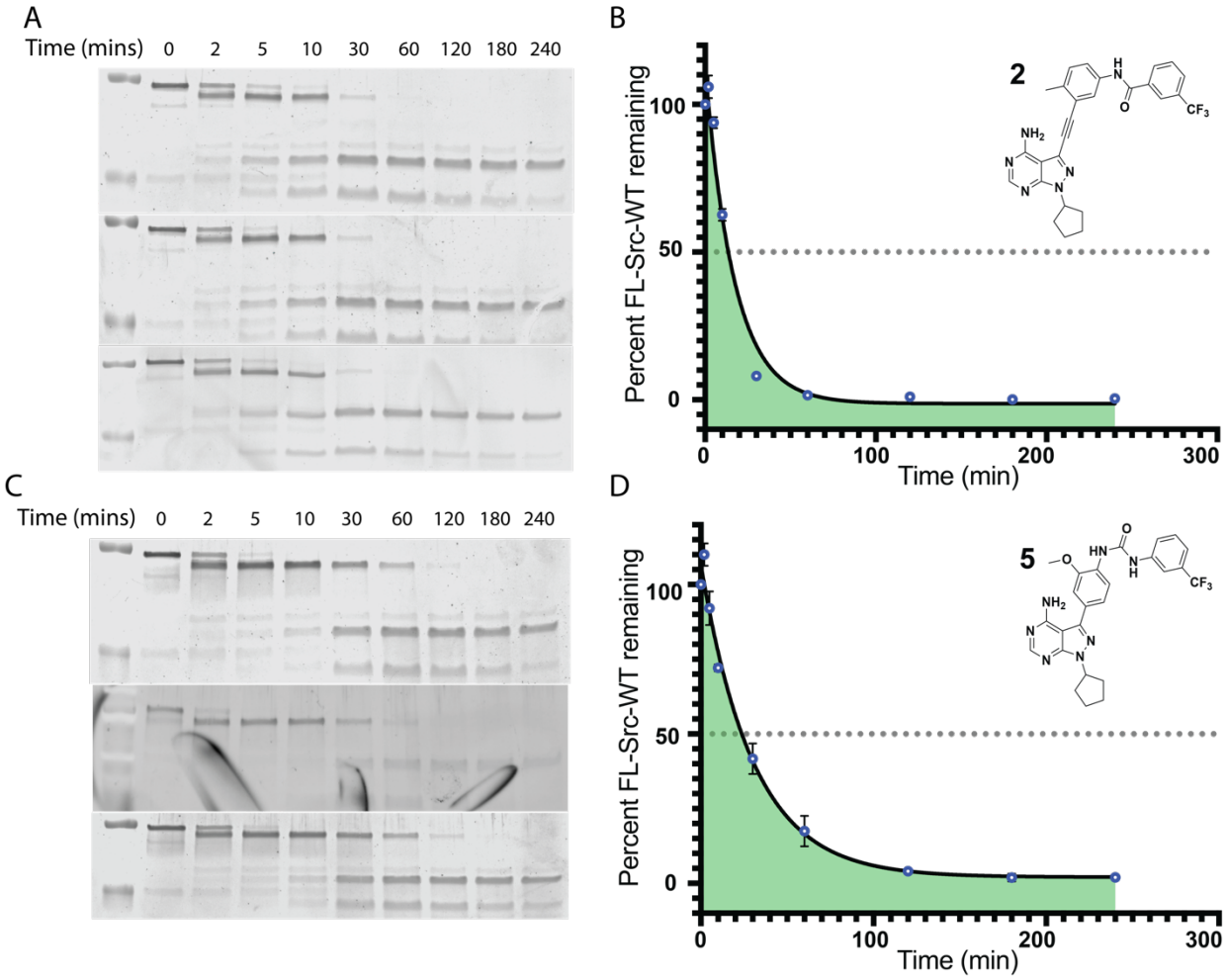

Half-life values for cleavage of Src bound to *helix αC-out-stabilizing inhibitors*.

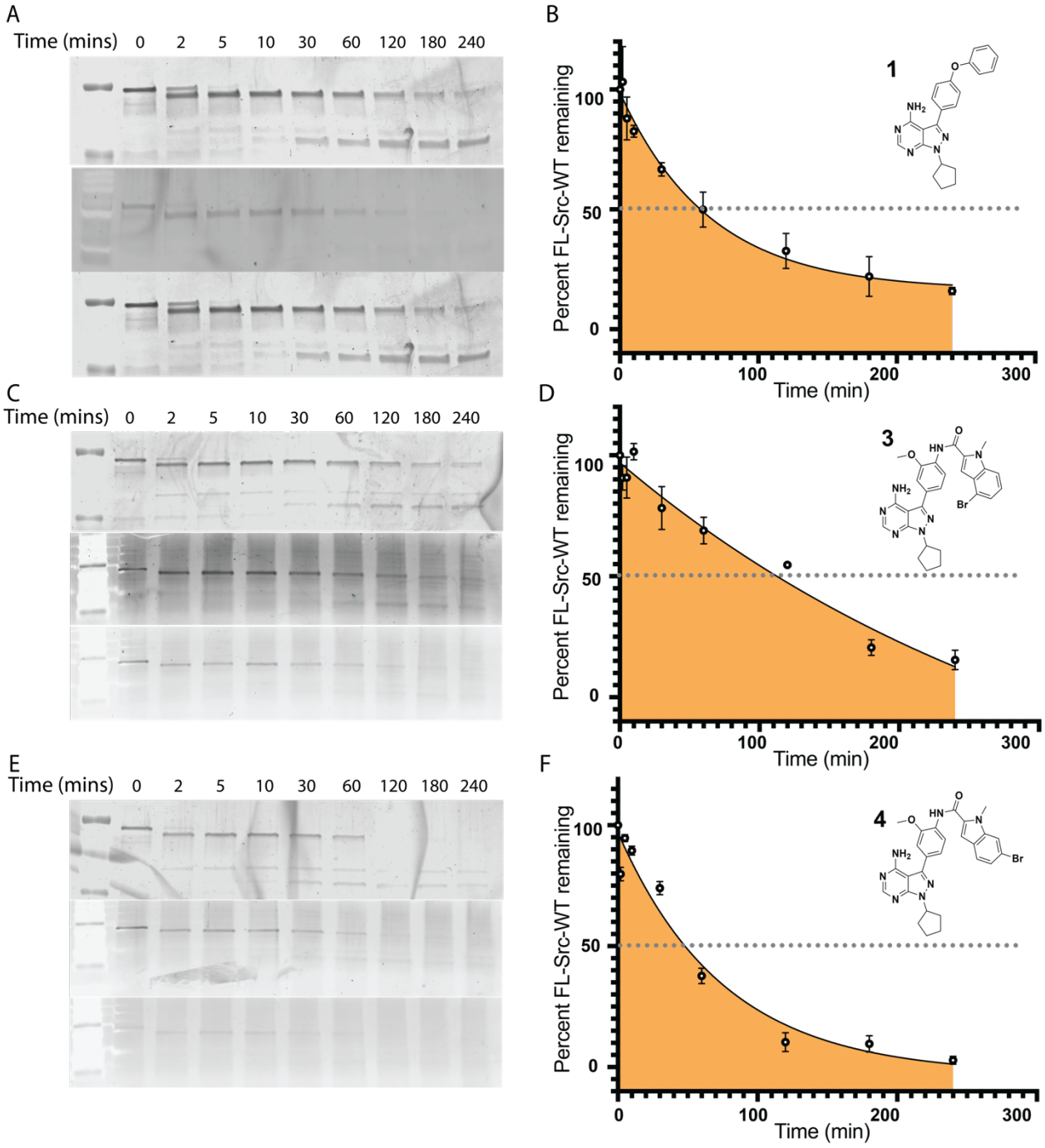

Half-life values for cleavage of Src bound to inhibitors 6-8.

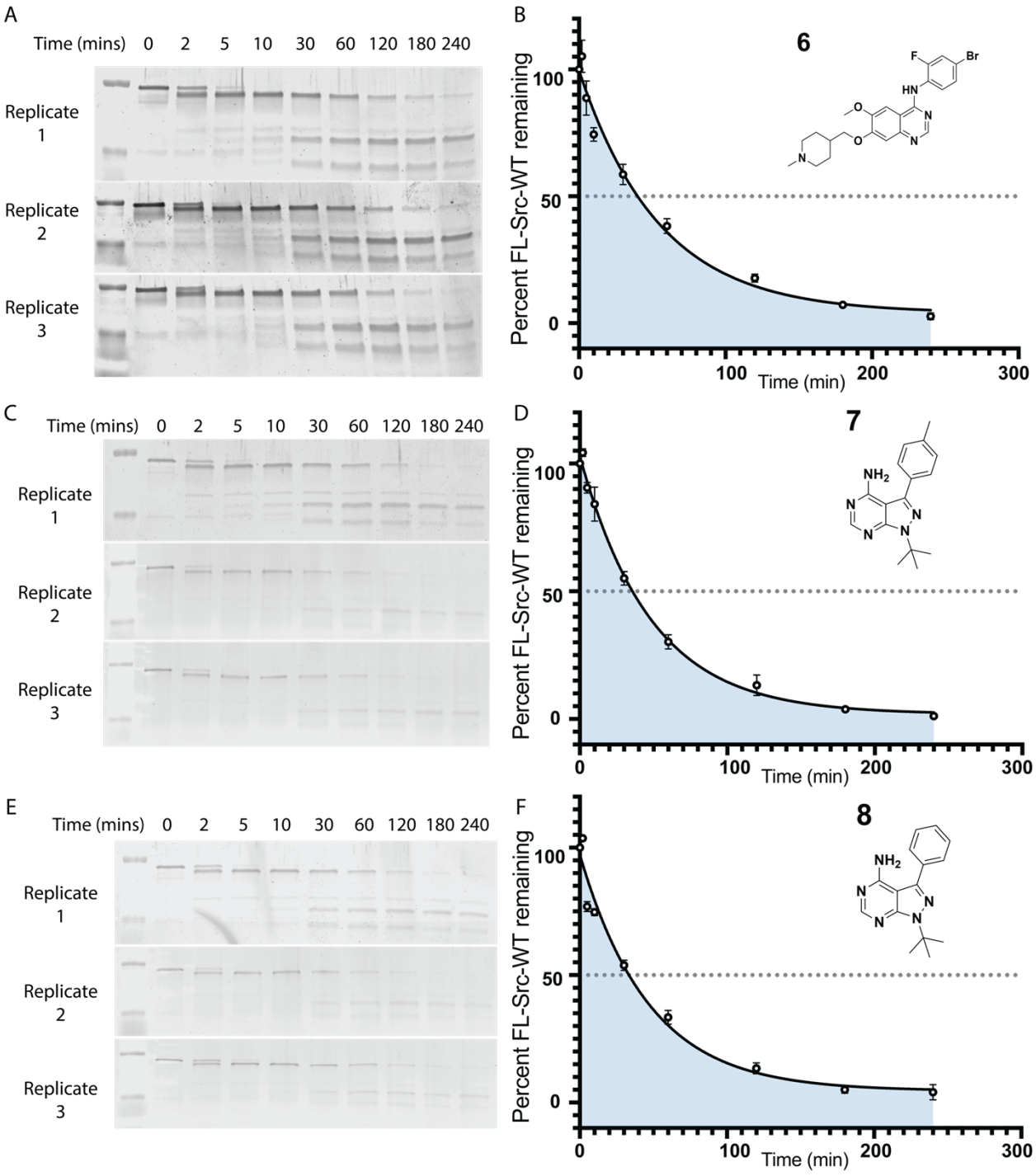

Half-life values for cleavage of Src bound to inhibitors 9-11.

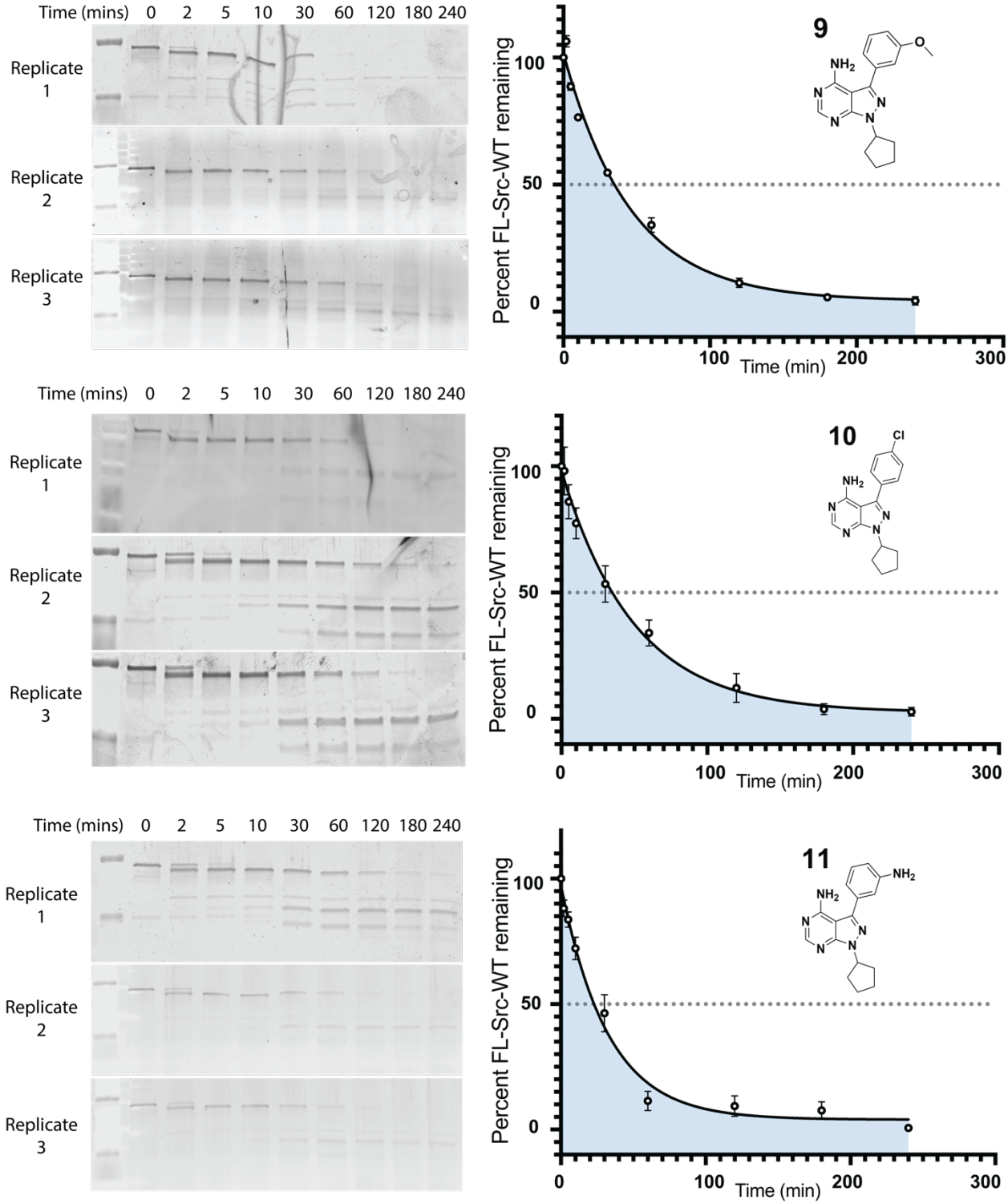

Half-life values for cleavage of Src bound to inhibitors 12-13.

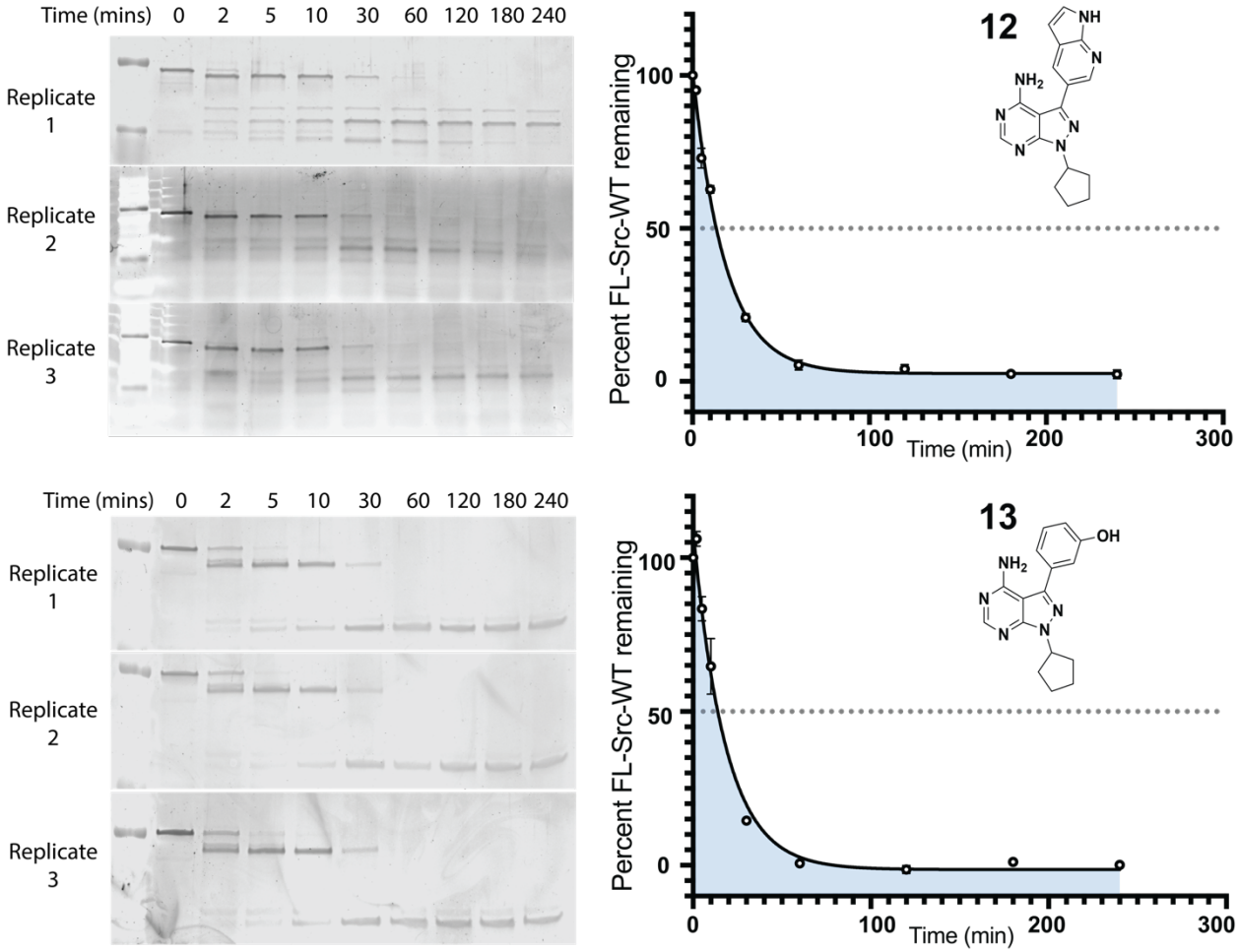

Determining the global conformation of 14-bound Src and 15-bound Src using thermolysin assay.

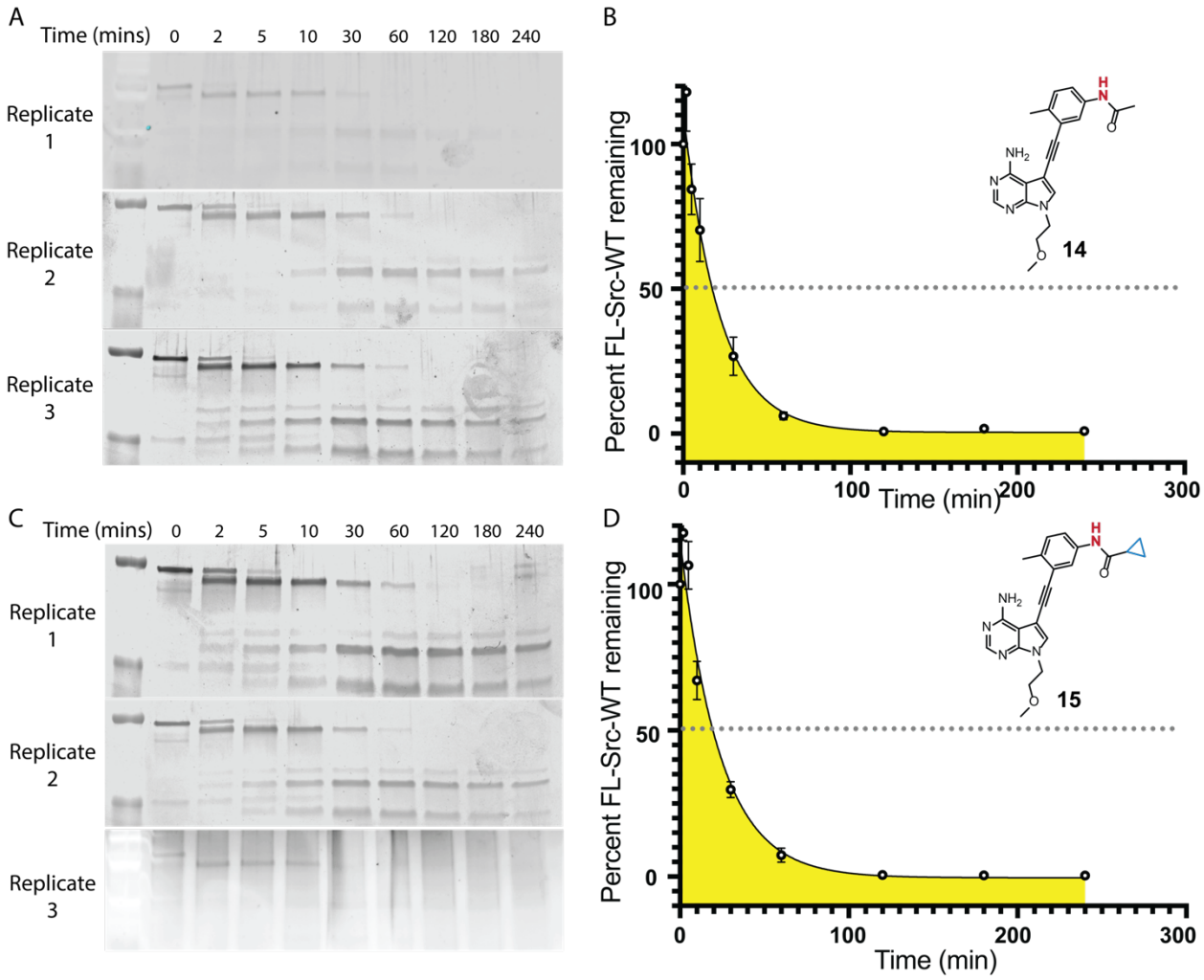

X-ray crystallography of Src/14 (PDB ID: 6WIW): Electron density maps of 14, Glu310 (helix aC) and DFG-motif (Asp404 and Phe405)

Chain A: electron density of inhibitor 14, Glu310, and Asp404.

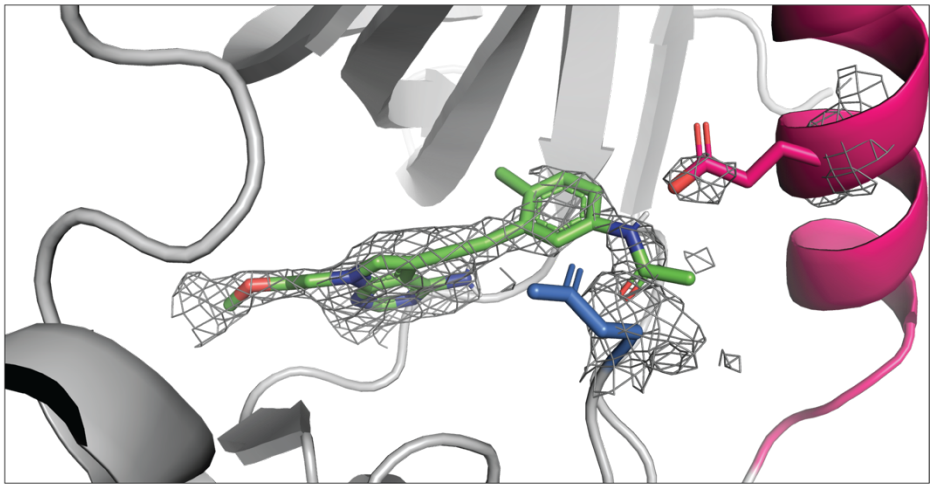

Chain B: electron density of inhibitor 14

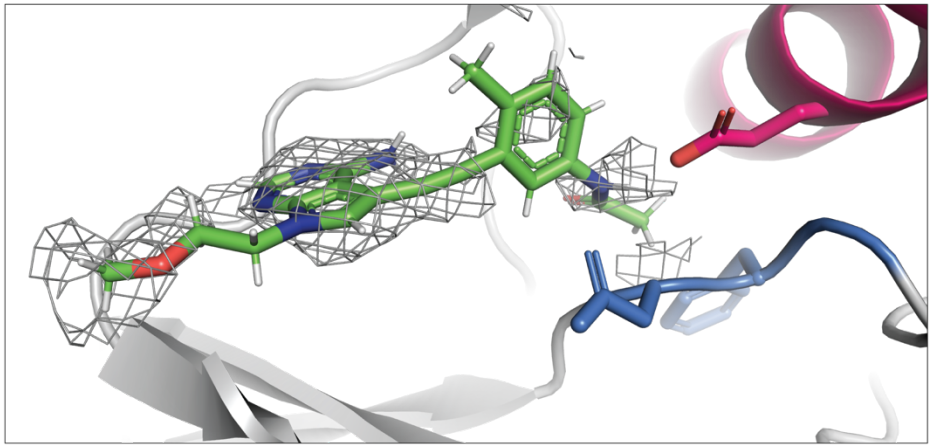

Chain B: electron density of Glu310, Asp404, Phe405

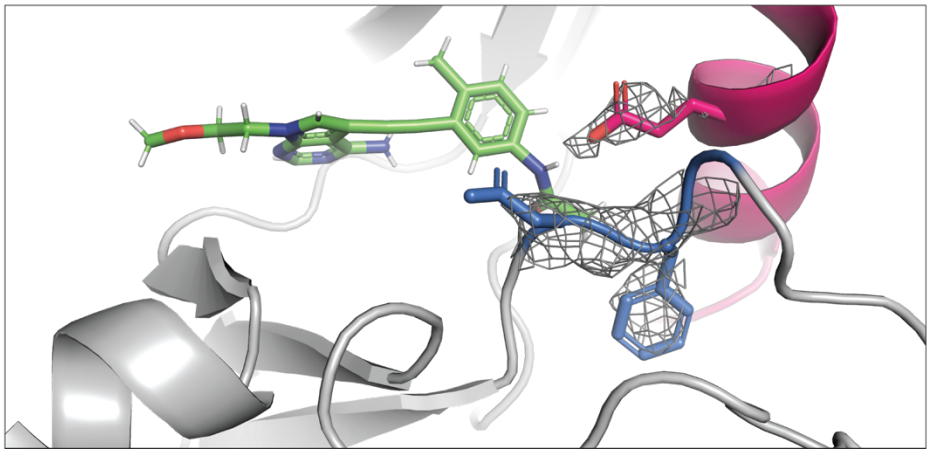

BIBLIOGRAPHY

(1) Taylor, S. S.; Keshwani, M. M.; Steichen, J. M.; Kornev, A. P., *Philos Trans R Soc Lond B Biol Sci* **2012,** *367* (1602), 2517-28.

(2) Johnson, L. N.; Lewis, R. J., *Chem Rev* **2001,** *101* (8), 2209-42.

(3) Kung, J. E.; Jura, N., *Structure* **2016,** *24* (1), 7-24.

(4) Zhao, Z.; Wu, H.; Wang, L.; Liu, Y.; Knapp, S.; Liu, Q.; Gray, N. S., *ACS Chem Biol* **2014,** *9* (6), 1230-41.

(5) Johnson, L. N., *Q Rev Biophys* **2009,** *42* (1), 1-40.

(6) Zhang, J.; Yang, P. L.; Gray, N. S., *Nat Rev Cancer* **2009,** *9* (1), 28-39.

(7) Mobitz, H., *Biochim Biophys Acta* **2015,** *1854* (10 Pt B), 1555-66.

(8) Davies, S. P.; Reddy, H.; Caivano, M.; Cohen, P., *Biochem J* **2000,** *351* (Pt 1), 95-105.

(9) Garnett, M. J.; Rana, S.; Paterson, H.; Barford, D.; Marais, R., *Mol Cell* **2005,** *20* (6), 963-9.

(10) Ahmad, M. K.; Abdollah, N. A.; Shafie, N. H.; Yusof, N. M.; Razak, S. R. A., *Cancer Biol Med* **2018,** *15* (1), 14-28.

(11) Hari, S. B.; Merritt, E. A.; Maly, D. J., *Chem Biol* **2014,** *21* (5), 628-35.

(12) Manning, G.; Whyte, D. B.; Martinez, R.; Hunter, T.; Sudarsanam, S., *Science* **2002,** *298* (5600), 1912-34.

(13) Maddika, S.; Chen, J., *Nat Cell Biol* **2009,** *11* (4), 409-19.

(14) Hu, S.; Xie, Z.; Onishi, A.; Yu, X.; Jiang, L.; Lin, J.; Rho, H. S.; Woodard, C.; Wang, H.; Jeong, J. S.; Long, S.; He, X.; Wade, H.; Blackshaw, S.; Qian, J.; Zhu, H., *Cell* **2009,** *139* (3), 610-22.

(15) Hatzivassiliou, G.; Song, K.; Yen, I.; Brandhuber, B. J.; Anderson, D. J.; Alvarado, R.; Ludlam, M. J.; Stokoe, D.; Gloor, S. L.; Vigers, G.; Morales, T.; Aliagas, I.; Liu, B.; Sideris, S.; Hoeflich, K. P.; Jaiswal, B. S.; Seshagiri, S.; Koeppen, H.; Belvin, M.; Friedman, L. S.; Malek, S., *Nature* **2010,** *464* (7287), 431-5.

(16) Poulikakos, P. I.; Zhang, C.; Bollag, G.; Shokat, K. M.; Rosen, N., *Nature* **2010,** *464* (7287), 427-30.

(17) Krishnamurty, R.; Brigham, J. L.; Leonard, S. E.; Ranjitkar, P.; Larson, E. T.; Dale, E. J.; Merritt, E. A.; Maly, D. J., *Nat Chem Biol* **2013,** *9* (1), 43-50.

(18) Leonard, S. E.; Register, A. C.; Krishnamurty, R.; Brighty, G. J.; Maly, D. J., *ACS Chem Biol* **2014,** *9* (8), 1894-905.
(19) Register, A. C.; Leonard, S. E.; Maly, D. J., *Biochemistry* **2014,** *53* (44), 6910-23.
(20) Feldman, H. C.; Tong, M.; Wang, L.; Meza-Acevedo, R.; Gobillot, T. A.; Lebedev, I.; Gliedt, M. J.; Hari, S. B.; Mitra, A. K.; Backes, B. J.; Papa, F. R.; Seeliger, M. A.; Maly, D. J., *ACS Chem Biol* **2016,** *11* (8), 2195-205.
(21) Housden, B. E.; Muhar, M.; Gemberling, M.; Gersbach, C. A.; Stainier, D. Y.; Seydoux, G.; Mohr, S. E.; Zuber, J.; Perrimon, N., *Nat Rev Genet* **2017,** *18* (1), 24-40.
(22) Weiss, W. A.; Taylor, S. S.; Shokat, K. M., *Nat Chem Biol* **2007,** *3* (12), 739-44.
(23) Knight, Z. A.; Shokat, K. M., *Cell* **2007,** *128* (3), 425-30.
(24) Murphy, J. M.; Nakatani, Y.; Jamieson, S. A.; Dai, W.; Lucet, I. S.; Mace, P. D., *Structure* **2015,** *23* (11), 2111-21.
(25) Ahler, E.; Register, A. C.; Chakraborty, S.; Fang, L.; Dieter, E. M.; Sitko, K. A.; Vidadala, R. S. R.; Trevilli-an, B. M.; Golkowski, M.; Gelman, H.; Stephany, J. J.; Rubin, A. F.; Merritt, E. A.; Fowler, D. M.; Maly, D. J., *Molecular Cell* **2019**, in press.
(26) Gonfloni, S.; Weijland, A.; Kretzschmar, J.; Superti-Furga, G., *Nat Struct Biol* **2000,** *7* (4), 281-6.
(27) Wang, L.; Perera, B. G.; Hari, S. B.; Bhhatarai, B.; Backes, B. J.; Seeliger, M. A.; Schurer, S. C.; Oakes, S. A.; Papa, F. R.; Maly, D. J., *Nat Chem Biol* **2012,** *8* (12), 982-9.
(28) Moellering, R. E.; Cravatt, B. F., *Chem Biol* **2012,** *19* (1), 11-22.
(29) Kang, K.; Park, J.; Kim, E., *Proteome Sci* **2016,** *15*, 15.
(30) Cravatt, B. F.; Wright, A. T.; Kozarich, J. W., *Annu Rev Biochem* **2008,** *77*, 383-414.
(31) Speers, A. E.; Adam, G. C.; Cravatt, B. F., *J Am Chem Soc* **2003,** *125* (16), 4686-7.
(32) Hong, V.; Steinmetz, N. F.; Manchester, M.; Finn, M. G., *Bioconjug Chem* **2010,** *21* (10), 1912-6.
(33) Khossravi, M.; Borchardt, R. T., *Pharm Res* **2000,** *17* (7), 851-8.
(34) Cheng, R. Z.; Uchida, K.; Kawakishi, S., *Biochem J* **1992,** *285 (Pt 2)*, 667-71.
(35) Houghton, E. A.; Nicholas, K. M., *J Biol Inorg Chem* **2009,** *14* (2), 243-51.
(36) Khossravi, M.; Borchardt, R. T., *Pharm Res* **1998,** *15* (7), 1096-102.
(37) Ramirez, D. C.; Mejiba, S. E.; Mason, R. P., *J Biol Chem* **2005,** *280* (29), 27402-11.

(38) Baskin, J. M.; Prescher, J. A.; Laughlin, S. T.; Agard, N. J.; Chang, P. V.; Miller, I. A.; Lo, A.; Codelli, J. A.; Bertozzi, C. R., *Proc Natl Acad Sci U S A* **2007,** *104* (43), 16793-7.
(39) Rutkowska, A.; Thomson, D. W.; Vappiani, J.; Werner, T.; Mueller, K. M.; Dittus, L.; Krause, J.; Muelbaier, M.; Bergamini, G.; Bantscheff, M., *ACS Chem Biol* **2016,** *11* (9), 2541-50.
(40) Blackman, M. L.; Royzen, M.; Fox, J. M., *J Am Chem Soc* **2008,** *130* (41), 13518-9.
(41) Serafimova, I. M.; Pufall, M. A.; Krishnan, S.; Duda, K.; Cohen, M. S.; Maglathlin, R. L.; McFarland, J. M.; Miller, R. M.; Frodin, M.; Taunton, J., *Nat Chem Biol* **2012,** *8* (5), 471-6.
(42) Bradshaw, J. M.; McFarland, J. M.; Paavilainen, V. O.; Bisconte, A.; Tam, D.; Phan, V. T.; Romanov, S.; Finkle, D.; Shu, J.; Patel, V.; Ton, T.; Li, X.; Loughhead, D. G.; Nunn, P. A.; Karr, D. E.; Gerritsen, M. E.; Funk, J. O.; Owens, T. D.; Verner, E.; Brameld, K. A.; Hill, R. J.; Goldstein, D. M.; Taunton, J., *Nat Chem Biol* **2015,** *11* (7), 525-31.
(43) Krishnan, S.; Miller, R. M.; Tian, B.; Mullins, R. D.; Jacobson, M. P.; Taunton, J., *J Am Chem Soc* **2014,** *136* (36), 12624-30.
(44) Miller, R. M.; Paavilainen, V. O.; Krishnan, S.; Serafimova, I. M.; Taunton, J., *J Am Chem Soc* **2013,** *135* (14), 5298-301.
(45) Liu, B. A.; Engelmann, B. W.; Nash, P. D., *FEBS Lett* **2012,** *586* (17), 2597-605.
(46) Tyanova, S.; Temu, T.; Sinitcyn, P.; Carlson, A.; Hein, M. Y.; Geiger, T.; Mann, M.; Cox, J., *Nat Methods* **2016,** *13* (9), 731-40.
(47) Szklarczyk, D.; Franceschini, A.; Wyder, S.; Forslund, K.; Heller, D.; Huerta-Cepas, J.; Simonovic, M.; Roth, A.; Santos, A.; Tsafou, K. P.; Kuhn, M.; Bork, P.; Jensen, L. J.; von Mering, C., *Nucleic Acids Res* **2015,** *43* (Database issue), D447-52.
(48) Szklarczyk, D.; Morris, J. H.; Cook, H.; Kuhn, M.; Wyder, S.; Simonovic, M.; Santos, A.; Doncheva, N. T.; Roth, A.; Bork, P.; Jensen, L. J.; von Mering, C., *Nucleic Acids Res* **2017,** *45* (D1), D362-D368.
(49) Heberle, H.; Meirelles, G. V.; da Silva, F. R.; Telles, G. P.; Minghim, R., *BMC Bioinformatics* **2015,** *16*, 169.
(50) Cox, J.; Mann, M., *Nat Biotechnol* **2008,** *26* (12), 1367-72.
(51) The Gene Ontology, C., *Nucleic Acids Res* **2017,** *45* (D1), D331-D338.
(52) Ashburner, M.; Ball, C. A.; Blake, J. A.; Botstein, D.; Butler, H.; Cherry, J. M.; Davis, A. P.; Dolinski, K.; Dwight, S. S.; Eppig, J. T.; Harris, M. A.; Hill, D. P.; Issel-Tarver, L.; Kasarskis, A.;

Lewis, S.; Matese, J. C.; Richardson, J. E.; Ringwald, M.; Rubin, G. M.; Sherlock, G., *Nat Genet* **2000,** *25* (1), 25-9.

(53) Xing, Z.; Chen, H. C.; Nowlen, J. K.; Taylor, S. J.; Shalloway, D.; Guan, J. L., *Mol Biol Cell* **1994,** *5* (4), 413-21.

(54) Tanaka, S.; Neff, L.; Baron, R.; Levy, J. B., *J Biol Chem* **1995,** *270* (24), 14347-51.

(55) Bromann, P. A.; Korkaya, H.; Courtneidge, S. A., *Oncogene* **2004,** *23* (48), 7957-68.

(56) Gao, X.; Hannoush, R. N., *J Am Chem Soc* **2014,** *136* (12), 4544-50.

(57) Weibrecht, I.; Leuchowius, K. J.; Clausson, C. M.; Conze, T.; Jarvius, M.; Howell, W. M.; Kamali-Moghaddam, M.; Soderberg, O., *Expert Rev Proteomics* **2010,** *7* (3), 401-9.

(58) Gao, X.; Hannoush, R. N., *Nat Chem Biol* **2014,** *10* (1), 61-8.

(59) Gao, X.; Hannoush, R. N., *Nat Protoc* **2014,** *9* (11), 2607-23.

(60) Soderberg, O.; Gullberg, M.; Jarvius, M.; Ridderstrale, K.; Leuchowius, K. J.; Jarvius, J.; Wester, K.; Hydbring, P.; Bahram, F.; Larsson, L. G.; Landegren, U., *Nat Methods* **2006,** *3* (12), 995-1000.

(61) Donepudi, M.; Resh, M. D., *Cell Signal* **2008,** *20* (7), 1359-67.

(62) Stenmark, H.; Aasland, R.; Toh, B. H.; D'Arrigo, A., *J Biol Chem* **1996,** *271* (39), 24048-54.

(63) Lombard, C. K.; Davis, A. L.; Inukai, T.; Maly, D. J., *Biochemistry* **2018,** *57* (40), 5897-5909.

(64) Chakraborty, S.; Inukai, T.; Fang, L.; Golkowski, M.; Maly, D. J., *ACS Chemical Biology* **2019**.

(65) Golkowski, M.; Vidadala, R. S.; Lombard, C. K.; Suh, H. W.; Maly, D. J.; Ong, S. E., *J Proteome Res* **2017,** *16* (3), 1216-1227.

(66) Kuriyan, J.; Eisenberg, D., *Nature* **2007,** *450* (7172), 983-90.

(67) Pellicena, P.; Kuriyan, J., *Curr Opin Struct Biol* **2006,** *16* (6), 702-9.

(68) Huse, M.; Kuriyan, J., *Cell* **2002,** *109* (3), 275-82.

(69) Taylor, S. S.; Kornev, A. P., *Trends Biochem Sci* **2011,** *36* (2), 65-77.

(70) Engen, J. R.; Wales, T. E.; Hochrein, J. M.; Meyn, M. A., 3rd; Banu Ozkan, S.; Bahar, I.; Smithgall, T. E., *Cell Mol Life Sci* **2008,** *65* (19), 3058-73.

(71) Sicheri, F.; Kuriyan, J., *Curr Opin Struct Biol* **1997,** *7* (6), 777-85.

(72) Kim, L. C.; Song, L.; Haura, E. B., *Nat Rev Clin Oncol* **2009,** *6* (10), 587-95.

(73) Jura, N.; Zhang, X.; Endres, N. F.; Seeliger, M. A.; Schindler, T.; Kuriyan, J., *Mol Cell* **2011,** *42* (1), 9-22.

(74) Boggon, T. J.; Eck, M. J., *Oncogene* **2004,** *23* (48), 7918-27.
(75) Fang, L.; Chakraborty, S.; Dieter, E. M.; Potter, Z. E.; Lombard, C. K.; Maly, D. J., *J Am Chem Soc* **2019,** *141* (30), 11912-11922.
(76) Ahler, E.; Register, A. C.; Chakraborty, S.; Fang, L.; Dieter, E. M.; Sitko, K. A.; Vidadala, R. S. R.; Trevillian, B. M.; Golkowski, M.; Gelman, H.; Stephany, J. J.; Rubin, A. F.; Merritt, E. A.; Fowler, D. M.; Maly, D. J., *Mol Cell* **2019,** *74* (2), 393-408 e20.
(77) Young, M. A.; Gonfloni, S.; Superti-Furga, G.; Roux, B.; Kuriyan, J., *Cell* **2001,** *105* (1), 115-26.
(78) Kwarcinski, F. E.; Brandvold, K. R.; Phadke, S.; Beleh, O. M.; Johnson, T. K.; Meagher, J. L.; Seeliger, M. A.; Stuckey, J. A.; Soellner, M. B., *ACS Chem Biol* **2016,** *11* (5), 1296-304.
(79) Seeliger, M. A.; Nagar, B.; Frank, F.; Cao, X.; Henderson, M. N.; Kuriyan, J., *Structure* **2007,** *15* (3), 299-311.
(80) Xu, W.; Doshi, A.; Lei, M.; Eck, M. J.; Harrison, S. C., *Mol Cell* **1999,** *3* (5), 629-38.
(81) Chakraborty, S.; Inukai, T.; Fang, L.; Golkowski, M.; Maly, D. J., *ACS Chem Biol* **2019,** *14* (6), 1249-1259.
(82) Tong, M.; Pelton, J. G.; Gill, M. L.; Zhang, W.; Picart, F.; Seeliger, M. A., *Nat Commun* **2017,** *8* (1), 2160.
(83) Agius, M. P.; Ko, K. S.; Johnson, T. K.; Kwarcinski, F. E.; Phadke, S.; Lachacz, E. J.; Soellner, M. B., *ACS Chem Biol* **2019,** *14* (7), 1556-1563.
(84) Skora, L.; Mestan, J.; Fabbro, D.; Jahnke, W.; Grzesiek, S., *Proc Natl Acad Sci U S A* **2013,** *110* (47), E4437-45.
(85) Hantschel, O.; Nagar, B.; Guettler, S.; Kretzschmar, J.; Dorey, K.; Kuriyan, J.; Superti-Furga, G., *Cell* **2003,** *112* (6), 845-57.
(86) Nagar, B.; Hantschel, O.; Young, M. A.; Scheffzek, K.; Veach, D.; Bornmann, W.; Clarkson, B.; Superti-Furga, G.; Kuriyan, J., *Cell* **2003,** *112* (6), 859-71.
(87) Nagar, B.; Hantschel, O.; Seeliger, M.; Davies, J. M.; Weis, W. I.; Superti-Furga, G.; Kuriyan, J., *Mol Cell* **2006,** *21* (6), 787-98.
(88) Sonti, R.; Hertel-Hering, I.; Lamontanara, A. J.; Hantschel, O.; Grzesiek, S., *J Am Chem Soc* **2018,** *140* (5), 1863-1869.
(89) Amatya, N.; Lin, D. Y.; Andreotti, A. H., *Biochem Soc Trans* **2019,** *47* (4), 1101-1116.
(90) Tong, M.; Seeliger, M. A., *ACS Chem Biol* **2015,** *10* (1), 190-200.

(91) Dar, A. C.; Lopez, M. S.; Shokat, K. M., *Chem Biol* **2008,** *15* (10), 1015-22.
(92) MacAuley, A.; Cooper, J. A., *Mol Cell Biol* **1989,** *9* (6), 2648-56.
(93) Cowan-Jacob, S. W.; Fendrich, G.; Floersheimer, A.; Furet, P.; Liebetanz, J.; Rummel, G.; Rheinberger, P.; Centeleghe, M.; Fabbro, D.; Manley, P. W., *Acta Crystallogr D Biol Crystallogr* **2007,** *63* (Pt 1), 80-93.
(94) Weisberg, E.; Manley, P. W.; Breitenstein, W.; Bruggen, J.; Cowan-Jacob, S. W.; Ray, A.; Huntly, B.; Fabbro, D.; Fendrich, G.; Hall-Meyers, E.; Kung, A. L.; Mestan, J.; Daley, G. Q.; Callahan, L.; Catley, L.; Cavazza, C.; Azam, M.; Neuberg, D.; Wright, R. D.; Gilliland, D. G.; Griffin, J. D., *Cancer Cell* **2005,** *7* (2), 129-41.
(95) Zhou, T.; Commodore, L.; Huang, W. S.; Wang, Y.; Thomas, M.; Keats, J.; Xu, Q.; Rivera, V. M.; Shakespeare, W. C.; Clackson, T.; Dalgarno, D. C.; Zhu, X., *Chem Biol Drug Des* **2011,** *77* (1), 1-11.
(96) Chan, W. W.; Wise, S. C.; Kaufman, M. D.; Ahn, Y. M.; Ensinger, C. L.; Haack, T.; Hood, M. M.; Jones, J.; Lord, J. W.; Lu, W. P.; Miller, D.; Patt, W. C.; Smith, B. D.; Petillo, P. A.; Rutkoski, T. J.; Telikepalli, H.; Vogeti, L.; Yao, T.; Chun, L.; Clark, R.; Evangelista, P.; Gavrilescu, L. C.; Lazarides, K.; Zaleskas, V. M.; Stewart, L. J.; Van Etten, R. A.; Flynn, D. L., *Cancer Cell* **2011,** *19* (4), 556-68.
(97) Horio, T.; Hamasaki, T.; Inoue, T.; Wakayama, T.; Itou, S.; Naito, H.; Asaki, T.; Hayase, H.; Niwa, T., *Bioorg Med Chem Lett* **2007,** *17* (10), 2712-7.
(98) Apsel, B.; Blair, J. A.; Gonzalez, B.; Nazif, T. M.; Feldman, M. E.; Aizenstein, B.; Hoffman, R.; Williams, R. L.; Shokat, K. M.; Knight, Z. A., *Nat Chem Biol* **2008,** *4* (11), 691-9.
(99) Garske, A. L.; Peters, U.; Cortesi, A. T.; Perez, J. L.; Shokat, K. M., *Proc Natl Acad Sci U S A* **2011,** *108* (37), 15046-52.
(100) Zhang, C.; Lopez, M. S.; Dar, A. C.; Ladow, E.; Finkbeiner, S.; Yun, C. H.; Eck, M. J.; Shokat, K. M., *ACS Chem Biol* **2013,** *8* (9), 1931-8.
(101) Seeliger, M. A.; Ranjitkar, P.; Kasap, C.; Shan, Y.; Shaw, D. E.; Shah, N. P.; Kuriyan, J.; Maly, D. J., *Cancer Res* **2009,** *69* (6), 2384-92.
(102) Shan, Y.; Seeliger, M. A.; Eastwood, M. P.; Frank, F.; Xu, H.; Jensen, M. O.; Dror, R. O.; Kuriyan, J.; Shaw, D. E., *Proc Natl Acad Sci U S A* **2009,** *106* (1), 139-44.
(103) Kung, A.; Schimpl, M.; Ekanayake, A.; Chen, Y. C.; Overman, R.; Zhang, C., *ACS Chem Biol* **2017,** *12* (6), 1499-1503.

(104) Zhang, C.; Kenski, D. M.; Paulson, J. L.; Bonshtien, A.; Sessa, G.; Cross, J. V.; Templeton, D. J.; Shokat, K. M., *Nat Methods* **2005,** *2* (6), 435-41.

(105) Bantscheff, M.; Eberhard, D.; Abraham, Y.; Bastuck, S.; Boesche, M.; Hobson, S.; Mathieson, T.; Perrin, J.; Raida, M.; Rau, C.; Reader, V.; Sweetman, G.; Bauer, A.; Bouwmeester, T.; Hopf, C.; Kruse, U.; Neubauer, G.; Ramsden, N.; Rick, J.; Kuster, B.; Drewes, G., *Nat Biotechnol* **2007,** *25* (9), 1035-44.

(106) Golkowski, M.; Brigham, J. L.; Perera, G. K.; Romano, G. E.; Maly, D. J.; Ong, S. E., *Medchemcomm* **2014,** *5* (3), 363-369.

(107) Golkowski, M.; Perera, G. K.; Vidadala, V. N.; Ojo, K. K.; Van Voorhis, W. C.; Maly, D. J.; Ong, S. E., *Mol Omics* **2018,** *14* (1), 26-36.

(108) Charras, G. T., *J Microsc* **2008,** *231* (3), 466-78.

(109) Wang, Q.; Pechersky, Y.; Sagawa, S.; Pan, A. C.; Shaw, D. E., *Proc Natl Acad Sci U S A* **2019,** *116* (19), 9390-9399.

(110) Wang, Q.; Vogan, E. M.; Nocka, L. M.; Rosen, C. E.; Zorn, J. A.; Harrison, S. C.; Kuriyan, J., *Elife* **2015,** *4*.

(111) Choi, Y.; Seeliger, M. A.; Panjarian, S. B.; Kim, H.; Deng, X.; Sim, T.; Couch, B.; Koleske, A. J.; Smithgall, T. E.; Gray, N. S., *J Biol Chem* **2009,** *284* (42), 29005-14.

(112) Hantschel, O., *Genes Cancer* **2012,** *3* (5-6), 436-46.

(113) Varnai, P.; Rother, K. I.; Balla, T., *J Biol Chem* **1999,** *274* (16), 10983-9.

(114) Morita, S.; Villalta, S. A.; Feldman, H. C.; Register, A. C.; Rosenthal, W.; Hoffmann-Petersen, I. T.; Mehdizadeh, M.; Ghosh, R.; Wang, L.; Colon-Negron, K.; Meza-Acevedo, R.; Backes, B. J.; Maly, D. J.; Bluestone, J. A.; Papa, F. R., *Cell Metab* **2017,** *25* (4), 883-897 e8.

(115) Saito, K.; Tolias, K. F.; Saci, A.; Koon, H. B.; Humphries, L. A.; Scharenberg, A.; Rawlings, D. J.; Kinet, J. P.; Carpenter, C. L., *Immunity* **2003,** *19* (5), 669-78.

(116) Seeliger, M. A.; Young, M.; Henderson, M. N.; Pellicena, P.; King, D. S.; Falick, A. M.; Kuriyan, J., *Protein Sci* **2005,** *14* (12), 3135-9.

(117) Kabsch, W., *Acta Crystallogr D Biol Crystallogr* **2010,** *66* (Pt 2), 133-44.

(118) McCoy, A. J., *Acta Crystallogr D Biol Crystallogr* **2007,** *63* (Pt 1), 32-41.

(119) Adams, P. D.; Grosse-Kunstleve, R. W.; Hung, L. W.; Ioerger, T. R.; McCoy, A. J.; Moriarty, N. W.; Read, R. J.; Sacchettini, J. C.; Sauter, N. K.; Terwilliger, T. C., *Acta Crystallogr D Biol Crystallogr* **2002,** *58* (Pt 11), 1948-54.

(120) Emsley, P.; Cowtan, K., *Acta Crystallogr D Biol Crystallogr* **2004,** *60* (Pt 12 Pt 1), 2126-32.